CONVENTIONAL ROOFS AS COLLECTORS IN A SOLAR-ASSISTED HEAT PUMP SYSTEM

BY

DENNIS LESLIE LOVEDAY, B.Sc.

A THESIS SUBMITTED TO THE UNIVERSITY OF ASTON IN BIRMINGHAM FOR THE DEGREE OF DOCTOR OF PHILOSOPHY

DEPARTMENT OF PHYSICS

JUNE, 1983

SUMMARY

The performance of a series configuration, solar-assisted heat pump system with sensible heat storage in water is evaluated. The system is installed in an occupied house near Basingstoke, U.K., and the solar assistance is provided by the conventional tiled roof of the dwelling. The results of system monitoring over one heating season are presented, and the saving in the requirement of purchased energy is estimated to be about 24% over a resistance heating system. A discussion of store modifications indicates that savings of up to 40% would be possible.

From further monitoring, empirical relations are obtained which characterise the in situ performance, in the U.K. climate, of the installed air source heat pump. These permit calculation of the heating capacity and the heating mode coefficient of performance from a knowledge of the psychrometric state of the source air.

An analytical model is presented of an air-heating solar collector, which incorporates the finite thickness and thermal conductivity of the absorber plate. Laboratory tests show the model to be applicable to a conventional tiled roof when used as an air heater; similar testing of corrugated metal panels is described. Further experiments show that wind over an untorched tiled roof increases the outlet air temperature and useful energy gain. A modified model is proposed to explain these effects.

Conventional tiled and metal roofs are suitable pre-heaters for air source heat pumps. Assessments, for the monitored installation, of no roof, tile roof and steel roof pre-heating give corresponding seasonal COP(H) values of 2.44, 2.50 and 2.57 (for the same fan power requirements).

The analytical models for roofs as air heaters, together with the performance relations for the heat pump, may be used in computer modelling applications to predict the performance of both newly-designed and retrofitted installations.

KEY WORDS

Solar-assisted heating; heat pumps; solar air panels; conventional roof absorption; solar heat simulation.

Submitted for the degree of Doctor of Philosophy, 1983, by
Dennis Leslie Loveday, B.Sc.

TO MY MOTHER, AND TO THE MEMORY

OF MY GRANDPARENTS

ACKNOWLEDGEMENTS

I wish to express my sincere thanks to Professor W.E.J. Neal for his supervision throughout the project, for much thought-provoking discussion, and for permission to use some of the illustrations from his Inaugural Lecture. I also wish to thank Dr. M. Pabon-Diaz and Dr. G.L.R. Mair for their helpful discussion on several aspects of the work.

Many thanks to the following: Mr. C.B. Symonds and Cmdr. R.E. Bird of Almondbury Developments Ltd., for their help in the installation and maintenance of part of the monitoring equipment; Messrs. J. Goff and E. Hodder of Normalair-Garrett Ltd., for the loan and installation of a Demand Profile Recorder and for the provision of data translation services; Mr. P. Loake of Lee-Dickens Ltd., for help in interfacing humidity sensors with the monitoring equipment; Dr. M.G. Hutchins of University College, Cardiff, for carrying out reflectivity measurements on surface samples; Messrs. F. Lane and H. Arrowsmith of the Physics Departmental Workshop for their assistance in the construction of items necessary during the course of this work, and Mr. T.J. Kennedy, the Departmental Superintendent, for his helpfulness at all times.

I acknowledge a studentship from the Science and Engineering Research Council and thank them, together with the University of Aston, for the financial assistance which enabled me to attend conferences in Lindau, West Germany, and Lyons, France.

For their help in the production of this thesis, I am grateful to Mr. R. Howes, Miss S. Clark, Mr. D. Whiteford and Mrs. D. James.

Finally, I wish to express my gratitude to Brian and Sheila Wilson, and their son Derek, for allowing their house to be used for monitoring purposes, and for their kind hospitality during visits. Without their co-operation and patience, much of this work would not have been possible.

Birmingham, December, 1982. D. L. Loveday.

PREFACE

THE PROJECT OBJECTIVES

The objectives of this project were as follows:

(i) to evaluate the performance over a heating season of an installed solar-assisted air-source heat pump system for domestic space and water heating, using a conventional tiled roof as the radiation absorber;

(ii) to determine the saving in purchased energy of the installed system over a 1:1 ratio resistance heating system;

(iii) to obtain in situ operation performance characteristics of the installed heat pump;

(iv) to determine the efficiency of a tiled roof as an air-heating solar collector, the improvement in the performance of the heat pump as a result of using the tiled roof to pre-heat the source air, and to consider the applicability for retrofitting to existing houses;

(v) to compare other roof structures with tiled roofs in the same context as (iv) above, and to consider their applicability in new building design;

(vi) to design a control system for improving the performance of the installation, in the light of operational experience and results.

Frontispiece: A test in progress on the section of tiled roof, using the indoor heating simulator.

CONTENTS

LIST OF FIGURES

LIST OF TABLES

LIST OF PHOTOGRAPHS

'this most excellent canopy the air, ...

this majestical roof .....'

Hamlet, Act II, Scene 2,

Shakespeare.

CHAPTER 1

ENERGY CONSERVATION AND HEAT PUMPS - INTRODUCTION AND BACKGROUND

The rate of consumption of fossil fuels, and in particular the prospect of depletion of the reserves of oil and natural gas in the relatively near future, has led in recent years to an increased interest in the so-called 'renewable' energy sources and into methods of energy conservation. The exploitation of renewable sources can provide both short term and long term benefits. In the short term, it offers the ability to conserve the existing supplies of fossil fuels. In the long term, electricity generated by the processes of nuclear fission and fusion, together with energy derived from the renewable sources, can contribute to form the basis for the supply of the future energy needs of mankind.

1.1 The Prospects for Energy Saving in the United Kingdom

In the United Kingdom, about 26% of the total annual energy consumption takes place in the domestic sector (Department of Energy, 1981). Attempts at saving energy in this area would therefore appear worthwhile from the points of view of reducing the U.K.'s total demand, and of providing financial savings to consumers by reducing their requirement of purchased energy.

A report by the Building Research Establishment (1975) states that of the total energy consumed domestically, an average of approximately 64% is used for space heating, 22% is used for water heating, and 14% is used for cooking, lighting and appliances. Thus, while the use of 'solar panels', for example, to heat water can offer savings, there

is much greater scope for savings if some provision could be made for space heating requirements. The report discusses various ways in which energy in housing could be conserved. One method is by the use of heat pumps, and a possible saving of close to 9% in the U.K.'s primary energy consumption is quoted.

1.2 Heat Pumps

1.2.1 Basic Principles

The principle of the heat pump was first put forward by William Thomson (1852) (who later became Lord Kelvin). The principle states that for the input of some work, heat is absorbed from a region of lower temperature and is rejected at a higher temperature in another region, i.e. low-grade heat (at a lower temperature) is upgraded to become high-grade heat (at a higher temperature). This can be achieved by the cyclic evaporation and condensation of a suitable working fluid, and such a machine, called a heat pump, can operate on an absorption cycle or a vapour compression cycle (Stoecker, 1958; ASHRAE, 1972; Rogers and Mayhew, 1978).

The efficiency of any machine is defined as the ratio of the useful effect obtained to the work input. Consider a heat pump operating between two regions of temperature T_1 and T_2, where $T_1 > T_2$ (Figure 1.1).

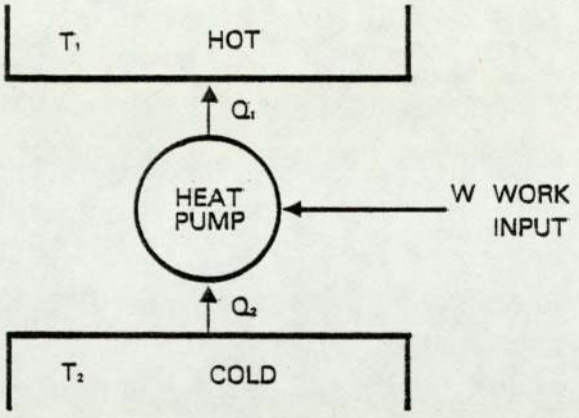

Figure 1.1 Thermodynamic operation of a heat pump.

For the work input W, an amount of energy Q_2 is extracted from the lower temperature region, or reservoir, and an amount of energy Q_1 is rejected to the higher temperature reservoir, such that:

$$Q_1 = Q_2 + W \qquad 1.1$$

Two efficiencies, or coefficients of performance (COP), can be defined for the heat pump (a reversed heat engine) depicted in Figure 1.1 - that in the heating mode, COP(H), and that in the cooling mode, COP(C). The term chosen depends upon whether the useful effect is that of heating or cooling (refrigeration). The heat pump and refrigerator are, therefore, one and the same machine.

$$\text{COP(H)} = Q_1/W \qquad 1.2$$

and

$$\text{COP(C)} = Q_2/W \qquad 1.3$$

Dividing equation 1.1 by W and substituting from equations 1.2 and 1.3 gives:

$$\text{COP(H)} = \text{COP(C)} + 1 \qquad 1.4$$

From discussions presented in many standard texts on thermodynamics

(see, for example, Zemansky, 1968), the COP(H) may be expressed, for T_1 and T_2 in Kelvins, as:

$$COP(H) = T_1/(T_1 - T_2) \qquad 1.5$$

and equation 1.5 represents the reversed Carnot efficiency. This is the maximum efficiency that is thermodynamically possible for a reversed heat engine operating between the absolute temperatures T_1 and T_2. It can be seen that for $T_1 > T_2$ the value of the COP(H) is greater than unity. Thus, using a heat pump to heat a house becomes attractive from the viewpoint of reducing one's running costs, since an amount of heat can be rejected to the living space which is in excess of the (purchased) work input to the pump, the difference being supplied by the low grade source. Further, the rejected heat is at a higher temperature and hence is more useful for heating purposes.

Figure 1.2 is a schematic diagram showing the basic components of a vapour compression cycle heat pump.

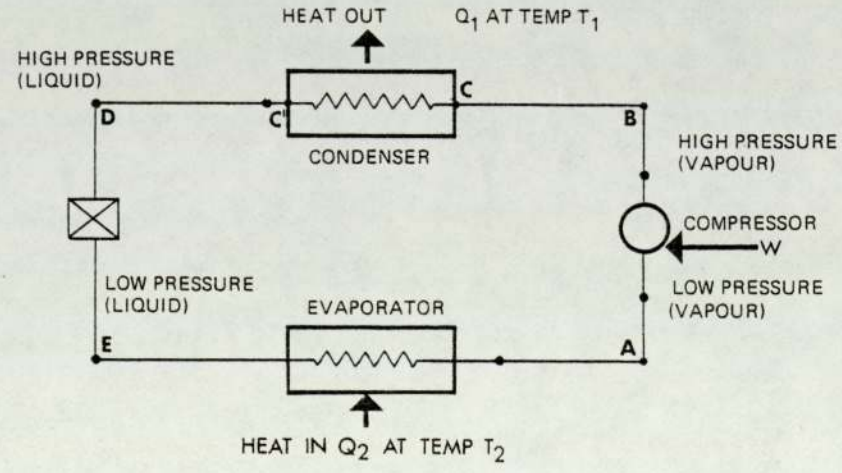

Figure 1.2 The basic heat pump components.

The working substance commonly used in such heat pumps is one of a range of organic refrigerants or 'Freons' (see, for example, ASHRAE, 1972). After evaporation with the absorption of heat at temperature T_2 (EA), the refrigerant vapour is compressed (AB). The high pressure superheated vapour is then cooled from a temperature T_3 (BC) and condensed (CC'), with the rejection of heat at a temperature T_1, where $T_1 > T_2$; (C'D) represents subcooling of the now liquid refrigerant. Passage through the expansion valve (DE) reduces the pressure for the cycle to be repeated. The cycle may be represented on a pressure versus specific enthalpy diagram (Figure 1.3).

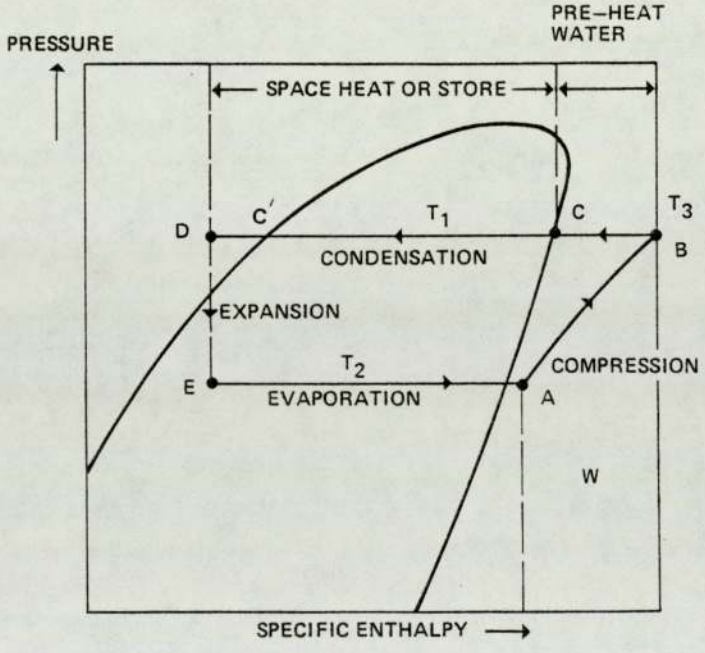

Figure 1.3 Pressure/enthalpy diagram for the basic heat pump cycle.

In practical heat pump cycles, the effects of pressure drops along pipes, frictional losses in the components and the temperature gradients necessary for heat transfer reduce the coefficient of performance to approximately half the ideal Carnot value. Actual COP(H) values in the range of 2-4 are common. The practical aspects

of heat pump design and engineering are discussed by Stoecker (1958), Ambrose (1966), ASHRAE (1972) and Rogers and Mayhew (1978).

1.2.2 Practical Heating Considerations

After Thomson's first enunciation of the principle, little practical work with heat pumps was able to be carried out, mainly due to the lack of available technology. The first heat pump in the U.K. was built by Haldane (1930) for domestic heating; the next, built by Sumner in 1946, was a large commercial unit. In 1952, a heat pump was used to heat the Festival Hall, London (Sumner, 1976). There has, until comparatively recently, however, been little interest in the use of heat pumps for domestic heating in the U.K. because, at a time when fossil fuels were relatively cheap, heat pumps were not considered cost-effective. By contrast, in the U.S.A., there has arisen a large number of domestic heat pump installations used mainly for air-conditioning purposes. This has led to a situation where the majority of heat pumps now available in the U.K. are American air-conditioning units with both heating and cooling capability.

The coefficient of performance of a heat pump not only gives rise to financial savings for the consumer but also leads to more efficient utilisation of primary fuel at the point of generation (Neal, 1980). In an electrically driven heat pump, a COP(H) of 3.6 is needed to achieve 100% use of primary fuel at the power station, assuming a generation efficiency of 33% and transmission losses of 5% (Figure 1.4).

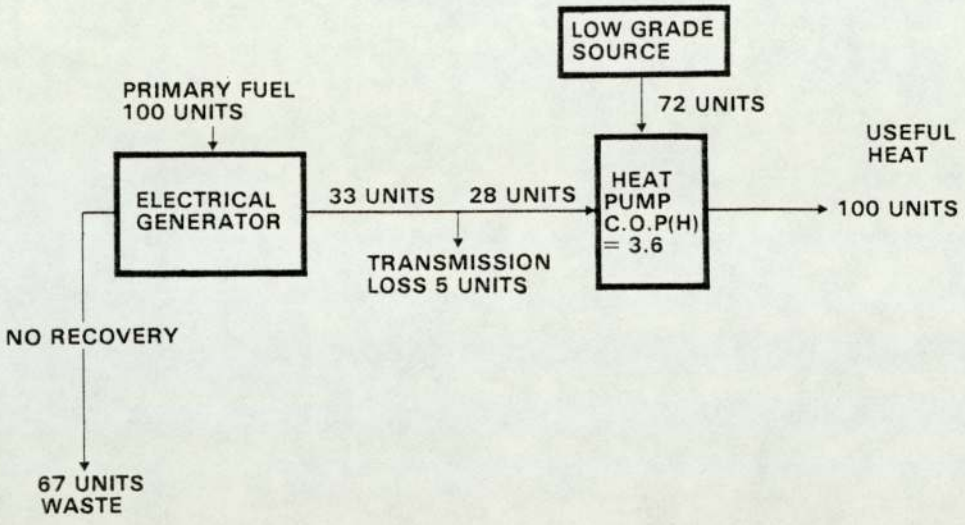

Figure 1.4 Utilisation of primary fuel for an electrically driven heat pump.

A heat pump's compressor may also be driven by means of a fossil-fueled engine (oil or gas) operating at the point of use. With, for example, 64% of the waste heat from the engine recovered and a COP(H) of 3, an overall efficiency of 135% in primary fuel usage can be realised. This is illustrated in Figure 1.5.

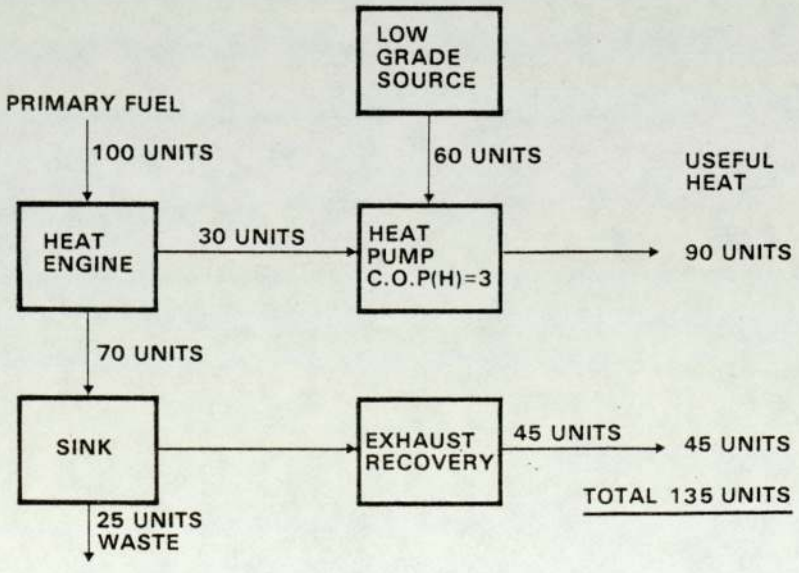

Figure 1.5 Utilisation of primary fuel with a gas driven heat pump.

There is, therefore, increasing interest in the development of gas driven heat pumps (see, for example, Hoggarth, 1981) and in the domestic use of absorption cycle heat pumps combined with solar energy or the burning of waste. Heat recovery from power stations is another possibility receiving attention. For the reason of primary fuel saving, much heat pump research is carried out in Sweden and West Germany, countries that rely heavily on imported primary fuel.

Heat pumps can use the air, the ground, or water as their source of low grade heat (Ambrose, 1966), and the designation of a heat pump as, for example, an air to water, air to air, or water to air etc. unit relates to the siting of the evaporator and condenser coils respectively. (Such types of heat pump and low grade heat sources are discussed by Stamper and Koral, 1979). Water (from, for example, a river or well) as the low grade source has the advantage of a higher specific heat capacity than air or the ground, and also has good heat transfer properties; the source temperature remains fairly constant. However, such a source is not available to the majority of users. Air has a lower specific heat capacity than water, and so large volumes need to be drawn across the evaporator. Another disadvantage, if used for space heating, is that heating demand is high when the ambient air temperature is low, and heat pump performance fluctuates with the temperature; this makes some form of supplementary heating necessary. There is the additional problem of frosting of the evaporator coils at low temperatures and high relative humidities. Nevertheless, due to its universal availability, air is the low grade source most commonly used. The ground offers a third source of low grade heat, and from about one metre down, its temperature becomes steadier as

depth increases. However, problems with frosting and heat transfer to the coil, excavation costs and the difficulties of maintenance to the evaporator after installation render it the least utilised of the three sources discussed.

1.2.3 Solar-Assisted Heat Pumps

For a fixed condensing temperature, the COP(H) of a heat pump can be improved by raising the temperature of the low grade source (air or water, for example). One method of achieving this is with the use of solar energy, and such systems are known as solar-assisted heat pump systems. They can be of the series or parallel configuration, or a combination of the two (Duffie and Beckman, 1980). In the series system, solar collectors or a store act as a supply to the evaporator of the heat pump, which then upgrades the heat to supply the load. In the parallel configuration, the solar collector system and the heat pump supply the load separately. In the combined, or dual system, there are two heat pump evaporators, one supplied by the solar collectors or store, the other by another source; the evaporator in use at any given time is dependent upon the source temperatures. For further discussion and comparison of these configurations, see Freeman et al (1979) and Hwang and Bessler (1979).

In the 1950's, a solar-assisted heat pump system was installed to heat an office building in Albuquerque, New Mexico, U.S.A., and in the U.K. a private dwelling at Rickmansworth was heated by a heat pump and passive solar assistance (see McVeigh, 1977). In recent years, interest has grown in solar-assisted heat pump systems, and installations in various parts of the world have been monitored (see

for example, Mumma and Sepsy, 1975; Terrell, 1978; Taussig et al, 1979; Lou et al, 1981; Aranovitch et al, 1981; Esbensen and Kristensen, 1981). Other developments have included flat-plate heat pump evaporators acting as solar collectors (Charters and Dixon, 1979), and the use of ground source heat pumps with restoration of the ground temperature by solar assistance, i.e. ground storage (Conseil et al, 1981). In the latter work, a mean coefficient of performance of 4-4.5 was reported.

It has been pointed out by Cottingham (1979) that in series configuration, solar-assisted heat pump systems, the possibility arises of using collectors of lower performance and hence lower cost, and work by Andrews (1979) supports this. Passive structures then become acceptable as solar collectors acting as pre-heaters for heat pumps. Bourne (1975) has described a house with a single-glazed roof admitting radiation to an attic space, which acts as a 'volume collector'. A heat pump then removes heat from the attic and heats a water store. Dean (1981) has described an enclosure, glazed on one side and with walls acting as insulated thermal masses, which surrounds a heat pump evaporator, while Dietrich (1981) has surveyed the development in the Federal Republic of Germany of energy roof systems and their relation to solar collectors and heat pump systems.

In many solar heating systems, including those with heat pumps, thermal energy storage is incorporated, mainly because of the intermittent nature of the energy source and because requirements are least when the source is most abundant. In heat pump installations, heat may be stored at times when a high COP(H) value can be achieved, and used later. The storage medium is frequently water, but rocks, pebbles

and certain chemical salts for latent heat storage are in use. Thermal energy storage is a very wide topic to which a great deal of recent research effort has been devoted. For further general reading, see, for example, Duffie and Beckman (1980), and Neal (1981a).

1.3 The Monitored System and the Research Objectives

1.3.1 The Monitored System

The research discussed in this thesis concerns the evaluation of a domestic space and water heating system. The installation may be classified as a series configuration solar-assisted heat pump system, and is installed in an occupied private dwelling near Basingstoke, U.K. Solar assistance is provided by a conventional tiled roof which pre-heats outdoor air before it passes over the evaporator of an air to water electrically driven heat pump. The condenser of the (split) heat pump supplies heat either directly to the load or to a water store. A detailed description of the system is deferred until Chapter 2. The advantage of this system is that the use of a conventional roof enhances the potential for retrofitting some form of solar-assisted heating system to existing buildings with a minimum of structural modifications. This is an important consideration, since about 70% of the U.K.'s housing stock for the year 2000 A.D. is already built. The system is also suitable for new constructions where, for example, the use of specialised collector equipment is precluded.

1.3.2 The Research Objectives

The objectives of this research were as follows:

(i) to evaluate the performance of the installed system over a heating season;

(ii) to determine the saving in purchased energy of the installed system over a 1:1 ratio resistance heating system;

(iii) to obtain in situ operation performance characteristics of the installed heat pump;

(iv) to determine the efficiency of a tiled roof as an air-heating solar collector, the improvement in the performance of the heat pump as a result of using the tiled roof to pre-heat the source air, and to consider the applicability for retrofitting to existing houses;

(v) to compare other roof structures with tiled roofs in the same context as (iv) above, and to consider their applicability in new building design;

(vi) to design a control system for improving the performance of the installation, in the light of operational experience and results.

CHAPTER 2

THE TEST HOUSE AND MONITORING EQUIPMENT

In this chapter, both the test house and the heating system, together with its mode of operation, are described in detail. The equipment installed to monitor the performance of the system is also described, including the necessary calibration techniques.

2.1 The Test House and Heating System

The house is a detached, owner-occupied, three-bedroom dwelling, with the living accommodation on two levels (total floor area 142m^2). It is situated in Long Sutton, near Basingstoke, U.K. The calculated rate of fabric heat loss from roof, walls and windows is 4.6 kW for an indoor/outdoor temperature difference of twenty degrees, and for windstill conditions. The total wall and window areas are 175m^2 and 25m^2 respectively; all windows are double-glazed and brush-sealed. The two sides of the roof face South East and North West, with a pitch of 25°. The roof is of a conventional tiles-on-laths construction, made up of brown-coloured 'Delta' tiles; each side is of area 55m^2.

The heating system comprises three main components - the conventional roof, a heat pump, and a thermal store. Figure 2.1 shows a cross-sectional view through the roof space.

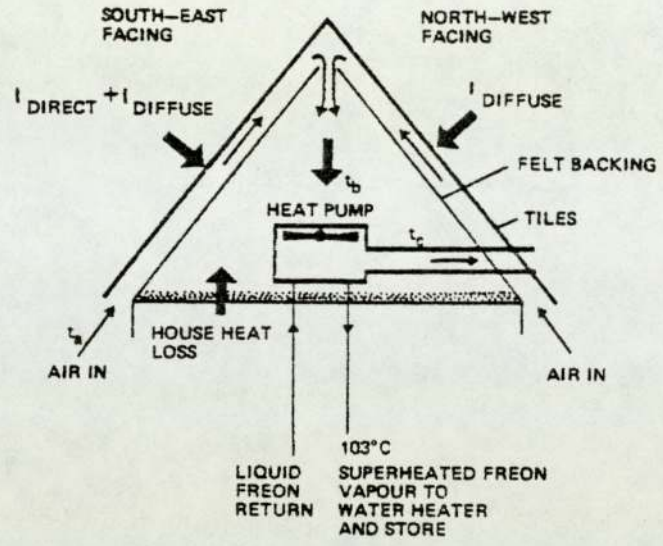

Figure 2.1 Cross-sectional view of the roof space.

The heat pump is a Lennox HP7 split unit, situated in the roof space (it could equally well be situated elsewhere and connected to the roof space by a duct). Air from outside the building at an external ambient temperature t_a is drawn, by the heat pump fan, through channels (on both sides of the roof) formed by the underside of the tiles and a backing of felt, which is attached to the lower side of the rafters. The air enters through an opening at the eaves and during its passage through the channels (which are about 0.1m wide) is raised in temperature by heat exchange with the tiles, which absorb both direct and diffuse solar radiation. A gap at the apex allows the heated air to enter the roof space, and it arrives at the evaporator of the heat pump at a temperature t_b. After crossing the evaporator coils, the air is expelled at a temperature t_c to the outdoor environment; generally $t_b > t_a > t_c$. The roof space is insulated from the rest of the dwelling with the equivalent of 0.15m of fibre glass wool. Any heat loss from the living space to the loft contributes to the value of

t_b and thus is partly, or fully, recycled. Figure 2.2 is a schematic diagram of the remainder of the system.

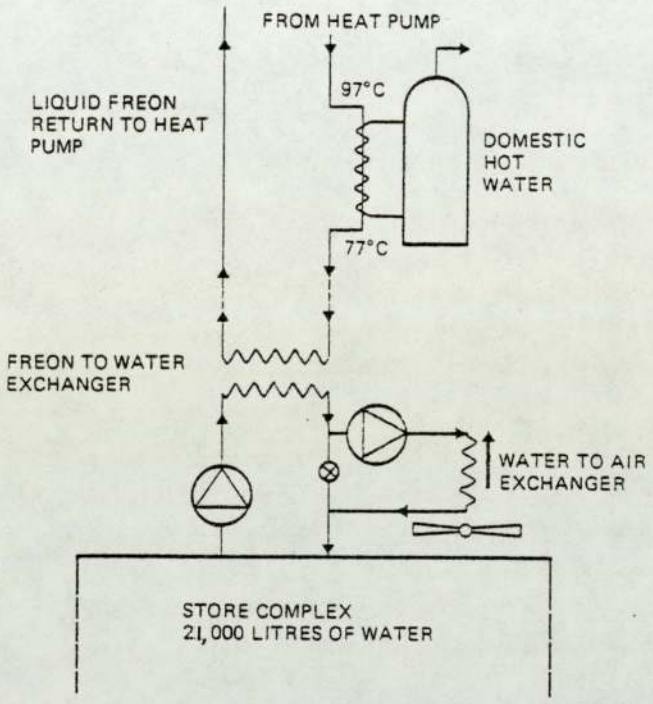

Figure 2.2 System for space and water heating, and storage.

After leaving the heat pump, the superheated refrigerant vapour ('R22') is cooled in a de-superheater to provide pre-heating for the domestic hot water (see Figure 1.3). The water is brought to its final usage temperature of 60°C by an electrical immersion heater. The condenser/store water heat exchanger is situated below the ground floor, and the refrigerant, condensing at a fixed temperature of 65°C, supplies heat to the store, either directly, or via the heat exchanger in the ducted warm air heating system. The store complex consists of approximately 21m^3 of water contained in three interconnected polypropylene bags recessed into the ground floor; it is therefore

contained within the building structure. The store water is designed to reach a temperature of 55°C. Figure 2.3 illustrates the whole system (the exchanger between the store and the warm air space heating system is shown separately for clarity. However, Figure 2.2 depicts the actual circuit). The system was designed and installed by Helix Multiprofessional Services of Reading, U.K.

The photographs at the end of this chapter further illustrate the test house installation. Photograph 2.1 is a general view of the house showing the South East facing front elevation. Photograph 2.2 is a close-up view of the gap at the eaves which allows the ingress of air to the roof space; the interlocking construction of the 'Delta' tiles is clearly visible. The heat pump, situated in the roof space, is shown in Photograph 2.3 with its safety grille removed to show the fan and, behind it, the evaporator. Photograph 2.4 shows one of the three polypropylene storage bags, below the ground floor, being filled with water; to the left is the recess for another bag. Each recess space is about 0.5m deep; the sides are lined with polystyrene whereas the base is covered with sand to a depth of 0.1m.

Charging of the store commences in October and the heat pump is normally operated only during daylight hours to maximise the heating mode coefficient of performance, COP(H). On occasions when the stored heat was depleted and the water temperature had fallen to about 25°C, the heat pump was operated throughout the night to aid store re-charge. The water from the condenser/store heat exchanger goes directly to the store, except when the thermostatically-controlled ducted warm air heating system demands heat; the water is then diverted via the air system heat exchanger. Any supplementary heating requirement

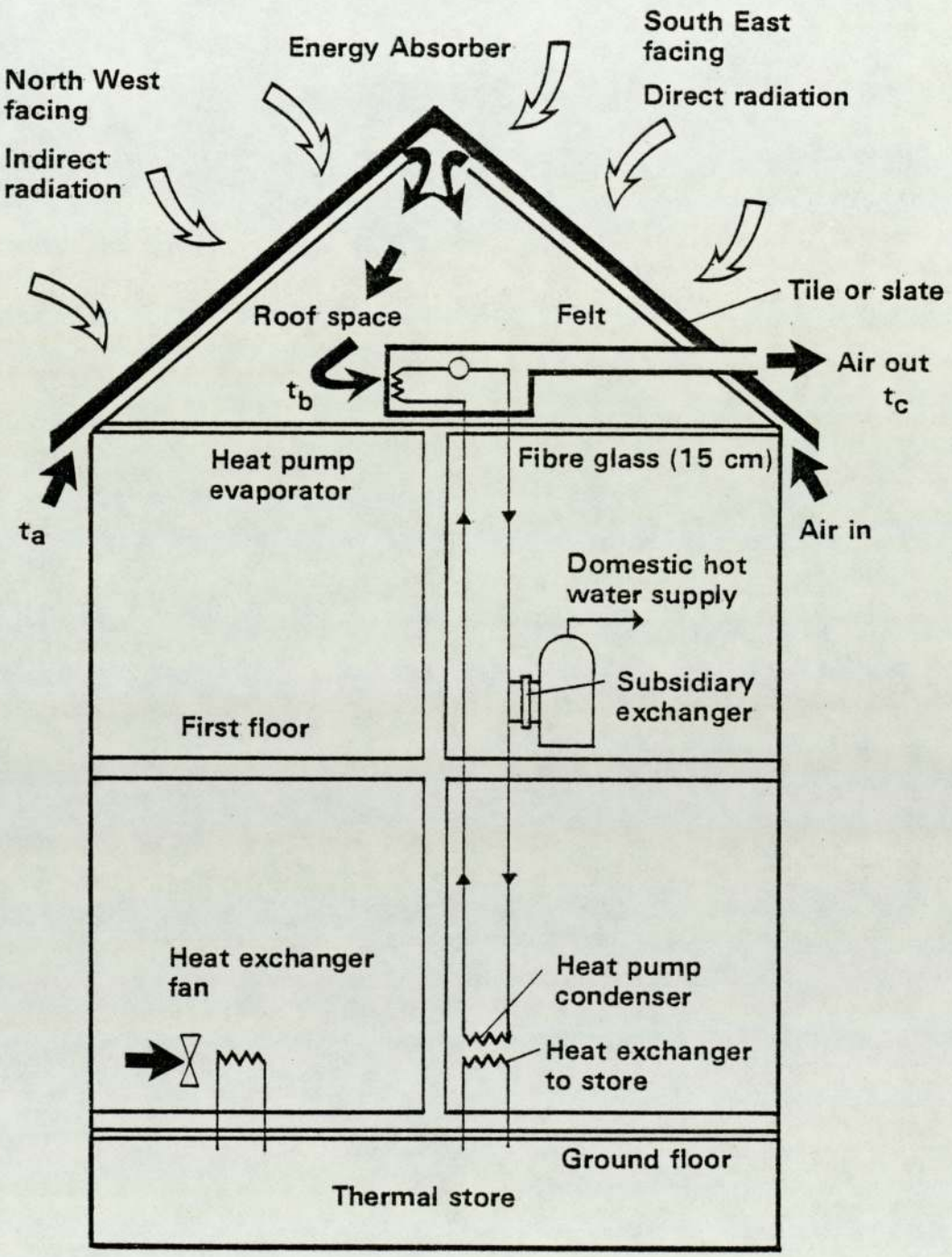

Figure 2.3 The complete space and water heating system.

is provided by portable electric resistance heaters. The system is switched off in April, at the end of the heating season.

2.2 Monitoring Equipment, Calibration and Deployment

2.2.1 Equipment and Calibration

The monitoring of the system was based upon measurements of temperatures (at appropriate positions), electricity and water consumptions, properties of the low grade heat source (air), and such other incidental values as were necessary. Solar radiation and weather data were provided by meteorological stations in the vicinity of the test site.

Surface and air (dry bulb) temperatures were measured using platinum resistance thin film sensors (Thermafilm 100 W 47) made by Matthey Electronics. Each was encased in a small radiation-shielded housing; the sensor for measuring the outdoor air dry bulb temperature (position 'a' in Figure 2.4) was additionally enclosed within a Stevenson screen.

The sensors were connected by four-core screened cables to a digital pyrometer (Newport, Type 267A) giving a temperature readout with a resolution of 0.1°C. Each sensor was connected in turn to the pyrometer by means of an electronic mercury-wetted contact switching system (designed by Almondbury Developments) with an input capability of up to thirty channels. Both the pyrometer and the switching system were incorporated in a single unit which was connected to a digital printer (Newport, Model 810); this gave a printed output of the temperature values on paper tape. Cable resistance compensation for lead lengths of up to 30 metres was effected electronically by means of an in-built circuit; calibration of the data acquisition system was

regularly checked against a standard 100 ohm precision resistance permanently connected to one channel. An in-built timer initiated a scan of the thirty channels once every hour, and also initiated the printout of the corresponding temperature values on the paper tape, this being periodically collected. This system resulted in an overall accuracy of about $\pm$ 0.15°C for individual temperature values; those sensors which were used to provide temperature differences were individually calibrated, leading to overall accuracies in temperature difference values of about $\pm$ 0.3 °C.

The relative humidity of the air was monitored at three locations - outdoors, and in the roof space at the entrance to and exit from the heat pump evaporator (corresponding to positions 'a', 'b' and 'c' in Figure 2.4). Three relative humidity probes (Lee Dickens, Model HP5) were used for this purpose. Their principle of operation was based upon the change in capacitance of a thin film, brought about by the moisture absorption properties of a special polymer used as the dielectric. The probes consisted of the capacitive thin film sensor and associated circuitry, and gave a voltage output proportional to the relative humidity of the environment in which they were placed. It was necessary to interface the output from the probes with the pyrometer and scanner unit described above in order to obtain values on an hourly basis. This was achieved by feeding the signal from each probe to its scanner input channel via separate potential divider networks. Each probe, when connected in the above manner to the pyrometer and scanner unit, was calibrated in the laboratory using a method of saturated salt solutions in containers to provide environments of constant relative humidity (Young, 1967). Five salts were used - magnesium chloride hexahydrate, sodium dichromate dihydrate, sodium chloride,

potassium chloride and potassium sulphate - providing reference points with relative humidity values (at 25°C) of 32.7%, 53.7%, 75.1%, 84.2% and 97.0% respectively. For each probe, a graph was produced of the pyrometer reading against relative humidity (corrected for temperature); to these graphs were fitted third degree polynomial expressions. These expressions were used in the analysis of the subsequent data printout, and values accurate to within about ± 3% relative humidity were obtained. Figure 2.4 illustrates the positions of some of the sensors for monitoring temperature and relative humidity.

The electrical consumptions of the heat pump compressor and fan, ancillary pumps and air blower, immersion heater, cooker and lights, and all mains supply outlets were measured with kilowatt-hour meters, the readings of which were recorded weekly by the occupants during the early monitoring period. Latterly, the consumption of the heat pump was monitored automatically by a Demand Profile Recorder, manufactured and installed by Normalair - Garrett Limited (N.G.L.). This recorded the average electrical demand over thirty-minute periods by the heat pump; the data was stored on cassette tape for translation by N.G.L.'s computer facilities, and printouts were subsequently dispatched to the author for analysis. This yielded the energy consumption of the heat pump (compressor and fan) on an hourly basis.

The remaining values recorded on site included the consumption of hot water, measured by a volume flow meter plumbed into the supply, and the speed of the air flow across the heat pump evaporator, measured periodically with a hot-wire anemometer. Values of atmospheric pressure, total and diffuse solar radiation, windspeed and direction, and other weather data were supplied from nearby weather stations.

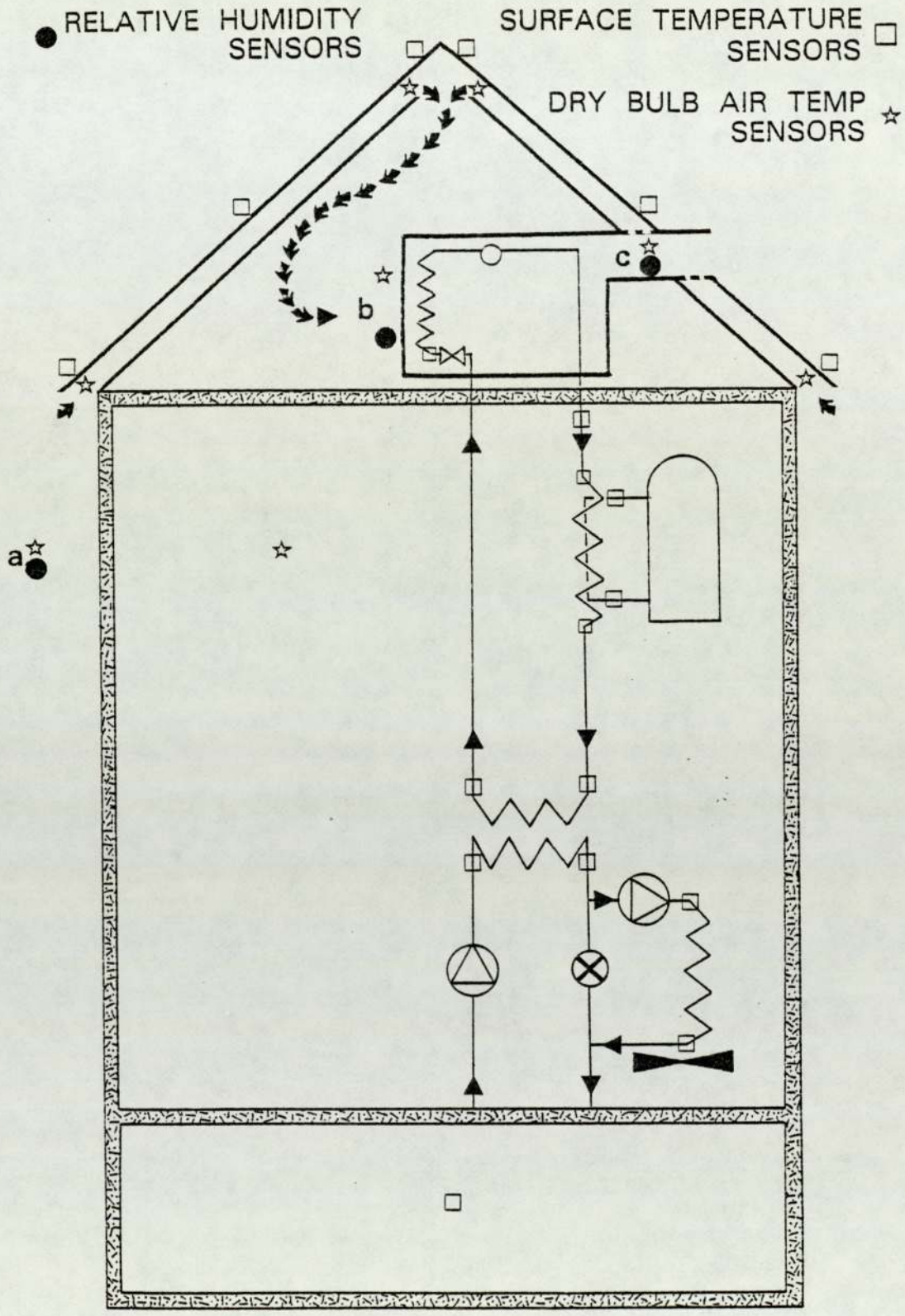

Figure 2.4 Positions of some of the monitoring sensors at the test house.

2.2.2 Deployment

Research commenced at the beginning of the 1977/78 heating season; in the time available, it was possible to install at the test house only the pyrometer/scanner unit with thirty temperature sensors, the water consumption meter and the kilowatt-hour meters for the monitoring of performance over that season. The hourly values of outdoor relative humidity (at position 'a'), and atmospheric pressure were provided by Boscombe Down weather station, 54 km W.S.W. of the site. Other weather data was supplied by the Meteorological Office at Bracknell, 26 km to the N.E. At the same time, equipment was set up for the monitoring of a similar heating installation in a second test house (with a slate roof) in London. At the end of the season, an almost full set of data had been obtained for the Basingstoke installation, but due to technical difficulties, this was not the case for the installation in London, and the monitoring equipment was subsequently removed from the latter for deployment elsewhere.

Failure of the Basingstoke monitoring equipment occurred during the 1978/79 heating season, preventing the recording of any reliable data for that period. The data acquisition system was then completely serviced and supplementary equipment prepared and installed for the 1979/80 heating season. This consisted of an additional pyrometer/scanner unit and sensors, the relative humidity sensors for positions 'a', 'b' and 'c', and the Demand Profile Recorder (installed by N.G.L.). The purpose of the additional equipment was to determine the in situ operating characteristics of the air-source heat pump over a heating season. However, the development of faults in different sections of the monitoring system and also in the heat pump itself resulted in

there being only 26 days between January and April 1980 for which full sets of data were simultaneously available; the heat pump performance was based on these. In addition, continual breakdowns of the outdoor relative humidity sensor (position 'a') made necessary the use of data from Boscombe Down weather station for this value once again. However, for the few days on which the on-site sensor functioned, the values of outdoor relative humidity which it provided agreed very closely with those from the weather station, so it was assumed reasonable to take the data from the weather station as being appropriate for the site in other considerations.

The analysis of the results of this research, therefore, took the form of obtaining in situ heat pump characteristics from the 1979/80 heating season data (presented in Chapter 5) and utilising those characteristics relating to air moisture content in the analysis of the heating system performance over the 1977/78 heating season (presented in Chapter 6). These chapters are preceded, however, by theoretical and laboratory experimental studies into the efficiency of conventional roofing materials when used as air-heating solar collectors.

Photograph 2.1: The South East facing front elevation of the test house.

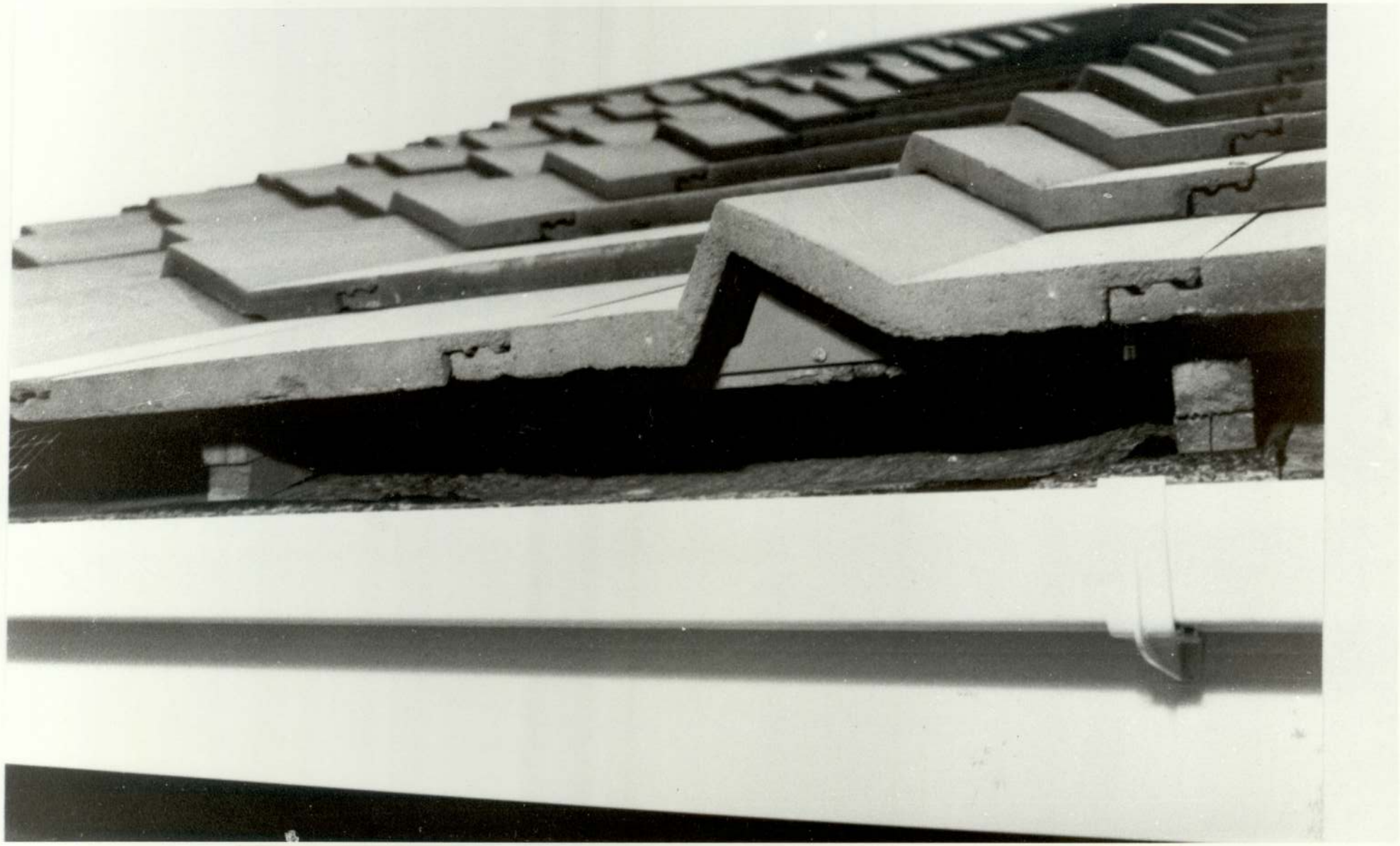

Photograph 2.2: The gap at the eaves which allows air ingress to the roof space.

Photograph 2.3: The heat pump in the roof space, its safety grille removed.

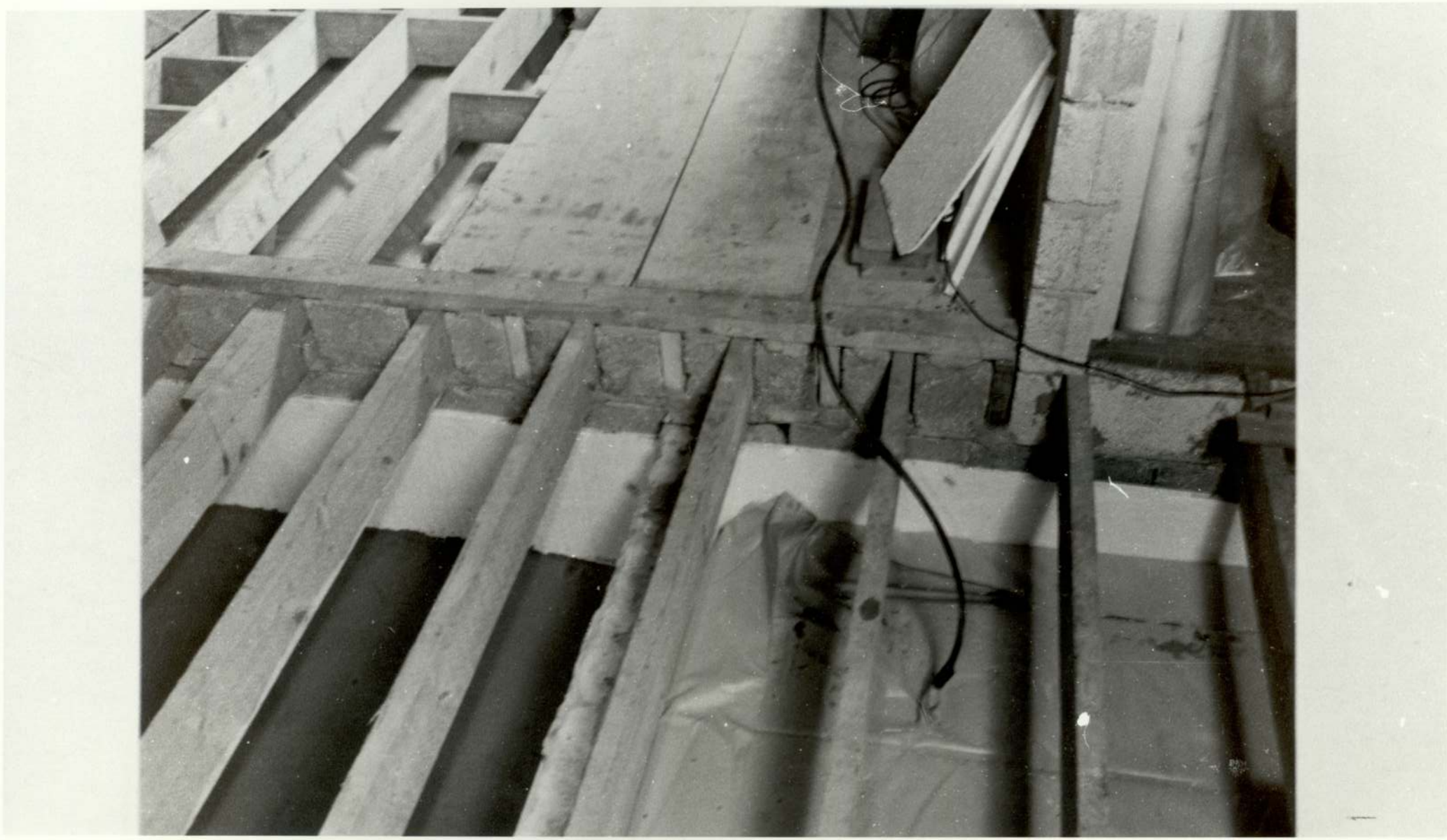

Photograph 2.4: A polypropylene storage bag being filled with water.

CHAPTER 3

THE PERFORMANCE OF CONVENTIONAL ROOFING MATERIALS AS ENERGY COLLECTORS

3.1 Introduction

The objective of this part of the work was to investigate the feasibility of utilising the existing roof of a house as a collector of solar energy. This would not only be of particular relevance for the retrofitting of some form of solar assisted heating system to the existing housing stock (removing the need and the cost of special panel installation), but could also be of benefit in the design of new buildings where the addition of fixtures to the roof structure or the use of certain materials are precluded. Glass, for example, may not be acceptable for certain locations.

A theoretical model is presented to describe the behaviour of a conventional roof as an energy collector within the context of the procedures and analysis currently employed in the testing of solar collectors. Laboratory testing was carried out to study the applicability of the model to both tiled and metal roofs, and to investigate, under controlled conditions, special properties of conventional roofs when used as air-heating energy collectors.

3.2 Collector Testing

3.2.1 Theoretical Background

There are numerous designs of solar collectors (see, for example,

McVeigh, 1977). A typical configuration for a flat plate collector is shown in Figure 3.1. Let the useful energy collected be q_u and let IA be the total incident energy, both per unit time for the collector

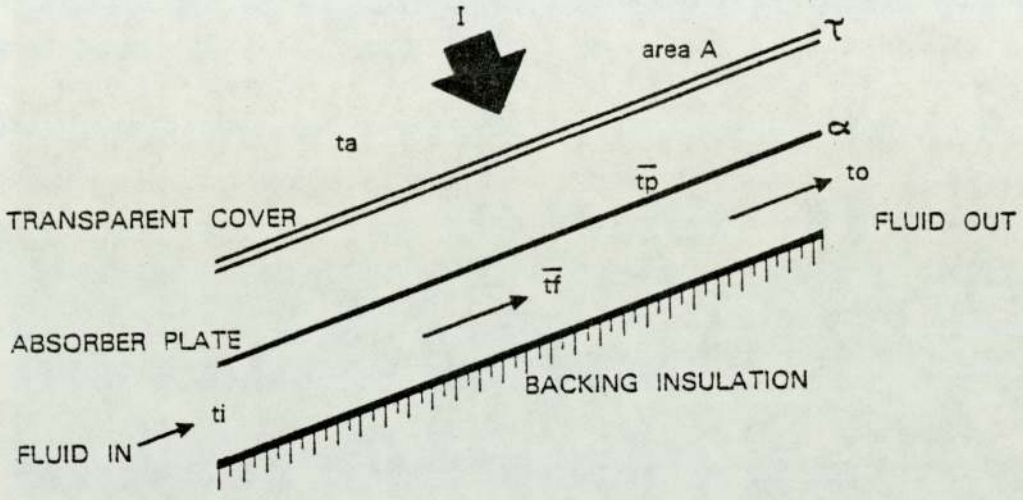

Figure 3.1 Section through a typical flat plate collector, with heat transfer fluid flowing behind the absorber plate.

area, A, considered; I is the incident radiation, τ and α the cover transmittance and plate absorptance respectively, $\bar{t}_p$ the average absorber plate temperature, $\bar{t}_f$, t_o and t_i the average heat transfer fluid temperature, fluid outlet and fluid inlet temperatures respectively, and t_a the surrounding ambient temperature.

The performance of the collector can be described by a consideration of the balance between the absorbed energy, the useful energy

removed and the energy losses. An analysis based on this approach was first carried out by Hottel and Woertz (1942). The steady state performance may then be expressed:

$$\eta = q_u/IA = (\tau\alpha)_e - U_L (\bar{t}_p - t_a)/I \qquad 3.1$$

where η, the efficiency, is defined as the ratio of the useful energy collected to the total energy incident; $(\tau\alpha)_e$ is the effective transmittance - absorptance product (Duffie and Beckman, 1974), and U_L the overall heat loss coefficient;

$$q_u = \dot{m} C_p (t_o - t_i) \qquad 3.2$$

where $\dot{m}$ and C_p are the mass flow rate for the collector area, A, considered, and specific heat of the transfer fluid respectively. Two additional factors have been introduced by Bliss (1959). These are:

the plate efficiency factor, F' = $\frac{\text{useful energy collection rate}}{\text{useful energy collection rate if the plate were at a temperature of } t_f}$

and the heat removal efficiency factor, F_R = $\frac{\text{useful energy collection rate}}{\text{useful energy collection rate if the plate were at a temperature of } t_i}$

These factors enable the steady state performance equation to be written:

$$\eta = F' (\tau\alpha)_e - F' U_L (\bar{t}_f - t_a)/I \qquad 3.3$$

or $$\eta = F_R (\tau\alpha)_e - F_R U_L (t_i - t_a)/I \qquad 3.4$$

The above forms, of what has now come to be known as the Hottel-Whillier-Bliss equation, are those most frequently used in collector testing, as it is usually more convenient to measure $\bar{t}_f$ or t_i than it is to measure $\bar{t}_p$; $(\tau\alpha)_e$, U_L and the factors F' and F_R are generally taken as constants (within limited operating conditions), and characterise the performance of a given collector.

3.2.2 Application to a Tiled Roof

A configuration of tiles on laths and a backing of felt with air (as a heat transfer fluid) flowing in the tile/felt duct can act as an air-heating device. Heat transfer analyses for air-heating collectors have been carried out by numerous authors, including Bliss (1959), Whillier (1964), Bansal and Kaushik (1980) and Parker (1981). Duffie and Beckman (1974) give expressions for F' and U_L for air-heating collectors with flow under the absorber plate, but the expressions are based on a single absorber plate temperature. The same 'thin plate' simplification is utilised in the derivations given by Bliss (1959), Whillier (1964), Bansal and Kaushik (1980) and Parker (1981). However, for the present analysis, it would be better to assume a tiled roof to be a thick, poorly conducting structure; one therefore has to assign finite values of thickness and thermal conductivity.

Whillier (1964) has assumed rear heat losses from air collectors to be zero, or that rear losses, when considered, are added to the front losses (Duffie and Beckman, 1974; Whillier, 1964). Bansal and Kaushik (1980) and Parker (1981) consider front and rear losses as occurring to the same uniform ambient temperature. When a section

of tiled roof is considered as an integral part of a roof and loft structure, however, the assumption of a uniform temperature surrounding the collector is not necessarily valid, since the loft space temperature can differ from that outside. This may not greatly affect a purpose-designed collector with a high level of backing insulation, but may have a significant effect in the case of felt alone. However, any rear heat losses in the case of the tiled roof collector are not actually 'losses' if the roof is used as a pre-heat system for an air source heat pump (as in the system monitored); this is because the heat eventually arrives at the heat pump, when considering the system as a whole. They must be regarded as losses in the following analysis in order to evaluate the performance of a roof as a solar collector in relation to the work of others. The analysis adopted is similar in approach to ones carried out by Duffie and Beckman (1980) and Parker (1981) for solar air heaters.

3.2.3 Heat Transfer Analysis for a Tiled Roof

Consider a section through a tiled roof being heated by radiation, Figure 3.2. The symbols used in the analysis are now defined:

I is the incident radiation, Wm^{-2};

τ is the transmittance of the cover plate (when installed), expressed as a fraction;

α is the absorptivity of the tiles, expressed as a fraction;

$(\tau\alpha)_e$ is the effective transmittance - absorptance product (Duffie and Beckman, 1974). Though, in this case, there are no covers, and $\tau = 1$, the notation $(\tau\alpha)_e$ will be retained.

The h - values which follow are the heat transfer coefficients (for radiation or convection), in $Wm^{-2}\ °C^{-1}$:

h_1 is for wind-induced convection from the upper tile surface to the ambient air at the front;

h_{r1} is for radiation exchange between the upper tile surface and the equivalent sky temperature, T_s;

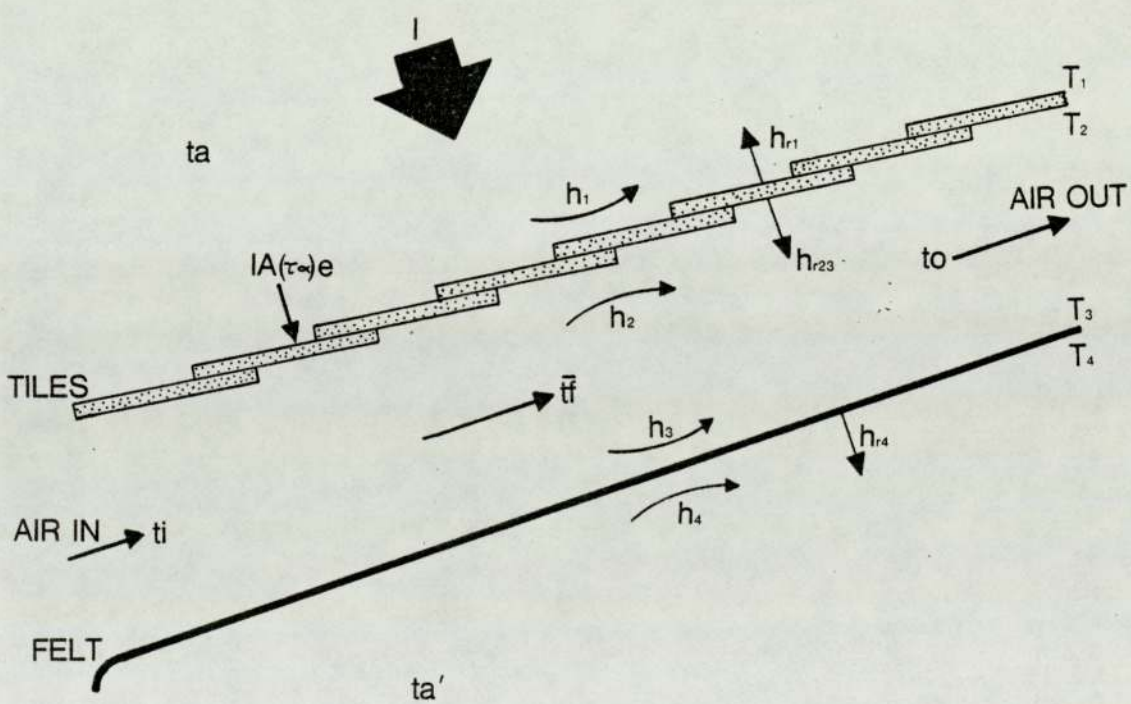

Figure 3.2 Section through a tiled roof, showing the duct formed by the roof tiles and a backing of roof felt.

h_2 is for convection from the lower tile surface to the airstream in the duct;

h_{r23} is for the net radiation exchange between the lower tile surface and upper felt surface forming the duct;

h_3 is for convection from the upper felt surface to the airstream;

h_4 is for convection from the lower felt surface to the ambient air at the rear;

h_{r4} is for radiation exchange between the lower felt surface and the environment at the rear.

The remaining symbols are defined as follows:

k_1, k_2 are the thermal conductivities of tile and felt respectively, $Wm^{-1}\,°C^{-1}$;

d_1, d_2 are the thicknesses of the tiles and felt respectively, m; (note that the k and d values can be adjusted to account for any air gaps between tiles, or for different materials);

U_t is the overall heat loss coefficient from the top surface of the roof, combining h_1 and h_{r1} - see later, $Wm^{-2}\,°C^{-1}$;

U_b is the overall heat loss coefficient from the back of the roof channel, combining k_2, d_2, h_4 and h_{r4} (and side losses in a heating simulator test section) - see later, $Wm^{-2}\,°C^{-1}$.

T_1, T_2 are the upper and lower tile surface temperatures respectively, °C;

T_3, T_4 are the upper and lower felt surface temperatures respectively, °C;

t_o, t_i are the fluid (air) outlet and inlet temperatures respectively, °C;

$\bar{t}_f$ is the average fluid temperature in the duct, °C;

t_a is the ambient air temperature at the front, °C;

t_a' is the ambient air temperature at the rear, °C;

$\dot{m}$ is the total mass flow rate of air in the duct for the tile section area, A, considered, kg s^{-1};

C_p is the specific heat capacity of air at constant pressure, J kg^{-1} $°C^{-1}$;

A is the area of tile section considered, m^2.

Q_u is the total rate of useful energy collection from the section of roof considered, W.

One may write the equation:

$$Q_u = \dot{m}C_p (t_o - t_i) \qquad 3.5$$

Initially, in order to simplify the analysis, the tiles are regarded as a flat plate of uniform thickness with no leakage of air to the airstream, the mass flow rate of air in the duct being only that which is drawn in at the inlet. No separate account is taken of the effect on heat transfer of the laths on which the tiles rest, a single overall convection heat transfer coefficient, h_2, being adopted. Heat losses at the sides (accounted for later) are neglected and thermal conductivity along the length of the tile plate is also neglected (Bansal and Kaushik, 1980), the analysis being restricted to one dimension only, and steady state conditions throughout. (The 'stepped' effect of a tiled roof, the effects of small air spaces between the overlapping tiles and the effects of laths and side heat losses are introduced later in the estimation of the heat transfer coefficients). At this stage, the analysis is restricted to that of obtaining a basic, general purpose, no-leakage model, incorporating the effect of an absorber plate with finite thickness and thermal conductivity.

An overall energy balance gives:

$$IA(\tau\alpha)_e = Q_u + U_tA\ (T_1 - t_a) + U_bA\ (T_3 - t_a') \qquad 3.6$$

An energy balance on the tiles gives:

$$IA(\tau\alpha)_e = U_tA\ (T_1 - t_a) + h_2A\ (T_2 - \bar{t}_f) + h_{r23}A\ (T_2 - T_3) \qquad 3.7$$

$$(k_1/d_1)\ A\ (T_1 - T_2) = h_2A\ (T_2 - \bar{t}_f) + h_{r23}A\ (T_2 - T_3) \qquad 3.8$$

An energy balance on the felt gives:

$$h_{r23}A\ (T_2 - T_3) = h_3A\ (T_3 - \bar{t}_f) + U_bA\ (T_3 - t_a') \qquad 3.9$$

An energy balance on the fluid gives:

$$Q_u = h_2A\ (T_2 - \bar{t}_f) + h_3A\ (T_3 - \bar{t}_f) \qquad 3.10$$

Eliminating T_2 between equations 3.9 and 3.10, substituting in 3.9 to obtain an expression for T_3 and then substituting for T_3 in the expression $U_bA\ (T_3 - t_a')$ yields:

$$U_bA\ (T_3 - t_a') = \left[\frac{U_bh_{r23}}{h_2(B+U_b)}\right] Q_u + \left[\frac{BU_b}{(B+U_b)}\right] A\ (\bar{t}_f - t_a') \qquad 3.11$$

where $B = [h_{r23} + (h_3h_{r23}/h_2) + h_3]$ 3.12

Eliminating T_2 between 3.7 and 3.8, substituting for T_3 to obtain an expression for T_1, and then substituting for T_1 in the expression $U_tA\ (T_1 - t_a)$ yields, after summing terms in $(\bar{t}_f - t_a)$:

$$U_tA\ (T_1 - t_a) = \left[\frac{U_tCd_1}{D}\right] IA(\tau\alpha)_e + \left[\frac{U_th_{r23}^2k_1}{h_2D(B+U_b)}\right] Q_u$$

$$+\left[\frac{U_tk_1\ (h_{r23}\ B + h_2\ B + h_2U_b)}{D(B+U_b)}\right] A\ (\bar{t}_f - t_a) + \left[\frac{U_tU_bk_1h_{r23}}{D(B+U_b)}\right] A\ (t_a' - t_a) \qquad 3.13$$

where $C = [h_2+h_{r23}+(k_1/d_1)]$ 3.14

and $D = [(h_2+h_{r23})(k_1+d_1U_t)+k_1U_t]$ 3.15

One may substitute equations 3.11 and 3.13 into equation 3.6, gather terms in $IA(\tau\alpha)_e$ and Q_u, and re-arrange:

$$Q_u = [k_1h_2\ (B + U_b)(h_2 + h_{r23})/E]\ IA(\tau\alpha)_e$$
$$- [U_tk_1h_2\ (h_{r23}\ B + h_2\ B + h_2U_b)/E]\ A(\bar{t}_f - t_a)$$
$$- [U_bh_2\ BD/E]\ A(\bar{t}_f - t_a')$$
$$- [U_tU_bk_1h_{r23}h_2/E]\ A(t_a' - t_a) \qquad 3.16$$

where $E = [h_2\ D\ (B + U_b) + h_{r23}\ (U_tk_1h_{r23} + U_bD)]$ 3.17

Equation 3.16 gives the useful energy collected for different ambient air temperatures at the front and rear of the roof collector, i.e. when $t_a \neq t_a'$. In many derivations, and for collector testing, the air surrounding a collector is taken as being at a uniform temperature, front and rear, i.e. $t_a = t_a'$. Using this equality, equation 3.16 can be reduced to:

$$Q_u = [k_1h_2\ (B + U_b)(h_2 + h_{r23})/E]\ IA(\tau\alpha)_e$$
$$- [[U_tk_1h_2\ (h_{r23}\ B + h_2\ B + h_2U_b) + U_bh_2BD]/E]\ A(\bar{t}_f - t_a) \qquad 3.18$$

Dividing both sides of equation 3.18 by IA (the total energy incident on the roof collector of area A) gives the efficiency, η:

$$\eta = Q_u/IA = [k_1h_2\ (B + U_b)(h_2 + h_{r23})/E]\ (\tau\alpha)_e$$
$$- [[U_tk_1h_2(hr_{23}\ B + h_2\ B + h_2U_b) + U_bh_2BD]/E][(\bar{t}_f - t_a)/I] \qquad 3.19$$

Equation 3.19 is in the form of equation 3.3, the Hottel-Whillier-Bliss equation:

$$\eta = F'(\tau\alpha)_e - F'U_L\ (\bar{t}_f - t_a)/I \qquad 3.3$$

Thus, equation 3.3 applies only when $t_a = t_a'$, i.e. it is a special condition. The more general case is that of $t_a \neq t_a'$, for which equation 3.16 applies.

From equation 3.19 (substituting E from 3.17), expressions for F' and U_L may be derived:

$$F' = \frac{[k_1 h_2 (B + U_b)(h_2 + h_{r23})]}{[h_2 D (B + U_b) + h_{r23}(U_t k_1 h_{r23} + U_b D)]} \qquad 3.20$$

$$U_L = \frac{[U_t k_1 h_2 (h_{r23} B + h_2 B + h_2 U_b) + U_b h_2 BD]}{[k_1 h_2 (B + U_b)(h_2 + h_{r23})]} \qquad 3.21$$

Where B and D are given by equations 3.12 and 3.15 respectively.

The overall top heat loss coefficient U_t is given by:

$$U_t = h_1 + h_{r1}[(T_1 - T_s)/(T_1 - t_a)] \qquad 3.22$$

where the radiative heat loss, though taking place to the sky at equivalent temperature T_s is, for convenience, referred to the ambient air temperature t_a (Duffie and Beckman, 1980). Note that if it is assumed that $T_s = t_a$, equation 3.22 reduces to:

$$U_t = h_1 + h_{r1} \qquad 3.23$$

The overall back heat loss coefficient U_b is given by:

$$[1/U_b] = [d_2/k_2] + [1/(h_4 + h_{r4})] \qquad 3.24$$

$$\text{or } U_b = [k_2(h_4 + h_{r4})]/[d_2(h_4 + h_{r4}) + k_2] \qquad 3.25$$

This assumes that the equivalent temperature for radiative exchange at the rear of the roof is the same as the ambient air temperature at the rear.

An expression for F_R, given by Bliss (1959), Whillier (1964) and by Duffie and Beckman (1974), and of general application to solar collectors, is:

$$F_R = (\dot{m}C_p/AU_L)[1-\exp(-F'AU_L/\dot{m}C_p)] \qquad 3.26$$

Expressions 3.20, 3.21 and 3.26 allow calculations to be made of F', U_L and F_R from values of the heat transfer coefficients appropriate to the type of collector and its environment under consideration. They may be compared with values of F', U_L and F_R obtained by experiment, and shown graphically (Figure 3.3, and Chapter 4).

The heat transfer analysis has shown that, when the ambient temperature at the front and rear of a tiled roof structure behaving as an air-heating solar collector are the same, a form of the Hottel-Whillier-Bliss equation is valid to describe this behaviour. General expressions for F' and U_L, appropriate to the condition $t_a = t_a'$ and for a collector having an absorber plate of finite thickness and thermal conductivity, have been derived. Values for these, together with F_R, may be calculated by insertion of the heat transfer coefficients, thermal conductivities and thicknesses appropriate to the type of collector or roof structure, and its environment. The calculated values may be compared with those obtained from experimental data.

3.2.4 Estimation of the Heat Transfer Coefficients

Theoretical analyses leading to expressions for the heat transfer coefficients in several simplified situations can be found in many

texts on heat transfer, for example, Kays, (1966); Eckert and Drake, (1972); Welty, (1978); Incropera and De Witt, (1981). In many (more complex) situations, however, it is necessary to rely on expressions obtained from experimental data. In all cases, appropriate relationships must be selected. For convective heat transfer, the choice of equation is dependent upon whether the convection is free or forced, laminar or turbulent, whether the flow is internal or over an external surface, and is dependent on the geometry of the surface. Radiative heat transfer is dependent on geometries and emissivities of surfaces. The prevailing conditions must first be ascertained.

The analytical model of section 3.2.3 can immediately be tested for the situation of the test house roof simply by inserting values for the heat transfer coefficients. These values are obtained from suitable expressions selected from the literature. Some of the symbols involved are now defined:

h is the heat transfer coefficient, $Wm^{-2}\ °C^{-1}$;

$\dot{m}$ is the mass flow-rate of the heat transfer fluid, $kg\ s^{-1}$;

v, v_1 are the velocities of the heat transfer fluid and wind respectively, ms^{-1};

g is the acceleration due to gravity, ms^{-2};

A' is the cross-sectional area of the duct, m^2;

P is the perimeter of the duct, m;

D_e is the equivalent diameter of a non-circular duct, m;

L is the characteristic length involved in a heat transfer problem, m;

ε is the emissivity of a surface, fraction of unity;

σ is the Stefan-Boltzmann constant, $Wm^{-2}\ K^{-4}$.

For the fluid properties:

ρ is the density, kg m^{-3};

μ is the dynamic viscosity, kg m^{-1} s^{-1};

ν is the kinematic viscosity, m^2 s^{-1};

k is the thermal conductivity, Wm^{-1} K^{-1};

Cp is the specific heat capacity at constant pressure, J kg^{-1} K^{-1};

β' is the volumetric coefficient of expansion, K^{-1};

α is the thermal diffusivity, m^2 s^{-1}.

For the dimensionless groups:

Re is the Reynolds number;

Nu is the Nusselt number;

Pr is the Prandtl number;

Gr is the Grashof number;

Ra is the Rayleigh number.

Some of the above are related as follows:

$$\dot{m} = A'v\rho \qquad 3.27$$

which is known as the continuity equation.

$$D_e = 4A'/P \qquad 3.28$$

$$Re = vL/\nu \qquad 3.29$$

$$Nu = hL/k \qquad 3.30$$

In the above two expressions, L may be replaced by D_e if internal flow is under consideration; for external flow, L is the plate length in the flow direction.

$$Pr = \nu / \alpha \qquad 3.31$$

$$Gr = g\beta' L^3 \Delta T / \nu^2 \qquad 3.32$$

where ΔT is the driving temperature difference.

$$Ra = g\beta' L^3 \Delta T / \nu\alpha \qquad 3.33$$

$$\text{Therefore, } Ra = GrPr \qquad 3.34$$

$$\nu = \mu/\rho \qquad 3.35$$

$$\text{and } \alpha = k/\rho Cp \qquad 3.36$$

For the situation of the tiled roof at the test house, it is now necessary to select appropriate expressions to determine the heat transfer coefficients.

The linearized radiation heat transfer coefficients are given by (Duffie and Beckman, 1980):

$$h_{r1} = \varepsilon_{tile}\sigma \quad (T_1^2+T_s^2)(T_1+T_s) \qquad 3.37$$

for radiation from the tiled surface (temperature T_1) to the sky (temperature T_s) with a view factor of unity. Similarly, for radiation from the rear of the felt backing to the roof space, where surface temperatures are assumed equal to t_a':

$$h_{r4} = \varepsilon_{felt}\sigma \quad (T_4^2 + t_a'^2)(T_4 + t_a') \qquad 3.38$$

For radiative exchange between two infinite parallel flat plates (tiles and felt):

$$h_{r23} = \sigma (T_2^2 + T_3^2)(T_2 + T_3)/[(1/\varepsilon_{tile}) + (1/\varepsilon_{felt})-1] \qquad 3.39$$

At the test site, the mean wind speed for the area was taken as

$4ms^{-1}$ (Rayment, 1976). At this speed, natural convection from the tile surface need not be considered, and an expression given by Duffie and Beckman (1980), for the wind-induced heat transfer coefficient for roof mounted collectors may be used:

$$h_1 = 8.6\ v_1^{0.6}/L'^{0.4} \qquad 3.40$$

where v_1 is the wind velocity in metres per second, and L' is the cube root of the house volume in metres.

At the rear surface of the felt in the loft, there is little, if any, forced movement of air over much of the surface, and free convection must be considered for the evaluation of h_4. Holman (1976) gives simplified expressions for free convection in air at atmospheric pressure. Evaluation of the product Gr Pr at the film temperature, $(T_4 + t_a')/2$, for the averages of these temperatures in the 1977-78 heating season results in a value for Gr $Pr > 10^9$. This indicates turbulent free convection, and the expression for a downward-facing heated flat plate is:

$$h_4 = 0.61\ (\Delta T/L^2)^{0.2} \qquad 3.41$$

where ΔT is the temperature difference (T_4-t_a'), and L is the mean of the length and width of the felt backing.

Each side of the test house roof is of length 4.52 m from eaves to ridge, and width 11.925 m; the tile/felt gap averages 0.1 m in width. Thus, h_2 and h_3 may be evaluated for forced convection in a rectangular duct of equivalent diameter $D_e \simeq 0.192$ m (calculated after accounting for the effect of rafters). The total mass flow rate of air for each side of the roof is 0.45 kg s^{-1}, and from

equation 3.27 a flow velocity, v, in the duct of 0.31 ms^{-1} is obtained. This leads to a value of Re of 4273 (fluid properties have been evaluated at the average fluid temperature in the duct). For internal flow, the critical Reynolds number is 2100, so the flow, in this case, is turbulent. Hatton and Quarmby (1963) have presented solutions for the case of turbulent flow between parallel plates with uniform heat flux on one side. They show their results to be of the same order as those obtained for round tubes using the Dittus Boelter equation:

$$Nu_{fd} = 0.024\ Re^{0.8}\ Pr^{0.4} \qquad 3.42$$

where Nu_{fd} is the fully developed Nusselt number. For values of Re appropriate to the present work, the values for Nu_{fd} were estimated by interpolating the results of Hatton and Quarmby (1963). These Nu_{fd} values were in good agreement with those calculated using equation 3.42. This expression was therefore adopted for the assessment, with acceptable accuracy, of heat transfer coefficients for internal flow, h_2 and h_3, in this analysis. The effect of the entrance region, where heat transfer coefficients are higher than the fully developed values, is accounted for from data supplied by Kays (1966). For the roof length, 4.52 m, and the calculated value of D_e:

$$Nu_m \simeq 1.05\ Nu_{fd} \qquad 3.43$$

where Nu_m is the mean Nusselt number with respect to the roof length. Thus, values for h_2 and h_3 may be estimated.

A structure of tiles on laths is a complex one for heat transfer purposes, and in an attempt to account for these complexities, further refinements were introduced to the expressions given above.

The laths were treated as roughness elements, so that the situation became one of turbulent flow in the entrance region of a rough rectangular duct. The effect of roughness is to increase the h-value, and Kays (1966) suggests an expression for air, $P_r = 0.7$, modified to:

$$Nu = Nu_{smooth} \, (f/f_{smooth})^{0.5} \qquad 3.44$$

where f is the friction coefficient. The friction coefficient can be found from a Moody chart (Moody, 1944), which plots f as a function of Re with e/D as a parameter; e is the absolute average roughness of a surface, and D is the diameter of a round pipe. In this case, D_e was substituted for D, and for the lath heights at the test house (averaged with the relatively smooth felt surface) it was estimated from equation 3.44 that:

$$Nu \simeq 1.476 \, Nu_{smooth} \qquad 3.45$$

Here, Nu_{smooth} is the value for Nu_m found from equation 3.43.

In this way, both the effects of the entrance region and roughness are included to produce a final Nusselt number $Nu = 1.55 \, Nu_{fd}$. This value is in reasonable agreement with the effects predicted by Cur and Sparrow (1979), who measured heat transfer coefficients along a periodically interrupted surface within a rectangular duct. Their results indicate that for fully developed turbulent flow, the h-values can be up to twice those for a continuous-walled duct, for $Re > 10^4$. Augmentation values for $Re < 10^4$ could not be given, but the enhancement effect is still valid.

No data could be found in the literature for heat transfer coefficients for stepped surfaces such as a tiled roof. It was therefore decided

to define an area enhancement factor (such as that given by Hollands and Shewen [1979] for a triangular duct collector) to account for the increased area due to the 'steps'. Thus, for a tiled roof, the enhancement factor is [1 + (a/A)], where 'A' is the normal flat area, and 'a' is the total step area, i.e. step height x step width x number of steps. For the test house roof, this factor was calculated to be 1.043, and acts as a multiplier to h_1 and h_2 (the effect on h_{r1} and h_{r23} was neglected).

The overlapping construction of a tiled roof results in gaps when one row of tiles is laid above the other (these give rise to wind leakage which is discussed in Chapter 4). The effect of these air layers is to impede heat transfer through the tile absorber 'plate' and effectively reduce the thermal conductivity. Treating the gaps as inclined still-air layers, the following expression for air (Duffie and Beckman, 1980) was used:

$$Nu = 1 + 1.44\,[1-(1708/Ra\cos\beta)]^{+}[1-[(\sin 1.8\beta)^{1.6}\,1708/Ra\cos\beta]] + [(Ra\cos\beta/5830)^{1/3}-1]^{+} \qquad 3.46$$

where β is the angle of inclination to the horizontal, and the + exponent means that only positive values of the terms in square brackets to which the exponent refers should be used (if negative, use zero). This expression is strictly valid for the lower plate being the hotter. However, for $\beta = 25°$ and a plate spacing taken to be about 0.001 m, the value for Nu was unity, indicating pure conduction. This led to an h-value for the air layer between tiles of about 25 - 30 $Wm^{-2}\,°C^{-1}$, and including estimates of radiation exchange between tile layers, an overall effective thermal conductivity of 0.69 $Wm^{-1}\,K^{-1}$ was calculated. This may be compared

with 0.8 Wm^{-1} K^{-1} for tile alone. An overall 'absorber plate' thickness of 0.027 m was estimated. For the Delta tile roof, these became the values for k_1 and d_1 for insertion into the model.

The above represents the theoretical basis for the estimates of heat transfer coefficients in the case of a tiled roof. As a result of the complex construction, several approximations and assumptions were necessary. The equations are used to estimate values for insertion in the model.

3.2.5 Application to the Test House Roof

From results for the 1977-78 heating season (Chapter 6), the average outdoor ambient air temperature t_a was found to be 7°C. The exit temperature of air at the roof ridge was measured to be 8.4°C (the average of the South East and North West facing contributions). Taking the air and surface temperatures in the loft to be at the same value, that of t_a' = 8.4°C, and taking values for T_1, T_2, T_3 and T_4 of 9.5°C, 9.0°C, 8.8°C and 8.6°C respectively, heat transfer coefficients were estimated from the expressions of the previous section. Values for k_2 of 0.17 Wm^{-1} K^{-1} and for d_2 of 0.0016 m were taken, and the average fluid temperature of the tile/felt airstream was taken as 7.7°C. Estimation of the sky temperature, T_s, cannot be exact. Duffie and Beckman (1974) have reported the expression:

$$T_s = t_a - 6 \qquad 3.47$$

and also the expression (Duffie and Beckman, 1980):

$$T_s = 0.0552\ t_a^{1.5} \qquad 3.48$$

for T_s, t_a in Kelvins. Using these equations, and for t_a = 7°C, values for T_s of 1°C and -14.4°C are obtained. An average value for T_s of -7°C was therefore adopted. In fact, T_s is unlikely to be as low as this because both expressions are for clear skies and no account is taken of ground reflectance.

Measurements made at University College, Cardiff, gave values for the emissivities of the Delta tiles and felt of 0.93 and 0.84 respectively (Chapter 4); a wind velocity of 4ms^{-1} was assumed. Table 3.1 summarises the heat transfer coefficients (rounded to the first decimal place) and the values for F', U_L and F_R calculated from equations 3.20, 3.21 and 3.26 (for the South East facing side of the test house roof).

HEAT TRANSFER COEFFICIENT	ESTIMATED VALUE, $Wm^{-2}°C^{-1}$	CALCULATED VALUES FOR F', U_L AND F_R
h_1	8.9	
h_{r1}	4.4	
U_t	37.6	F': 0.09
h_2	3.5	
h_3	3.4	
h_{r23}	4.0	U_L: 55
h_4	0.2	
h_{r4}	4.3	
U_b	4.3	F_R: 0.07

Table 3.1 Heat transfer coefficients and values for F', U_L and F_R using the no-leakage model for the test house roof. The units of U_L are $Wm^{-2}°C^{-1}$.

The model was developed for a roof without wind leakage between tiles; the test house roof can be assumed, as a first approximation,

to have little wind leakage because of the size and interlocking construction of the tiles (see Photograph 2.2).

To estimate the temperature rise of air resulting from passage under each side of the tiled roof, use must be made of the equations:

$$\eta = F_R(\tau\alpha)_e - F_R U_L (t_i - t_a)/I \qquad 3.4$$

$$\text{and} \quad (t_o - t_i) = \eta I A/\dot{m}Cp \qquad 3.49$$

From the radiation figures recorded at the Bracknell Weather Centre, the average value of total radiation on a horizontal surface for the heating season 1977/78 was 144 Wm^{-2}, of which 64% was diffuse (i.e. 92 Wm^{-2}). Assuming an average seasonal loading of 25% on the above value for a surface inclined at 25° to the horizontal, and facing South East (Temps and Coulson, 1977)(this average loading was confirmed by calculations for individual days), the average total radiation incident on the South East facing side of the roof was estimated to be about 180 Wm^{-2}; radiation on the North West facing side was 92 Wm^{-2} (assumed to be diffuse only).

For Delta tiles under AM2 solar radiation, the value for $(\tau\alpha)_e$ is 0.76 (Chapter 4); the values calculated for F_R and U_L are substituted into equation 3.4, and for $t_i = t_a = 7°C$, a value for η of 0.053 is calculated. Sustituting the appropriate values into equation 3.49 gives, for the South East facing side of the test house roof, a temperature rise for the airstream of 1.14°C. Assuming the same values of F_R and U_L apply to the North West facing side of the roof, but for $I = 92\ Wm^{-2}$, a similar calculation results in an air temperature rise of 0.58°C. For equal air mass flow rates from each side, the overall

air temperature rise after passage under the test house roof becomes $(1.14 + 0.58)/2 \simeq 0.9°C$. However, repeating the above procedure for $t_i = 7°C$, but with t_a replaced by an average surrounding ambient air temperature, $t_{a(av)}$, for the roof 'collector', where:

$$t_{a(av)} = (t_a + t_a')/2 \qquad 3.50$$

(i.e. $t_{a(av)} = [7.0 + 8.4]/2 = 7.7°C$), results in an overall temperature rise of air from South East and North West facing sides of the test house roof of $(1.46 + 0.90)/2 \simeq 1.2°C$. This figure may take more account of heat losses to the loft from the living space of the house.

The above figures of 0.9°C and/or 1.2°C may be compared with the test house measured value of 1.4°C for the average temperature rise of air over the heating season 1977/78 provided by the tiled roof (Chapter 6). In view of the approximations made in the analysis as a result of the complexity of a tiles on laths structure, the agreement is thought to be very good, and to show the suitability of the model for predicting the temperature rises to be expected from a conventional roof when used as an air-heating solar collector. In the next section, a further comparison is made, that between the calculated values of F_R and U_L and values obtained from measurements at the test house.

3.2.6 Standard Test Procedures

To make meaningful comparisons of the thermal performance of different solar collectors, tests need to be conducted under similar conditions, and the results presented in a standard format. In this respect,

several 'standard test procedures' have been devised by various authorities.

The National Bureau of Standards (NBS) test procedure (Hill and Kusada, 1974) is based on equation 3.3; the American Society of Heating, Refrigerating and Air-Conditioning Engineers (ASHRAE) test procedure (ASHRAE 93-77, 1978) is based on equation 3.4. In each of these, the results presentation is in the form of a graph of efficiency, η, plotted against $(\bar{t}_f - t_a)/I$ or $(t_i - t_a)/I$ respectively; a straight line is obtained in each case. In the NBS procedure, the gradient and efficiency intercept are $F'U_L$ and $F' (\tau\alpha)_e$ respectively, whereas in the ASHRAE procedure they are F_RU_L and $F_R (\tau\alpha)_e$ respectively.

The NBS and ASHRAE procedures stipulate that outdoor tests should be conducted with radiation levels of not less than 630 Wm^{-2}. Such intensities of radiation lasting for extended periods of time are not common in Northern Europe; this led, therefore, to the formulation of the Bundesverband Solarenergie (BSE) test procedure (BSE, 1978). In this procedure, heat loss tests are conducted indoors. Jenkins (1979) has compared the efficiency plots of five liquid-heating collectors tested according to the ASHRAE and BSE procedures and has found the results to be in good agreement (after transposing the BSE results into the ASHRAE format). The format given in the ASHRAE procedure is widely used in collector testing work, and so was chosen for the presentation of the experimental results in this thesis (Chapters 3 and 4). In addition, graphs were plotted in the NBS format, and from these, values for F' and U_L were obtained; these were compared with calculated values (see Chapter 4).

The NBS and ASHRAE procedures allow for the testing of collectors using air as the heat transfer fluid. However, both Parker (1981) and Hill and Streed (1976) have pointed out that values of F' and U_L for air-heating collectors may exhibit significant errors compared with those for liquid-heating collectors. This is because equation 3.3 is valid only at a certain point in the flow path (as F' and U_L are weak functions of temperature), and in liquid-heating collectors, the variation in fluid temperature from inlet to outlet is generally smaller than with air-heating collectors. It may be possible to reduce the uncertainty in the values of F' and U_L by having shorter lengths of air-heating collector under test (giving a reduced temperature rise), but this could introduce problems due to unrepresentative flow regimes (Mumma et al, 1978). Comparative tests for air-heating collectors should not be affected, provided the ducts are of approximately the same dimensions; in addition, the error is reduced if fluid temperature rises are not too large (this being the case at the test house and in the laboratory tests to follow). Nevertheless, to the best of the author's knowledge, no specialised testing procedures have been put forward for air-heating collectors.

Using the ASHRAE format, it is possible to produce efficiency graphs for the test house roof from which values for F_R and U_L may be obtained. These may then be compared with the values calculated from the model. In situ efficiency characteristics for the South East facing side of the test house roof were determined from hourly values of the appropriate temperatures and hourly values of the levels of total and diffuse solar radiation incident on a horizontal surface. The radiation data was recorded at Bracknell Meteorological

Office, about 26 km to the North East.

From the data recorded for the period February to April 1980, days with sufficiently high levels of direct beam solar radiation were selected for analysis. The total radiation incident on the South East facing surface of the roof, inclined at 25° to the horizontal, was calculated for each hourly period using a method described by Duffie and Beckman (1980) and originally reported by Liu and Jordan (1963). This takes into account diffuse reflection from the ground. A ground reflectivity value of 0.2 was assigned, together with the values of latitude and longitude for the test site. Values for the equation of time were obtained from the American Ephemeris and Nautical Almanac for the Year 1950, published by the United States Naval Observatory (1948).

The air temperature in the loft differed from the external air temperature, and hence equation 3.16 applies. However, to produce an efficiency graph in the format described by the ASHRAE 93-77 (1978) test procedure, it was necessary to assume an average surrounding ambient air temperature, $t_{a(av)}$, (equation 3.50), where t_a is the outside ambient air temperature, and the loft air temperature t_b was taken for t_a' (t_b corresponds to t_a' in equation 3.16). Two plots of efficiency, η, against $(t_i - t_{a(av)})/I$ were produced, one for $I \geqslant 650$ Wm^{-2}, and the other for I in the range 300 - 650 Wm^{-2}, where I is the total radiation intensity incident on the inclined South East facing side of the test house roof; the reason for this was because the higher radiation level relates to that stipulated in the ASHRAE procedure, while the lower radiation level relates to conditions more usual in the United Kingdom. The

total air mass flow rate in each case was taken as 0.45 kg s^{-1} (which is 0.04 kg s^{-1} per metre width). These plots (best-fit lines) are shown in Figure 3.3. The results include the effect of any airstream heating from the loft space (which accounts for the negative values of $(t_i - t_{a(av)})/I$) and so give the overall efficiency which can be expected.

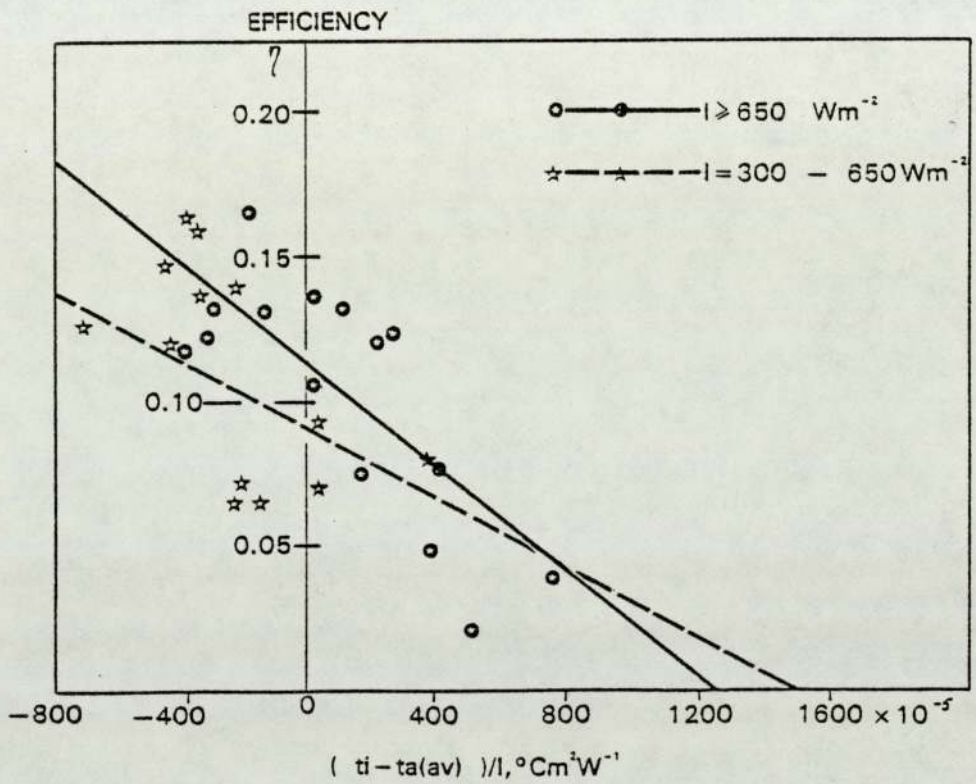

Figure 3.3 Efficiency versus $(t_i - t_{a(av)})/I$ for the South East facing side of the tiled roof at the test house (best fit lines).

A $(\tau\alpha)_e$ value to AM2 solar radiation of 0.76 was taken for the Delta tiles, and from the linefits to the outdoor results, values for F_R and U_L were calculated. These are shown in Table 3.2, where they are compared with the values calculated from the model for the season 1977/78.

η TEST CONDITIONS AND COMMENTS	GRAPHICAL				CALCULATED	
	$F_R U_L$	$F_R(\tau\alpha)_e$	F_R	U_L	F_R	U_L
OUTDOORS, $I \geqslant 650 Wm^{-2}$	9 ± 4 ($\pm 2\sigma$)	0.11 ± 0.01 ($\pm 2\sigma$)	0.15	61	0.07	55
OUTDOORS, $I = 300\text{-}650$ Wm^{-2}	6 ± 7 ($\pm 2\sigma$)	0.09 ± 0.02 ($\pm 2\sigma$)	0.12	51		

Table 3.2 Comparison of graphical F_R and U_L values with the seasonal values calculated using the no-leakage model, Delta-tiled roof. The units of U_L are $Wm^{-2}{}^{\circ}C^{-1}$.

The agreement between graphical and calculated values for F_R and U_L is good, considering the inaccuracies involved, which further indicates that the no-leakage model is suitable for calculating air temperature rises and values for F', F_R and U_L for tiled roofs used as air-heating solar collectors. As shown in Chapter 4, the calculated value of F_R will be increased, and U_L decreased, if any leakage takes place between the tiles.

Figure 3.3 may be compared with Figure 3.4, which shows the efficiency characteristics of a double-glazed flat plate solar air heater (with flow under the absorber) given in ASHRAE 93-77 (1978) and originally reported by Hill et al (1978). This highlights the fact that, compared with the Delta-tile roof, the specially designed panel has a lower heat loss coefficient (assuming a $(\tau\alpha)_e$ value of 0.75), and can run with higher inlet fluid temperatures. It is

concluded that a tiled roof structure has a role to play as a pre-heating device for an air source heat pump, since it is comparably efficient for small temperature rises.

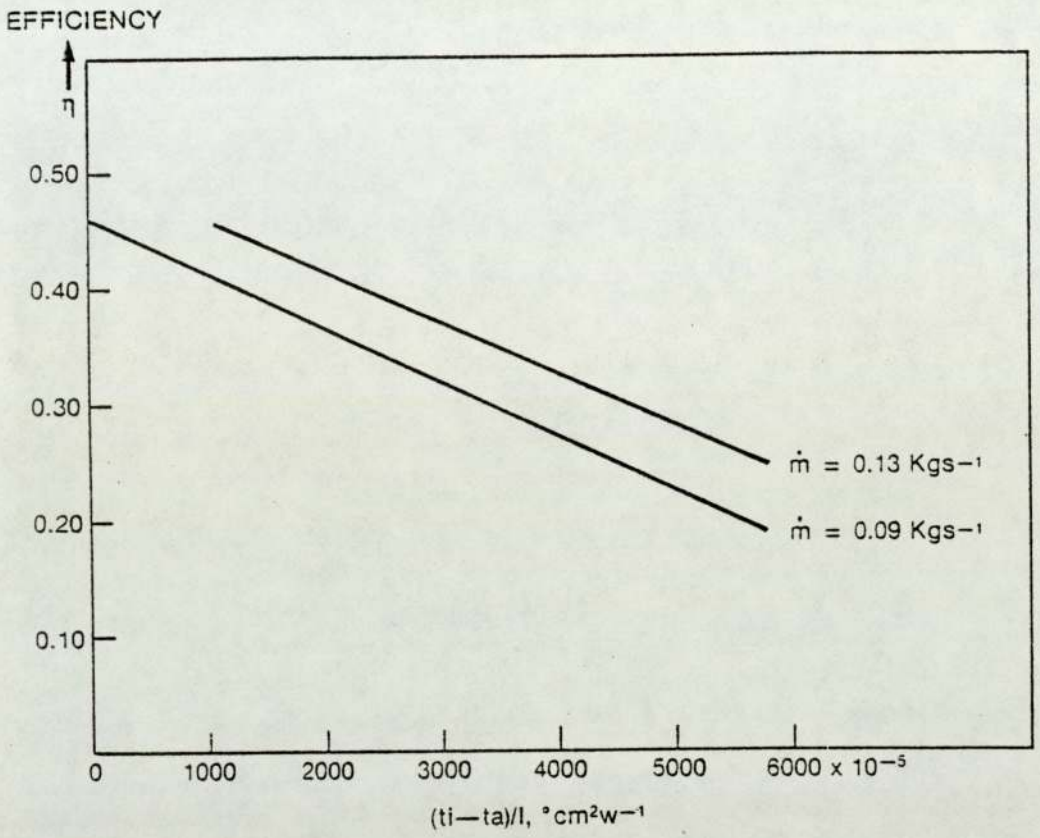

Figure 3.4 Efficiency versus $(t_i - t_a)/I$, air panel; (from Hill, Jenkins and Jones, 1978).

The feasibility of using other types of conventional roofs as solar collectors was investigated by laboratory testing. This permitted further examination of the use of the no-leakage model in estimating the performance of tiled roofs and also enabled the applicability of the model to other roof types to be determined. In addition, specific properties of conventional roofs when used as energy collectors could be studied under more controlled conditions.

3.2.7 Solar Simulators

Indoor testing of solar collectors offers advantages over outdoor testing (see, for example, Simon and Harlamert, 1973; Gillett, 1977; Dittes and Goettling, 1979) in that conditions may be closely controlled which in turn reduces scatter in efficiency plots and aids comparison of results. 'Solar simulators' are usually employed to provide the necessary radiation levels and to reproduce the solar spectrum, and several have been described (Yass and Curtis, 1974; Gillett, 1977; Krusi and Schmid, 1979); their use, however, gives rise to special problems.

The main concern is with the spectrum of the radiation source, which must coincide as closely as possible with the solar spectrum for a particular air mass. This, and other factors, such as beam parallelism, uniformity of radiation distribution on the test area, intensity variation, source manoeuvrability and life are discussed by Gillett (1977) and by Laidler and Bainbridge (1979). Several types of lamp have been used for solar simulation, such as the xenon high pressure lamp (Boettner and Miedler, 1963) the tungsten halogen lamp (Simon and Harlamert, 1973), and the compact source iodide (CSI) lamp (Gillett, 1977; Laidler and Bainbridge, 1979; Krusi and Schmid, 1979).

Another problem is the simulation indoors of a thermal environment which is representative of that found outdoors. A method of maintaining the radiant temperature of the walls and the indoor ambient air temperature at the same value is outlined by Dittes and Goettling (1979). This helps to provide a constant field of view tempera-

ture for the collector under test. The significance of longwave radiation in collector tests is discussed by Green and Gillett (1979), and methods of correcting for the effects of thermal radiation from the enclosure, lamp bulbs and support gantry are presented by Gillett et al (1980). It has been shown (Green, 1979) that wind and ambient temperature have the more significant effect on the performance of a collector outdoors than does the effective sky temperature. Indoors, the effect of wind can easily be simulated by means of a fan, while a temperature of about 20°C for ambient air is common (though air-conditioned rooms could offer control of this variable).

3.3 A Heating Simulator

A facility giving full spectral simulation is expensive. In view of this, and for the present work, a simulator was constructed which reproduced the heating effect of solar radiation rather than its actual spectrum (initially reported by Loveday et al, 1981).

3.3.1 Simulator Design and Construction

The simulator was firstly designed to test the thermal performance of a roof structure similar to that of the test house. Modifications were subsequently made to allow for the testing of other roof structures (corrugated metal panels). The design was such that approximately $1m^2$ sections of conventional roofing structures could be assembled upon a supporting steel framework. Each roof structure was set at an angle of 20° to the horizontal (approximately the same as at the test house) in an attempt to reproduce the heat transfer coefficients, which are themselves a function of surface inclination (Diamant, 1977).

The heat source consisted of a gantry of sixteen Philips 300 watt tungsten filament infra red reflecting (IRR) heat lamps, arranged in a symmetrical 4 x 4 array. The array dimensions were calculated, using the manufacturer's data, to produce a reasonably uniform intensity distribution on the $1m^2$ test surfaces, 0.5m below the glass envelopes of the lamps. The voltage across the lamps (and hence their intensity) was controlled by a bank of transformers. The lamp gantry, also inclined at 20° to the horizontal, was fixed above the support framework.

An air pre-heating module containing transformer-controlled resistance-heating elements was attached to the duct entrance of each roof section, and a crossflow fan was attached at the duct exit. Another crossflow fan simulated the effect of a $2ms^{-1}$ wind parallel to the test surfaces. The roof structures were built on a wheeled rectangular subframe allowing limited mobility which in turn gave easier access during 'roof' changeovers.

Two types of roof were tested, of tiles and of metal. The tiled roof section consisted of rows of red 'Dreadnought' tiles on laths, with a gap 0.1m in width separating them from a sanded bitumen felt backing. Panels packed with closed cell rubber were used to produce airtight seals at the sides and to reduce heat losses from the sides. The metal roof panels consisted of corrugated steel and aluminium backed with isocyanate foam insulation 0.05m thick (as supplied by the manufacturers). The insulation, together with the corrugations, formed air flow channels trapezoidal in section, of heights 0.025m (steel) and 0.038m (aluminium). The upper surface of the steel panel was coated with a plastic finish ('Plastisol'),

dark brown in colour, while the upper surface of the aluminium panel was finished with colour bond (also dark brown), stucco embossed.

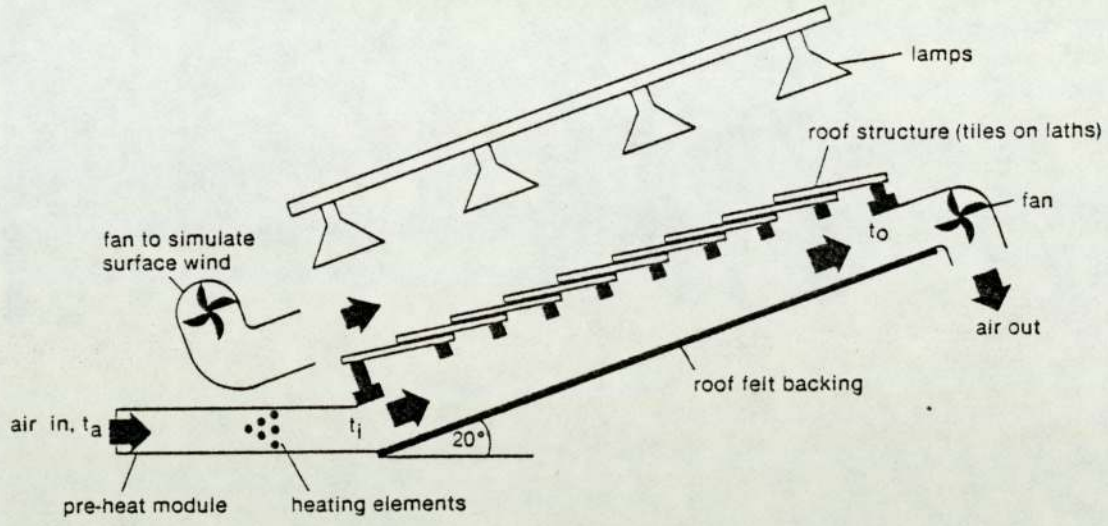

Figure 3.5 Schematic diagram of the heating simulator with the tiled roof section fitted.

A schematic diagram of the simulator with the tiled roof section fitted is shown in Figure 3.5, while the colour photograph at the front of the thesis shows a test in progress on the tiled roof section. Photographs 3.1, 3.2 and 3.3 (at the end of this chapter) show the general construction of the simulator with the corrugated steel panel fitted, together with some of the control and data acquisition equipment.

3.3.2 Instrumentation and Calibration

The airstream temperature differences across the pre-heating module and across the roof sections were measured with copper/constantan thermopiles giving voltage outputs to a high impedance digital voltmeter of 1μ V resolution. Each thermopile was made from 0.315mm diameter

thermocouple wire; six and eight-junction thermopiles were used to measure the temperature difference values ($t_i - t_a$) and ($t_o - t_i$) (see Figure 3.5) respectively, when testing the tiled roof section. When testing the metal panels, twelve-junction thermopiles were used for both temperature differences. All the junctions of each thermopile were radiation-shielded (Rogers and Mayhew, 1978). Each thermopile was calibrated against a platinum resistance thermometer, and the thermoelectric powers of each are presented in Table 3.3.

THERMOPILE AND SITUATION OF USE	THERMOELECTRIC POWER, °C μV^{-1}	ERROR, $\pm$ 3 st. dev.
6-JUNCTION, ($t_i - t_a$), TILED ROOF	0.00816	$\pm$0.00048
8-JUNCTION, ($t_o - t_i$), TILED ROOF	0.00611	$\pm$0.00020
12-JUNCTION, ($t_i - t_a$), METAL PANELS	0.00435	$\pm$0.00004
12-JUNCTION, ($t_o - t_i$), METAL PANELS	0.00423	$\pm$0.00005

Table 3.3 Thermopile thermoelectric powers.

Surface temperatures were measured with platinum resistance sensors of the type used at the test house (see Chapter 2), and mercury-in-glass thermometers indicated the temperature of the ambient air at several points around the simulator.

Duct airspeeds were measured with a hot-wire anemometer; 'traverses' were carried out, averages of a large number of readings were

taken, and these were used in the calculation of the air mass flow rates. Tests were conducted at values for the averaged air mass flow rate measured at the inlet of 0.106 ± 0.004 kg s^{-1} and 0.029 ± 0.004 kg s^{-1} for the tiled roof section, and at a single value of 0.034 ± 0.004 kg s^{-1} for the metal panels. The values near 0.030 kg s^{-1} were selected because they were close to the value for the air mass flow rate in each side of the roof at the test house. In addition, mass flow rates were measured at the outlet to determine the leakage rates to or from the duct airstream. For each experiment, the specific mass flow rate value is stated.

3.3.3 Radiation Characteristics

The radiation intensity I, Wm^{-2}, from the sixteen-lamp array was measured with an Eppley pyranometer. Sets of readings were recorded for various lamp voltage settings, and from the readings, initial recorded radiation intensities were calculated based on the manufacturer's calibration. These formed the basis of a pre-selection procedure in which two lamp voltage settings were chosen at which to conduct laboratory tests. The values chosen were 160V and 100V, which corresponded to initial radiation intensities of 736 Wm^{-2} (recorded) and 278 Wm^{-2} (recorded) respectively. These were selected because the former relates to conditions stipulated in the ASHRAE procedure (ASHRAE 93-77, 1978) at which collectors to date have been tested, and because the latter relates more closely to U.K. conditions. Corrections to the recorded values are necessary when using the Eppley pyranometer in this way and these are discussed later. The coefficient of variation (Krusi and Schmid, 1979) of the radiation intensity over the $1m^2$ test surfaces was calculated

to be about 16% for each voltage setting. This may be compared with values of about 15% (Krusi and Schmid, 1979) and 20% (Gillett et al, 1980) for two solar simulators using CSI lamps.

Treating the IRR lamp filaments as black body radiators at temperatures of 2093 $\pm$ 50K and 1765 $\pm$ 50K (corresponding to voltage settings of 160V and 100V respectively), the use of Wien's displacement law allows calculation to be made of the wavelengths at which maximum radiation emission occurs. These values are 1.39 μm and 1.64 μm for the lamps at 160V and 100V respectively, and compare with a value of about 0.5 μm for solar radiation.

Some of the radiation emitted by the filaments undergoes absorption by the glass envelopes of the lamps. The values of transmittance of the IRR lamp 'hard glass' for the wavelength ranges 0-0.3 μm, 0.3-2.7 μm, and 2.7-3.6 μm and 3.6 μm and beyond are given as zero, 0.835, 0.184 and zero respectively (Philips Lighting Division, 1982). The fraction of the total radiant energy emitted by a black body, temperature T, between zero and some value λT may be expressed (Duffie and Beckman, 1980) by:

$$\frac{E_{(0 - \lambda T)}}{\sigma T^4} = \int_0^{\lambda T} \frac{C_1 \, d(\lambda T)}{\sigma (\lambda T)^5 \, (e^{C_2/\lambda T} - 1)} \qquad 3.51$$

where $E_{(0 - \lambda T)}$ is the radiant energy per unit area per unit time between the values zero and λT from a black body, C_1 and C_2 are Planck's first and second radiation constants respectively, σ is the Stefan-Boltzmann constant, λ is the wavelength of the radia-

tion emitted and T is the absolute temperature of the black body source. Values of this integral have been calculated by Sargent (1972) for various wavelength intervals and are presented in tabular form by Duffie and Beckman (1974). Using these values, and the transmittance values above, the radiant energy reaching a test surface in particular wavelength intervals may be expressed as a percentage of the total energy reaching the surface after leaving the glass envelopes of the IRR lamps. This is given in Table 3.4.

WAVELENGTH INTERVAL, μm	% OF TOTAL ENERGY LEAVING IRR LAMP GLASS	
	LAMPS AT 100V	LAMPS AT 160V
0.3 - 2.8	95.2%	96.7%
2.8 - 3.6	4.8%	3.3%

Table 3.4 Energy in certain wavelength intervals reaching a test surface, expressed as a percentage of the total leaving the IRR lamp glass.

The Eppley pyranometer is calibrated for the measurement of solar radiation. Hence its use for measuring radiation intensities from sources of other spectral distributions requires the introduction of corrections based on the transmission of the domes and the absorption of the thermopile to that distribution. At the earth's surface, the solar spectrum ranges from about 0.3 - 2.5 μm, whereas the spectral range of the output from the IRR lamps is 0.3 - 3.6 μm. The pyranometer thermopile is covered by two hemispherical domes of Schott glass, each of 0.002 m thickness. From data supplied by the manufacturers (Eppley Laboratory, Inc., 1982) and from Duffie and Beckman (1974), the transmission, τ, for each dome is 0.9 and an

estimated value of 0.38 for radiation in the spectral ranges 0.29 - 2.8 μm and 2.8 - 3.6 μm, respectively. The thermopile sensor is coated with Parson's Black optical laquer, which has uniform absorption properties throughout the wavelengths of solar and terrestrial radiation (Fritschen, 1965). The absorptivity, α, of Parson's Black is 0.98 and 0.97 for radiation in the spectral ranges 0.29 - 2.8 μm and 2.8 - 3.6 μm respectively (Touloukian, 1972).

From the above data, separate $\tau\tau\alpha$ products were obtained for both spectral ranges, and from the manufacturer's constant (applicable for solar radiation, and hence to the range 0.29 - 2.8 μm), a separate constant was calculated for the range 2.8 - 3.6 μm. These constants were:

range: 0.29 - 2.8 μm, $1 Wm^{-2} \equiv 10.40 \times 10^{-6}$ volts;

range: 2.8 - 3.6 μm, $1 Wm^{-2} \equiv 1.84 \times 10^{-6}$ volts;

Using the two constants, and the data in Table 3.4, simultaneous equations were set up which were then solved to give the intensity of radiation from the IRR lamps falling on a test surface in the two spectral ranges. For the lamps at 100V the values are 276 Wm^{-2} in the range 0.3 - 2.8 μm, and 14 Wm^{-2} in the range 2.8 - 3.6 μm, giving a total intensity from the lamps of 290 Wm^{-2} for the range 0.3 - 3.6 μm. This may be compared with the initial value of 278 Wm^{-2} calculated by direct use of the manufacturer's constant. A similar calculation for the lamps at 160V gives values of 731 Wm^{-2} and 25 Wm^{-2} for the ranges 0.3 - 2.8 μm and 2.8 - 3.6 μm respectively; the total output is therefore 756 Wm^{-2} (compared with the initial value of 736 Wm^{-2} obtained from direct use of the manufacturer's constant).

There is an additional effect to be considered. Studies by Drummond and Roche (1965) have shown that absorption of radiation by the glass domes of Eppley pyranometers can have an effect on the instrument calibration constant. In the case of the IRR lamps, a significant amount of radiation in the range 2.8 - 3.6 μm is absorbed by the domes, so the effect of this on calculated results was estimated using the data of Drummond and Roche(1965). Their work involved the use of filters which absorbed in particular sections of the solar spectrum, and from measurements taken they were able to calculate a multiplication correction factor for each filter to reduce the measured energy values to true energy values (typical correction factors were 0.94, 0.91).

For the IRR lamps, estimates of the amount of radiation absorbed by the domes of the Eppley were made (neglecting reflection), and, based on the results of Drummond and Roche, correction factors were estimated for each particular setting of the lamps. These correction factors were typically in the range 0.99 - 0.98, so it can be seen that the effect is small in comparison with that for solar radiation. Note that included in the calculation procedure to arrive at these factors is the longwave radiation from the lamp glass and gantry. Note also that the calculation procedure is iterative. Thus, the total intensities from the lamps at 100V and 160V become 286 Wm^{-2} and 740 Wm^{-2} respectively.

There are additional sources of radiation for a test surface from both the glass envelopes of the lamps and the lamp support gantry, while the laboratory windows act as 'sinks'. For tests on the tiled roof surface, the wooden side panels, used for sealing purposes,

act as sources, while for the metal panels, the tinplate end seals act as sources of diffuse reflectance. Corrections for these thermal radiation inputs were made using the method given by Gillett et al (1980), with the relevant view factors evaluated from expressions given by Siegel and Howell (1981). All corrections to the incident radiation are summarised in Tables 3.5 - 3.8 for both the tiled and metal roofs. Note that the values for thermal radiation given in Tables 3.7 and 3.8 are excess over a black body at ambient temperature (with the exception of the diffuse reflection from the end seals), and are average figures only; they are shown simply to indicate the order of magnitude of the correction. The actual values were calculated for each individual experiment and the final radiation intensity for each experiment is stated in Chapter 4.

LAMP VOLTAGE	RADIATION INTENSITIES, Wm^{-2}			CORRECTION FACTOR FOR DOME ABSORPTION	TOTAL RADIATION INCIDENT FROM LAMPS, Wm^{-2}
	INITIALLY RECORDED	ACTUAL, CALCULATED			
		0.3-2.8μm	2.8-3.6μm		
100	278	276	14	x0.987	286
160	736	731	25	x0.979	740

Table 3.5 Corrections, and values for radiation from the IRR lamps incident on the tiled roof in the heating simulator.

LAMP VOLTAGE	RADIATION INTENSITIES, Wm^{-2}			CORRECTION FACTOR FOR DOME ABSORPTION	TOTAL RADIATION INCIDENT FROM LAMPS, Wm^{-2}
	INITIALLY RECORDED	ACTUAL, CALCULATED			
		0.3-2.8μm	2.8-3.6μm		
100	278	275	14	x0.986	285
160	740	735	25	x0.977	743

Table 3.6 Corrections, and values for radiation from the IRR lamps incident on the metal panels in the heating simulator. (The differences between Tables 3.5 and 3.6 are caused by differing lamp/test surface distances).

LAMP VOLTAGE	LAMP GLASS		GANTRY		WINDOWS		SIDE PANELS	
	V.F.	RADN.	V.F.	RADN.	V.F.	RADN.	V.F.	RADN.
100	0.097	12	0.196	13	0.057	-7	0.018	1
160	"	25	"	14	"	-7	"	1

Table 3.7 View factors (V.F.) and thermal radiation inputs (RADN.), Wm^{-2}, for the tiled roof in the simulator (typical values only).

LAMP VOLTAGE	LAMP GLASS		GANTRY		WINDOWS		END SEALS	
	V.F.	RADN.	V.F.	RADN.	V.F.	RADN.	V.F.	RADN.
100	0.112	13	0.211	14	0.059	-7	0.038	1
160	"	29	"	15	"	-7	"	3

Table 3.8 Average view factors (V.F.) and thermal radiation inputs (RADN.), Wm^{-2}, for the metal panels in the simulator (typical values only).

3.4 Summary

A heat transfer analysis has been carried out for a tiled roof structure behaving as an air-heating solar collector, which has shown that when the ambient air temperatures at the front and rear of the structure are equal, a form of the Hottel-Whillier-Bliss equation applies. Expressions for F' and U_L, appropriate to the condition $t_a = t_a'$, were then derived. These expressions are of general application to the case of a no-leakage air-heating solar collector with an absorber plate of finite thickness and thermal conductivity. Application of the no-leakage model to the tiled roof of the test house gave values for F_R, U_L and the air temperature rise which are considered to be in good agreement with those measured.

The use of standard procedures for testing solar collectors, together with some of the advantages and problems associated with indoor testing using solar simulators, have been commented upon; the construction and instrumentation of a heating simulator using infra red reflecting lamps has been described. The characteristics of the radiation source in the simulator have been discussed,

together with corrections to the measured values of incident radiation, and calculations were made of the thermal radiation inputs from the glass envelopes of the lamps, the lamp support gantry, other constructional elements, and windows. The final values for the total radiation incident on a test surface in the simulator were found to be, approximately:

305 Wm^{-2} and 773 Wm^{-2}, $\pm$ 25 Wm^{-2}, for the tiled roof;

306 Wm^{-2} and 783 Wm^{-2}, $\pm$ 25 Wm^{-2}, for the metal panels;

for the two operating conditions employed in the indoor tests (actual values vary slightly for each test).

Photograph 3.1: The heating simulator, showing the general construction. To the left are the controls for the lamps and the duct fan.

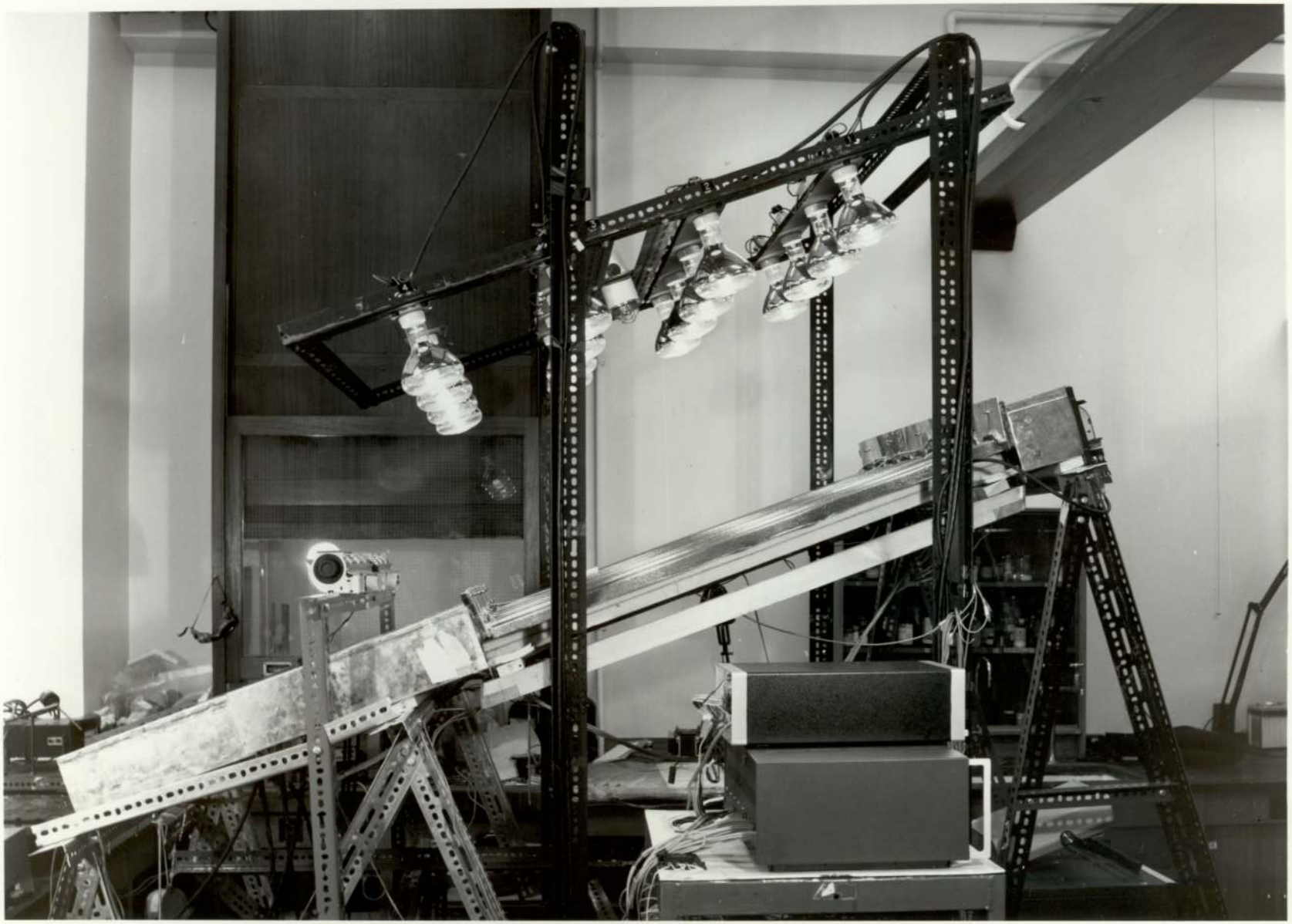

Photograph 3.2: Side view of the heating simulator.

Photograph 3.3: The heating simulator, showing the air pre-heating module and, above it, the fan for simulating surface wind.

CHAPTER 4

LABORATORY TESTS, RESULTS AND DISCUSSION

4.1 Absorptivity of Roof Tiles and Metal Panels

Values for the absorptivities of roof tiles and metal panel surfaces to both IRR and solar radiation spectral distributions were obtained from reflectivity measurements made by Dr. M. G. Hutchins at University College, Cardiff, using an Ultra Violet/Visible/Near Infra Red Perkin Elmer 330 spectrophotometer, of spectral range 0.185 - 2.500 μm. Three samples of the 'Dreadnought' tiles used in the laboratory test roof were tested, as were four samples of 'Delta' tiles, used for the roof of the test house, and a sample from both the steel and aluminium panels. The percentage reflectivity of each sample was recorded graphically through the spectral range 0.3 - 2.1 μm and the results dispatched to the author for analysis The spectral reflectance vs. wavelength plots for the steel ('Plastisol' coating, 'Van Dyke Brown') and aluminium (colour bond, stucco embossed, 'Van Dyke Brown') panels are shown in Figures 4.1 and 4.2 (all Figures and Tables are at the end of this chapter).

The absorptivities over the IRR radiation distributions (taken to be those of a black body at 2093K and 1765K) and over the air mass two solar spectrum (due to Moon, and reported in the Smithsonian Physical Tables, 1954) were calculated using the methods of selected and weighted ordinates described in a publication by the American Society for Testing and Materials (1979) and by Olson (1963).

Firstly, the absorptivity of each Dreadnought and Delta tile sample to the AM 2 solar spectrum was calculated using the selected ordinate method, and twenty selected ordinates. The average absorptivity for the four Delta tile samples was found to be 0.76 $\pm$ 0.01 (for the range 0.3 - 2.1 μm). The average absorptivity (to AM 2 solar radiation) of the entire test surface of Dreadnought tiles in the laboratory heating simulator was found to be 0.64 $\pm$ 0.01 (for the range 0.3-2.1 μm); this average value resulted from a weighting technique based on the number of tiles in the section of laboratory roof which resembled the colour tint of each of the three samples tested. The absorptivities of both the steel and aluminium panels were found to be 0.92 $\pm$ 0.01 (for the range 0.3 - 2.1 μm).

Secondly, the absorptivity of each tile and metal panel sample to the radiation distribution from the IRR lamps when operated at 160V and 100V was calculated using the weighted ordinate method. In this method, the absorptivity is obtained by evaluation of:

$$\alpha = 1 - \left[\sum_{\lambda_1}^{\lambda_2} (E_\lambda \cdot R_\lambda \cdot \Delta\lambda) / \sum_{\lambda_1}^{\lambda_2} (E_\lambda \cdot \Delta\lambda) \right] \qquad 4.1$$

where E_λ is the spectral energy distribution of the source over a certain wavelength interval, R_λ is the absolute spectral reflectivity over the same wavelength interval, λ_1 and λ_2 are the limits of the wavelength range considered (0.3 - 2.1 μm), and $\Delta\lambda$ is the wavelength interval concerned (a width of 0.05 μm being taken).

Equation 3.51 gives the fraction $E_{(0-\lambda T)}/\sigma T^4$ of the total radiant energy emitted by a black body, absolute temperature T, between the values 0 and λT. The fraction of energy, $E_{(\lambda_a - \lambda_b)}/\sigma T^4$, within

a certain wavelength interval (λ_a to λ_b, say) may then be found from:

$$E_{(\lambda_a - \lambda_b)}/\sigma T^4 = E_{(0 - \lambda_b T)} / \sigma T^4 - E_{(0 - \lambda_a T)}/\sigma T^4 \qquad 4.2$$

Multiplying by the total energy of the black body distribution, σT^4, gives the actual energy within the wavelength interval λ_a to λ_b; this is equal to the value $E_\lambda \Delta\lambda$ for the same wavelength interval. Thus, equation 3.51 may be used to find values for $E_\lambda \Delta\lambda$. However, in the calculation of α (equation 4.1), since σT^4 would appear in both the numerator and the denominator and cancel, the fractional value $E_{(\lambda_a - \lambda_b)}/\sigma T^4$ may be taken in place of $E_\lambda \Delta\lambda$.

The weighting was carried out over the black body distributions for temperatures of 2093K and 1765K in $\Delta\lambda$ increments of 0.05 μm; in the case of the laboratory test surface of Dreadnought tiles, further weighting was carried out, based once again on the number of tiles in the laboratory roof section which resembled the colour tint of each of the three samples tested. Values for the average surface absorptivities of the tiles are given in Table 4.1, and those for the metal panels in Table 4.2. A sample of the calculation using the weighted ordinate method is given in Table 4.3.

The values of $R_\lambda \; E_{(\lambda_a - \lambda_b)}/\sigma T^4$ and $E_{(\lambda_a - \lambda_b)}/\sigma T^4$ were summed over the range 0.3 - 2.1μm. The absorptivity was then found from:

$$\alpha = 1 - \frac{\sum_{\lambda = 0.3}^{\lambda = 2.1} R_\lambda \; E_{(\lambda_a - \lambda_b)}/\sigma T^4}{\sum_{\lambda = 0.3}^{\lambda = 2.1} E_{(\lambda_a - \lambda_b)}/\sigma T^4} \qquad 4.3a$$

$$= 1 - \frac{\sum_{\lambda = 0.3}^{\lambda = 2.1} R_\lambda E_{(\lambda_a - \lambda_b)}}{\sum_{\lambda = 0.3}^{\lambda = 2.1} E_{(\lambda_a - \lambda_b)}} \qquad 4.3b$$

$$= 1 - \frac{\sum_{\lambda = 0.3}^{\lambda = 2.1} R_\lambda E_\lambda \Delta\lambda}{\sum_{\lambda = 0.3}^{\lambda = 2.1} E_\lambda \Delta\lambda} \qquad 4.3c$$

Surface absorptivities for the wavelength range 2.1 - 3.6 μm were assumed to be the average values for the range 0.3 - 2.1 μm (the reflectance curves varied smoothly in the case of the tile samples, and, in the case of the metal samples, exhibited little variation at all - see Figures 4.1 and 4.2). This assumption was necessary because it was not possible to obtain specific reflectance values for the wavelength range of interest.

From measurements of broad band thermal emissivities, also carried out at University College, Cardiff, surface absorptivities for wavelengths beyond 3.6 μm were obtained by treating the surfaces as grey bodies and then employing Kirchhoff's law for radiation. Summaries of surface absorptivities in the spectral ranges 2.1 - 3.6 μm, and beyond 3.6 μm, are presented in Tables 4.4 and 4.5, while Table 4.6 shows some of the measured emissivity values.

Application of the appropriate absorptivity values to the intensities of radiation in each wavelength range (Chapter 3, section 3.3.3) enabled values of the total absorbed energy (per unit area), $I\ (\tau\alpha)_e$, to be calculated for each experiment. Dividing these values by I,

the total incident radiation, overall values for $(\tau\alpha)_e$ were arrived at for use in the indoor tests (note that as there were no transparent covers, the transmissivity, τ, was unity). Overall values for $(\tau\alpha)_e$ were found to be 0.45 ± 0.10 for the Dreadnought tile roof section, 0.92 ± 0.05 for the steel panel, and 0.93 ± 0.05 for the aluminium panel.

4.2 Validation of the No-Leakage Model

The theoretical model describing the behaviour of a no-leakage air-heating solar collector having an absorber plate of finite thickness and thermal conductivity was used in Chapter 3 to predict both the temperature rise of air and the values of F', U_L and F_R for the tiled roof of the test house. The values obtained showed good agreement with those measured at the site. It is now possible to examine further the validity of the model by applying it to a section of sealed tile roof tested in the laboratory. In addition, its applicability to corrugated metal roofs can be investigated by tests on the steel and aluminium panels. The comparison of experimental and calculated values for F' and U_L will also determine to what extent a relatively inexpensive simulator with IRR lamps could be used for testing the performance of tile and metal roofs as energy collectors.

Efficiency graphs are generated by varying the duct inlet fluid temperature, t_i, while holding the air mass flow rate and radiation intensity at constant values. Plotting the efficiency, η, against $(t_i - t_a)/I$ provides values for F_R and U_L; plotting η against $(\bar{t}_f - t_a)/I$ provides values for F' and U_L. The latter graph may be obtained from the same set of data as that used to

obtain the former, because if $\bar{t}_f$ is taken as:

$$\bar{t}_f = (t_o + t_i) / 2 \qquad 4.4$$

it can be shown that:

$$(\bar{t}_f - t_a) = (t_i - t_a) + 0.5\,(t_o - t_i) \qquad 4.5$$

(Note that defining $\bar{t}_f$ in this way produces a value F_{av} [Duffie and Beckman, 1980] rather than the true F', where F_{av} is approximately the same as F'. F_{av} may be converted to F_R [and hence to the true F' by equation 3.26] from the expression given by Duffie and Beckman [1980]; for the small temperature rises encountered in the indoor tests, the difference betwen F_{av} and F' was very small, about 2% in the worst case. Thus the notation F' for values obtained experimentally, will be retained).

For the conditions of each indoor test, heat transfer coefficients are estimated, and the values inserted into the model to obtain values for F' and U_L. Validation is carried out by comparing the calculated values for F' and U_L with those obtained experimentally.

4.2.1 Estimation of the Heat Transfer Coefficients for the Laboratory Tests

This is carried out in a similar manner to that described in Chapter 3, section 3.2.4, but some modifications are necessary because of the effects of the indoor environment and the simulator construction.

For indoor testing, it is common to take the 'sky' temperature, T_s,

as equal to the ambient air temperature, t_a, in the laboratory. Thus the value of U_t is given by equation 3.23, and t_a replaces T_s in equation 3.37.

A crossflow fan simulated a wind of average value $2ms^{-1}$ parallel to the test surfaces. This value is relatively small compared with those encountered outdoors, and it was considered worthwhile to check if any 'mixed' (i.e. both forced and free) convection was present. This is determined by calculation of the value of (Gr/Re^2), and then by adoption of the following criteria (Incropera and DeWitt, 1981):

if $(Gr/Re^2) \gg 1$, 'pure' free convection;

if $(Gr/Re^2) \simeq 1$, mixed convection;

if $(Gr/Re^2) \ll 1$, 'pure' forced convection.

Values of the above parameter were calculated for each experiment in which a wind was applied, (Re based on the plate length), and it was found that 'pure' forced convection was the dominant mode throughout.

Green et al (1980) state that, for collector testing, a wind speed of $2ms^{-1}$ is adequate to ensure results reproducibility, and recommend that the following relation be used for evaluation of the wind induced heat transfer coefficient:

$$h_1 = 3.0 + 7.4v_1^{0.5} \qquad 4.6$$

where v_1 is the air velocity parallel to the surface of the collector. This expression was used for the indoor tests. In tests without a surface wind, an expression by Welty (1978) for turbulent free convection from a horizontal upward-facing flat plate was used to determine h_1:

$$h_1 = 1.52\ (\Delta T/L)^{0.33} \qquad 4.7$$

where ΔT is the temperature difference $(T_1 - t_a)$ and L the plate length. This gave a value for h_1 of about 3 $Wm^{-2}{}^{\circ}C^{-1}$, close to that given by Green et al (1980) for free convection from an inclined collector during indoor testing.

Overall thermal conductivity through the tile 'plate' was assessed in a similar way to that described in section 3.2.4, by considering thin air layers between overlapped tiles. This led to values for k_1 of, on average, 0.37 $Wm^{-1}K^{-1}$ and for d_1 of 0.0206m for insertion in the no-leakage model (compared with the thermal conductivity of tile of 0.8 $Wm^{-1}K^{-1}$).

In the simulator, edge losses in the case of the tiled roof may become important (for the metal panels there are no 'edges', as such). These were treated in a manner suggested by Duffie and Beckman (1980), where they are referenced to the collector area. The edge loss coefficient, U_e, is given by:

$$U_e = (U_{side}\ A_{side}) / A \qquad 4.8$$

where U_{side}, A_{side} are the U- value and total area of the sides of the tiled roof duct, respectively, and A is the ordinary flat plate area of the roof. It was necessary to determine an overall U_e value for the insulating materials of the duct edging. For the tile roof experiments, this was estimated to be 0.74 $Wm^{-2}{}^{\circ}C^{-1}$. This was added to the value for U_b calculated from equation 3.25, to produce a value U_b' (equal to the sum of U_b and U_e) for insertion into the model in the place of U_b. Note that in estimating h_4, for $3 \times 10^5 < GrPr < 3 \times 10^{10}$, the following

expression given by Welty (1978) was used:

$$h_4 = 0.59 \, (\Delta T/L)^{0.25} \qquad 4.9$$

where ΔT is the temperature difference $(T_4 - t_a')$, and L is the average length of side of the felt backing panel.

For internal flow, the relatively short length of roof test section leads to heat transfer coefficients substantially higher than the fully developed values. This is caused by higher rates of heat transfer across the developing boundary layers of the entrance region. In addition, the type of entrance can also increase the Nusselt number and hence the internal heat transfer coefficients h_2 and h_3. In the simulator, the pre-heat module/roof test section entrance would give rise to this. Both these effects are discussed by Kays (1966), and from the data presented, the combined effects of entrance length and entrance type were estimated, for the one metre test section lengths, to be:

$$Nu_m \simeq 2 \, Nu_{fd} \qquad 4.10$$

for the tiled roof,

$$Nu_m \simeq 1.19 \, Nu_{fd} \qquad 4.11$$

for the steel panel, and

$$Nu_m \simeq 1.22 \, Nu_{fd} \qquad 4.12$$

for the aluminium panel; (Nu_m and Nu_{fd} are, respectively, the mean and fully developed Nusselt numbers).

For the tiled roof section, the effect of laths was once again treated as described in section 3.2.4, and by using equation 3.44

it was estimated:

$$Nu \simeq 1.359\ Nu_{smooth} \qquad 4.13$$

where Nu_{smooth} is the value for Nu_m found from equation 4.10 so as to include all effects. The fully developed Nusselt number was found using equation 3.42, with values for D_e of 0.216m for the tiled roof section (to the base of the tiles), 0.0329m for the steel panel flutes and 0.0378m for the aluminium panel flutes. Note that for the metal panels, Re, $\dot{m}$, and hence h_2 and h_3, in this case relate to flow in a single flute or channel, formed by the corrugations. Figure 4.3 is an illustration showing the construction of the metal panels. Note also that the flow channels were not smooth, but frequently had 'blobby' surfaces, which, it was estimated, enhance the Nusselt numbers as:

$$Nu \simeq 1.072\ Nu_{smooth} \qquad 4.14$$

for the steel panel, and

$$Nu \simeq 1.127\ Nu_{smooth} \qquad 4.15$$

for the aluminium panel (Nu_m from equations 4.11 and 4.12 being taken for Nu_{smooth}).

For the Dreadnought tile roof section, the area enhancement factor, $[1 + (a/A)]$, for the stepped surface was calculated to be 1.0636, and is a multiplier for h_1, h_{r1} and h_2. The flow channels of the metal panels are trapezoidal in section, and the h-values were enhanced by firstly finding $h/(\sin \theta/2)$ for the angled sides, where θ is the angle at the projected apex of the channel and h the relevant heat transfer coefficient, i.e. h_1, h_{r1} or h_2, for the flat surface area. Secondly, for the 'flat' top part of the channel, the ordinary flat surface area h-value was retained, and then the

values $h/(\sin \theta/2)$ and h combined in a weighting technique based on the projected area - refer to Figure 4.4 and the equation below:

$$h_2 = h_{2flat} \left[[m/(s+m)] + [s/(s+m)][1/(\sin \theta/2)] \right] \qquad 4.16$$

where s and m are the dimensions indicated in Figure 4.4 and the subscript 'flat' refers to h-values based on the ordinary flat surface area. This gave enhancement factors for h_{1flat}, h_{r1}, and h_{2flat} of 1.278 for the steel panel and 1.585 for the aluminium panel.

There are flat sections between the flow channels of the metal panels; for these, h_1 and h_{r1} will take their usual 'flat' surface values, whereas no values for h_2, h_3 or h_{r23} are applicable because no fluid flow occurs beneath the absorber plate in these regions. To take this into account, a further overall weighting technique, based on surface areas, was devised, which led to the final overall enhancement factors for the metal panel heat transfer coefficients given below.

For the steel panel:

$$h_1 = 1.171\ h_{1flat} \qquad 4.17$$

(the same factor applies to h_{r1});

$$h_2 = 0.788\ h_{2flat} \qquad 4.18$$

(the same factor applies to h_{r23});

and $$h_3 = 0.617\ h_{3flat} \qquad 4.19$$

For the aluminium panel:

$$h_1 = 1.315\ h_{1flat} \qquad 4.20$$

(the same factor applies to h_{r1});

$$h_2 = 0.853\ h_{2flat} \qquad 4.21$$

(the same factor applies to h_{r23});

and $h_3 = 0.538\ h_{3flat}$ 4.22

The evaluation of the enhancement factor relations is based on flow channel geometry and dimensions, and is a tedious procedure. It is, however, necessary to carry it out, because the no-leakage model presented earlier is based on the overall length and width dimensions of a collector panel, and is for the geometry of fluid flow beneath the whole absorber plate, not just through individual channels. Therefore, to use this model, the values for the heat transfer coefficients to be inserted must be related to the geometry which has been modelled - hence the relations 4.17 to 4.22 which attempt to treat the metal panels as 'equivalent flat plates'.

The expressions and procedures outlined in this section were used to estimate the heat transfer coefficients for the conditions of each laboratory test. These values were inserted into the no-leakage model, and the values obtained for F', U_L and F_R were compared with those obtained experimentally.

4.2.2 Application to the Section of Sealed Tile Roof

Figures 4.5 and 4.6 are plots of efficiency, η, against $(t_i - t_a)/I$ obtained for the section of Dreadnought tiles in the simulator, all gaps and tile overlaps having been sealed so as to prevent wind leakage into the airstream. The values of I and $\dot{m}$ stated with the Figures (and in key code summaries - see the Tables) are, respectively, the level of IRR (and thermal) radiation, and

the air mass flow rate in the duct appropriate to that particular test. It can be seen that the application of wind reduces the efficiency. From these graphs, values for F_R and U_L were deduced, while from plots of η against $(\bar{t}_f - t_a)/I$ (not shown) values were deduced for F' and U_L. The results are summarised in Tables 4.8 and 4.9, while Table 4.7 shows a convenient key code for summarising the test conditions. Table 4.10 summarises the values estimated for the heat transfer coefficients for the two experiments.

After substitution of the heat transfer coefficients, the values for F' and U_L predicted by the author's no-leakage model, which takes account of the finite thickness and thermal conductivity of the absorber plate, were compared with values obtained by substitution of the (adapted) h-values into the expressions for F' and U_L derived by Parker (1981) for a bare plate collector with air flow under the absorber, and into expressions presented by Duffie and Beckman (1980) for a similar collector geometry (Type 'e', page 238). The latter models do not take into consideration the finite thermal conductivity and thickness of the absorber plate, but treat it as thin, and highly conducting. Table 4.11 summarises the values calculated using each model and compares them with the values obtained experimentally.

It can be seen that the agreement between the graphical and calculated values for F' and U_L is moderately good, and that the no-leakage model gives better agreement overall than do the models of Parker (1981) or Duffie and Beckman (1980). This is because the author's model is the most suitable for the geometry of a thick, poorly-conducting absorber plate, as is the case with a tiled roof.

Its use in this context would be better for conservative design than the other models. Note that it was assumed throughout that, in the laboratory, $t_a = T_s$, the 'sky' temperature. If the wall temperatures are taken to be less than the ambient air temperature, then the calculated U_L values increase, and this gives better agreement. This would have a bigger effect for test condition A, where there was no surface wind. Thus the importance of the 'sky' temperature should not be overlooked when testing uncovered collectors. Also, the surface roughness of the tiled roof (an effect not accounted for) would increase the calculated U_L values.

Substitution of the F' and U_L values, calculated using the no-leakage model, into equation 3.26 (tile roof section area equal to $1.188m^2$) gives values for F_R of 0.24 and 0.14 for test conditions A and B respectively. These may be compared with the respective experimental values for F_R of 0.23 and 0.19 (Table 4.9).

Limitations to the accuracy of the calculated, but more especially the experimental, results will be discussed more fully at the end of the next section. As a result, it was concluded that the no-leakage model is valid to predict the general performance of a tiled roof when used as an air-heating solar collector.

4.2.3 Application to the Metal Panels

Plots of efficiency, η, against $(t_i - t_a)/I$ for the steel panel are shown in Figures 4.7 and 4.8, while Figures 4.9 and 4.10 show corresponding results for the aluminium panel. Results for two

levels of radiation are presented, the higher level corresponding to that stipulated in the ASHRAE 93-77 (1978) test procedure, and the lower level corresponding to conditions more realistic for the U.K. In each case, efficiencies appear higher for the lower radiation level. This is thought to be the result of inaccuracies in the results obtained from the simulator. The causes of the graphical inaccuracies are discussed at the end of this section. In addition, at the lower radiation level, the efficiency plots were found to be more sensitive to the laboratory ambient temperature, which is in agreement with the findings of Green (1979).

Values for F_R and U_L were found from the above plots, while values for F' and U_L were found from plots of η against $(\bar{t}_f - t_a)/I$ (not shown). Tables 4.12 - 4.14 summarise the results.

Table 4.15 summarises the values estimated for the heat transfer coefficients for the tests on the metal panels. For the steel panel, values taken for k_1, d_1, k_2 and d_2 were 55$Wm^{-1}K^{-1}$, 0.0007m, 0.031 $Wm^{-1}K^{-1}$ and 0.05m respectively; for the aluminium panel, the corresponding values were 202 $Wm^{-1}K^{-1}$, 0.0008m, 0.031 $Wm^{-1}K^{-1}$ and 0.05m.

The applicability of the no-leakage model to the metal panels may now be tested. The panels are well-sealed units, so the no-leakage condition is satisfied. The values for the heat transfer coefficients were substituted into the expressions for F' and U_L from the no-leakage model and into the expressions of Parker (1981), and Duffie and Beckman (1980) for flat plate collectors with flow under the absorber. However, the construction of the metal panels is that of trapezoidal flow channels separated by strips of flat plate. Together, these form the

absorber plate, the rear surface of which is bonded to the isocyanate foam backing; the surface of the foam in contact with the corrugated plate is covered with a layer of metallic foil. Thus the metal panels could be regarded as resembling a collector consisting of tubes which form an integral part of a flat metal plate, the spacings between the tubes acting as fins (refer to Figure 4.3 and compare it with Figure 4.11). It was therefore decided to additionally substitute adapted h-values into expressions given by Duffie and Beckman (1980) for a 'fin and tube' collector of the geometry depicted in Figure 4.11 (Type (c), page 237). For this collector type:

$$U_L = U_t + U_b \qquad 4.25$$

$$F' = 1/[(WU_L/\pi Dh) + (W/[D+(W-D)F])] \qquad 4.26$$

where $$F = [\tanh m (W-D)/2] / [m(W-D)/2] \qquad 4.27$$

and $$m = \sqrt{U_L / k\delta} \qquad 4.28$$

In the above expressions, W is the centre to centre distance between tubes, D the tube diameter, k and δ the thermal conductivity and thickness respectively of the absorber plate; h is the fluid/tube heat transfer coefficient. For the metal panels, h was taken as the average of the h_2 and h_3 values in the trapezoidal duct, excluding the enhancement given by equations 4.18, 4.19 or 4.21, 4.22 (used for relating the panel to its 'equivalent flat plate'). In addition, D was taken as simply the width of the trapezoidal duct. The results are summarised in Table 4.16, where they are compared with the experimental values for F' and U_L.

From an inspection of Table 4.16 it can be seen that results based on the no-leakage model, and the models of Parker (1981) and Duffie and Beckman (1980) for a flat plate collector give almost identical values for F' and U_L. This is to be expected, because the metal panels approximate closely to the condition of a thin, highly conducting absorber plate, for which the latter two models were derived. The no-leakage model then tends towards the results from these models for decreasing absorber plate thickness and for increasing thermal conductivity. Compare this with the sealed tiled roof results, where the no-leakage model gives the best agreement overall to the graphical values. However, it is apparent from Table 4.16 that the performance of the metal panels can be described much better by regarding them as 'fin and tube' collectors, as would be suggested by their geometry. Adoption of this approach would mean that several of the tedious area enhancement factor calculations described earlier could be dispensed with. Note that the no-leakage model would be applicable to a construction which gives a single flow channel.

Substitution of the F' and U_L values, calculated using the 'fin and tube' model, into equation 3.26 (steel and aluminium panel areas $1.123m^2$ and $0.933m^2$ respectively, based on the overall widths and lengths) gives values for F_R of 0.53 for the steel panel, test conditions C and D, and 0.50 for the aluminium panel, test conditions E and F. These may be compared with the experimentally measured F_R values of 0.53, 0.46 for the steel panel, test conditions C, D respectively, and 0.53, 0.48 for the aluminium panel, test conditions E, F (Table 4.14).

An inspection of the results in Tables 4.11 and 4.16, however, shows an overall lack of very close agreement between the graphical and calculated results, particularly in the case of U_L.

This is thought to be due to several factors. The calculated values were based on the assumption that, in the laboratory, $t_a = T_s$. This may not be the case, and, as stated earlier, a wall temperature several degrees below t_a would bring the calculated U_L values further into agreement. The values for h_1 were determined for smooth surfaces; roughness would increase these values and hence the U_L values. A 'tiles on laths' structure is a complex one for heat transfer purposes, and so the estimation of h-values can only be approximate. In the no-leakage model, F' and U_L are most strongly influenced by the values of U_t, U_b, k_1, d_1 and h_2. It is therefore recommended that the heat transfer coefficients, particularly h_1 and h_2, for a tiled (stepped) surface, and for a laths structure, be evaluated by careful experimentation, as should values for trapezoidal ducts, for conditions appropriate to the use of these structures as solar collectors. In arriving at figures for insertion into the model, approximations were necessary in obtaining values for k_1 and d_1, and in the treatment of side heat losses (Duffie and Beckman, 1980) for the tiled roof section.

During the analysis, it was noticed that the graphical results, and the value of U_L in particular, were highly sensitive to the laboratory ambient temperature, which was not known accurately. This, combined with the wall temperatures, means that the test sections may have been responding to some effective ambient temperature different from t_a as measured. This would particularly affect an uncovered collector,

more so than glazed units which are better insulated from their test environment. Increased dependence on the wall temperatures would also result from the fairly low windspeeds ($2ms^{-1}$) used in the indoor tests. It is recommended that for indoor tests on uncovered collectors, attention be paid to accurate measurement of the ambient and wall temperatures in the laboratory and to the temperatures of the collector surfaces, and that higher wind speeds be employed, say about $4ms^{-1}$. Consideration should be given to tests in controlled environmental chambers.

The design of the simulator pre-heat module was such that part of the roof duct could 'see' the heating elements, and this could influence the results. This would be most marked in test conditions 'D' and 'F', where the high levels of IRR radiation necessitated higher heating element voltages to generate the full efficiency graphs. It is therefore recommended that to quantify this effect, the pre-heating entrance to the test sections be modified. Edge effects of the test section would also influence the experimental results.

The problems associated with the indoor testing of the roof sections leads to the conclusion that the experimental results presented for efficiency serve only to give the order of magnitude of the F' and U_L values. In view of this, it is concluded that the moderate agreement between the experimental and calculated values is sufficiently good to validate the author's no-leakage model for the prediction of the performance of flat plate collectors when the absorber plate is thick and poorly conducting (such as a tiled roof). In addition, the similarity in behaviour of the no-leakage model to

other flat plate models presented in the literature increases confidence in its validity. It is indicated that a 'fin and tube' model is the most suitable for describing the performance of metal panels of the geometry considered.

For future investigations, it is recommended that the heating simulator be modified, and that improved measuring procedures for surface, ambient and laboratory wall temperatures be adopted. A higher artificial wind speed for uncovered collectors should also be adopted, so as to reduce dependence on wall temperatures, and to remove the uncertainty of any natural convection that may be present; a speed of $2ms^{-1}$, as recommended by Green et al (1980), may be sufficient for covered collectors.

For the testing of solar collectors, it is better to conduct indoor testing in special rooms with a carefully controlled environment, and the findings of the present work indicate that this would be especially important for uncovered collectors. Furthermore, the problem of relating collector performances obtained from indoor tests to those in the field is a common one. Gillett (1980) discusses the effects of cover plate heating, diffuse radiation and variation of longwave radiation on efficiency and the implications for mixed indoor/outdoor tests, concluding that these tests over-estimate the efficiency in poorly designed collectors. Gillett, Rawcliffe and Green (1980) state that indoor thermal radiation raises the efficiency by 2 - 3%.

The results have shown that the inexpensive heating simulator is suitable for producing efficiency characteristics which are only an

order of magnitude indication of the indoor performance of the tile and metal roofs as collectors; since the characteristics presented in the thesis relate to IRR radiation, they should not be taken as representative of the outdoor performance that could be expected. They are, however, adequate for model validation purposes and for the comparative investigation of other thermal effects (discussed in the next section). (Note that the use of the simulator for the testing of glazed collectors would lead to an additional complication because of the higher proportion of infra red radiation in the spectral output of the IRR lamps. Infra red absorption by the glazing would then lead to unrepresentative cover temperatures compared with those attained under the solar spectrum. Differing absorptivities of the tile and metal panel surfaces to the IRR and solar spectra have been discussed in section 4.1).

It would be easier and more appropriate to carry out indoor testing using a proper solar simulator. Better agreement with results calculated from the model may then follow, because of more accurate information on surface absorptivity, and more favourable experimental conditions.

4.3 Investigation of Wind Leakage in a Tile Roof Structure

During the preliminary testing of the heating simulator with the tiled roof section unsealed, it was observed that, in certain cases, the application of wind enhanced, rather than reduced, the measured efficiency characteristics. In the sealed condition, the effect disappeared. Qualitatively, the enhancement was thought to be due to air from outside entering the tile/felt airstream through the untorched tile overlaps. In so doing, heat is removed from the

tile upper surfaces and the energy is transported to the airstream in the duct. The effect is illustrated in Figure 4.12. When a simulated wind was applied over the tile surface, higher values of the air outlet temperature, t_o, were observed.

Further experimentation was carried out in order to quantify the effects mentioned. A theoretical model is proposed in an attempt to explain them, and this 'wind-leakage model' is then applied to two sets of experimental results for the section of unsealed tile roof.

4.3.1 Increase in the Airstream Temperature Rise

The increase in the airstream temperature rise, $(t_o - t_i)$, was investigated in the laboratory by heating the unsealed tile roof structure under IRR radiation with no surface wind. After equilibrium had been reached, the wind fan was switched on, applying a $2ms^{-1}$ wind over the tile upper surfaces. The temperature differences $(t_o - t_i)$ in the duct and $(t_i - t_a)$ were then recorded with time, and graphs plotted. These are shown in Figures 4.13, 4.14 and 4.15, where each plot is numbered. The last graph, Figure 4.15, relates to the tiled roof after sealing and to the steel panel, which act as 'control' experiments. The temperature difference $(t_i - t_a)$ is not shown on the graphs, but remained constant throughout each test. For each test, the air mass flow rate in the duct was measured at both inlet and outlet, and with the wind fan both on and off. In this way, an estimate of the total wind ingress, or leakage, $\dot{m}_w$, for the test section could be made. Tests were conducted at two levels of IRR radiation, and for two basic duct mass flow rates set by the duct fan. The results are summarised

in Table 4.17.

The mass flow rates are the averages of several sets of readings for each test condition. The suction leakage, labelled $\dot{m}_s$ in Table 4.17, is found by subtracting the $\dot{m}$ value measured at the inlet from that measured at the outlet for the case where the external wind fan is off. The suction leakage arises from the Bernoulli effect, where the differing air velocities above and below the tile surfaces create a pressure differential. The total wind leakage, $\dot{m}_w$, for the test section, is found by subtracting the inlet $\dot{m}$ value from the outlet $\dot{m}$ value for the case where the external wind fan is on. Negative values of $\dot{m}_s$ or $\dot{m}_w$ indicate leakage out of the test section. The accuracy of measurement for individual values was $\pm$ 0.004 kg s^{-1}, so positive or negative values for $\dot{m}_s$ and $\dot{m}_w$ smaller than 0.008 kg s^{-1} cannot be regarded as significant under the test conditions.

The graphs (Figures 4.13, 4.14) show that with the application of an external wind over an untorched tile surface, the temperature t_o, and hence the difference $(t_o - t_i)$ (as t_i remains constant), in the duct immediately rises. After a period of time, a new equilibrium state is reached, which can be at a higher (denoted by a '+' sign) or lower (denoted by a '-' sign) value of $(t_o - t_i)$ than the initial (no surface wind) equilibrium state, shown at the start of the plot. Comparing plots 1 with 3 and plots 2 with 4 and referring to the test conditions (Table 4.17) shows that increasing the incident radiation level serves only to increase the temperature of the air injected into the duct airstream (because of higher surface temperatures) and hence to increase the t_o value (greater heights of peaks).

Comparing plots 1 with 2 in Figure 4.13 and plots 3 with 4 in Figure 4.14 shows that the air mass flow rate in the duct is a very critical value in determining the magnitude of the effect of wind application to an unsealed tiled roof. At low duct flow rates, the application of an external wind has a big effect on $(t_o - t_i)$, enhancing the useful gain more than the top heat loss, and thus leading to a higher overall performance when the tile roof is used as an air-heating solar collector. At high duct flow rates, external wind application has a much lesser effect on $(t_o - t_i)$. This is thought to be the result of the fact that, at the higher duct flow rates, there is already substantial leakage into the duct taking place as a result of suction (see Table 4.17, plots 2 and 4), so that when a wind is applied, this has little additional effect and in fact serves to reduce the overall performance by enhancing heat loss from the upper surface more than further enhancing the useful gain. The final equilibrium states for plots 2 and 4 are therefore lower than the initial states.

In the cases of the tiled roof after sealing and the steel panel (a well-sealed unit), Figure 4.15, it can be seen that wind application immediately reduces the value of $(t_o - t_i)$ and hence performance; there are no peaks. Comparing the initial states of plots 5 and 2 (sealed and unsealed tile roof, respectively, and both for the high duct flow rate) shows that the initial steady state for the unsealed case is higher than that for the sealed case. This indicates that the suction effect is already taking place before wind application, which is in agreement with the above hypothesis. For plots 1 and 6, the initial steady states are at approximately the same level; these are for the low duct flow rate so little suction is taking place in the unsealed case. This is confirmed by measurement.

From the results of plot 5, (Table 4.17), the sealed tile roof with the high duct flow rate, there appears to be a significant leakage out of the test section. This must occur from the sides, and shows the edge effects present in the heating simulator (at the low duct flow rate, leakage in or out is negligible).

The experiments described confirm that in the case of an untorched tile roof, wind leakage into the duct increases the $(t_o - t_i)$ value, and hence t_o, and in so doing, can enhance the efficiency characteristics. At high duct flow rates, and no external wind, significant suction leakage occurs. The application of wind in such cases does not further enhance performance, but reduces it (i.e. it is a comparative effect). Several authors have discussed the effects of leaks on the efficiency of air-heating solar collectors (see Close and Yusoff, 1978; Mumma et al 1978). In the present work, benefit is derived since the ingressing leakage air passes over the upper surfaces of the tiles, which are hotter than the lower surfaces. Thus, a supplementary heat source is introduced which raises the outlet air temperature, t_o (this could be regarded as a distinction between 'hot' and 'cold' leaks into a collector).

Optimisation studies, based on further experimentation and the wind-leakage model (see section 4.3.2), should be carried out to determine the best operating condition for a tiled roof in terms of duct flow rate, pressure drops, wind leakage and average meteorological wind speed for a particular area, to extract the maximum benefit from the effects discussed in this section. It is concluded that efficiency enhancement, as a result of wind leakage into the airstream, is increased by reducing the basic fan-induced duct mass flow rate.

4.3.2 A Proposed Theoretical Model

In this section, a simple theoretical approach is proposed to take into account the wind leakage effect described in the previous section. It is known that supplementary energy is introduced to the duct airstream, and that this energy is obtained at the expense of the initial heat loss from the upper tile surface. Thus, it was decided to approach the problem as one of a re-distribution of energy.

Consider an unsealed section of tile roof, area A, with a wind blowing over the upper surface (Figure 4.16). Let Q_u be the useful energy gain by normal heat transfer with the underside of the tiles, and let Q_W be the energy introduced as a result of wind leakage.

$$Q_u = \dot{m}\, C_p\, (t_o"-t_i) \qquad 4.29$$

and

$$Q_W = \dot{m}_w\, C_p\, (t_{inj} - t_a) \qquad 4.30$$

where $\dot{m}$ and $\dot{m}_w$ are, respectively, the mass flow rate drawn at the duct inlet and the total wind leakage mass flow rate for the area, A, considered; $t_o"$ represents the final outlet temperature reached by the air of mass flow rate $\dot{m}$, after normal heat exchange with the lower surfaces of the tiles, but modified because of the injection of warm air along the length of the roof duct; t_{inj} is the temperature at which the wind leakage air is injected to the airstream; t_i and t_a are the air temperature at the duct inlet, and above the upper tile surface respectively; C_p is the specific heat capacity of air at constant pressure. One may now write a re-arranged form of equation 3.1 to include the wind-leakage energy:

$$IA(\tau\alpha)_e = (Q_u + Q_W) + [U_L A(\bar{t}_p - t_a) - Q_W] \qquad 4.31$$

where the remaining symbols are defined in Chapter 3. By introducing the plate efficiency factor with wind leakage, F'_W, defined as:

$$F'_W = \frac{\text{useful + leakage energy collection rate}}{\text{useful + leakage energy collection rate if the tile plate were at a temperature of } \bar{t}_f}$$

it can be shown that:

$$\eta_W = (Q_u + Q_W)/IA = F'_W(\tau\alpha)_e - F'_W U_{LW}(\bar{t}_f - t_a)/I \qquad 4.32$$

where the subscript 'W' indicates that wind leakage is now involved; also $\bar{t}_f$ is the average fluid temperature, but with wind leakage to the airstream, and t_o will be the overall outlet temperature from the duct, including the leakage air. Thus, a form of the Hottel - Whillier - Bliss equation is still valid to describe the behaviour of the tiled roof collector with wind leakage. The useful energy is enhanced while the heat loss is (effectively) reduced (i.e. a fraction of the initial top heat loss is returned as useful energy), and efficiency characteristics obtained in the heating simulator for the unsealed section of tiled roof showed higher F' values, and lower U_L values, than those of the corresponding 'sealed' experiment. To quantify this effect, and the effect of the higher outlet temperature, t_o, discussed in section 4.3.1, values for Q_u and Q_W must be found. Note that Q_u in the unsealed case is not the useful energy for the simple case of a sealed tile roof section, because the injection of warm air takes place along the length of the roof duct, and so will modify the useful energy gain by the normal exchange process with the undersurfaces of the tiles. The approach to the problem is now presented in more detail.

The simplifying assumptions are, in general, the same as those adopted in section 3.2.3, but now injection of air is considered to take place at the tile overlaps in the lateral direction only, and not through any longitudinal gaps (in fact, nearly all the longitudinal gaps will have a solid tile surface beneath because of the staggered construction of each row, so this assumption is reasonable as a first approximation). Each tile row is then treated as a separate small sub-collector, the output from one row becoming the input to the next, and so on, for the full length of roof from eaves to ridge. The temperature rise of the stream air for each tile row is the result of normal heat exhange with the solid tile undersurface (this can be modified - see later). At the end of each tile row, a mass flow rate of air $\dot{m}'_w$ at temperature t_{inj} is injected at the discreet overlap strip; this mixes with the duct airstream to produce a mass flow rate of air increased by an amount $\dot{m}'_w$ and at a temperature found by mixing the respective duct and injection stream temperatures in the ratios of the mass flow rates. This then forms the input to the next tile row. The procedure is schematically illustrated in Figure 4.17.

Each tile sub-collector is numbered 1, 2, 3 ....n etc. For r rows of tiles there are (r - 1) overlaps, and $\dot{m}'_w$ is found from:

$$\dot{m}'_w = \dot{m}_w/(r - 1) \qquad 4.33$$

where $\dot{m}_w$ is the total wind leakage into the duct for the tile roof section area A considered, and $\dot{m}'_w$ is the leakage at each overlap. This assumes equal leakage at each overlap. The injected air enters the overlap at temperature t_{ent} and is injected to the airstream at temperature t_{inj}. It is further assumed that t_{ent} and t_{inj} are

constant for the entire roof length. One may now write, for the n^{th} tile row:

$$\eta_n = -F_R U_L (t_{i\,n} - t_a)/I + F_R(\tau\alpha)_e \qquad 4.34$$

where $t_{i\,n}$ is the inlet temperature to the n^{th} tile row, found by mixing the main stream, at temperature $t_{o\,(n-1)}$, and the injected stream, at temperature t_{inj}, in the ratios of the mass flow rates. The outlet temperature from the n^{th} tile row, $t_{o\,n}$, after normal heat exchange with the underside is given by:

$$t_{o\,n} = \eta_n [IA_n/(\dot{m} + \sum_{o}^{(n-1)} \dot{m}'_w)C_p] + t_{i\,n} \qquad 4.35$$

where A_n is the exposed area of the n^{th} tile row.

Now inject the stream $\dot{m}'_w$ at temperature t_{inj}:

$$t_{i(n+1)} = [1/(\dot{m} + \sum_{o}^{n} \dot{m}'_w)][(\dot{m} + \sum_{o}^{(n-1)} \dot{m}'_w)t_{o\,n} + \dot{m}'_w t_{inj}] \qquad 4.36$$

giving the inlet temperature to the $(n+1)^{th}$ tile row, $t_{i(n+1)}$. Note that for a constant t_{inj} and $\dot{m}'_w$, the effect of injection on the air temperature in the duct becomes less with increasing duct length. This procedure can be repeated for the full length of tile roof to provide the final outlet temperature, t_o, from an unsealed tile roof with wind leakage into the duct.

To use the procedure, it is necessary to know the value of t_{inj}. For each tile overlap, D_e is 0.002 m, and evaluation of Re (velocity found from equation 3.27 for the mass flow rate $\dot{m}'_w$) indicates

laminar flow. The local Nusselt number, Nu, for laminar flow between two flat plates with one side insulated and the other side heated with a constant heat flux is given, for Pr = 0.7, by Duffie and Beckman (1980) as:

$$Nu = Nu_{fd} + \frac{0.00190\ (RePrD_e/L)^{1.71}}{1 + 0.00563\ (RePrD_e/L)^{1.17}} \qquad 4.37$$

where Nu_{fd} = 5.4 and L is the plate length. Evaluating this expression for the length of the tile overlap and the narrow tile spacing showed that the average Nu was almost the same as the value for Nu_{fd}. This led to h-values in the overlaps of about 70 $Wm^{-2}{}^{\circ}C^{-1}$. Hence, by assuming values for t_{ent} and the tile surface temperatures in the overlaps, a value for t_{inj} may be estimated. However, a value was subsequently determined by measurement; this was found to agree well with that calculated by the above. Further measurements conducted in relation to the use of the wind-leakage procedure are described in section 4.3.3.

In equation 4.34 of the wind-leakage procedure, values for F_R (obtained from F') and U_L should, strictly speaking, be determined for each individual tile row for the appropriate airstream mass flow rate beneath that row. As a simplifying approximation, however, F', F_R and U_L were evaluated for the average mass flow rate in the whole duct, which is, for the area, A, of roof considered, $\dot{m} + (\dot{m}_w/2)$. The no-leakage model derived and tested earlier can be used to obtain these values, using h-values for the appropriate temperatures and mass flow rates.

While heat transfer coefficients h_1 and h_2 could be determined as before for a solid wall surface, an additional refinement may be introduced. The unsealed tile roof with wind leakage may be regarded as a porous surface, with suction on the upper side, and injection on the lower side. These effects are discussed in several heat transfer texts (see, for example, Kays, 1966; Eckert and Drake, 1972) where it is shown that suction increases heat transfer by thinning the boundary layer and injection decreases heat transfer by thickening the boundary layer. Thus, for the tiled roof, h_1 would increase and h_2 would decrease; F', F_R and U_L could therefore be evaluated for a porous surface with modified values for h_1 and h_2.

Estimation of Re for external flow over the tiles with a $2ms^{-1}$ wind indicates laminar flow (the critical Re being 5×10^5). Kays (1966) gives, for a laminar boundary layer, values for $Nu_x\ Re_x^{-0.5}$ for various Pr numbers and for different values of $(u_1/v_1)(\rho v_1 x/\mu)^{0.5}$, where x is the distance along the plate from the leading edge, u_1 is the fluid velocity normal to the surface due to suction, v_1 is the free-stream wind velocity parallel to the surface, and the remaining symbols are defined in Chapter 3. An estimation of u_1 and the other values from measurements for the conditions of two experiments (see section 4.3.3) led to average increases in Nu over a solid wall case of between 172% and 187%. Thus the increased value of h_1 for suction may be estimated.

For turbulent forced convection between parallel plates with injection, Lee and Gill (1964) have established the relation:

$$h/h_o = \alpha' \phi' / (e^{\alpha' \phi'} - 1) \qquad 4.38$$

where h and h_o are, respectively, the heat transfer coefficients with and without injection, α' is 1/1.1 for injection (1/1.2 for suction), and ϕ' is given by:

$$\phi' = Re_{wall} Pr \qquad 4.39$$

and

$$Re_{wall} = Du / \nu \qquad 4.40$$

where Re_{wall} is the wall Reynolds number, D is the plate separation, u is the transverse fluid velocity at the wall (i.e. the normal component) and ν the kinematic viscosity. Estimation of u and the other values led to:

$$h \simeq 0.0784\ h_o \qquad 4.41$$

and

$$h \simeq 0.0852\ h_o \qquad 4.42$$

for the test conditions of the two experiments to be described. Thus the reduced value of h_2 for injection may be estimated. The values for h_1 and h_2, modified for suction and injection respectively, may be inserted into the no-leakage model to obtain values for F', F_R and U_L to be used in equation 4.34 of the wind-leakage model. It is possible to obtain, therefore, two sets of values for F_R and U_L, one for a porous wall with the modified boundary layers, and the other for a solid wall. Both sets are used in the next section.

The value for Q_u, the useful energy gain by normal heat exchange with

the tiles, will differ in the unsealed case from that in a sealed case because of the injection of warm air. The value $Q_{u\ n}$ for the n^{th} tile row is calculated using (refer again to Figure 4.17):

$$Q_{u\ n} = (\dot{m} + \sum_{o}^{(n-1)} \dot{m}'_w)Cp(t_{o\ n} - t_{i\ n}) \qquad 4.43$$

The Q_u values for each tile row are then summed to arrive at the total Q_u value for the full length of roof (note that insertion of the total Q_u value in equation 4.29 would produce the value of t_o" for a known value of t_i). Q_W is found from equation 4.30. Adding the total Q_u and Q_W values gives the full useful energy for the unsealed tile roof with wind leakage into the airstream.

So far, the wind-leakage model may be used to predict both the final outlet temperature and the actual total useful energy for an unsealed tiled roof. It may be possible to extend the model in order to theoretically predict F'_W and U_{LW} values (refer to equation 4.32). In an attempt to do this, the no-leakage model was modified to account for the additional useful energy, in the following manner.

For the temperatures and conditions of a wind-leakage case, one may calculate, using the no-leakage model, values for F' and U_L based on the duct air mass flow rate as measured at the inlet (i.e. simple $\dot{m}$'), and no leakage. A value for useful energy may then be found, and since this will not be the true, or actual, useful energy for the particular wind-leakage case, call it the pseudo-useful energy, Q'_u. The actual total useful energy ($Q_u + Q_W$) for the

case of leakage may be calculated using the proper procedure described. Thus, an effective wind-leakage energy, Q'_W, could be evaluated, such that:

$$(Q'_u + Q'_W) = (Q_u + Q_W) \qquad 4.44$$

The following modification to the no-leakage model, when applied to a leakage case, is now proposed.

Since the effective wind-leakage energy, Q'_W, has been obtained at the expense of heat loss from the upper surface, the heat transfer coefficient h_1 can be re-defined as:

$$h_{1W} = h_1 - Q'_W \;/\; A(T_1 - t_a) \qquad 4.45$$

where h_{1W} is an effective convection heat transfer coefficient for wind leakage (the remaining symbols are defined elsewhere).

The effective wind-leakage energy Q'_W is an addition to the energy gained by the airstream in passage under the tiles. The heat transfer coefficient h_2 can be re-defined as:

$$h_{2W} = h_2 + Q'_W/A(T_2 - \overline{t}_f) \qquad 4.46$$

where h_{2W} is an effective convection heat transfer coefficient for wind leakage.

The newly-defined h-values are for use in a no-leakage (i.e. solid wall) model. Thus, the additional energy Q'_W must be 'apparently'

conducted through the tile absorber plate. By re-arranging equation 3.8, one can re-define the thermal conductivity k_1 as:

$$k_{1W} = [d_1/(T_1-T_2)][h_{2W}(T_2-\bar{t}_f) + h_{r23}(T_2-T_3)] \qquad 4.47$$

where k_{1W} is an effective absorber plate thermal conductivity for wind leakage.

Replacing h_1 by h_{1W} in equations 3.22 or 3.23 results in a value U_{tW}, an effective overall top heat loss coefficient for wind leakage; replacing U_t, h_2 and k_1 in equations 3.20 and 3.21 by U_{tW}, h_{2W} and k_{1W} results in theoretical values for F'_W and U_{LW}.

In this section, a model has been proposed to account for the effects of wind leakage in a tile roof structure when used as an air-heating solar collector. Using the model, it is possible to calculate values for the final outlet temperature of the duct air, the actual useful energy gain, and values for F'_W and U_{LW}. It is useful to summarise the procedure as follows:

(a) Using the no-leakage model, obtain average values for F' and U_L for an average duct mass flow rate of $\dot{m} + (\dot{m}_w/2)$. Values for a solid and/or porous wall may be calculated.

(b) Using the value of F' above, calculate a value for F_R for insertion into equation 4.34, together with U_L (these are average values to be used for each sub-collector). Calculate a value of η for a given t_i, and then calculate t_o from equation 4.35.

(c) Inject a wind-leakage stream $\dot{m}'_w$ at temperature t_{inj} and mix in the ratios of the mass flow rates to get the entry

temperature for the next sub-collector (equation 4.36). Repeat the process (equations 4.34 - 4.36) for each tile for the full length of roof. Hence obtain the final outlet temperature.

(d) Calculate the Q_u values for each sub-collector (equation 4.43) and sum for the full length of roof. Calculate Q_W from equation 4.30. Adding the total Q_u and Q_W values gives the total actual useful energy gain for the whole roof.

(e) Use the no-leakage model for the temperatures and conditions of the wind leakage case, but with the mass flow rate as measured at the inlet, and no leakage, to calculate a pseudo-useful energy, Q_u'. From the actual total useful energy, evaluate an effective wind-leakage energy Q_W' (equation 4.44).

(f) Use Q_W' to define the effective values h_{1W}, U_{tW}, h_{2W} and k_{1W}. Insert these into the no-leakage model and obtain values for F_W' and U_{LW}.

Parts (e) and (f) can be repeated for a set of experimental efficiency data, but with Q_u' replaced by a pseudo-useful energy value Q_u'' obtained from the experiment and based on the 'simple' $\dot{m}$ value as measured at the duct inlet and the measured temperature rise across the collector. Calculating a corresponding Q_W'' value leads to values for F_W' and U_{LW}. These should be the same as those found by pure calculation.

In the next section, the wind-leakage model is applied to two sets of experimental data.

4.3.3 Application to the Section of Unsealed Tile Roof

Before the wind-leakage model could be applied, further experimental results were necessary in order to utilise all aspects of the model to the full. Thus, values for the velocities of suction (upper tile surface) and injection (lower tile surface) were measured as, approximately, $0.9ms^{-1}$ and $0.16ms^{-1}$ respectively, in directions almost tangential to the surfaces. From these, normal velocity components were estimated which led to the Nu increases (suction) or decreases (injection) over the solid wall case given in the previous section.

Measurements for the overlap entry temperature, t_{ent}, led to the following empirical correlation:

$$t_{ent} \simeq \left[[(T_1 + t_a)/2] + t_a \right] /2 \qquad 4.48$$

while measurements of the injection temperature, t_{inj}, showed temperature rises ($t_{inj} - t_{ent}$) in the region of 1-3°C. These agreed with values obtained from calculation of t_{inj} using equation 4.37 of the previous section. The temperature of the injected air was also observed to increase for successive rows. This effect was not included in the present wind-leakage procedure, but the model is sufficiently flexible for this effect to be incorporated if required.

Values for the total leakage rate, $\dot{m}_w$, appropriate to the test conditions, were obtained from the measurements detailed in section 4.3.1. The assumptions of equal mass injection per unit time at

each overlap, and in the lateral direction only, were, on the whole, confirmed by measurement to be valid.

The wind-leakage model was applied for the conditions of two efficiency plots generated for the section of unsealed tile roof in the heating simulator. The experimental conditions are summarised in Table 4.18.

Using the same theoretical approach as described in sections 4.2.1 and 4.3.2 for evaluation of heat transfer coefficients, the following values were obtained for an average duct mass flow rate of $\dot{m} + (\dot{m}_w/2)$ - refer to part (a) of the procedure summary, section 4.3.2. The values, for both solid and porous wall cases, are presented in Table 4.19.

From the no-leakage model, the following values for F', U_L and F_R were calculated:

test condition G (SOLID: $F' = 0.13$; $U_L = 34\ Wm^{-2}{}^{\circ}C^{-1}$; $F_R = 0.12$.
(POROUS: $F' = 0.03$; $U_L = 76\ Wm^{-2}{}^{\circ}C^{-1}$; $F_R = 0.03$.

test condition H (SOLID: $F' = 0.29$; $U_L = 34\ Wm^{-2}{}^{\circ}C^{-1}$; $F_R = 0.29$.
(POROUS: $F' = 0.08$; $U_L = 77\ Wm^{-2}{}^{\circ}C^{-1}$; $F_R = 0.08$.

Using these values for F_R and U_L and equations 4.34, 4.35 and 4.36, values for the final outlet temperature from the laboratory test section were calculated (eight rows of tiles, seven overlaps) - refer to parts (b) and (c) of the procedure summary, section 4.3.2. To illustrate the procedure, a sample of the calculation (for test condition G, tile row 3 [i.e. n = 3], with the porous wall F_R and U_L

values, and with rounded figures) is now presented:

For tile row 3: $t_{i3} = 23.203°C$; $t_a = 20.760°C$; $I = 304\ Wm^{-2}$; $(\tau\alpha)_e = 0.45$; $F_R = 0.03$; $U_L = 76\ Wm^{-2}°C^{-1}$.

Using equation 4.34 and the above data, $\eta_3 = -0.0048$.

For tile row 3: $A_3 = 0.1426m^2$, and $(\dot{m} + \dot{m}'_w + \dot{m}'_w) = 0.0198kg\ s^{-1}$.

From equation 4.35, $t_{o3} = 23.193°C$.

Now add $\dot{m}'_w = 0.0024kg\ s^{-1}$ at temperature $t_{inj} = 25.2°C$ and mix in the ratios of the mass flow rates (equation 4.36):

From equation 4.36, $t_{i4} = 23.410°C$.

Thus, the input temperature to tile row 4 is obtained. The procedure above is repeated for each successive row for the roof length from eaves to ridge. For the laboratory section of eight rows of tiles, Tables 4.20 and 4.21 present the inlet (t_i) and outlet (t_o) temperatures for each tile row calculated using the procedure illustrated. Table 4.20 relates to test condition G, and to the porous wall values for F_R and U_L. The difference between the value of t_{i4} shown in Table 4.20 and that shown above is the result of rounding errors. Note the cooling that takes place, by the normal heat exchange process, for each individual tile from inlet to outlet. The values are given to three decimal places merely to show this effect. Table 4.21 relates to test condition H, and to the solid wall values for F_R and U_L.

Table 4.22 presents the final outlet temperatures, t_o, together with temperature rise values $(t_o - t_i)$, for both test conditions, as calculated using the wind-leakage model. They are compared with the corresponding measured values.

Inspection of Table 4.22 shows that the wind-leakage model predicts approximately the right outlet temperature and hence the temperature rise for an unsealed tile roof, and particularly for high leakage rates at lower radiation levels.

Treating the tile absorber plate first as a solid wall and then as a porous wall (i.e. including the effects of suction and injection on the boundary layers) produces slightly differing results. If one defines a leakage fraction, L.F., as:

$$\text{L.F.} = \frac{\text{Total leakage mass flow rate into the duct, } \dot{m}_w}{\text{Total mass flow rate in the duct, as measured at the outlet, } (\dot{m} + \dot{m}_w)}$$

for the total area under consideration, then, for test condition G, L.F. = 0.0177/0.0324 = 0.546, or about 55%; for test condition H, L.F. = 0.0140/0.1201 = 0.117, or about 12% ($\dot{m}$ is the duct mass flow rate as measured at the inlet). Now note that, in Table 4.22, the porous wall approach gives the better agreement to the measured values of t_o and $(t_o - t_i)$ for test condition G, where the higher L.F. applies, whereas the solid wall approach is better in test condition H, where the lower L.F. applies. However, further measurements would need to be obtained for a variety of carefully controlled test conditions to ascertain whether the above observations are significant.

Utilising equation 4.43, a total value for Q_u for the full test section length may be found for both test conditions. These (rounded) values are, for condition G, - 2.2 Watts (i.e. the air loses energy - refer to Table 4.20), and, for condition H, 84.5 Watts. Equation 4.30 gives the values for Q_W, which are 75.7 Watts (condition G) and 81.0 Watts (condition H). Thus, for test condition G, leakage provides the only useful energy contribution. Adding the total Q_u and Q_W values gives the total actual useful energy, $(Q_u + Q_W)$, for the roof with wind leakage - refer to part (d) of the procedure summary. The values are summarised below:

$(Q_u + Q_W) = 73.5$ Watts (test condition G);

$(Q_u + Q_W) = 165.5$ Watts (test condition H).

Calculated values for F_W' and U_{LW} are found by firstly evaluating heat transfer coefficients for the test conditions G and H, based on the mass flow rate as measured at the duct inlet, and for a solid wall. Insertion of these in the no-leakage model gives values for F' and U_L for substitution into a rearranged form of equation 3.3; this provides a value for Q_u', a pseudo-useful energy, for each test condition. Equation 4.44 then gives a value for Q_W', an effective wind-leakage energy - refer to part (e) of the procedure summary. The rounded values are:

$Q_W' = 68.8$ Watts (test condition G);

$Q_W' = 84.1$ Watts (test condition H).

Use of the values for Q_W' and equations 4.45, 4.46 and 4.47 leads to values for h_{1W}, h_{2W} and k_{1W}. These are summarised in Table 4.23, together with the h-values obtained for use in the no-leakage model (procedure summary, part (e)).

Insertion of the effective values U_{tW}, k_{1W} and h_{2W} in place of U_t, k_1 and h_2 in the no-leakage model provides calculated values for F_W' and U_{LW} (wind-leakage procedure summary, part (f)).

Parts (e) and (f) of the procedure may be repeated for an experimentally-based pseudo-useful energy, $Q_u"$, in place of Q_u'. 'Simple' efficiency plots for test conditions G and H were obtained in the heating simulator. The measured useful energy in these cases was based on the air mass flow rate as measured at the duct inlet, and the temperature rise as measured across the outlet and inlet. Clearly, this cannot be the actual useful energy gain, so let it be designated as the experimental pseudo-useful energy, $Q_u"$. An effective experimental wind-leakage energy, $Q_W"$, may now be calculated from an expression similar to that of equation 4.44:

$$(Q_u" + Q_W") = (Q_u + Q_W) \qquad 4.49$$

From the efficiency plots for conditions G and H, average values of $Q_u"$ were obtained for each; from equation 4.49, an average value for $Q_W"$ was calculated for each experiment. These were:

$Q_W"$ = 53.1 Watts (test condition G);

$Q_W"$ = 4.5 Watts (test condition H).

The above values for $Q_W"$ were then added to each of the experimentally measured $Q_u"$ values to produce the 'true' wind-leakage efficiency characteristics for test conditions G and H. These are shown in Figures 4.18 and 4.19. The results of linefits are given in Table 4.24, while Table 4.25 summarises the experimental values for F_W', U_{LW} and F_{RW} (subscript 'W' refers to the case of wind leakage). Comparison of the F_W' and U_{LW} values for test condition G with the

corresponding F' and U_L values for the sealed case (test condition B, Table 4.11) shows that the effect of wind leakage is to enhance the value of F' and reduce the value of U_L.

The purpose of the latter exercise is to show that 'true' efficiency plots and F'_W and U_{LW} values can be obtained from any set of 'simple' experimental efficiency data, by using the wind-leakage model (note that leakage rates and relevant temperatures must be known). These values for F'_W and U_{LW} should agree with those obtained by calculation based on the pseudo-useful energy Q'_u. The comparison is shown in Table 4.26.

The agreement between the 'experimental' and calculated values for F'_W and U_{LW} is seen, in general, to be fairly good, except for the value of U_{LW} in test condition H. This could be due to the factors discussed in section 4.2.3 for the sealed condition. A single overall value for Q_W", found from equation 4.49, was added to each of the measured Q_u" values based on the inlet mass flow rate and the measured temperature differences $(t_o - t_i)$; this is a simplification. Also, the values calculated for h_{1W}, h_{2W} and k_{1W} (equations 4.45 - 4.47) are very sensitive to temperature differences.

Substitution of the F'_W and U_{LW} values, calculated using the wind-leakage model based on Q'_u, into equation 3.26 gives values for F_{RW} of 0.42 and 0.69 for test conditions G and H respectively. These may be compared with the respective 'experimental' values for F_{RW} of 0.57 and 0.63 (Table 4.25).

It is concluded that the wind-leakage model presented is adequate to predict the outlet air temperature (from a known inlet temperature) from an untorched tile roof when used as an air-heating solar collector, and also the actual useful energy gain from two energy sources - normal heat exhange with the lower surfaces of the tiles, and wind leakage. The correct trends are predicted in the theoretical calculation of F'_W and U_{LW}, i.e. that of raising the value of F' and lowering the value of U_L compared with the case of a sealed roof. The model permits the 'true' efficiency graph to be generated from a set of results based on pseudo-useful energies. It is recommended, however, that further, more detailed experimentation be devised to test the model to the full.

Knowledge of typical leakage rates for various types and constructions of tiles on laths is important for the proper performance evaluation of conventional roofs as air-heating solar collectors. Values could be obtained from experimental equipment similar in construction to that of the heating simulator. It is suggested that investigations should commence into the feasibility of developing a novel design of collector incorporating a louvered, variable-slot absorber plate with airflow across the upper surface.

4.4 Comparison of Time Constants

The time constant of a collector is defined in ASHRAE 93-77 (1978) as the time required for the quantity $(t_{o\ final} - t_i)/(t_{o\ initial} - t_i)$ to fall to 36.8% of its initial value. With the heating simulator, the time constants of the roof structures were measured by initially

holding the system in a steady state condition, with $t_i = t_a$ (i.e. no air pre-heating) and I = 305 Wm^{-2}; the lamps were then switched off, reducing the incident radiation to zero, and the value of $(t_o - t_i)$ was recorded as a function of time. Values of the time constants for each structure, with and without wind, were calculated, and are presented in Table 4.27, where they are compared with that of the air panel of Hill et al (1978).

The significantly longer time constants of the tiled roof section, compared with those of the metal panels and purpose-designed panel, render its response time slower to transient weather conditions. Note that for the laboratory section of tiled roof with a wind of $2ms^{-1}$, the time constant for the unsealed condition is shorter than that for the sealed condition; this is because of the leakage through the tile structure. MacGregor (1979) has reported that from tests on water heating collectors, a large absorber plate thermal capacity (proportional to the time constant) gives only a slight reduction in the overall seasonal energy collected. A 'heavier' collector has a heat storage capability which can be exploited by running the system to a later time. When a tiled roof is used as the pre-heater for a heat pump, the heat pump switch-on can be set back in the morning and the pump allowed to operate until later into the evening to recover some of the stored energy (and also to take advantage of house heat loss in the evening, depending on family occupancy patterns).

4.5 Estimates of Fan Power

The theoretical fan power, P_{th}, required to draw a mass flow rate $\dot{m}$ of air, density ρ, through a duct or collector is given by (ASHRAE 93-77, 1978):

$$P_{th} = \dot{m}\, \Delta p/\rho \qquad 4.50$$

where Δp is the operational pressure difference. The pressure difference $p_1 - p_2$, where p_1 is the static pressure at the duct inlet and p_2 the static pressure at the duct outlet, may be calculated from an expression given by McAdams (1954):

$$p_1 - p_2 = [(f \rho v_m^2/2\, D_e)(x_2 - x_1)] + g\rho(z_2 - z_1) \qquad 4.51$$

where $(x_2 - x_1)$ is the duct length between outlet and inlet, $(z_2 - z_1)$ is the difference in the height between outlet and inlet for an inclined duct, f is the friction factor, v_m is the mean velocity of the air in the duct, D_e is the duct equivalent diameter and g is the acceleration due to gravity.

Evaluation of the above expressions for the laboratory roof test sections, together with relations for the appropriate types of entrance and exit (McQuiston and Parker, 1977), and including changes in velocity pressure so as to arrive at the total pressure drop, led to the results summarised in Table 4.28; also shown are the comparisons with the actual fan power required.

For the test house, calculation of the static pressure drop for

air flow in the channel, but for no net change in height (as the heat pump and eaves are at the same level) gave a value of 0.2 Pa. Taking the height into account, the value would be 23.7 Pa. Accordingly, the theoretical fan power requirement would be low, and not compatible with the value for supplied fan power experienced on site. It was concluded that the performance of the installed fan was in response to pressure drops additional to those of the tile/felt air channels. It was noted that the measured air flow rate through the fan on site was significantly less than that quoted by the manufacturer. This could be due to blockages in the evaporator coil matrix, and to the nature of the wall exit, which incorporated a flap to exclude birds.

The motor and static efficiencies of the installed propeller fan were estimated to be 55% and 30% respectively, based on the manufacturer's data. The fan motor was rated 1/3 h.p. (249 Watts). For a measured mass flow rate of 0.9 kg s^{-1}, the total theoretical fan power, P_{th}, and total operational pressure drop, Δp, (i.e. inclusive of velocity pressure), were estimated as 78.6 Watts and 110.2 Pa respectively, for the existing roof system. On this basis, an attempt was made to assess the fan power consumption for a roof made up of the steel panels tested in the laboratory. Both the North West and South East facing sides of the test house roof were considered to be of steel and the value of 0.9 kgs $^{-1}$ was taken for the total air mass flow rate. As a result of the increased resistance to flow presented by the steel panels, as found in the laboratory tests, ducting between the steel roof ridge and heat pump inlet was considered to be installed. The net resistance of this system was estimated to be 48.8 Pa (for no

additional change in velocity pressure compared with the existing system), which is additional to the 110.2 Pa for the existing system. The total operational pressure drop for the fan would be, therefore, 159.0 Pa. From the fan laws (McQuiston and Parker, 1977), one may write:

$$P_{a\ sh} / P_{b\ sh} = (p_a/p_b)^{1.5} \qquad 4.52$$

where P_{sh} is the shaft power and p is the total pressure drop. Using this expression, a value for shaft power of 431 Watts was calculated. For an electrical efficiency of 55%, a value of 780 Watts was obtained for the fan power consumption with a steel roof and ducting. Table 4.29 summarises the estimates.

Thus, a fan power of about 780 Watts would be needed to draw a mass flow rate of 0.9 kg s^{-1} through a steel roof and ducting, a substantial increase over the fan power required to draw the same mass flow rate through the existing test house roof. This value is used in Chapter 7.

For the tile roof, the average seasonal air temperature rise is 1.4°C (see Chapter 6). For a steel roof, the average temperature rise is estimated to be 3.0°C (see Chapter 7). Use of equation 3.5 for these temperature rises and for an air mass flow rate of 0.9 kg s^{-1} gives values for the average rate of useful energy gain of the air passing through each roof system of 1268 Watts (tile roof) and 2716 Watts (steel roof). These figures may be compared with the figures for supplied fan power of 450 Watts and 780 Watts for the tile and

steel roofs respectively. However, a decision concerning the benefits to be obtained by using a steel roof should be based on the evaluation of the system performance as a whole (see Chapter 7).

4.6 Summary

Values for $(\tau\alpha)_e$ have been deduced for Dreadnought and Delta tile surfaces and for the corrugated metal panels, both for IRR radiation in the indoor heating simulator and for AM2 solar radiation. These values were utilised in the theoretical models.

The no-leakage model derived in Chapter 3, together with other models, has been applied to the roof sections tested in the laboratory, and the values for F' and U_L, calculated from insertion of estimated heat transfer coefficients, have been compared with values obtained experimentally. This has shown that the no-leakage model is valid to describe the behaviour of a tiled roof used as an air-heating solar collector, and that the performance of the corrugated metal panels is best described by a 'fin and tube' model, presented by Duffie and Beckman (1980). Limitations to the accuracy of experimental results obtained with the heating simulator have been discussed, and modifications to reduce uncertainties have been suggested.

Wind leakage into an unsealed tile roof structure was found to raise the value of F' and lower the value of U_L compared with results from a sealed roof. In addition, the outlet air temperature was found to be increased. Experiments to investigate and quantify these effects have been described, and a wind-leakage model has been

proposed in an attempt to explain the results. The model has been shown to adequately predict the outlet air temperature (from a known inlet temperature) from an unsealed tile roof, and can be used to calculate the useful energy gain. It predicts an increase in the value of F' and a decrease in the value of U_L for a change from a sealed to an unsealed condition. It may also be used to produce 'true' efficiency graphs from sets of data based on experimental pseudo-useful energies.

Measurements of time constants for the test sections have been carried out and estimations have been made of fan power requirements; the results have been related to the test house situation.

Conventional roofs may be utilised as pre-heaters for air source heat pumps (in a domestic or industrial retrofit situation, for example), and the models presented can be used in conjunction with heat pump performance characteristics to predict the expected values for heating mode coefficients of performance, COP(H). An agricultural application for such roofs might be near - ambient temperature grain and hay drying (see Ferguson and Bailey, 1981).

LAMP VOLTAGE	SURFACE ABSORPTIVITY, α , TO IRR RADIATION, RANGE 0.3 - 2.1 μm	
	DREADNOUGHT (ROOF SECTION)	DELTA
160	0.40 $\pm$ 0.02	0.66 $\pm$ 0.02
100	0.38 $\pm$ 0.02	0.66 $\pm$ 0.02

Table 4.1 Average surface absorptivities of tiles to IRR radiation, for the range 0.3 - 2.1 μm.

LAMP VOLTAGE	SURFACE ABSORPTIVITY, α, TO IRR RADIATION, RANGE 0.3 - 2.1 μm	
	STEEL PANEL	ALUMINIUM PANEL
160	0.92 $\pm$ 0.02	0.93 $\pm$ 0.02
100	0.92 $\pm$ 0.02	0.93 $\pm$ 0.02

Table 4.2 Surface absorptivities of metal panels to IRR radiation, for the range 0.3 - 2.1 μm.

WAVE LENGTH λ, μm	λT, μm K	FRACTION OF ENERGY BETWEEN O AND λT	$\frac{E(\lambda_a - \lambda_b)}{\sigma T^4}$ %	λ VALUE AT WHICH TO TAKE THE R_λ VALUE, μm	R_λ VALUE (CORRECTED) OF THE SAMPLE TESTED, %	$\frac{R_\lambda E(\lambda_a - \lambda_b)}{\sigma T^4}$
"	"	"	"	"	"	"
"	"	"	"	"	"	"
0.95	1988.4	0.0650	)			
			) 1.691	0.975	37.8	63.92
1.00	2093.0	0.0819	))			
			) 1.861	1.025	41.0	75.74
1.05	2197.7	0.1005	))			
			) 2.003	1.075	43.8	87.63
1.10	2302.3	0.1205	)			
"	"	"	"	"	"	"
"	"	"	"	"	"	"

Table 4.3 Sample of the weighted ordinate method ($\Delta\lambda$ = 0.05 μm) employed on a Dreadnought tile sample for a black body distribution with T = 2093K.

LAMP VOLTAGE	SURFACE ABSORPTIVITY, α , TO IRR RADIATION, RANGE 2.1 - 3.6 μm			
	TILES		METAL PANELS	
	DREADNOUGHT	DELTA	STEEL	ALUMINIUM
160	0.51	0.71	0.92	0.93
100	0.51	0.71	0.92	0.93

Table 4.4 Surface absorptivities to IRR radiation, for the range 2.1 - 3.6 μm.

LAMP VOLTAGE	SURFACE ABSORPTIVITY, α, TO IRR RADIATION, RANGE BEYOND 3.6 μm			
	TILES		METAL PANELS	
	DREADNOUGHT	DELTA	STEEL	ALUMINIUM
160	0.85	0.93	0.87	0.86
100	0.85	0.93	0.87	0.86

Table 4.5 Surface absorptivities to IRR radiation, for the range beyond 3.6 μm.

SURFACE	AVERAGE EMISSIVITY, ± 0.04
DREADNOUGHT TILES	0.85
DELTA TILES	0.93
SANDED BITUMINOUS FELT	0.84
STEEL PANEL:	
UPPER SURFACE ('PLASTISOL')	0.87
LOWER SURFACE	0.83
ALUMINIUM PANEL:	
UPPER SURFACE (COLOUR BOND)	0.86
LOWER SURFACE	0.44

Table 4.6 Some of the measured broad band thermal emissivity values.

TEST CONDITIONS FOR THE SEALED TILE ROOF	$I = 305\ Wm^{-2}$; $\dot{m} = 0.029\ kg\ s^{-1}$ (inlet and outlet); no wind	$I = 304\ Wm^{-2}$; $\dot{m} = 0.029\ kg\ s^{-1}$ (inlet and outlet); wind $2ms^{-1}$
KEY CODE	A	B

Table 4.7 Key code summarising the sealed tile roof test conditions.

TEST CONDITIONS	$F_R U_L$ ($\pm 3\sigma$)	$F_R (\tau\alpha)_e$ ($\pm 3\sigma$)	$F' U_L$ ($\pm 3\sigma$)	$F' (\tau\alpha)_e$ ($\pm 3\sigma$)
A	-5.8 $\pm$ 2.0	0.11 $\pm$0.02	-6.5 $\pm$2.6	0.12 $\pm$0.03
B	-8.3 $\pm$3.5	0.08 $\pm$0.02	-9.8 $\pm$5.1	0.10 $\pm$0.03

Table 4.8 Linefit results to the efficiency graphs for the section of sealed tile roof; $(\tau\alpha)_e = 0.45$.

TEST CONDITIONS	FROM η VS $(t_i - t_a)/I$		FROM η VS $(\bar{t}_f - t_a)/I$	
	F_R	U_L	F'	U_L
A	0.23	25	0.26	25
B	0.19	45	0.22	44

Table 4.9 Experimental values for F_R, F' and U_L for the section of sealed tile roof. The units of U_L are $Wm^{-2}\ °C^{-1}$.

HEAT TRANSFER COEFFICIENT	ESTIMATED VALUES, $Wm^{-2}\ °C^{-1}$	
	TEST CONDITION A	TEST CONDITION B
h_1	3.3	14.3
h_{r1}	5.6	5.5
U_t	8.9	19.8
h_2	4.0	4.0
h_3	3.7	3.7
h_{r23}	4.6	4.5
h_4	0.8	0.7
h_{r4}	5.0	5.0
U_b'	6.2	6.1

Table 4.10 Heat transfer coefficients for the two laboratory tests on the section of sealed tile roof.

SEALED TILE ROOF SECTION	TEST CONDITION A		TEST CONDITION B	
	F'	U_L	F'	U_L
EXPERIMENTAL VALUES	0.26	25	0.22	44
CALCULATED VALUES, USING EXPRESSIONS OF:				
AUTHOR	0.26	18	0.15	35
PARKER (1981)	0.32	16	0.19	30
DUFFIE AND BECKMAN (1980)	0.28	15	0.19	26

Table 4.11 Comparison of the experimental F' and U_L values with calculated values based on the author's no-leakage model, and other models, for the section of sealed tile roof. The units of U_L are $Wm^{-2}\ °C^{-1}$.

TEST CONDITIONS FOR THE METAL PANELS	$I = 306\ Wm^{-2}$; $\dot{m} = 0.036\ kg\ s^{-1}$ (inlet and outlet); wind $2 ms^{-1}$	$I = 781\ Wm^{-2}$; $\dot{m} = 0.036\ kg\ s^{-1}$ (inlet and outlet); wind $2\ ms^{-1}$	$I = 307\ Wm^{-2}$; $\dot{m} = 0.031\ kg\ s^{-1}$ (inlet and outlet); wind $2\ ms^{-1}$	$I = 784\ Wm^{-2}$; $\dot{m} = 0.031\ kg\ s^{-1}$ (inlet and outlet); wind $2\ ms^{-1}$
KEY CODE	C	D	E	F

Table 4.12 Key code summarising the metal panels test conditions.

TEST CONDITIONS AND PANEL TYPE	$F_R U_L$ ($\pm 3\sigma$)	$F_R (\tau\alpha)_e$ ($\pm 3\sigma$)	$F' U_L$ ($\pm 3\sigma$)	$F' (\tau\alpha)_e$ ($\pm 3\sigma$)
C STEEL	-14.6 $\pm$1.2	0.49 $\pm$0.02	-18.7 $\pm$2.0	0.63 $\pm$0.04
D STEEL	-14.5 $\pm$0.7	0.42 $\pm$0.01	-18.6 $\pm$1.1	0.54 $\pm$0.02
E ALUMINIUM	-16.2 $\pm$0.6	0.49 $\pm$0.01	-21.4 $\pm$1.1	0.65 $\pm$0.02
F ALUMINIUM	-15.3 $\pm$0.5	0.44 $\pm$0.01	-19.8 $\pm$0.9	0.58 $\pm$0.01

Table 4.13 Linefit results to the efficiency graphs for the metal panels; $(\tau\alpha)_e$ = 0.92 (steel) and 0.93 (aluminium).

TEST CONDITIONS AND PANEL TYPE	FROM η VS $(t_i - t_a)/I$		FROM η VS $(\bar{t}_f - t_a)/I$	
	F_R	U_L	F'	U_L
C STEEL	0.53	27	0.69	27
D STEEL	0.46	32	0.59	32
E ALUMINIUM	0.53	31	0.70	31
F ALUMINIUM	0.48	32	0.62	32

Table 4.14 Experimental values for F_R, F' and U_L for the metal panels. The units of U_L are $Wm^{-2}\,{}^{\circ}C^{-1}$.

HEAT TRANSFER COEFFICIENT	ESTIMATED VALUES, $Wm^{-2}\ °C^{-1}$, FOR EACH TEST CONDITION AND PANEL TYPE			
	C, STEEL	D, STEEL	E, ALUMINIUM	F, ALUMINIUM
h_1	15.8	15.8	17.7	17.7
h_{r1}	6.2	6.4	6.9	7.1
U_t	22.0	22.2	24.6	24.8
h_2	15.7	15.8	16.1	16.1
h_3	12.3	12.3	10.2	10.2
h_{r23}	1.6	1.7	1.4	1.4
h_4	0.7	0.8	0.7	0.8
h_{r4}	5.6	5.7	5.5	5.6
U_b	0.6	0.6	0.6	0.6

Table 4.15 Heat transfer coefficients for the laboratory tests on the metal panels.

METAL PANELS	VALUES FOR F' AND U_L, FOR EACH TEST CONDITION AND PANEL TYPE							
	C, STEEL		D, STEEL		E, ALUM.		F, ALUM.	
	F'	U_L	F'	U_L	F'	U_L	F'	U_L
EXPERIMENTAL VALUES	0.69	27	0.59	32	0.70	31	0.62	32
CALCULATED VALUES, USING EXPRESSIONS OF:								
AUTHOR	0.44	23	0.44	23	0.41	26	0.41	26
PARKER (1981)	0.44	23	0.44	23	0.41	26	0.41	26
DUFFIE AND BECKMAN (1980):								
FLAT PLATE	0.43	23	0.43	23	0.41	25	0.41	25
FIN AND TUBE	0.67	23	0.67	23	0.62	25	0.62	25

Table 4.16 Comparison of the experimental F' and U_L values with calculated values based on the author's no-leakage model, and other models, for the metal panels. The units of U_L are $Wm^{-2}\ °C^{-1}$.

PLOT NUMBER	STRUCTURE TESTED	TEST CONDITIONS					LEAKAGE DUE TO:	
		RADN.LEVEL, I, Wm^{-2}	$\dot{m}$ VALUES, $kg\ s^{-1}$				SUCTION ONLY, $\dot{m}_s$	WIND, $\dot{m}_w$
			WIND FAN OFF		WIND FAN ON			
			INLET	OUTLET	INLET	OUTLET		
1	UNSEALED TILE ROOF	305	0.033	0.033	0.015	0.032	0	0.017
2		305	0.109	0.127	0.102	0.130	0.018	0.028
3		773	0.033	0.033	0.015	0.032	0	0.017
4		773	0.112	0.122	0.106	0.120	0.010	0.014
5	SEALED TILE ROOF	305	0.135	0.121	0.136	0.125	-0.014	-0.011
6		305	0.038	0.037	0.036	0.036	-0.001	0
7	STEEL PANEL	306	0.034	0.038	0.036	0.038	0.004	0.002
8		783	0.038	0.036	0.037	0.036	-0.002	-0.001

Table 4.17 Test conditions and results for the wind leakage tests (refer to Figures 4.13, 4.14, 4.15). Rounded figures.

TEST CONDITIONS FOR THE UNSEALED TILE ROOF	$I = 304\ Wm^{-2}$; $\dot{m}_{inlet} = 0.015\ kg\ s^{-1}$; $\dot{m}_{outlet} = 0.032\ kg\ s^{-1}$; $\dot{m}_{w} = 0.017\ kg\ s^{-1}$; wind $2ms^{-1}$; $t_{ent} \simeq 22.7\ °C$; $t_{inj} \simeq 25.2\ °C$.	$I = 773\ Wm^{-2}$; $\dot{m}_{inlet} = 0.106\ kg\ s^{-1}$; $\dot{m}_{outlet} = 0.120\ kg\ s^{-1}$; $\dot{m}_{w} = 0.014\ kg\ s^{-1}$; wind $2ms^{-1}$; $t_{ent} \simeq 26.5\ °C$; $t_{inj} \simeq 30.4\ °C$.
KEY CODE	G	H

Table 4.18 Key code summarising the unsealed tile roof test conditions.

HEAT TRANSFER COEFFICIENT	ESTIMATED VALUES, $Wm^{-2}\ °C^{-1}$	
	TEST CONDITION G	TEST CONDITION H
h_1	(14.3 (SOLID) ((24.4 (POROUS)	(14.3 (SOLID) ((26.8 (POROUS)
h_{r1}	5.4	5.7
U_t	(19.7 (SOLID) ((30.0 (POROUS)	(20.0 (SOLID) ((32.5 (POROUS)
h_2	(3.3 (SOLID) ((0.3 (POROUS)	(14.3 (SOLID) ((1.2 (POROUS)
h_3	3.1	13.4
h_{r23}	4.4	4.5
U_b'	6.0	6.1

Table 4.19 Heat transfer coefficients for part (a) of the wind leakage procedure.

TILE NUMBER	1	2	3	4	5	6	7	8
t_i	22.540	22.924	23.203	23.415	23.581	23.714	23.823	23.914
t_o	22.541	22.917	23.193	23.403	23.568	23.700	23.809	23.900

Table 4.20 Inlet and outlet air temperatures for each tile sub-collector, test condition G, porous wall values for F_R and U_L, $t_{inj} \simeq 25.2$ °C.

TILE NUMBER	1	2	3	4	5	6	7	8
t_i	26.810	27.009	27.165	27.314	27.456	27.591	27.720	27.843
t_o	26.946	27.106	27.259	27.404	27.543	27.675	27.801	27.921

Table 4.21 Inlet and outlet air temperatures for each tile sub-collector, test condition H, solid wall values for F_R and U_L, $t_{inj} \simeq 30.4$ °C.

TEST CONDITION	t_o VALUE, °C			$(t_o - t_i)$ VALUE, °C		
	MEASURED	CALCULATED		MEASURED	CALCULATED	
		SOLID	POROUS		SOLID	POROUS
G	23.92	24.16	23.90	1.38	1.62	1.36
H	28.32	27.92	27.35	1.51	1.11	0.54

Table 4.22 Comparison of calculated and experimental values for t_o and $(t_o - t_i)$ for the wind leakage cases.

HEAT TRANSFER COEFFICIENT	ESTIMATED VALUES, $Wm^{-2}\ °C^{-1}$ FOR EACH TEST CONDITION	
	G	H
h_1 (h_{1W})	14.3 (5.1)	14.3 (7.4)
h_{r1}	5.4	5.7
U_t (U_{tW})	19.7 (10.5)	20.0 (13.1)
k_1 (k_{1W})	0.36 (0.67)	0.36 (11.86)
h_2 (h_{2W})	1.7 (34.4)	13.3 (42.3)
h_3	1.6	12.5
h_{r23}	4.4	4.5
U_b'	6.0	6.1

Table 4.23 Heat transfer coefficients and thermal conductivities (actual and effective) for use in parts (e) and (f) of the wind-leakage procedure (based on Q_u').

TEST CONDITIONS	$F_{RW}\ U_{LW}$ ($\pm$ 3σ)	$F_{RW}\ (\tau\alpha)_e$ ($\pm$ 3σ)	$F'_W\ U_{LW}$ ($\pm$ 3σ)	$F'_W\ (\tau\alpha)_e$ ($\pm$ 3σ)
G	-8.6 $\pm$1.5	0.25 $\pm$0.01	-13.0 $\pm$3.5	0.31 $\pm$0.03
H	-35.7 $\pm$3.7	0.28 $\pm$0.01	-44.4 $\pm$5.7	0.35 $\pm$0.02

Table 4.24 Linefit results to the efficiency graphs for the section of unsealed tile roof; $(\tau\alpha)_e$ = 0.45.

TEST CONDITIONS	FROM η VS $(t_i - t_a)/I$		FROM η VS $(\bar{t}_f - t_a)/I$	
	F_{RW}	U_{LW}	F'_W	U_{LW}
G	0.57	15	0.69	19
H	0.63	57	0.78	57

Table 4.25 'Experimental' values for F_{RW}, F'_W and U_{LW} for the section of unsealed tile roof. The units of U_L are $Wm^{-2}\ ^{\circ}C^{-1}$.

UNSEALED TILE ROOF SECTION	TEST CONDITION G		TEST CONDITION H	
	F'_W	U_{LW}	F'_W	U_{LW}
'EXPERIMENTAL' VALUES, BASED ON Q_u"	0.69	19	0.78	57
CALCULATED VALUES, BASED ON Q'_u	0.59	15	0.75	19

Table 4.26 Comparison of the 'experimental' F'_W and U_{LW} values, both with calculated values from the wind-leakage model. The units of U_{LW} are $Wm^{-2}\ °C^{-1}$.

STRUCTURE TESTED	TIME CONSTANTS, MINUTES	
	WINDSTILL	WIND 2ms^{-1}
TILED ROOF SECTION: UNSEALED SEALED	108 -	40 52
CORRUGATED STEEL PANEL	10	7
CORRUGATED ALUMINIUM PANEL	10	6
DOUBLE-GLAZED AIR PANEL (HILL ET AL, 1978)	-	12.7*

Table 4.27 Time constants.

* Tested outdoors, windspeed unspecified.

TEST SECTION AND MASS FLOW RATE	TOTAL PRESSURE DROP, Δp, Nm^{-2}	THEORETICAL FAN POWER, P_{th}, WATTS	FAN POWER CONSUMED,* WATTS
DREADNOUGHT . TILES $m = 0.029$ kg s^{-1}	4.9	0.12	0.24
STEEL PANEL . $m = 0.033$ kg s^{-1}	15.7	0.43	0.43
ALUMINIUM PANEL . $m = 0.031$ kg s^{-1}	15.3	0.40	0.37

Table 4.28 Pressure drops and fan power estimates for the laboratory test sections.

* After accounting for set efficiency, based on manufacturer's data.

TYPE OF ROOF AND MASS FLOW RATE	FAN TOTAL OPERATIONAL PRESSURE DROP, Δp, Nm^{-2}	THEORETICAL FAN POWER, P_{th}, WATTS	FAN POWER SUPPLIED, WATTS
THE EXISTING TILE ROOF . $m = 0.9$ kg s^{-1}	110.2	78.6	450
A CORRUGATED STEEL ROOF AND DUCTING . $m = 0.9$ kg s^{-1}	159.0	113.5	780

Table 4.29 Operational pressure drops and fan power estimates for the existing, and for a steel, roof at the test house.

Figure 4.1 Spectral reflectance vs. wavelength for the steel panel (Ward Bros. Ltd., 'Plastisol' coating, 'Van Dyke Brown' 08B29).

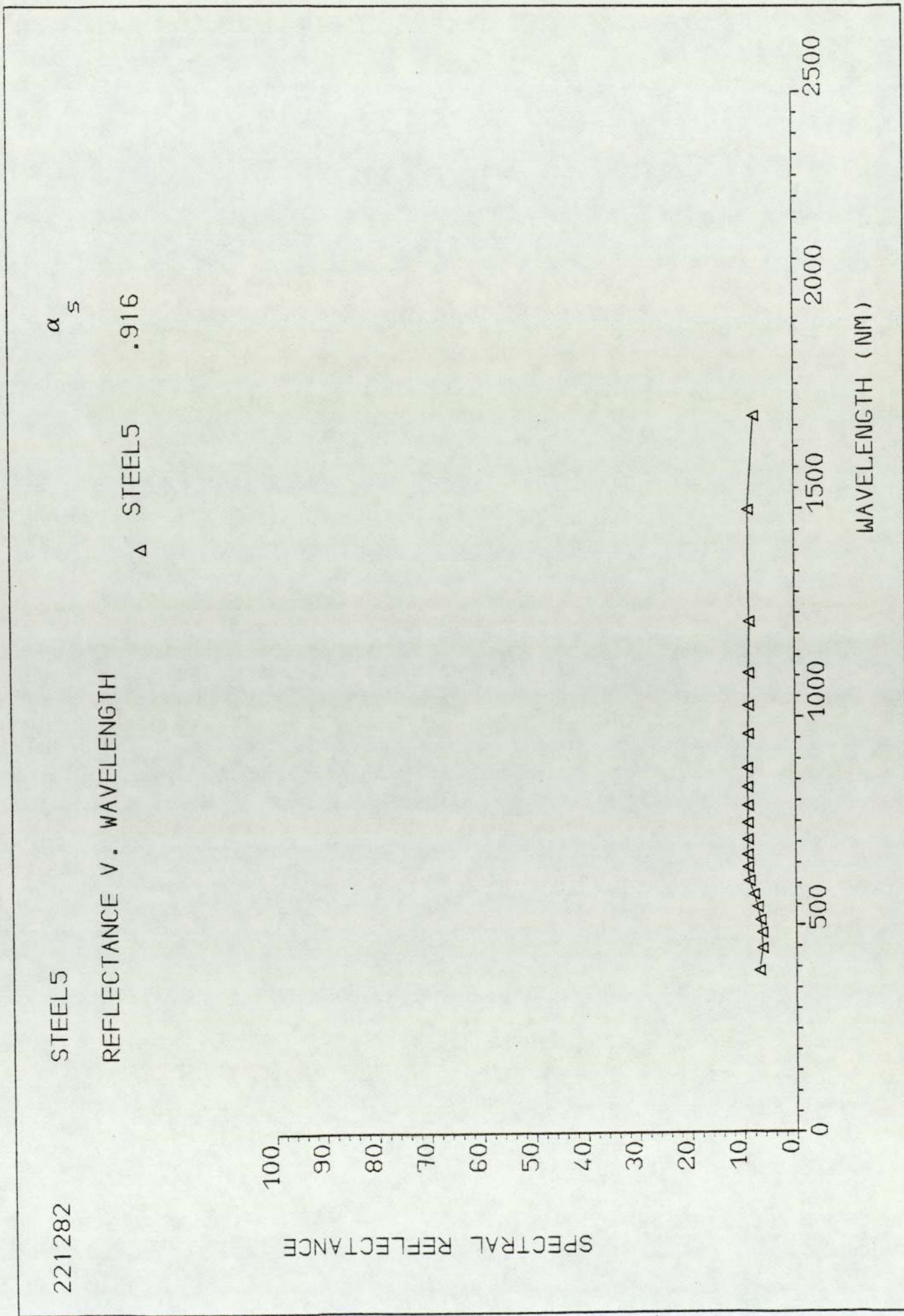

Figure 4.2 Spectral reflectance vs. wavelength for the aluminium panel (British Aluminium Co. Ltd., colour bond, stucco embossed finish, 'Van Dyke Brown' 08B29).

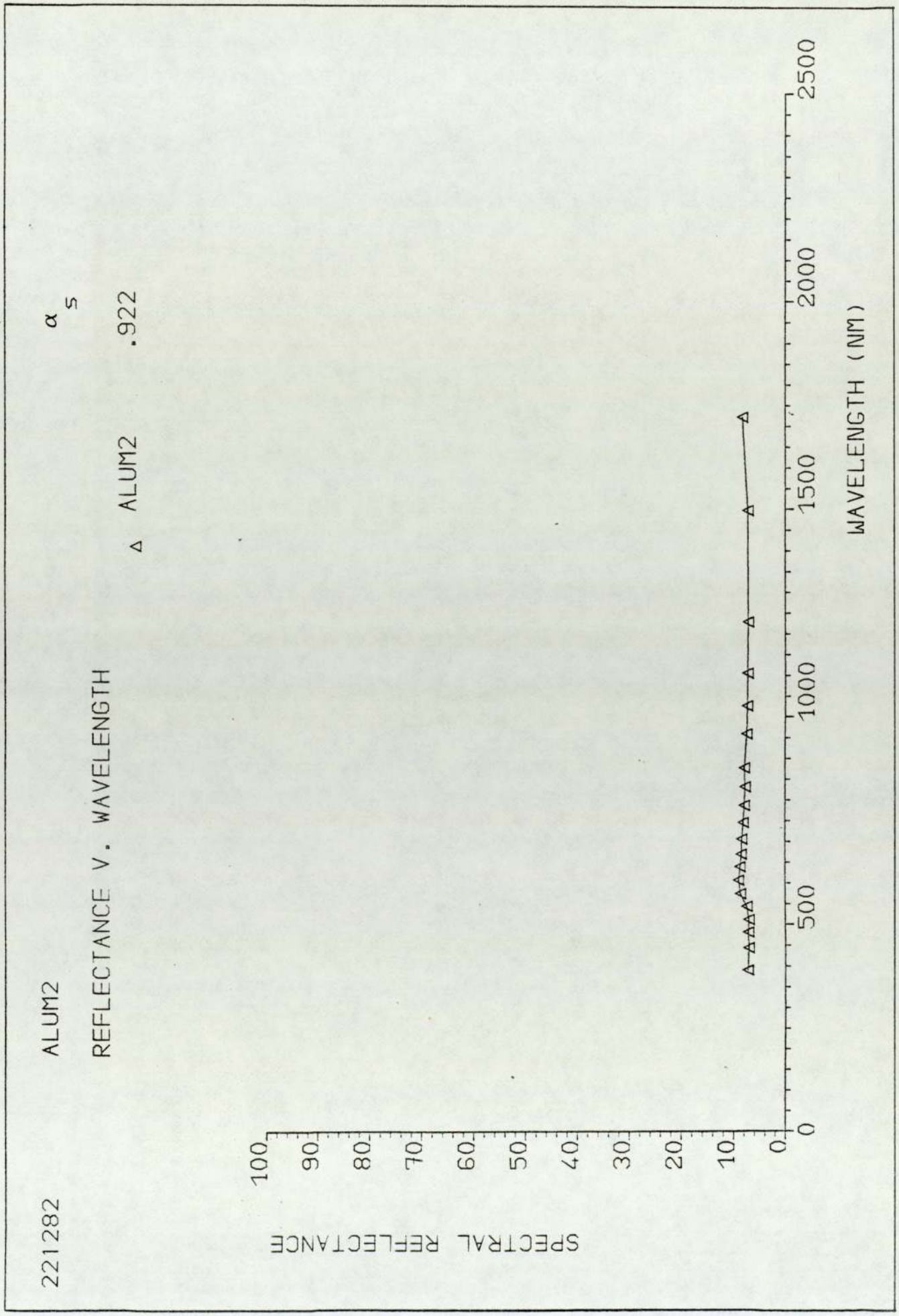

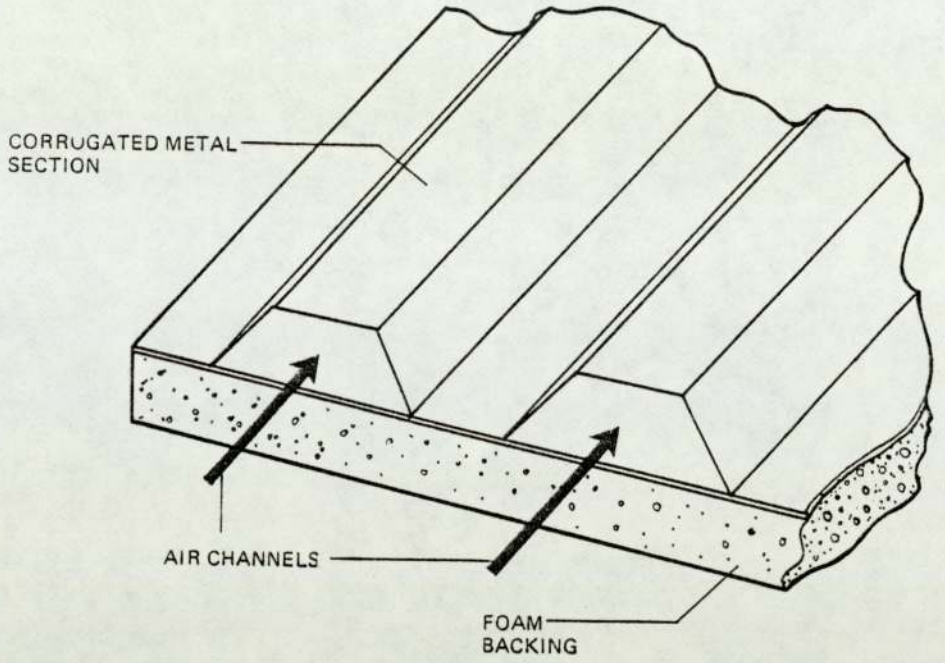

Figure 4.3 Illustration showing the construction of the metal panels.

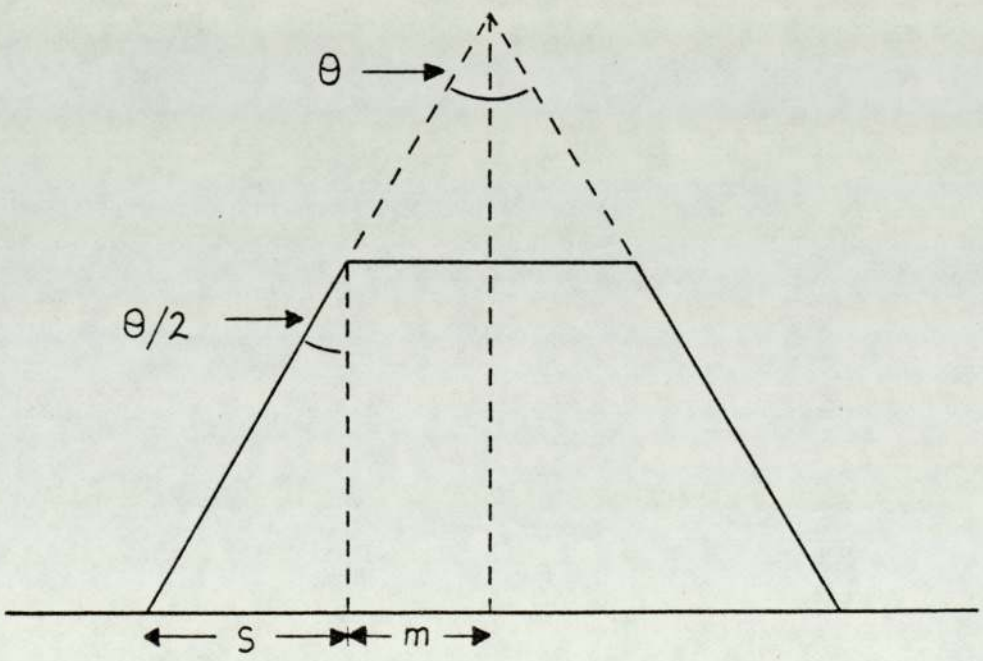

Figure 4.4 Cross section of one of the trapezoidal flow channels in the metal panels.

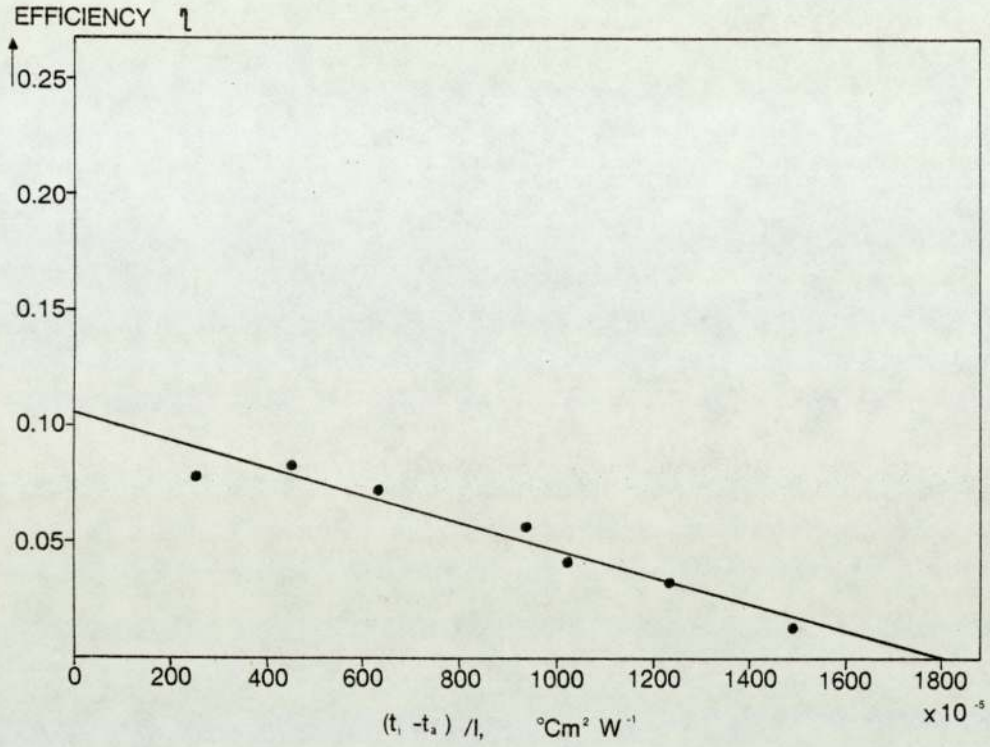

Figure 4.5 Efficiency versus $(t_i - t_a)/I$, sealed tile roof section; $I = 305\ Wm^{-2}$; $\dot{m} = 0.029\ kg\ s^{-1}$; no wind.

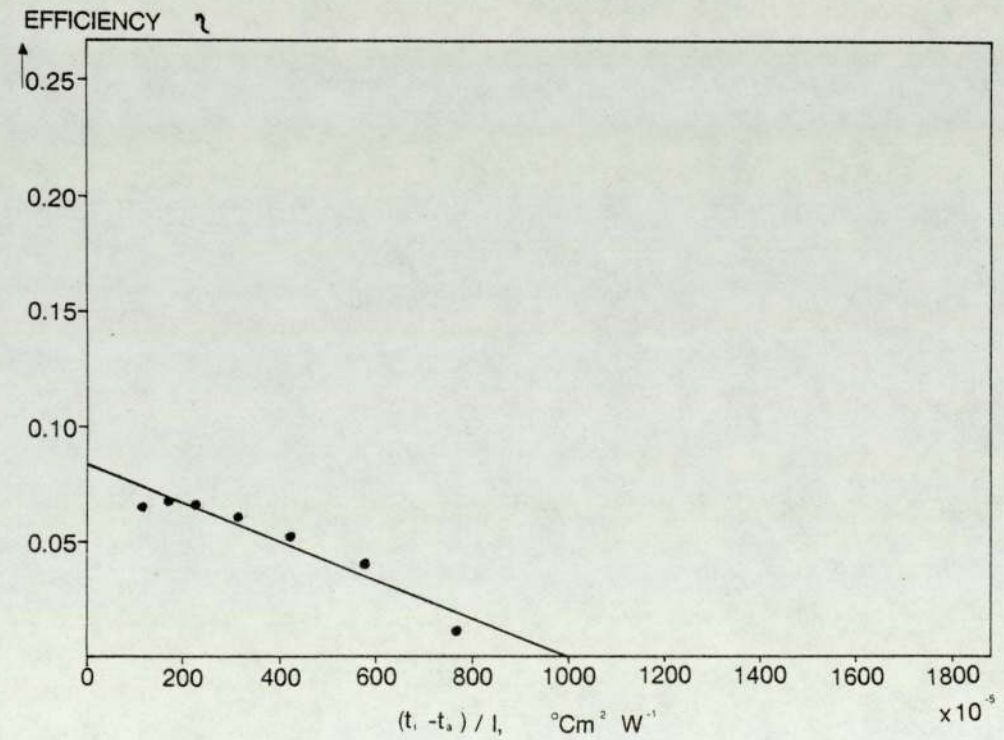

Figure 4.6 Efficiency versus $(t_i - t_a)/I$, sealed tile roof section; $I = 304\ Wm^{-2}$; $\dot{m} = 0.029\ kg\ s^{-1}$; wind $2ms^{-1}$.

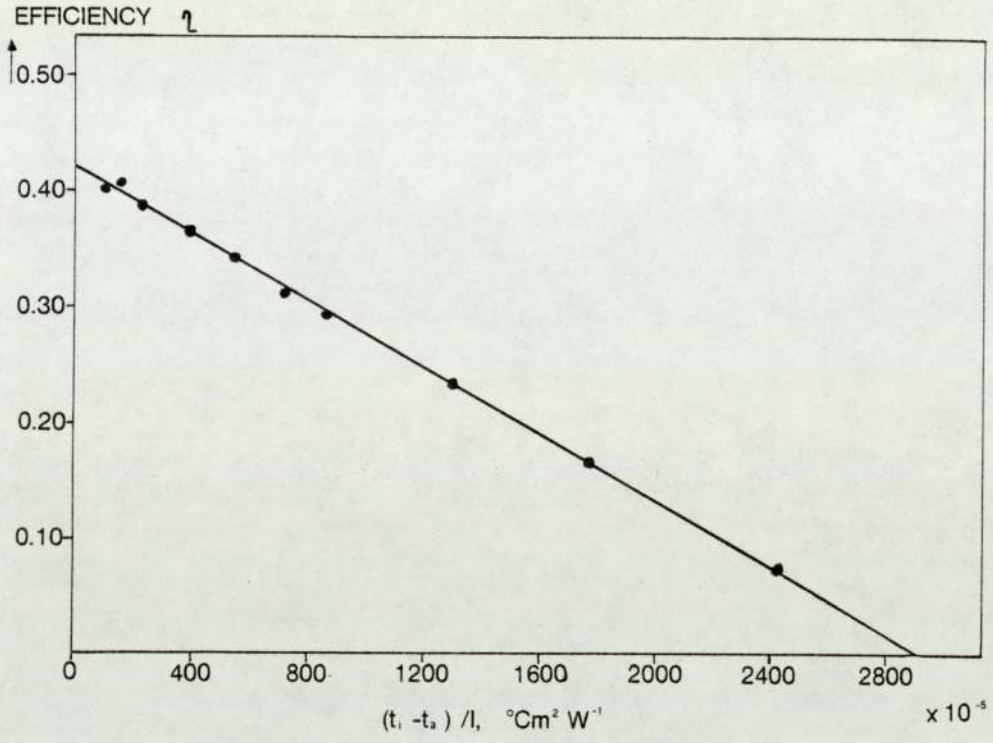

Figure 4.7 Efficiency versus $(t_i - t_a)/I$, steel panel; $I = 781\ Wm^{-2}$; $\dot{m} = 0.036\ kg\ s^{-1}$; wind $2ms^{-1}$.

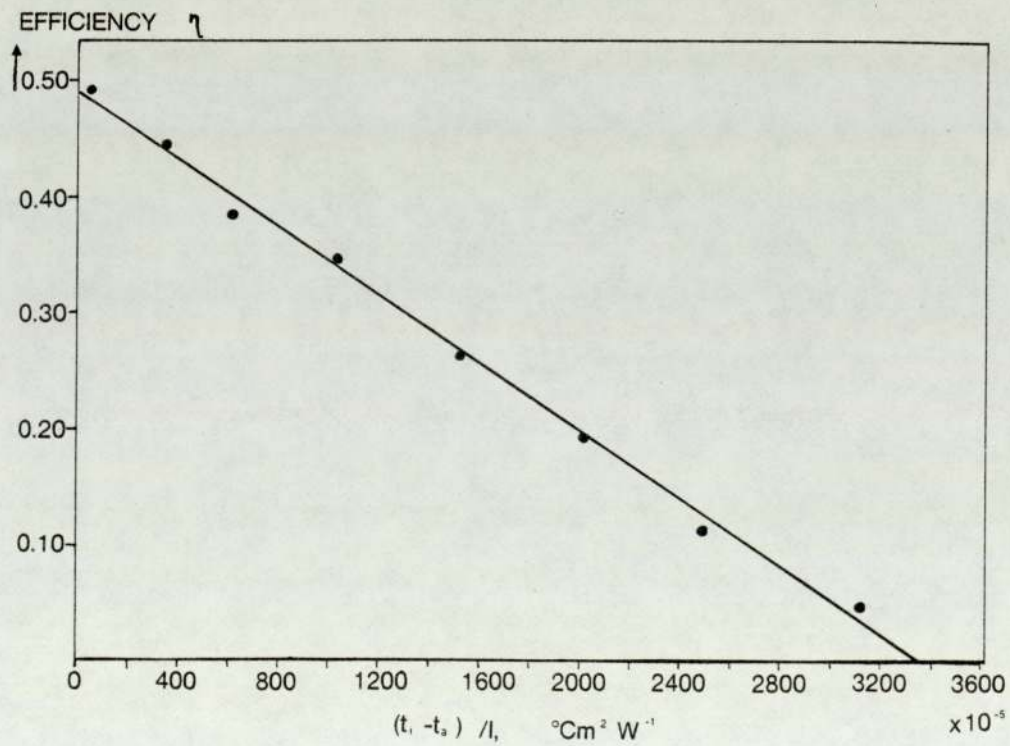

Figure 4.8 Efficiency versus $(t_i - t_a)/I$, steel panel; $I = 306\ Wm^{-2}$; $\dot{m} = 0.036\ kg\ s^{-1}$; wind $2ms^{-1}$.

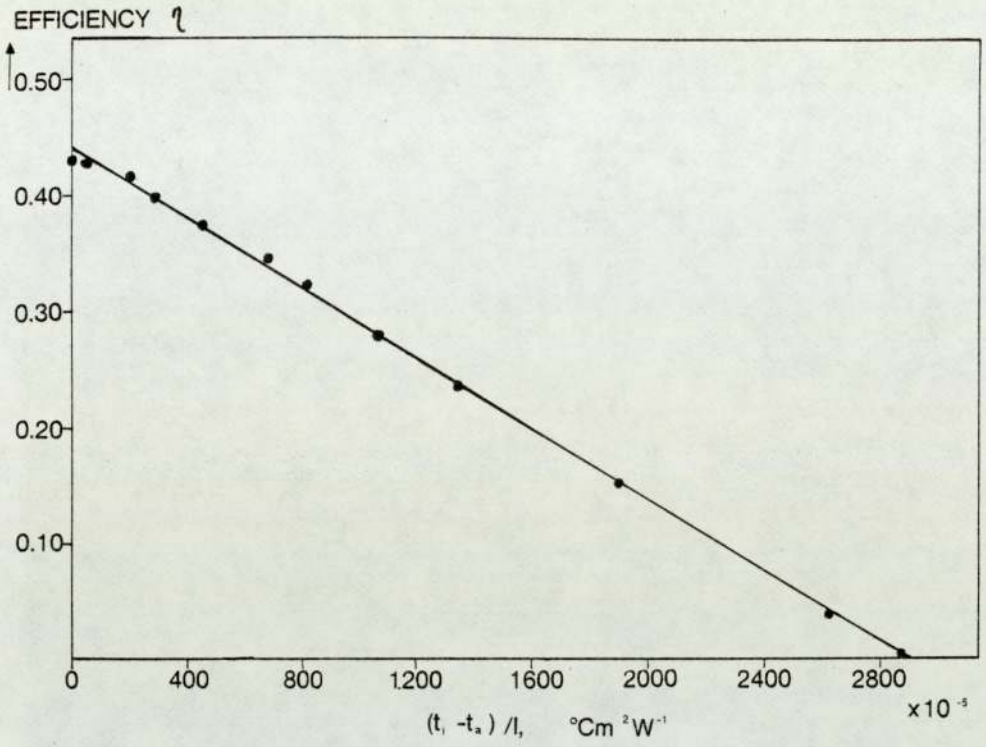

Figure 4.9 Efficiency versus $(t_i - t_a)/I$, aluminium panel; $I = 784\ Wm^{-2}$; $\dot{m} = 0.031\ kg\ s^{-1}$; wind $2ms^{-1}$.

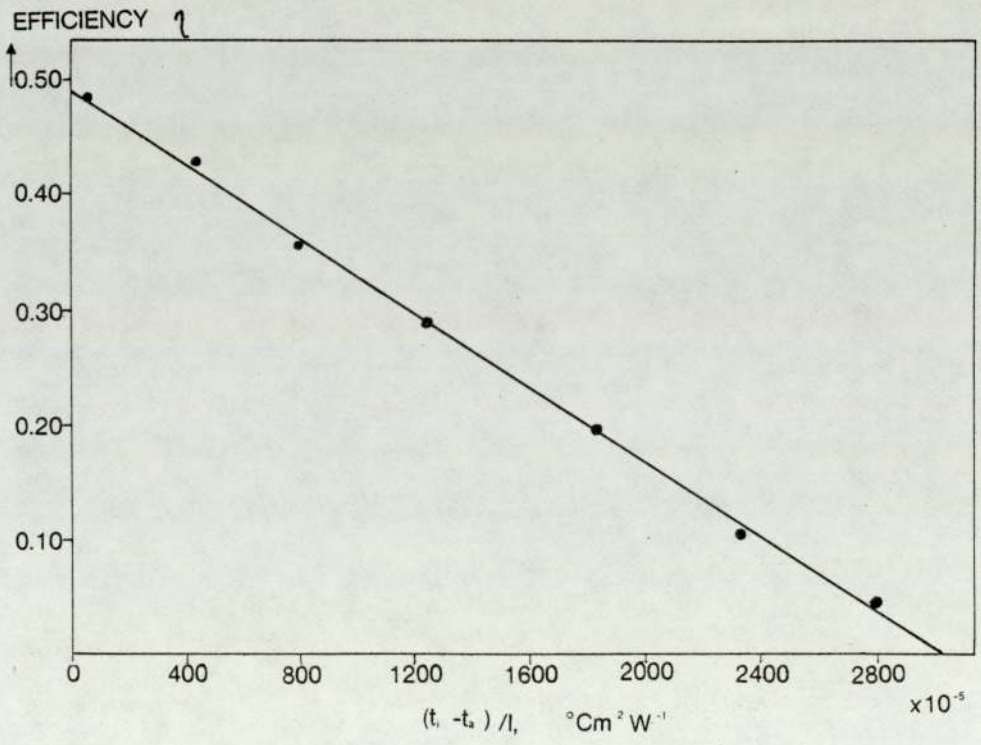

Figure 4.10 Efficiency versus $(t_i - t_a)/I$, aluminium panel; $I = 307\ Wm^{-2}$; $\dot{m} = 0.031\ kg\ s^{-1}$; wind $2ms^{-1}$.

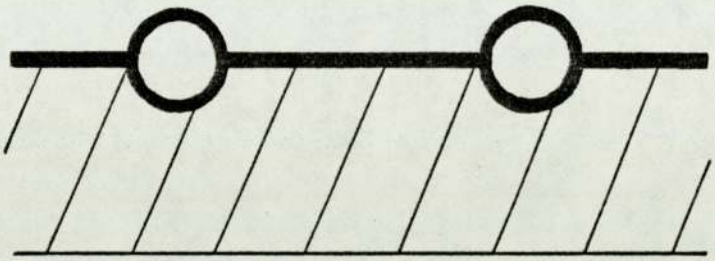

Figure 4.11 Schematic illustration of one type of 'fin and tube' solar collector.

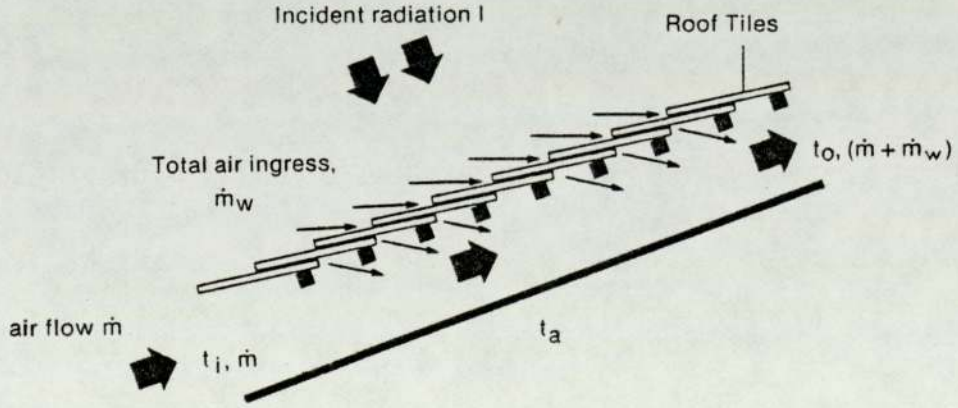

Figure 4.12 Air leakage to the tile/felt airstream.

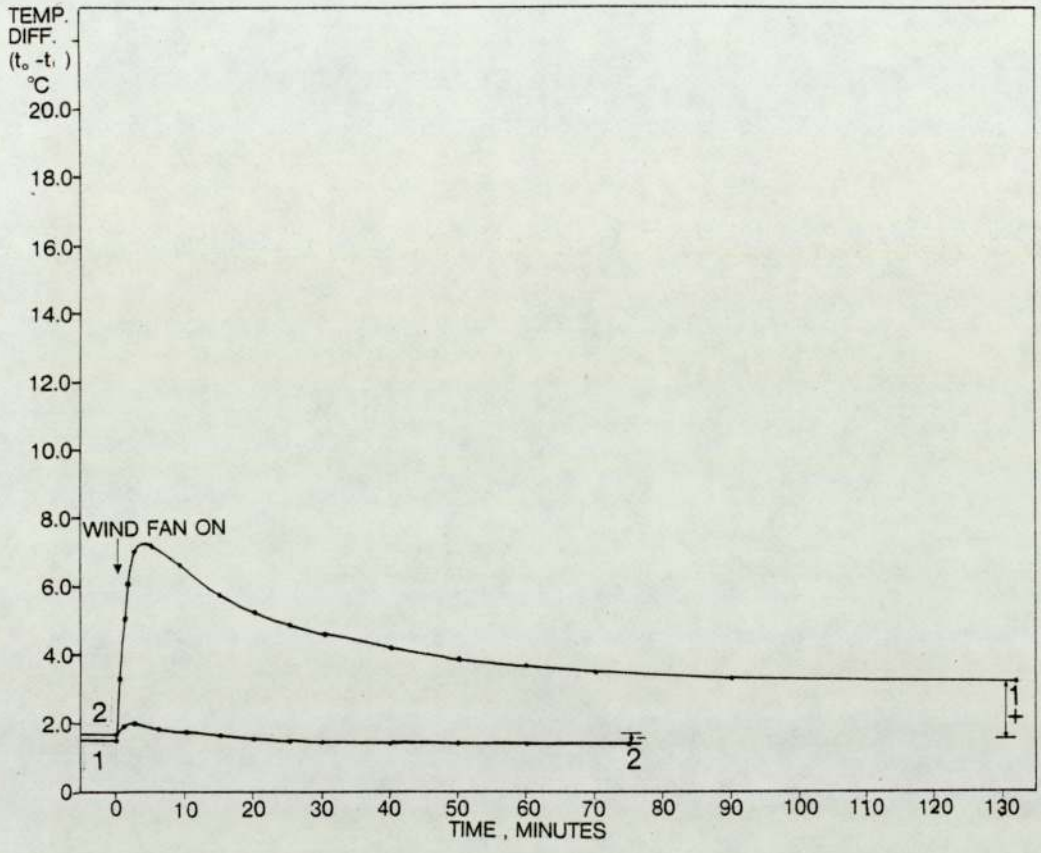

Figure 4.13 Effect of surface wind application to the unsealed tile roof section, I = 305 Wm^{-2}.

Plot 1: $\dot{m}_{inlet}$ = 0.033 kg s^{-1}.

Plot 2: $\dot{m}_{inlet}$ = 0.109 kg s^{-1}.

(Initial steady state values, wind fan off).

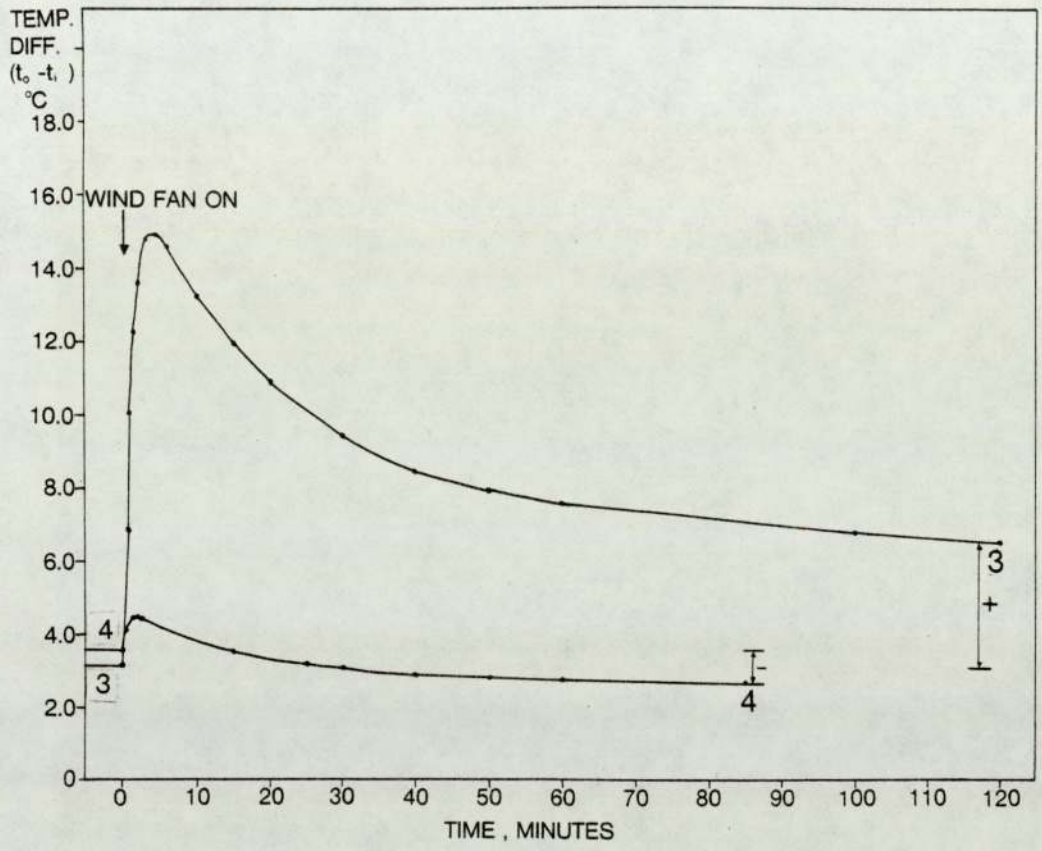

Figure 4.14 Effect of surface wind application to the unsealed tile roof section, I = 773 Wm^{-2}.

Plot 3: $\dot{m}_{inlet}$ = 0.033 kg s^{-1}.

Plot 4: $\dot{m}_{inlet}$ = 0.112 kg s^{-1}.

(Initial steady state values, wind fan off).

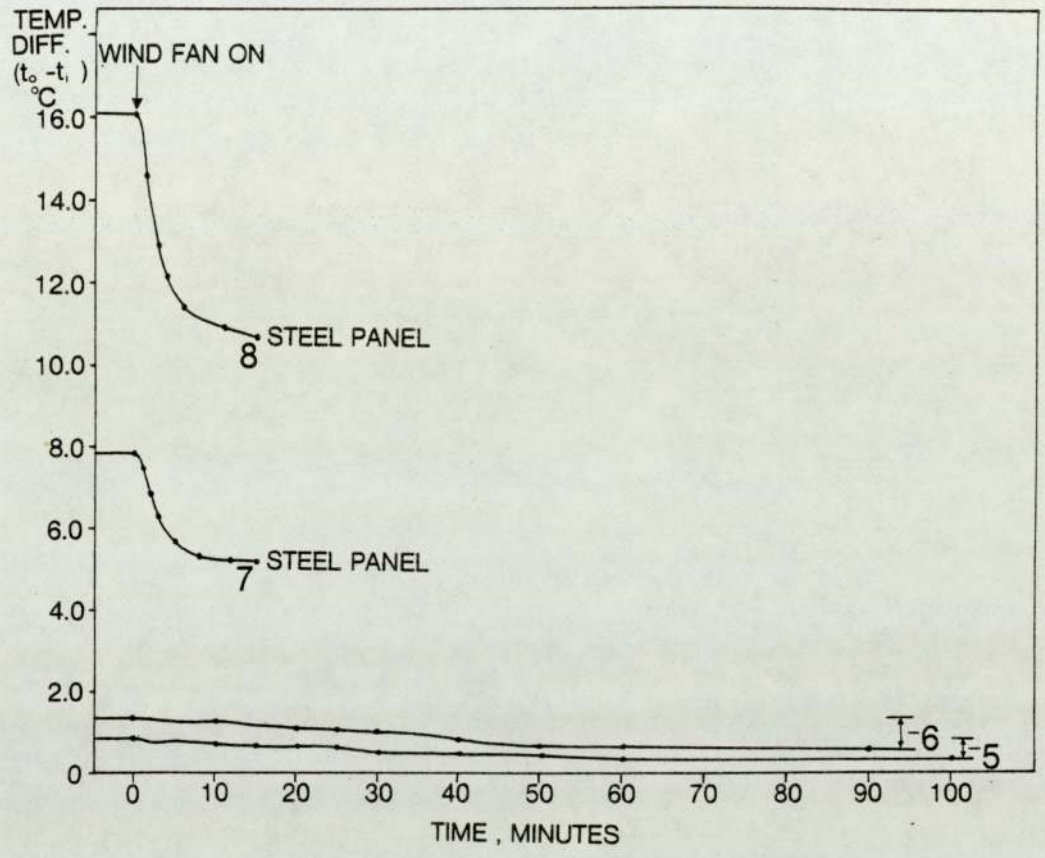

Figure 4.15 Effect of surface wind application to the sealed tile roof section (plots 5, 6) and to the steel panel (plots 7, 8).

Plot 5: $I = 305\ Wm^{-2}$, $\dot{m}_{inlet} = 0.135\ kg\ s^{-1}$.

Plot 6: $I = 305\ Wm^{-2}$, $\dot{m}_{inlet} = 0.038\ kg\ s^{-1}$.

Plot 7: $I = 306\ Wm^{-2}$, $\dot{m}_{inlet} = 0.034\ kg\ s^{-1}$.

Plot 8: $I = 783\ Wm^{-2}$, $\dot{m}_{inlet} = 0.038\ kg\ s^{-1}$.

(Initial steady state $\dot{m}$ values, wind fan off).

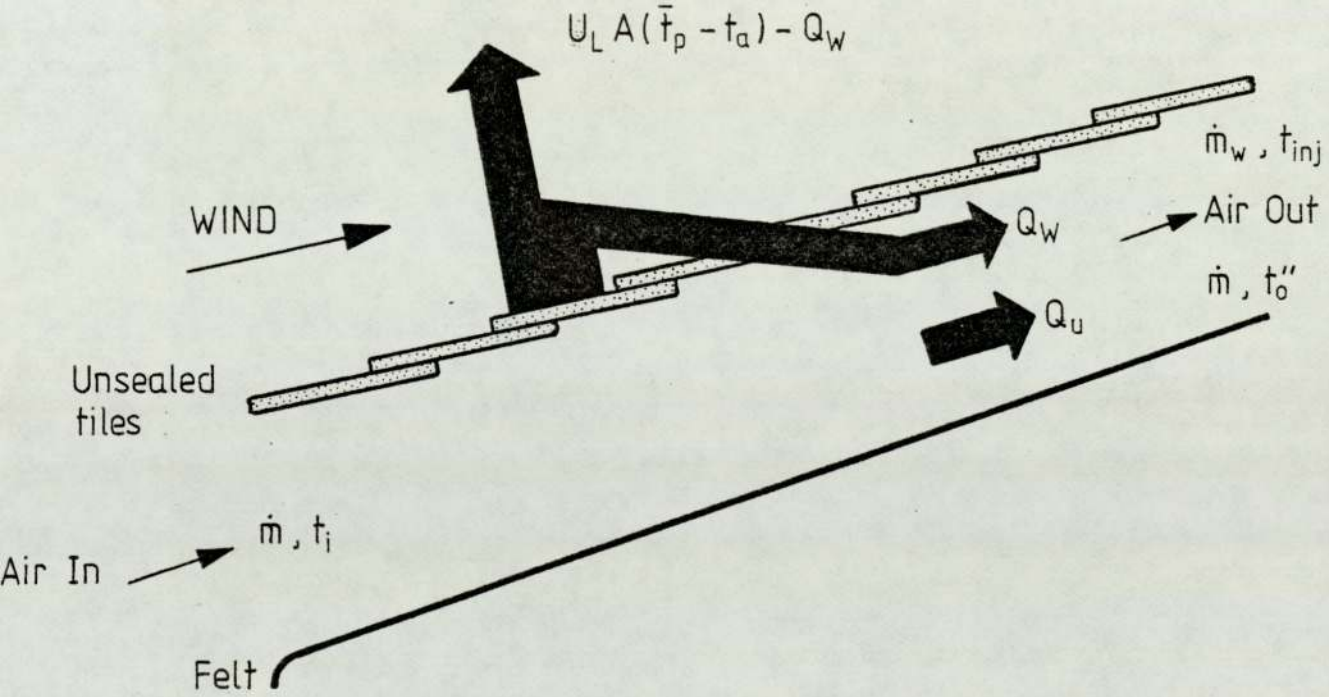

Figure 4.16 Schematic illustration of the overall energy re-distribution approach to the wind leakage effect.

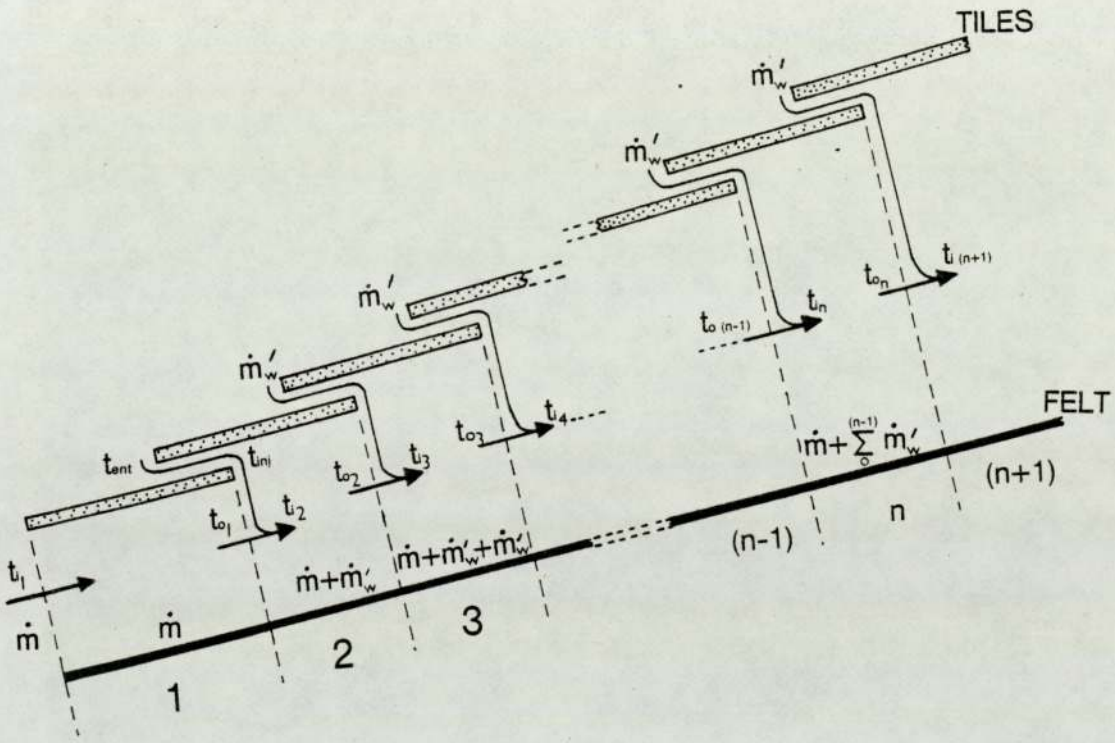

Figure 4.17 Schematic illustration of the wind leakage analysis procedure.

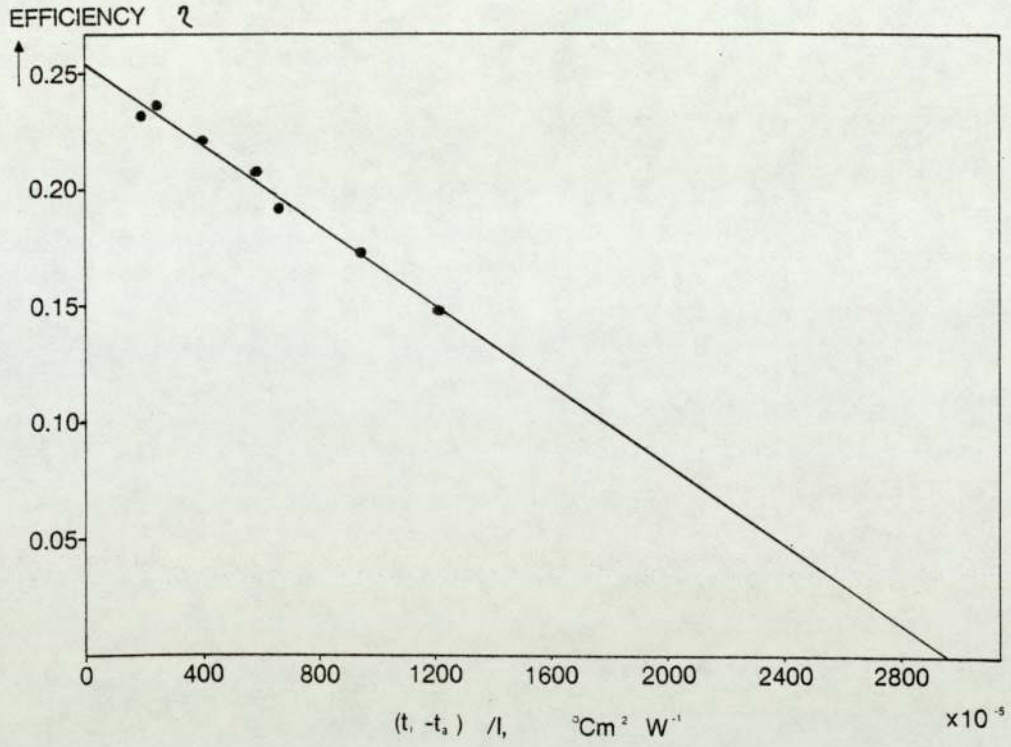

Figure 4.18 'True' efficiency versus $(t_i - t_a)/I$, unsealed tile roof section; $I = 304\ Wm^{-2}$; $\dot{m}_{inlet} = 0.015\ kg\ s^{-1}$, $\dot{m}_w = 0.017\ kg\ s^{-1}$; wind $2ms^{-1}$.

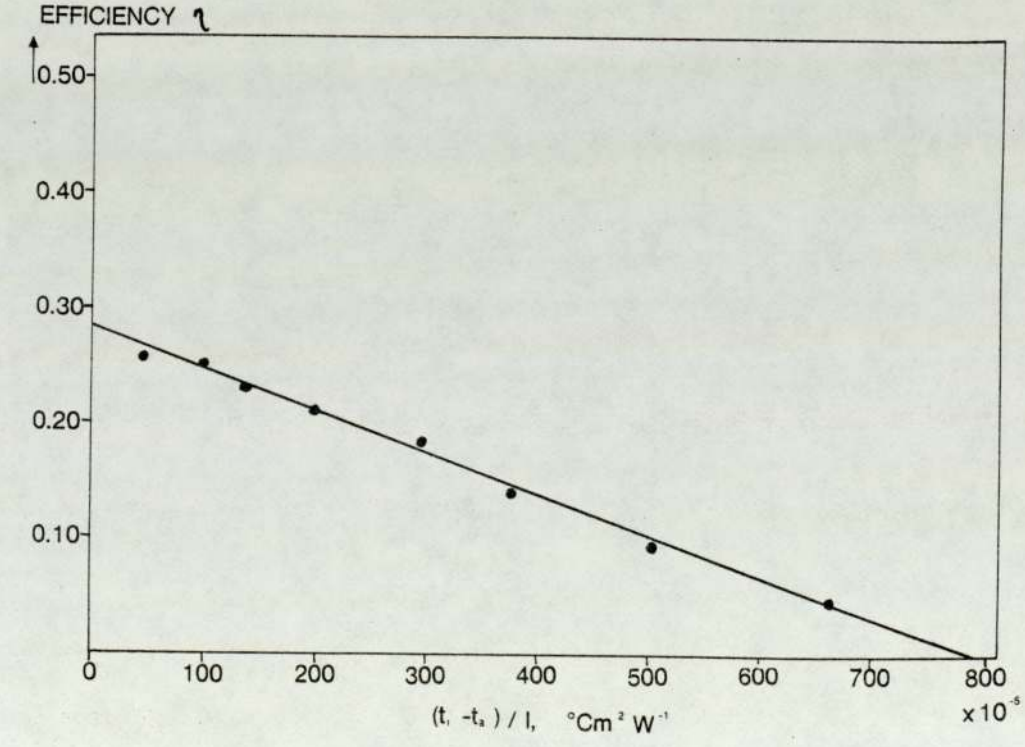

Figure 4.19 'True' efficiency versus $(t_i - t_a)/I$, unsealed tile roof section; $I = 773\ Wm^{-2}$; $\dot{m}_{inlet} = 0.106\ kg\ s^{-1}$, $\dot{m}_w = 0.014\ kg\ s^{-1}$; wind $2ms^{-1}$.

CHAPTER 5

THE IN SITU PERFORMANCE OF THE HEAT PUMP

5.1 Introduction

Discrepancies have been reported between heat pump field operating characteristics and manufacturers' data (see, for example, Norbäck, 1975 and Parken et al, 1977). There may be several reasons for this, one of which could be that manufacturers base their data on the results of tests performed under controlled laboratory conditions; disagreements may then arise when the heat pump is operated in different modes or under different conditions of temperature or humidity.

Heat pumps currently available for domestic use in the U.K. are mainly American in origin and are primarily designed as air-conditioning units (i.e. both heating and cooling capability). In the U.K., however, cooling is seldom a requirement, and several authors (e.g. Blundell et al, 1977; Heap, 1979) recognise the need for a heating mode only heat pump designed specifically for the U.K. The heat pump at the test house is a Lennox HP7 unit (model 411VFF) with a nominal heating capacity of 9.54 kW at an air source temperature of 7°C. It was not specifically designed for the U.K. market, and was being operated in the heating mode only. Also, it had been converted for air to water operation, whereas it had been designed for air to air operation. Obtaining the performance characteristics for this type of heat pump from data obtained on site would therefore be useful, not only because the characteristics could be compared with those of the manufacturer, but also because

they enable predictions to be made of performance in U.K. conditions and could be utilised in future computer modelling exercises. In addition, such characteristics would be an aid in the analysis of the performance for the monitored heating season (see section 2.2.2).

Heat pump characteristics were deduced from data recorded during the 1979/80 heating season. Particular attention was paid to performance analysis in terms of moist air thermodynamics, since the climate of the U.K. is relatively damp.

5.2 Heat Pump Analysis

5.2.1 Nomenclature

Q_2 is the total rate of heat energy extraction from moist air, kW;

Q_S' is the rate of sensible heat energy extraction from moist air, kW;

Q_L' is the rate of latent heat energy extraction from moist air, kW;

P_c is the rate of electrical energy consumption by the heat pump compressor, kW;

P_f is the rate of electrical energy consumption by the heat pump fan, kW;

P_t is the total rate of electrical energy consumption (compressor + fan) by the heat pump, kW;

$\dot{m}$ is the total mass flow rate of air crossing the heat pump evaporator (from both sides of the test house roof), kg s^{-1};

C_p is the specific heat capacity of dry air at constant pressure, kJ kg^{-1} K^{-1};

L is the specific latent heat of evaporation of water, kJ kg^{-1};

t_e is the heat pump evaporator coil temperature, °C;

t is the dry bulb temperature of air, °C;

ϕ is the relative humidity of air, %;

g is the moisture content of air, kg kg^{-1} of dry air;

h is the specific enthalpy of air, kJ kg^{-1} of moist air;

ρ is the density of air, kg m^{-3};

p_{at} is the atmospheric pressure, bar or mm Hg (specified in the text);

p_s is the water vapour pressure, bar or mm Hg (specified in the text);

p_{ss} is the saturated water vapour pressure bar or mm Hg (specified in the (text).

The suffices 'a', 'b' and 'c' refer to the following locations respectively (see Figure 2.4): outside the test house; at the entry to the heat pump evaporator; at the exit from the heat pump evaporator; they are applicable to the quantities t, ϕ, g and h above. The suffices 'dry' or 'moist' indicate dry air or moist air respectively, and are applicable to the quantities $\dot{m}$ and ρ above.

5.2.2 Theoretical Considerations

The analysis of moist air was carried out using relations given in the National Engineering Steam Tables, 1964, Section C1 of the IHVE Guide, Book C, 1970, 'Air Conditioning Engineering' by Jones, (1973), and the 'Handbook of Chemistry and Physics, 1973/74', published by the Chemical Rubber Company, U.S.A., (1973).

The pressure of water vapour in saturated air, p_{ss}, in bar, at a temperature t, in °C, is given by:

$$\log_{10} p_{ss} = 28.59051 - 8.2 \log_{10} (t + 273.16) + 0.0024804 (t + 273.16) - [3142.31/(t + 273.16)] \quad 5.1$$

and the water vapour pressure in air, p_s , by:

$$p_s = p_{ss} \phi / 100 \quad 5.2$$

The moisture content of air, g, in kg kg^{-1} of dry air at positions 'a', 'b' and 'c', for p_{at} (assumed the same at each position) and p_s in bar, may then be calculated from a knowledge of t and ϕ, using equations 5.1, 5.2 and:

$$g = 0.622 \, p_s/(p_{at} - p_s) \quad 5.3$$

The specific enthalpy of moist air, h, at positions 'a', 'b' and 'c' is obtained from:

$$h = 1.007 \, t - 0.026 + g \, (2501 + 1.84 \, t) \quad 5.4$$

where h is in kJ kg^{-1} for t in °C and g in kg kg^{-1} of dry air.

The density of moist air may be calculated from the relation:

$$\rho_{moist} = 1.2929 \, [273.13/(t + 273.16)] \, [(p_{at} - 0.3783 \, p_s)/760] \quad 5.5$$

The density of moist air at position 'b', $\rho_{b\,moist}$, was used in all calculations. The mass flow rate of moist air, $\dot{m}_{moist}$, crossing the heat pump evaporator, was then calculated from:

$$\dot{m}_{moist} = 0.740 \, \rho_{b\,moist} \quad 5.6$$

since the total volume flow rate of air across the heat pump evaporator was measured to be 0.740 $m^3 \, s^{-1}$. The total energy

(sensible + latent) removed from the air per second, Q_2, is given by:

$$Q_2 = \dot{m}_{moist} (h_b - h_c) \qquad 5.7$$

The heat pump coefficient of performance in the heating mode, COP(H), is defined as the ratio of the rate of energy output to the rate of electrical energy supply:

$$COP(H) = (Q_2 + P_c)/P_t \qquad 5.8$$

From in situ measurements of the air temperatures and relative humidity values at positions 'a', 'b' and 'c', the atmospheric pressure and the rates of electrical energy consumption, it is possible for calculations to be made of other thermodynamic properties of moist air, the quantities of energy extracted from it and the COP(H) of the heat pump, using the equations given in the above section.

5.2.3 Sensible and Latent Heat Contributions

In order to assess the relative contributions of sensible and latent heat to the total energy Q_2 extracted in unit time by the heat pump, consider the following analysis.

Q_2 is made up from two sources, sensible and latent heat, i.e.

$$Q_2 = Q_S' + Q_L' \qquad 5.9$$

where $$Q_S' = \dot{m}_{dry} C_p (t_b - t_c) \qquad 5.10$$

and $$Q_L' = \dot{m}_{dry} L (g_b - g_c) \qquad 5.11$$

The value of $\dot{m}_{dry}$ is calculated (see equation 5.6) from:

$$\dot{m}_{dry} = 0.74C \quad \rho_{b\ dry} \qquad 5.12$$

The value of $\rho_{b\ dry}$ (taken at position 'b') is given by:

$$\rho_{b\ dry} = \rho_{o}\ (T_o/T_b)\ (p_{at}/p_o) \qquad 5.13$$

where ρ_o is the density of air at the known values of pressure and absolute temperature p_o and T_o respectively, and $\rho_{b\ dry}$ the density at a pressure and absolute temperature (at position 'b') of p_{at} and T_b respectively. The dry air value for the mass flow rate, $\dot{m}_{dry}$ in equation 5.11, is taken because the units of $(g_b - g_c)$ are in kg kg^{-1} of dry air.

Using equations 5.8 to 5.11, one may write:

$$COP(H) = [\dot{m}_{dry}\ L\ (g_b - g_c) + \dot{m}_{dry}\ C_p\ (t_b - t_c) + P_c]/P_t \qquad 5.14$$

Neglecting any difference in fan power, P_f, which may arise as a result of drawing dry air and water vapour separately, and assuming the same compressor power, P_c, in each case (results have shown P_c to be independent of air moisture content), one can define two coefficients, A and B, such that:

$$A = (Q_L' + P_c)/P_t \qquad 5.15$$

and

$$B = (Q_S' + P_c)/P_t \qquad 5.16$$

Now, using equations 5.8 and 5.9, one may write:

$$COP(H) = (Q_S' + Q_L' + P_c)/P_t \qquad 5.17$$

which may also be written as:

$$COP(H) = Q_L'/P_t + (Q_S' + P_c)/P_t \qquad 5.18$$

From equations 5.15, 5.16 and 5.18 one arrives at the expression:

$$COP(H) = [A - (P_c/P_t)] + B \qquad 5.19$$

In section 5.3.1 (to follow), A and B are given as functions of $(g_b - g_c)$ and t_b respectively, and P_c is given as a function of t_b. P_t may be calculated from:

$$P_t = P_c + P_f \qquad 5.20$$

where P_f, the fan power, has been assumed constant throughout at 0.45 kW (manufacturer's data). Hence, the COP(H) may either be calculated directly from the enthalpy changes in moist air (section 5.2.2) or may be found by means of equation 5.19 (section 5.2.3).

In the sections which follow, empirical relations are presented (derived from in situ measurements at the test house) which, when used in conjunction with the preceding equations, allow calculation to be made of the heat pump's rate of energy extraction from the air (both sensible and latent contributions), its rate of energy output and its COP(H) for any known set of atmospheric conditions.

5.3 In Situ Results

The values of the air dry bulb temperature were recorded each hour at the test house at positions 'a', 'b' and 'c' (Figure 2.4). The evaporator coil temperature was measured on refrigerant entry. Relative humidity was recorded hourly at positions 'b' and 'c'; as discussed in Chapter 2, the values at 'a' were supplied by Boscombe Down weather station. Use was made of mean sea level atmospheric pressure values recorded at the same station and corrected for the

height above sea level of the test house site. The Demand Profile Recorder collected the data from which the hourly energy consumptions of the heat pump compressor and fan were deduced.

There were 26 days between January and April 1980 for which complete sets of data were available, together with full calibration, and it is from this data that the heat pump performance characteristics were derived. Measured values were plotted, one against the other, and, where appropriate, equations which were presented in the preceding sections were used to arrive at other values, which were also plotted. The linefits made to the graphs yielded the relations which follow. One such graph, that of t_b versus t_c, is shown in Figure 5.1. The broken line is that of $t_b = t_c$, and is drawn for comparison.

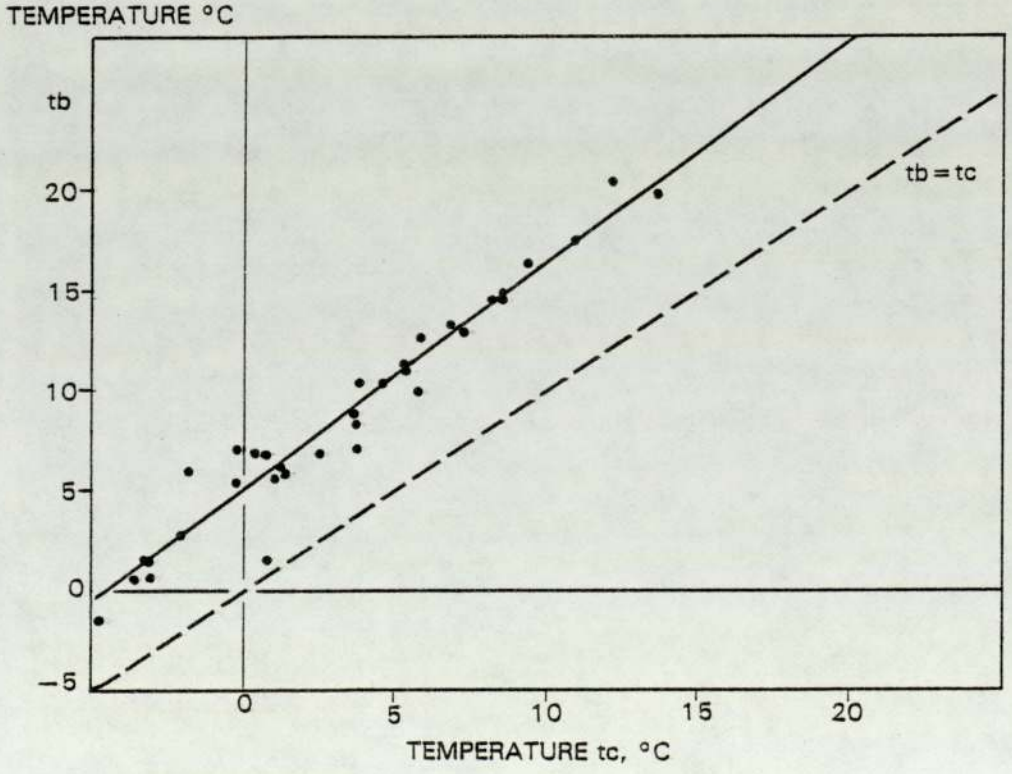

Figure 5.1 Relation between t_b and t_c, in °C, for the test house heat pump.

5.3.1 Heat Pump Performance

The air dry bulb temperature drop across the evaporator, for t_b and t_c in °C, is given by the empirical relation derived from Figure 5.1:

$$t_b = 1.17\ t_c + 4.25 \qquad 5.21$$

Errors: 1.17 ± 0.05 (2 st. dev.); 4.25 ± 0.31 (2 st. dev.).

Measured range of t_b: - 1.0°C to 25.0°C.

The drop in air moisture content across the evaporator, for g_b and g_c in kg kg^{-1} of dry air, is given by:

$$g_b = 1.03\ g_c + 0.0005 \qquad 5.22$$

Errors: 1.03 ± 0.22 (2 st. dev.); 0.0005 ± 0.001 (2 st. dev.).

Measured range of g_b: 0.003314 to 0.007665 kg kg^{-1} of dry air.

The compressor power, P_c, is related to the dry bulb temperature of the air entering the heat pump, t_b, (for P_c in kJ consumed per hour, and t_b in °C) by:

$$P_c = 199\ t_b + 8662 \qquad 5.23$$

Errors: 199 ± 19 (2 st. dev.); 8662 ± 217 (2 st. dev.).

Measured range of t_b: - 1.0°C to 25.0°C.

P_c is related to the heat pump evaporator temperature, t_e, (for P_c in kJ consumed per hour, and t_e in °C) by:

$$P_c = 315\ t_e + 10530 \qquad 5.24$$

Errors: 315 ± 38 (2 st. dev.); 10530 ± 117 (2 st. dev.).

Measured range of t_e: - 9.6°C to 6.2°C.

From a knowledge of the pressure, dry bulb temperature and relative humidity of air on entry to the heat pump evaporator, the above relations enable prediction to be made of the corresponding psychrometric state of the expelled air. This permits calculation of the enthalpy change in the air (equation 5.4), and knowledge of the moist air mass flow rate allows calculation of Q_2, the energy extracted from the air in unit time by the heat pump. The value of P_t may be obtained from equation 5.20 (by knowing P_f and deducing P_c from equation 5.23, if necessary); thus the COP(H) may be found (equation 5.8).

As an alternative, equation 5.19 can be used to estimate the COP(H) from an initial knowledge of p_{at}, t_b, ϕ_b and P_f only. Use the relevant equations to arrive at a value for g_b; equation 5.22 relates g_b and g_c, and P_c is related to t_b by equation 5.23. Equation 5.20 then provides a value for P_t. Values for coefficients A and B may be obtained from the following (for g_b and g_c in kg kg^{-1} of dry air, and t_b in °C):

$$A = 673\ (g_b - g_c) + 0.893 \qquad 5.25$$

Errors: 673 ± 22 (2 st. dev.); 0.893 ± 0.020 (2 st. dev.).
Measured range of $(g_b - g_c)$: -0.000860 to 0.001508 kg kg^{-1} of dry air.

$$B = 0.022\ t_b + 2.045 \qquad 5.26$$

Errors: 0.022 ± 0.010 (2 st. dev.); 2.045 ± 0.111 (2 st. dev.).
Measured range of t_b: -1.0°C to 25.0°C.

Relations 5.21 and 5.22 may also be utilised, together with equations 5.10 and 5.11, in the assessment of the sensible and latent heat contributions to Q_2. In the derivation of relations 5.25 and 5.26

from measured results, ρ_o (equation 5.13) was taken as 1.294 kg m^{-3} at values for T_o and p_o of 273K and 760mm mercury respectively. A constant value of 1.004 kJ kg^{-1} K^{-1} was adopted for C_p throughout.

For the 26 days of measured results, the overall average contributions of sensible and latent heat to the total energy extracted from the air by the heat pump was found to be ∿ 65% and ∿ 35% respectively. A sample of average values for individual days is shown in Table 5.1.

DATE (D/M/Y)	CONTRIBUTIONS TO THE TOTAL HEAT EXTRACTED	
	SENSIBLE HEAT	LATENT HEAT
"	"	"
"	"	"
9/2/80	53%	47%
10/2/80	68%	32%
11/2/80	61%	39%
12/2/80	66%	34%
14/2/80	60%	40%
29/2/80	75%	25%
"	"	"
"	"	"

Table 5.1 Sample values of the daily average sensible and latent heat contributions, %, to the total energy extracted from the air by the heat pump.

This gives an indication of the relative importance of the latent heat constribution, and justifies the analysis in terms of moist air thermodynamics.

5.3.2 Change in Air Moisture Content, Positions 'a' to 'b'

The change in air moisture content which takes place between outdoors (position 'a') and the entry to the heat pump evaporator (position 'b') is given (for g_a and g_b in kg kg^{-1} of dry air) by:

$$g_a = 0.96\ g_b \qquad 5.27$$

Error: 0.96 ± 0.10 (2 st. dev.).

Measured range of g_b: 0.003314 to 0.007665 kg kg^{-1} of dry air.

This result indicates that the roof tiles of the test house may have a hygroscopic effect, since measurements showed that the air frequently contained more moisture after passage under the tiles. Expression 5.27 was used in the analysis of the performance during the 1977/78 heating season (Chapter 6). However, an assumption that there is no change in moisture content from positions 'a' to 'b' may be satisfactory for other roof systems acting as pre-heaters for a heat pump, particularly in the case of a metal roof (see Chapter 7).

5.4 Summary

A set of empirical relations describing the in situ performance characteristics of an American heat pump using air as its low grade energy source and operating in the U.K. climate has been presented. These relations enable calculations to be made of the instantaneous values of the rate of energy extraction from moist air, Q_2, the latent and sensible heat contributions, Q_L' and Q_S', and the COP(H), from a knowledge of the instantaneous values of

pressure, dry bulb temperature and relative humidity of the air on entry to the evaporator, and also the air mass flow rate and fan power. An expression (5.27) relating the outdoor air moisture content to that on evaporator entry has been given, and this, together with expression 5.22, is used in the heating season analysis in the next chapter. Some of the relations given exhibit large errors, but this is to be expected as the results were obtained on site in an essentially uncontrolled environment.

The characteristics can be used to predict the performance of this type of heat pump when used in conjunction with other roof pre-heating systems, utilising the appropriate theoretical model for the 'collector' considered (see Chapter 7, for example), or utilising the relevant efficiency graphs, if available. Using additional characteristics (presented in Chapter 6), it is possible to compare data obtained from the heat pump's seasonal (1977/78) in situ operation with that quoted by the manufacturer (section 6.4.4, Chapter 6). The heat pump characteristics may be used as data input in computer modelling applications.

CHAPTER 6

PERFORMANCE OF THE SYSTEM OVER ONE HEATING SEASON

6.1 Introduction

The system was monitored for the heating season commencing October 1977 and ending April 1978. For this period, the number of monthly degree-days (Department of Energy, 1977) calculated for a base temperature of 15.5°C and for an assumed indoor air temperature of 18.3°C for the Thames Valley area totalled 1813 (Energy Management, 1979). This compares with a total for the same area of 1862 degree-days for the period October to April, taken from the monthly figures averaged over the twenty years up to 1979 (Energy Management, 1981). This indicates that the monitored heating season was slightly milder than average. The performance analysis of the system was not, however, based on degree-day figures, but on the actual values of indoor and outdoor air temperatures measured on site. This was because the average indoor air temperature of the test house differed from the value of 18.3°C assumed in the Department of Energy degree-day figures.

As discussed in Chapter 2, all temperatures, electrical energy consumptions and hot water usage were measured on site, while atmospheric pressure (corrected for the height above sea level of the test site) and outdoor relative humidity values were provided by Boscombe Down weather station. In addition, an average value for the ground temperature at a depth of 0.9 metres was calculated from Meteorological Office data (section 6.3.4).

6.2 Energy Balance Analysis

The energy flows considered in the analysis are illustrated in Figure 6.1 (all figures are at the end of this chapter).

6.2.1 Nomenclature

All units are in kW.

Q_2 is the rate of energy extraction from the air by the heat pump;

P_C is the rate of energy consumption by the heat pump compressor;

Q_W is the rate of energy supply by the heat pump to the domestic hot water;

Q_{PH} is the rate of energy supply to the living space from the condenser via the air heating system before transfer into the store;

Q_S is the rate of energy supply to the store;

Q_{SH} is the rate of energy supply from the store via the air heating system;

Q_{SL} is the rate of heat loss from the store to the living space;

Q_L is the rate of heat loss from the store to the ground through the store sides and base;

Q_{HL} is the sum of the rates of fabric heat loss (from the living space) through the walls and ceiling, and the ventilation heat loss;

Q_{INC} is the rate of energy supply arising from incidental gains;

Q_{SG} is the rate of energy supply arising from solar gains;

Q_{SUPP} is the rate of energy supply arising from supplementary electric space heating.

6.2.2 Analysis

The total rate of supply of energy by the heat pump was taken as $(Q_2 + P_c)$, since this then includes any refrigerant line heat losses (which are within the building structure). Q_W, the contribution from the heat pump to the domestic hot water load, is supplied by a de-superheater. The remainder of this load is supplied by an electrical immersion heater. Losses from the domestic hot water system to the living space can, if necessary, be included in the incidental gains, Q_{INC} (section 6.3.5).

Two control volumes are considered - that of the living space and that of the store. While there is heat loss from the living space into the loft, it would have to be reduced by a fraction dependent upon the number of hours of heat pump operation in a given time, since the heat pump recycles part or all of this loss when running. For simplicity, this element of the heat loss has not been specified as a separate term, but has been taken into account in the heat loss term Q_{HL} (ceiling losses represent only about 10% of the total fabric loss of the dwelling).

Considering the living space, and equating the rates of energy supply and loss:

$$(Q_2 + P_c) - Q_W + Q_{INC} + Q_{SG} + Q_{SUPP} + Q_{SH} + Q_{SL} = Q_S + Q_{HL} \qquad 6.1$$

Similarly, for the store complex:

$$Q_S = Q_{SL} + Q_{SH} + Q_L \qquad 6.2$$

By combining equations 6.1 and 6.2, i.e. effectively considering a single living space/store control volume, and introducing Q_{IMM}, the

rate of electrical energy supply for immersion heating, so as to include both space and water heating loads, one arrives at the following equation:

$$(Q_2 + P_c) + Q_{INC} + Q_{SG} + Q_{SUPP} + Q_{IMM} = Q_W + Q_{IMM} + Q_L + Q_{HL} \qquad 6.3$$

Now introduce Q_T, which represents the total change in stored energy in a given time interval. Q_T can be positive, negative, or zero, depending upon whether the left hand side of equation 6.3 is greater than, less than, or equal to the right hand side. Hence, one may write:

$$(Q_2 + P_c) + Q_{INC} + Q_{SG} + Q_{SUPP} + Q_{IMM} = Q_W + Q_{IMM} + Q_L + Q_{HL} + Q_T \qquad 6.4$$

This means that the energy supplied in a given time interval equals the energy to the load plus the stored energy in the same time interval. When the supply of energy exceeds the load, the excess is available for storage; when the supply cannot fully meet the load requirements, the deficit is made up by energy drawn from the store. Equation 6.4 forms the basis of the performance analysis of the system, and accounts for both space and water heating.

6.3 Energy Calculations

All energy flow rates were calculated on an average weekly basis in units of kWh per week.

6.3.1 Heat Pump Output, $(Q_2 + P_c)$, and the COP(H)

From the hourly measurements, an average value for each week was derived for appropriate quantities. Values of g_a were calculated using the equations of section 5.2.2, and those of g_b and g_c using relations 5.27 and 5.22. Weekly average values for Q_2, P_c and the

COP(H) were then calculated for the 25-week heating season, commencing 18 October 1977 and ending 10 April 1978.

6.3.2 Energy for Domestic Hot Water, $Q_W + Q_{IMM}$

From the measurement of the total amount of hot water used in the heating season, the average daily usage was found to be $0.242m^3$ or 242 litres, which is somewhat higher than the expected average usage of 135 litres day $^{-1}$ for a three-occupant household, based on a consumption of 45 litres person $^{-1}$ (Whittle and Warren, 1978). Energy to heat this water to its final draw-off temperature of 60°C came from two sources - the heat pump super-heated refrigerant vapour and an electrical immersion heater. From the measurements of temperatures in the water heating system and the electricity consumption of the immersion heater, it was found that, on average, 26% of the total domestic hot water load was met by energy from the heat pump; this is Q_W, and is about 21 kWh week^{-1}. The rest of the hot water load was met by the electrical immersion heater; this is Q_{IMM}, and is about 60 kWh week $^{-1}$.

6.3.3 Fabric and Ventilation Heat Loss, Q_{HL}

The ventilation rate of a building may be determined by either the air change method or the crack method (IHVE Guide, Book A, 1970; ASHRAE, 1972). The air change method, and the procedure described by the Building Research Establishment (1976) were adopted for this work.

The total floor area (ground and first floors) of the living space is $141.7m^2$, and the ceiling height 2.44m, giving a total volume of

approximately 346m^3. Deducting 10% of this for cupboards and other 'dead space' gives an air change volume of 311m^3. Since the test house has no flue, a rate of 0.5 air changes per hour was taken, giving a volume change of 156m^3 hr^{-1}, or 26208m^3 $week^{-1}$. A cubic metre of air requires 0.00033 kWh of energy to raise its temperature through 1°C, leading to a value for the test house of 8.7 kWh $week^{-1}$ for each degree temperature difference between the indoor and outdoor air. This is the rate of ventilation heat loss.

The rate of fabric heat loss (per degree temperature difference) from the test house was obtained by multiplying the external wall and window areas and the ceiling area with the appropriate U-values (Diamant, 1977) of the construction materials and then summing the individual 'UA' values.

The loss rate thus obtained was 4.6 kW for an internal to external temperature difference of twenty degrees, under windstill conditions.

Exposure loading of the fabric loss rate is arbitrary, though a value of 15% has been quoted (ASHRAE, 1972). It was decided, however, to calculate another value for the fabric heat loss rate under a known wind speed condition and by interpolating linearly between this and the windstill value, to arrive at a loading for a typical windspeed for the area. At a windspeed of 6 ms^{-1}, the fabric loss rate increased to 5.3 kW (for a twenty degree temperature difference). The mean wind speed for the area was taken as 4 ms^{-1} (Rayment, 1976), representing a loading of 10% on the windstill figure for the rate of fabric heat loss. A further loading of 5% was added to take account of sky radiation effects (Siviour, 1979a). This resulted in an average value

for the fabric heat loss rate of 5.3kW for a twenty degree temperature difference, or 44.5 kWh $week^{-1}$ for each degree temperature difference, indoors to outdoors.

The total rate of heat loss (ventilation + fabric) for the test house, Q_{HL}, is therefore approximately 53 kWh $week^{-1}$ $°C^{-1}$. Measured values provided the relevant temperature differences.

6.3.4 Store Heat Loss, Q_L

The store complex consists of three interconnected water-filled polypropylene bags, positioned into recesses in the ground floor of the test house. Each recess is about 0.5m deep. The bags rest on a layer of sand 0.1m deep, below which is concrete and then the ground; the bags are surrounded on their sides by polystyrene 0.05m thick. The U-values for the structure and materials are 0.6 Wm^{-2} K^{-1} for the top surface (store to living space), 0.6 Wm^{-2} K^{-1} for the sides (store to ground) and 2.0 Wm^{-2} K^{-1} for the base (store to ground). The corresponding surface areas are 44.7m^2 (top), 16.0m^2 (sides) and 44.7m^2 (base).

The rate of actual heat loss from the store, Q_L, is that taking place from the sides and base only, since top 'losses' are to the living space and hence remain within the system. From calculation of the products of U-values and areas, the value of Q_L was found to be 17 kWh $week^{-1}$ $°C^{-1}$, the temperature difference being that between the store and the ground.

From dimensions and depth measurements, the volume of water in the store was calculated to be $21m^3 \pm 5\%$ (a mass of 21×10^3 kg). The temperature of this water was monitored hourly by a sensor placed at the centre of the side of one of the bags. A separate measuring exercise showed little evidence of store temperature stratification, other than the water temperature around the top, sides and base of the bags being slightly cooler than that in the centre (of the order of 1 or 2°C). This effect was greatest when the water circulating pumps were off, and was more marked at the top and base of each bag rather than the sides. It was concluded that the regularly monitored store temperature was reasonably representative of the average value throughout.

The average ground temperature for the season was calculated from mean monthly values (over a thirty-year period, 1931/61) of earth temperature at a depth of 0.92m for Winchester, Hampshire, published by the Meteorological Office; this value was 8°C. However, a value of 10°C was taken due to proximity to the store. This correction was based on measurements of soil temperature at a depth of about 0.5m made outside the test house; a progressive increase in soil temperature was observed to take place as the distance between the test house and the temperature sampling point was reduced.

6.3.5 Incidental Gains, Solar Gain and Supplementary Heating, Q_{INC}, Q_{SG} and Q_{SUPP}

The average electricity consumption for cooking and lighting, immersion heating and power supply outlets was found, from measurements over the season, to be 7.5, 8.5 and 29.6 kWh day^{-1} respectively. The following assumptions were then made:

(i) of the energy used for cooking and lighting, 90% produces heat, the remainder being lost to the drainage;

(ii) of the energy used in domestic water heating, 50% helps supply the house heat loss (Siviour, 1979b), the remainder being lost to the drainage;

(iii) of the energy drawn from domestic outlets, 60% is for supplementary resistance heating, and of the remainder, 85% produces useful heat, the rest being lost in outdoor use, for example, workshop use.

These assumptions led to an average value for the rate of supply of supplementary heating, Q_{SUPP}, of 124 kWh week^{-1}, and a value for the rate of supply due to incidental gains from cooking, lighting, appliances and hot water heat loss of 22.6 kWh day^{-1}. The figure for incidental gains is in general agreement with values quoted by various authors, and summarised by Siviour (1979b). From the same reference, values of 2 kWh day^{-1} and 4 kWh day^{-1} respectively were added for the insulation effects of curtains and the heat output by occupants, giving a final figure for incidental gains, Q'_{INC}, of 198 kWh week^{-1} including, or Q_{INC} of 158 kWh week^{-1} excluding, the 50% contribution from domestic water heating. Note that the latter value, Q_{INC}, is adopted throughout this chapter and the next, since space and water heating are treated as separate entities and then summed.

A value for Q_{SG} of 2000 kWh year^{-1}, or 38 kWh week^{-1} was taken as the contribution to space heating resulting from the solar energy gain of a well-insulated double-glazed dwelling in the U.K. (Siviour, 1977).

6.4 Seasonal Performance - Results

The performance interpretation was based on equation 6.4, the energy values being calculated on a weekly basis using the results of the previous sections and the appropriate temperature differences. The values of Q_W, Q_{INC} and Q_{SG}, however, were taken as constant throughout the season. Also, since no data was available on supplementary heat usage with time, a correlation between Q_{SUPP} and the outdoor ambient air temperature, t_a, was assumed. Thus, Q_{SUPP} was taken as 124 kWh for a week with an average t_a value of 7.0°C (the seasonal average t_a value), and then 17.7 kWh added (or subtracted) for each degree below (or above) this value of t_a.

6.4.1 Energy Supply and Load

Figure 6.2 shows the variation in Q_{HL}, Q_L and $(Q_2 + P_c)$ over the season, while Figure 6.3 shows the seasonal variations of the total load (taken as the sum of Q_{HL}, Q_L, Q_W and Q_{IMM}) and the total supply (taken as the sum of $[Q_2 + P_c]$, Q_{INC}, Q_{SG}, Q_{SUPP} and Q_{IMM}). Averaged over the entire 25-week season, the values of Q_{HL}, Q_L and $(Q_2 + P_c)$ are 608, 359 and 715 kWh week^{-1} respectively; those of the total load and total supply are, respectively, 1048 and 1094 kWh week^{-1}.

A comparison of the actual change in stored energy each week, Q_T, with the estimated change is shown in Figure 6.4. The actual variation in energy is calculated from the measurements of the weekly changes in temperature of the stored mass of water. The estimated variation comes from equation 6.4, and is the result of the assumptions made in this performance analysis concerning, for example, occupancy patterns

and supplementary energy usage, i.e. the fact that it was an occupied residence under test; general values had to be attributed to such items as Q_W, Q_{IMM}, Q_{INC}, Q_{SG} and Q_{SUPP}. Also, assumptions were made in arriving at the load figures. Considering this, it can be seen that the shapes of the estimated and actual variations are in overall agreement, though individual values show some discrepancy. It is concluded, therefore, that the analysis procedure, with its assumptions, is valid for showing the general trends of the system.

The graph of the actual energy changes shows, in general, a smaller variation than that of the estimated changes. This is thought to be due to the foundations and nearby ground under the house behaving as a secondary store, and acting as a 'buffer' against large temperature changes in the water store. This effect is particularly marked when one observes the periods from January to February, and from mid-March to April; during the charging in October, the difference between the actual and estimated Q_T could then be due to raising the temperature of the ground and foundations.

Table 6.1 was obtained by summing the weekly energy values, and shows, on a monthly basis, the total supply, total load and the estimated total energy stored.

MONTH	TOTAL LOAD, kWh	TOTAL SUPPLY, kWh	ESTIMATED TOTAL ENERGY STORED, kWh
OCT.*	1234	2158	924
NOV.	4193	4224	31
DEC.	5462	5318	-144
JAN.	4505	4808	303
FEB.	4638	4633	-5
MAR.	4164	4485	321
APR.*	2022	1725	-297

Table 6.1 Performance figures on a monthly basis for the heating season 1977/78 (rounded figures).

* Two weeks only

Over the entire season, the total values of $(Q_? + P_c)$, $(Q_{INC} + Q_{SG})$, Q_{IMM} and Q_{SUPP} are 17868, 4887, 1492 and 3106 kWh respectively; summing these values gives a seasonal total supply of 27353 kWh. Similarly, the total values of Q_{HL}, Q_L, Q_W and Q_{IMM} are 15200, 8975, 525 and 1492 kWh respectively; summing these gives a seasonal total load of 26192 kWh.

Summing the actual Q_T values over the season results in a net gain of about 373 kWh to the store. This represents the difference between the initial and final states of the store at the beginning and end of the monitoring period. In October, when monitoring commenced, the store temperature was 15°C, whereas in April, at the cessation of monitoring, it was 30°C. The seasonal total value for Q_T can thus be looked upon as the energy required to raise the stored mass of water

from its initial temperature of 15°C to an assumed minimum useful temperature of 25°C, plus an additional 5°C (which could be regarded as a 'system mismanagement penalty' on the part of the occupants). This stored energy, then, must be included as an addition to the load since the analysis is restricted to the 25-week operation of the heat pump (whereas, in fact, the stored energy provided benefit beyond the month of April). This will result in a slightly more 'pessimistic' view of performance as regards savings on purchased energy (section 6.5).

The sum of the seasonal totals of load and stored energy is thus 26192 + 373 = 26565 kWh, while the seasonal total of supplied energy is 27353 kWh. The system is therefore balanced to within 788 kWh, or about 3%. This balance is thought to be very good in view of the assumptions made in the performance analysis. Note that Figures 6.2, 6.3, 6.4 and Table 6.1 contain this imbalance (which represents about 32 kWh $week^{-1}$).

6.4.2 Air Heating Performance of the Tiled Roof System

Figure 6.5 is a graph of the seasonal variations of the outdoor ambient air temperature, t_a, and the temperature t_b of the air after it has passed under the roof tiles to the entrance of the heat pump. This shows the effect the roof system has in raising the air temperature; the average increase over the season was about 1.4°C. Higher temperature rises (up to twelve degrees on the South East facing side of the roof) have been recorded on individual days (see Figure 6.8, for example) but this is dependent upon conditions. Airstreams from both the South East facing and North West facing sides of the tiled

roof contribute to the final temperature of entry, t_b, to the heat pump evaporator, as does heat loss into the loft from the living space. This was discussed by Neal et al (1979), when it was found that of the total energy extracted by the heat pump in the 1977/78 heating season, approximately 77.0%, 17.5% and 5.5% came from ambient, solar and heat loss sources respectively (assuming that all the heat loss from the living space into the loft goes in full to raise the temperature of the incoming air to the heat pump).

The effect of the tiled roof on the performance of the heat pump is discussed in Chapter 7.

6.4.3 Heat Pump Coefficient of Performance and Heating Capacity

The seasonal variation in the weekly average COP(H) values is shown in Figure 6.6. However, a single overall value for the season, the seasonal COP(H), may be defined as:

$$\text{seasonal COP(H)} = \frac{\text{total heat pump energy output for the season}}{\text{total heat pump (electrical) energy input for the season}} \qquad 6.5$$

The value for the 1977/78 seasonal COP(H) was 2.45. A plot of the weekly average values of COP(H) against t_b, in °C, is shown (as the solid line) in Figure 6.7. The linefit to this yields the following relation:

$$\text{COP(H)} = 0.043\ t_b + 2.139 \qquad 6.6$$

Errors: 0.043 ± 0.043 (2 st. dev.); 2.139 ± 0.393 (2 st. dev.).

Measured range of t_b: 1.7°C to 16.2°C.

This may be compared with the empirical relationship obtained by Heap (1976a) for a range of heat pumps operating in the U.K. climate:

$$COP(H) = 0.058\ t_s + 2.186 \qquad 6.7$$

where t_s is the source temperature in °C.

Figure 6.7 also shows, as a broken line, the weekly average COP(H) as a function of the weekly average outdoor ambient air temperature, t_a, in °C. The linefit gives:

$$COP(H) = 0.041\ t_a + 2.207 \qquad 6.8$$

Errors: 0.041 ± 0.043 (2 st. dev.); 2.207 ± 0.340 (2 st. dev.).

Measured range of t_a: - 0.5°C to 14.1°C.

The latter graph is useful for 'at a glance' forecasting of the approximate average COP(H) to be expected in this system, from a knowledge of the outdoor temperature. The possibility of a simple control system for the heat pump arises here, especially if the ambient air temperature can be predicted in advance. A method of achieving this has been described by Hays et al (1979). Note, however, that the graphs of Figure 6.7 are based on weekly average figures which therefore limits the accuracy in applications involving smaller time intervals. For more accurate COP(H) prediction, some form of control system based on the equations presented in Chapter 5 would be necessary. Broader aspects of heat pump system control have been discussed by Neal (1981b).

Figure 6.8 shows the variation of ambient and heat pump inlet air temperatures over a single day, while Figure 6.9 shows the hourly COP(H) variation over the same day. The COP(H) values in the evening

are greater than those in the early part of the morning. This is caused by the heat storage effect of the roof tiles in the evening (and their corresponding thermal inertia in the morning) and also by increased heat loss from the living space into the loft during the evening, as a result of the family's occupancy patterns. As discussed in Chapter 4, section 4.3.3, the heat pump on/off times could be adjusted to take advantage of this effect.

The average weekly heating capacity of the heat pump, $(Q_2 + P_c)$, in kW, as a function of t_b, in °C, is given by:

$$(Q_2 + P_c) = 0.145\ t_b + 7.4 \qquad 6.9$$

Errors: 0.145 ± 0.094 (2 st. dev.); 7.4 ± 0.9 (2 st. dev.).
Measured range of t_b: 1.7°C to 16.2°C.

6.4.4 Comparison of Heat Pump Performance with the Manufacturer's Specification

It is now possible to compare data obtained from the results of seasonal in situ operation of the heat pump with that provided by the manufacturer. The values for the heating capacity and the COP(H) at +7°C and -7°C (source temperature) given by the manufacturer for the HP7 heat pump (model 411VFF) were compared with those of $(Q_2 + P_c)$ and COP(H) calculated using equations 6.9 and 6.6 respectively, with values for t_b the same as the source temperatures above. The results are shown in Table 6.2. For the values compared, the actual in situ performance differs from that quoted by the heat pump manufacturer, this being particularly marked in the case of the COP(H). As discussed

in Chapter 5, this may be due to differences between the manufacturer's test conditions and those encountered in the outdoor environment.

	MANUFACTURER'S VALUE	VALUE CALCULATED FROM SEASONAL IN SITU RESULTS
HEATING CAPACITY, kW, AT +7°C	9.54	8.42
COP(H) AT +7°C	3.05	2.44
HEATING CAPACITY, kW, AT -7°C	5.67	6.39*
COP(H) AT -7°C	2.25	1.84*

Table 6.2 Comparison of the manufacturer's performance values with those calculated from seasonal in situ results.
* Extrapolated values, as the measured range of t_b was from 1.7°C to 16.2°C only.

6.5 Savings on Purchased Energy

In this, and subsequent sections (Chapter 7), savings are presented in terms of the requirement of purchased energy. No attempt is made to discuss financial savings, since this is dependent upon the prevailing tariffs for the energy source purchased, whether electricity, oil or gas.

The savings have been estimated by comparing the seasonal loads, supplies and requirements of purchased energy of the test house and existing heating system with those of the same house, but without the heat pump or the store; in the latter case, a 100% efficient heating system is taken as being installed, i.e. electrical resistance

heating. This system was chosen to simplify comparison; note that in an oil or gas-fired system, boiler inefficiencies would need to be taken into account. The seasonal loads and supplies of the existing system were found by adding the relevant weekly values; Q_T represents the total change in stored energy over the season, and, being a net gain, appears as an addition to the load. The energy (for space and water heating) purchased over the season, including that of ancillary pumps and fans, Q_{AN}, and immersion heating, Q_{IMM}, was deduced from the readings of kilowatt-hour meters. The 3% imbalance (section 6.4.1) between load and supply was corrected by adjusting the value of the supplmentary heating requirement (this will render the figures for percentage savings slightly 'optimistic' - see later). Table 6.3 gives the seasonal values for the existing system. The symbols previously defined as rates of energy supply, loss or consumption (section 6.2.1) are, for simplicity, retained, but they now refer to the total energy over the season for each quantity concerned. Where the symbols refer to totals over other time intervals (weekly, monthly, etc.), this is clearly indicated in the text, as, for example, in the earlier part of this chapter, and in Chapter 7.

	SEASONAL ENERGY TOTALS, kWh		
ITEM	LOAD	SUPPLY	PURCHASED
Q_{HL}	15200		
Q_L	8975		
Q_W	525		
Q_{IMM}	1492	1492	1492
Q_2		11516	
P_c		6352	
P_t			7290
Q_{AN}			1874
$(Q_{INC} + Q_{SG})$		4887	
Q_T	373		
Q_{SUPP}		2318	2318
TOTALS	26565	26565	12974

Table 6.3 Load, supply and requirement of purchased energy for the existing system.

The energy figures for the same house, but without the heat pump or store are given in Table 6.4. The value for Q_{HL} remains the same, but the value for Q_L is now that of heat loss from the living space through the floor to the ground (i.e. no store). For the same materials and areas, this loss was estimated to be about 187 kWh week^{-1} or 4675 kWh for the season. Since the resistance heating system employed was considered to be 100% efficient, Q_{AN} was taken as zero. The values for Q_{INC} and Q_{SG} were considered to remain the same, as was the domestic hot water requirement, $Q_W + Q_{IMM}$ (which now has no

contribution from any heat pump). The entire space and water heating load must now be met by purchased energy except for that supplied by the incidental gains.

	SEASONAL ENERGY TOTALS, kWh		
ITEM	LOAD	SUPPLY	PURCHASED
Q_{HL}	15200		
Q_L	4675		
Q_W) Q_{IMM})	2017	2017	2017
$Q_{INC} + Q_{SG}$		4887	
Q_{SUPP}		14988	14988
TOTALS	21892	21892	17005

Table 6.4 Estimated load, supply and requirement of purchased energy with a resistance heating system.

The two cases of the house with and without the monitored system may now be compared. The saving in purchased energy with the system is 17005 - 12974 = 4031 kWh over the season. This represents a percentage saving of (4031/17005) x 100% = 23.7% over the case of the same house but without the system. Note that the value of Q_{HL} in Table 6.3 does not allow for recycled heat losses during heat pump operation. When this is taken into account, the decrease in the seasonal value of Q_{HL} is estimated to be about 36kWh. This increases the value of 23.7% for percentage saving, but by a negligible amount (0.2%).

The above figures relate to the removal of the 3% imbalance from Q_{SUPP} only. If the imbalance is removed equally from Q_{INC} and Q_{SUPP} and the above procedure repeated, the figure for percentage saving becomes 23.2% (the value 4031 kWh remains the same). This may be compared with the figure 23.7% above. To the nearest whole number, the difference is 1%. However, to avoid confusing the incidental gains, the value 23.7%, or ≈ 24%, will be adopted, and balancing will be carried out on Q_{SUPP} only. It is concluded, therefore, that the monitored system, used in its present mode, results in savings of about 24% over the case of the same house but with a 1:1 ratio resistance heating system installed (i.e. a system in which 1 kWh of energy purchased produces 1 kWh of useful heating, as opposed to the COP of a heat pump system). Possible changes to the existing system and their effect on savings of purchased energy are discussed in the next chapter.

6.6 Summary

An energy balance for the test house and heating system has been carried out, resulting in an expression upon which the seasonal performance analysis could be based. From a combination of measured data and characteristics relating to changes in air moisture content (given in Chapter 5) for the heat pump and tiled roof system, values for the heating output and COP(H) of the heat pump were calculated for each week of the heating season. In addition, the procedures employed in calculating for each week the fabric, ventilation and store heat losses, the heat pump contribution to the energy required for the heating of domestic hot water, the incidental and solar gains, and the supplementary heating, have been described.

The seasonal performance has been presented in graphical (weekly) and tabular (monthly) forms, together with a comparison of estimated and actual changes in the energy stored throughout the season. This comparison showed good general agreement, from which it was concluded that the analytical procedure adopted is valid for showing the general behaviour of the system; from the smaller variation in actual changes compared with estimated changes in stored energy, it was concluded that the ground and house foundations may be acting as a secondary store. Further, it has been shown that the procedure balances the energy flows of the system to within about 3%.

The passage of air under both sides of the tiled roof resulted in an increase in the air temperature of, on average, 1.4°C over the season; of the total energy extracted from the air by the heat pump, it was found (Neal et al, 1979) that approximately 77.0%, 17.5% and 5.5% came from ambient, solar and heat loss sources respectively. The value for the seasonal COP(H) was 2.45.

An empirical relation between the weekly average COP(H) and the weekly average dry bulb temperature, t_b, in °C, of the air entering the heat pump was found to be:

$$COP(H) = 0.043\ t_b + 2.139 \qquad 6.6$$

which may be compared with one obtained by Heap (1976a). Relations have additionally been presented between the weekly average COP(H) and t_a, and the heating capacity ($Q_2 + P_c$) and t_b. Graphs showing the variation of t_a, t_b and the COP(H) over a single day have also been shown.

Values obtained from the seasonal in situ performance characteristics of the heat pump differed from those given by the manufacturer for the heating capacity and COP(H) at two values of source temperature.

The saving in the requirement of purchased energy as a consequence of using the monitored system as opposed to a 1:1 ratio resistance heating system to heat the test house was found to be 4031 kWh, or about 24% over the season.

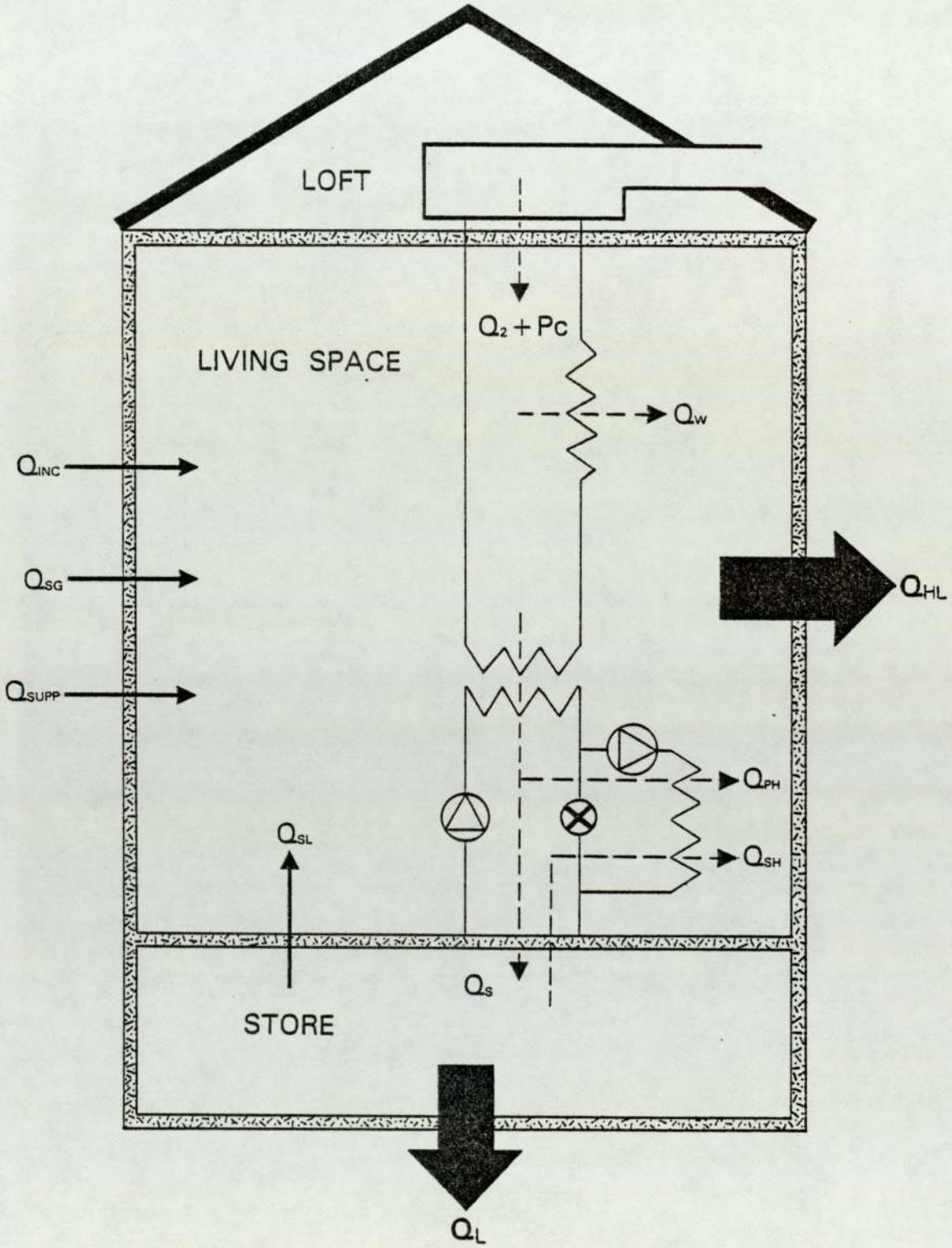

Figure 6.1 The energy flows considered in the test house analysis.

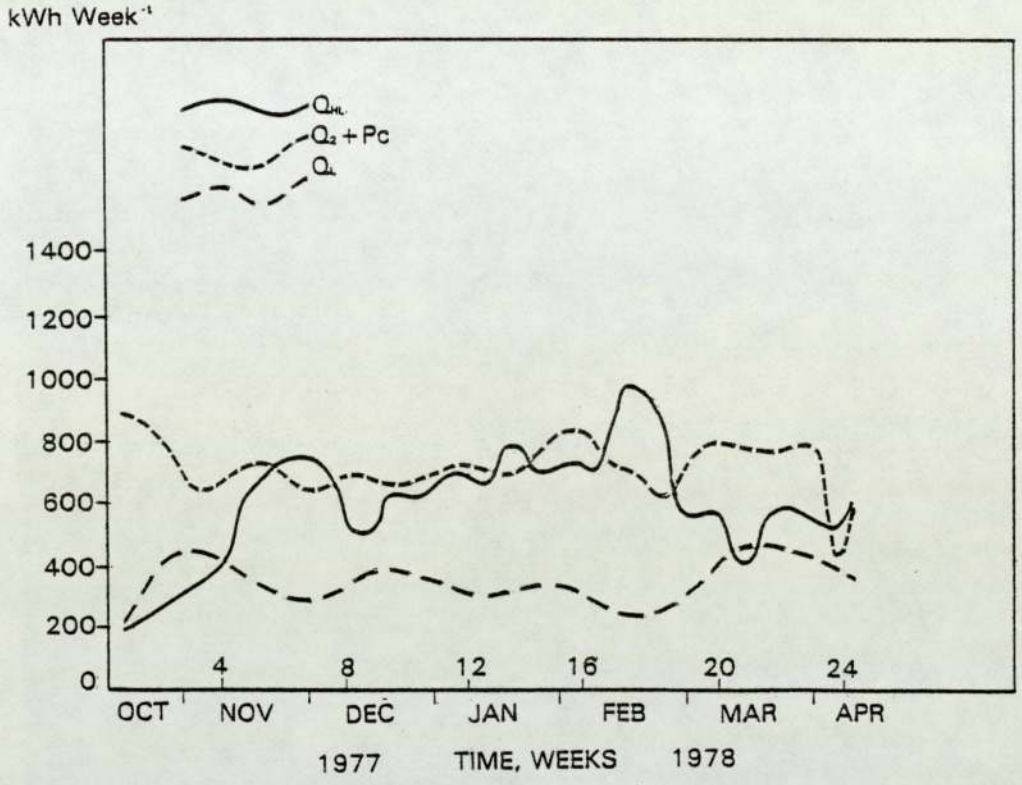

Figure 6.2 Variation in the weekly average values of Q_{HL}, Q_L and $(Q_2 + P_C)$ over the heating season.

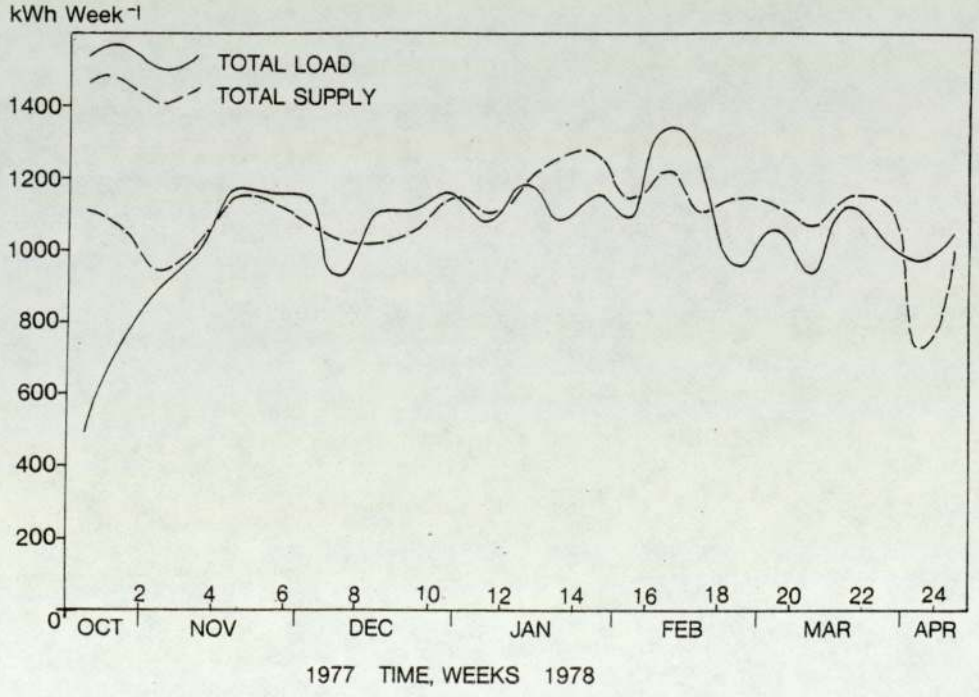

Figure 6.3 Variation in the weekly average values of the total load and total supply over the heating season.

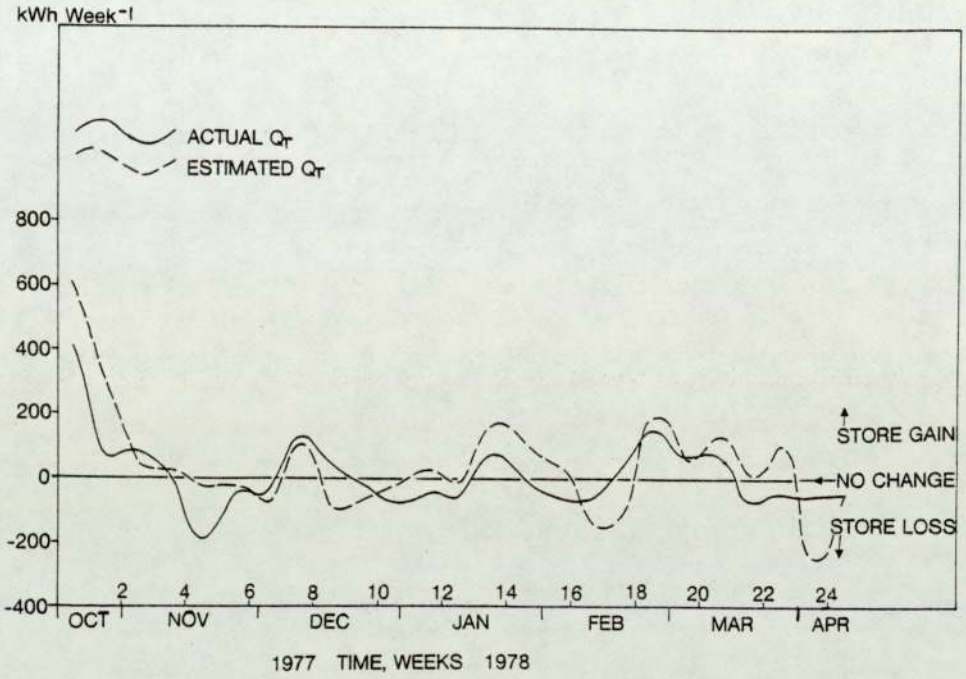

Figure 6.4 Comparison of the actual and estimated weekly changes in stored energy, Q_T, over the heating season.

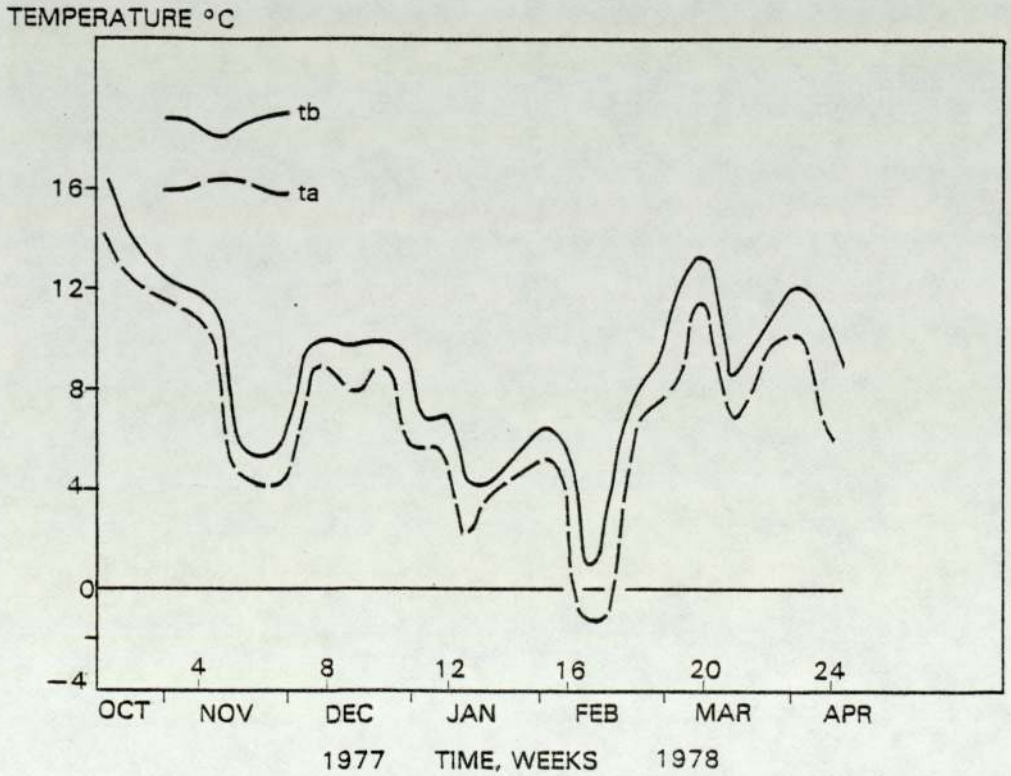

Figure 6.5 Variation in the weekly average values of t_a and t_b over the heating season.

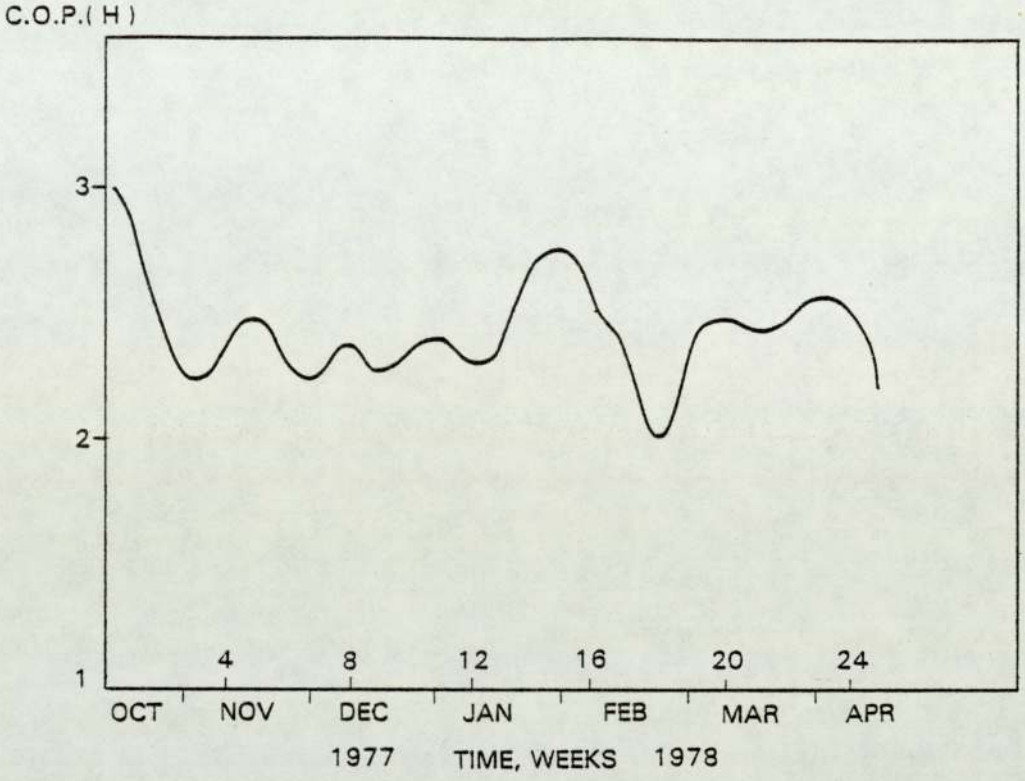

Figure 6.6 Variation in the weekly average COP(H) values over the heating season.

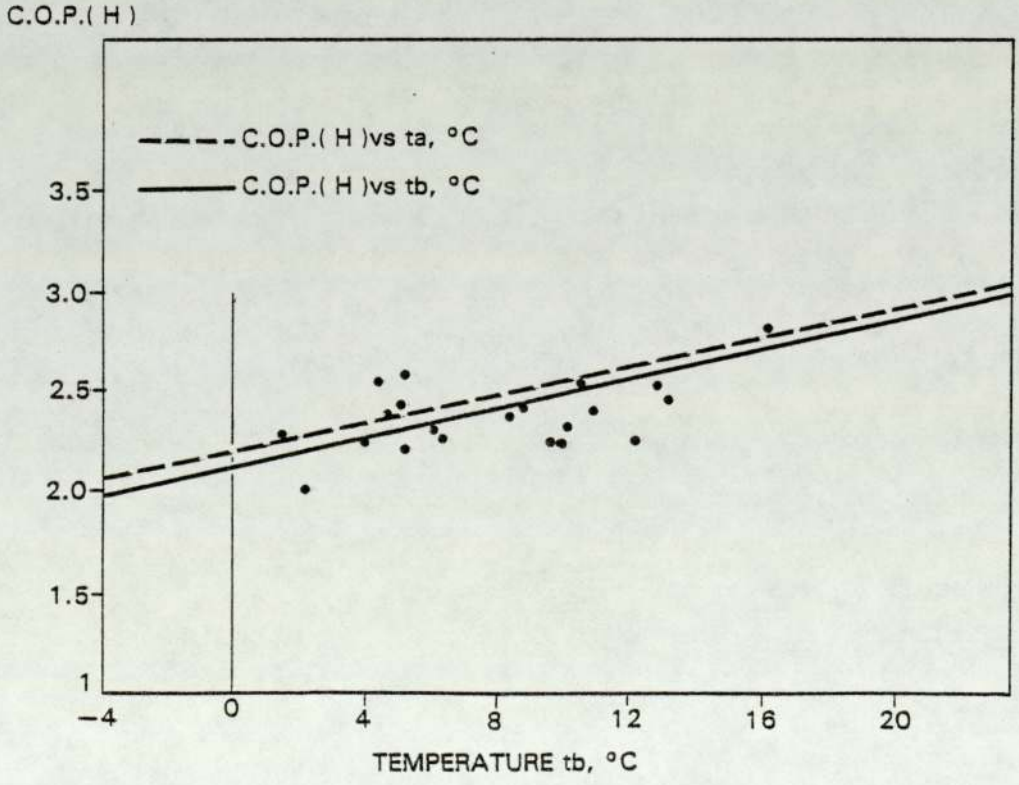

Figure 6.7 The weekly average COP(H) as a function of the weekly average values of t_b and of t_a. The graph points relate to the line COP(H) vs. t_b.

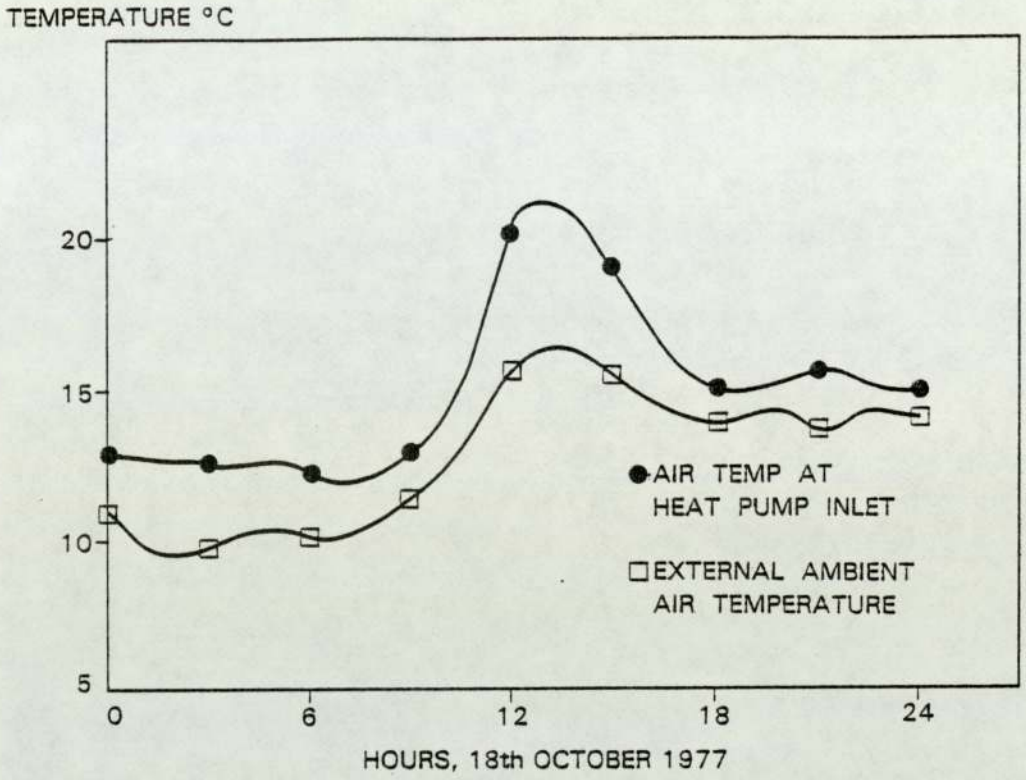

Figure 6.8 Variation in the external ambient air temperature, t_a, and the heat pump inlet air temperature, t_b, over a single day.

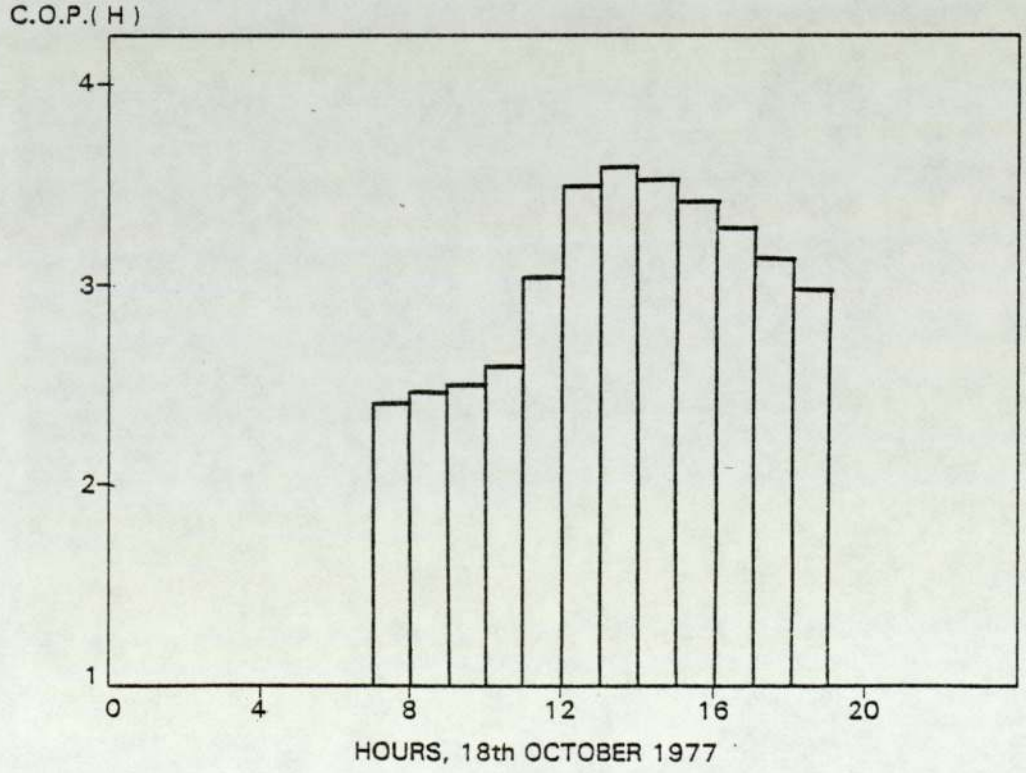

Figure 6.9 Variation in the hourly COP(H) value over the same day as in Figure 6.8.

CHAPTER 7

A DISCUSSION OF STORE MODIFICATIONS, AND OF THE EFFECTS OF THE TILED AND OTHER ROOF SYSTEMS

7.1 Introduction

In an attempt to improve the performance of the installed heating system, several modifications to the existing store of the test house are considered, and their effect on the saving of purchased energy discussed. The changes considered are those of improved insulation and reduction in store size, the latter of which would improve the prospects for retrofitting applications.

The latter part of this chapter is concerned with the effect, on the performance of the monitored heat pump, of using the tiled roof as the air pre-heater as opposed to using air drawn directly from outside without any pre-heating. In addition, the effect of using corrugated steel roofing panels, of the type discussed in Chapter 4, as air pre-heaters is assessed. All comparisons are based on the performance characteristics (Chapters 5 and 6) of the same monitored heat pump, and the comparative figures for the savings in purchased energy are calculated with reference to the monitored system.

Comments are made with regard to the cost-effectiveness of the store modifications. The analysis of a corrugated steel roof as an air pre-heater for the heat pump is not presented in the context of a cost-effective option for the householder, but is regarded as of interest from the point of view of indicating the performance of an installation

incorporating such a roof.

A discussion of the effects of modifications to the components of the heat pump is beyond the scope of this work, but such studies have been carried out by Blundell (1976) and by Carrington (1978). It was, however, necessary to consider changes to the hours of operation of the monitored heat pump to accommodate the effects of two of the modifications discussed in this chapter. The heat pump, as installed, was normally operated within the time period 0700 hours to 1900 hours. In the comparisons where more energy is supplied because of improved performance, the actual running time of the heat pump has been reduced, but was still constrained to be within the same time period, i.e. no consideration was given to night operation, when ambient air temperatures would be lower.

7.2 Modifications to the Store

7.2.1 Reduction in the Store Size

In the heating season analysed in Chapter 6, the maximum temperature recorded for the water in the store was 40°C, whereas the design temperature maximum was 55°C. This discrepancy was partly the result of heat losses from the store and the condenser heat exchanger, and partly the result of the design of the hot air system (which was able to remove heat from the water before it reached the store - see Figure 2.2). The minimum recorded store temperature during system operation was 25°C; thus the maximum temperature change in the store for the heating season was 15°C (with the exception of the initial charging period). In the existing storage mass of 2 1320 kg of water, this corresponded to a maximum energy change of 373 kWh.

The store could be returned to its maximum design temperature of 55°C by simply halving its mass. Thus, a store of 50% of the original mass of water (i.e. 10657 kg) could provide the same usable energy capacity of 373 kWh for a temperature change of 55°C (maximum) to 25°C (taken to be the minimum useful temperature). The condenser heat exchanger and hot air system remain unchanged.

The rate of heat loss from the reduced store was estimated by assuming the same store depth as the original, but with the reduced store covering only half the ground floor area, i.e. 22.4m^2. For the same U-values, the loss rate from the reduced store was calculated to be 8.6 kWh week^{-1} °C^{-1}, and that from the living space to the ground, through the remaining floor area, to be 7.7 kWh week^{-1} °C^{-1}. Average temperatures for the reduced store, ground, and living space were taken as 40°C, 10°C and 19°C respectively. This led to a value for Q_L, taken as being made up of store loss and loss through the floor, of 258 + 69 = 327 kWh week^{-1}. For the 25-week season, this amounts to 8 175 kWh. Since the store temperature was 15°C at the beginning and 30°C at the end of the heating season, this leads to a value for Q_T, the overall remaining stored energy, of 187 kWh for the reduced mass of water.

The effect on the saving of purchased energy with the reduced store may now be assessed. The estimated load, supply and requirement of purchased energy for the system with the reduced store are shown in Table 7.1 for the 1977/78 heating season. The balance between load and supply is achieved by adjustment to the figure for supplementary heating. Comparing this system with the case of the same house without the heat pump or store, but with a 1:1 ratio resistance

heating system (Table 6.4), gives a value for the saving in purchased energy of 17005 - 11988 = 5017 kWh over the season, a percentage saving of about 30%. This compares with a value of 24% saving with the existing store size.

	SEASONAL ENERGY TOTALS, kWh		
ITEM	LOAD	SUPPLY	PURCHASED
Q_{HL}	15200		
Q_L	8175		
Q_W	525		
Q_{IMM}	1492	1492	1492
Q_2		11516	
P_c		6352	
P_t			7290
Q_{AN}			1874
$Q_{INC} + Q_{SG}$		4887	
Q_T	187		
Q_{SUPP}		1332	1332
TOTALS	25579	25579	11988

Table 7.1 Estimated load, supply and requirement of purchased energy for the system with a 50% reduced store.

For the heating season monitored, the system operating with a 50% smaller store could therefore have fulfilled the same role as the existing system with the original store, and with less supplementary heat usage.

7.2.2 Further Insulation of the Existing Store

The existing store has its outer sides insulated with polystyrene, giving an overall side U-value of 0.6 $Wm^{-2} K^{-1}$, and rests on a sand base, giving an overall base U-value of 2.0 $Wm^{-2} K^{-1}$. This latter high U-value is, in fact, an installation fault, since better thermal insulation should have been included during construction. This led to the substantial heat losses from the store which were encountered in the monitored heating season (359 kWh $week^{-1}$, on average). Improvements should therefore be made in this area.

If the store base/ground U-value was brought to 0.6 $Wm^{-2} K^{-1}$ (the same as the sides), the total store heat loss rate would fall to 6.2 kWh $week^{-1} °C^{-1}$. This could be achieved with, for example, a base layer of 'styrofoam' (a form of polystyrene) 0.04m thick. The compression strength of styrofoam is 2.5×10^5 Pa, compared with 5.0×10^3 Pa for a water column 0.5m in height; it could therefore support the store. Assuming an average store temperature of 50°C and a ground temperature of 8°C (due to reduced heat leakage), the value for Q_L becomes 260 kWh $week^{-1}$, or 6500 kWh for the season. For beginning and end of season store temperatures of 15°C and 30°C respectively, Q_T becomes 373 kWh.

In order to balance the load and supply in Table 7.2, a reduction in $(Q_2 + P_c)$, and hence in the running hours of the heat pump, is required, as well as adjustment to the value for Q_{SUPP} (zero in this case). The 'excess' of supply over the load is 157 kWh; subtracting this from the total supplied by the heat pump, $(Q_2 + P_c)$, and assuming the same seasonal COP(H) of 2.45, a value for P_t of 7229 kWh for the

season is obtained. This is a reduction of 7290 - 7229 = 61 kWh, or about 2.44 kWh week^{-1} on the value for the existing system. For the heat pump rating of 3.48 kW (on average), the reduction in operating time would be 0.1 hours day $^{-1}$. However, the value of the seasonal COP(H) may change as a result of the different times of operation, which would in turn affect P_t and the reduction in running hours again.

The process is therefore an iterative one, but the present approximation is considered adequate in view of the inaccuracies of the overall analysis. In addition, the values of Q_W and Q_{AN} will differ, but this is negligible.

	SEASONAL ENERGY TOTALS, kWh		
ITEM	LOAD	SUPPLY	PURCHASED
Q_{HL}	15200		
Q_L	6500		
Q_W	525		
Q_{IMM}	1492	1492	1492
Q_2)			
)		17711	
P_c)			
P_t			7229
Q_{AN}			1874
$Q_{INC} + Q_{SG}$		4887	
Q_T	373		
Q_{SUPP}		0	0
TOTALS	24090	24090	10595

Table 7.2 Estimated load, supply and requirement of purchased energy for the system with improved insulation to the existing store.

The savings in purchased energy over the case of the same house but with the 1:1 ratio resistance heating system (Table 6.4) are 17005 - 10595 = 6410 kWh, or about 38%. Hence, insulating the existing store saves more on purchased energy than simply halving the store size.

7.2.3 Insulation of the 50% Reduced Store

The two options discussed so far lead to the consideration of a third option, that of insulating the 50% reduced store of section 7.2.1. For a store base/ground U-value of 0.6 $Wm^{-2}\,K^{-1}$ and a base surface area of 22.4m^2, the rate of store heat loss becomes 3.2 kWh $week^{-1}$ $°C^{-1}$; the rate of heat loss through the remaining floor area is 7.7 kWh $week^{-1}$ $°C^{-1}$. For the assumed average values of temperature for the store, ground and living space of 55°C, 8°C and 19°C respectively, the total rate of heat loss, Q_L, (taken as the sum of store and floor losses) is therefore 235 kWh $week^{-1}$, or 5875 kWh for the season. For start and end of season store temperatures of 15°C and 30°C respectively, Q_T becomes 187 kWh.

To obtain the load and supply balance in Table 7.3, a reduction in (Q_2 + P_c) and hence in the running hours of the heat pump must again be considered. The 'excess' supply is 968 kWh, and for the same seasonal COP(H) of 2.45, P_t must equal 6898 kWh for the season. The reduction in P_t from its original value of 7290 kWh is therefore 392 kWh, or 15.68 kWh $week^{-1}$. For an average heat pump compressor and fan rating of 3.48 kW, the reduction in operating time is about 0.64 hours day^{-1}. Again, this ignores any change in the seasonal COP(H) value which may be a consequence of the new time settings; changes in Q_W and Q_{AN} are neglected.

The savings in purchased energy over the case of the same house but with the 1:1 ratio resistance heating system (Table 6.4) are 17005 - 10264 = 6741 kWh, or about 40%.

	SEASONAL ENERGY TOTALS, kWh		
ITEM	LOAD	SUPPLY	PURCHASED
Q_{HL}	15200		
Q_L	5875		
Q_W	525		
Q_{IMM}	1492	1492	1492
Q_2)			
)		16900	
P_c)			
P_t			6898
Q_{AN}			1874
$Q_{INC} + Q_{SG}$		4887	
Q_T	187		
Q_{SUPP}		0	0
TOTALS	23279	23279	10264

Table 7.3 Estimated load, supply and requirement of purchased energy for the system with the store 50% reduced in size, and with improved insulation.

With regard to the cost-effectiveness of the three store modifications discussed, the first option of reduction in the store size would be the least expensive to carry out. Since the existing store is modular, consisting of three bags, one could be removed and the quantity of

water adjusted to the required value in the remaining two. However, the latter two options involving additional insulation offer greater savings in purchased energy; of these, there is little difference in the amount of purchased energy saved, but insulation of the reduced store would be the more cost-effective since less insulation material would be required.

The discussion of these three cases of store modifications is of interest since it indicates the scope for improvement in the savings of purchased energy. However, a full analysis by computer model would need to be carried out in order to arrive at the optimum combination of store size and insulation thickness for cost-effectiveness (having regard for the limits imposed by the condensing temperature of the existing heat pump).

7.3 The Effect of Different Roof Systems

In the following sections, the improvement to the performance of the heat pump as a result of using the tiled roof as a pre-heating device for the source air, as opposed to drawing the air directly from outside, is assessed. The possible effect of using corrugated steel roofs for this purpose is also discussed.

7.3.1 The Effect of the Existing Tiled Roof

The value for the seasonal COP(H) of the heat pump was found, using the expression $(Q_2 + P_c)/P_t$ with the seasonal values for Q_2, P_c and P_t, to be 2.45 (section 6.4.3). The average seasonal value of the air dry bulb temperature (for the hours of heat pump operation)

on entry to the evaporator, t_b, was 8.4°C (these values being based on the average of weekly figures). Inserting this value for t_b into equation 6.6:

$$COP(H) = 0.043\ t_b + 2.139 \qquad 6.6$$

gives a value for the seasonal COP(H) of 2.50, which agrees with the value calculated previously to within about 2%. It is concluded that equation 6.6 may therefore be used, with acceptable accuracy, to estimate the seasonal COP(H) resulting from the use of non pre-heated ambient air and air from a corrugated steel roof as sources for the heat pump. (If greater accuracy is required, it is necessary to use the relations given in Chapter 5).

The saving in purchased energy with the existing tiled roof (and system) is 4031 kWh, or 24% over the case of the same house but with the 1:1 ratio resistance heating system (section 6.5). This result was based on the actual measured values for t_b and t_c from the monitored heating season, 1977/78. In assessing the effect of using non pre-heated air drawn directly from outdoors, or the effect, as an air pre-heater, of a roof made up of corrugated steel panels, it will be necessary to use the empirical relations 5.21 and 5.22 to obtain the values for t_c and g_c. It is, therefore, useful to re-calculate a value for the saving in purchased energy for the existing system in the monitored heating season using relations 5.21 and 5.22, and seasonal average values for t_b, g_b and the moist air mass flow rate. This will be a test of the reliability of the relations in seasonal performance calculations and also will provide a figure against which the savings resulting from the no pre-heating and

steel roof pre-heating cases may be compared (since in the latter two cases, use of relations 5.21 and 5.22 is the only method of assessment).

The seasonal value for t_b was 8.4°C, and that for g_b was calculated to be 0.005528 kg kg^{-1} of dry air. Inserting these values in equations 5.21 and 5.22, values for t_c of 3.55°C and for g_c of 0.004882 kg kg^{-1} of dry air are obtained. The enthalpy change in the air crossing the evaporator is found from equation 5.4, and taking an average value of 0.9 kg s^{-1} for the mass flow rate of moist air, Q_2 is calculated (from a knowledge of the total number of hours of heat pump operation) to be 12344 kWh for the season. This compares with a value of 11516 kWh in section 6.5; the agreement is to within 7%.

The total operating time of the heat pump in the heating season was 2093 hours, and for a fan rating of 0.45 kW, the total seasonal value for P_f is 942 kWh. Taking equations 5.8 and 5.20 and re-arranging, one arrives at:

$$(COP(H)-1)\ P_c + COP(H)\ P_f = Q_2 \qquad 7.1$$

Using the value 2.50 for the seasonal COP(H) obtained earlier in this section, and the values for Q_2 and P_f of 12344 kWh and 942 kWh respectively, values for P_c of 6659 kWh and hence for P_t of 7601 kWh are obtained from equations 7.1 and 5.20. By the method of balancing seasonal load and supply employed previously, and assessing the requirement of purchased energy, a saving of 17005 - 12150 = 4855 kWh is realised over the case of the same house but with the 1:1 ratio resistance heating system (Table 6.4). This compares with the value

of 4031 kWh estimated in section 6.5, i.e. a difference of 20%. Expressed as a percentage, this saving is 29%, compared with the value of 24% found earlier.

It can be seen that the method of estimating savings in purchased energy using relations 5.21 and 5.22 gives only moderate agreement with the results of the method based on the weekly calculated values. However, since the former method is used in both the no pre-heating and steel roof pre-heating cases, it will not affect the comparative nature of the results. Therefore, the value adopted in the following sections for the savings in purchased energy provided by the existing tiled roof and system is, for comparison purposes, 29%.

7.3.2 The Effect of Having No Roof Pre-heating

Many heat pump installations use, as the low grade energy source, air drawn directly from outdoors without any pre-heating. The performance of the monitored heat pump with ambient air used directly as the source may be estimated by inserting the seasonal average values for t_a and g_a from the 1977/78 heating season into equations 6.6, 5.21 and 5.22. In this way, the benefit derived from the tiled roof pre-heater may be assessed.

The seasonal average value of t_a (based on the average of weekly figures for the hours of heat pump operation) was 7.0°C; substituting this for t_b in equation 6.6 gives the seasonal COP(H) as 2.44 (compared with 2.50 with the tiled roof). The seasonal value for g_a was 0.005758 kg kg^{-1} of dry air, and if the heat pump utilises ambient air directly, these values for t_a and g_a become the values for t_b and g_b to insert

in equations 5.21 and 5.22. This gives a value for t_c of 2.35°C and a value for g_c of 0.005105 kg kg^{-1} of dry air. Taking an average value for the moist air mass flow rate of 0.9 kg s^{-1} leads to a seasonal value for Q_2 of 11995 kWh. From equation 7.1, for a seasonal COP(H) of 2.44 and a value for P_f of 942 kWh, P_c becomes 6734 kWh and hence, from equation 5.20, the value for P_t is 7676 kWh. Balancing the seasonal load and supply gives a requirement for purchased energy of 12499 kWh and therefore a saving over the case of the same house but with the 1:1 ratio resistance heating system (Table 6.4) of 17005 - 12499 = 4506 kWh, or 26.5%.

Comparison with the figures for the existing tiled roof (section 7.3.1) shows that its use provides a saving of 4855 - 4506 = 349 kWh over the season, and that the effect of the tiled roof pre-heater on the seasonal COP(H) of the heat pump is to raise it from a value of 2.44 to one of 2.50 (an improvement of 2.5%). Though the benefits of utilising the tiled roof as a pre-heater may appear only modest, there is an additional aspect to be considered. All air-source heat pumps suffer from the problem of frost formation on the evaporator coils as a result of moisture in the air. One method of clearing this frost is by the initiation of a 'defrost cycle', where the flow of refrigerant is reversed and the evaporator assumes the role of the condenser for a short period of time (typically several minutes). Other methods of defrosting include the use of electric heaters and water sprays. These, together with the sensors which control defrost operation, are discussed by Ambrose (1966) and by McMullan and Morgan (1981). Defrosting tends to occur more frequently under conditions of high relative humidity and air temperatures near 1°C (Heap, 1979); these conditions are often met in the U.K. climate.

With the monitoring equipment employed, it was not possible to record either the number or the duration of defrost cycles for the heat pump at the test house. An indication of likely defrost performance may, however, be obtained from an interpretation of the data published for other monitored systems. Blundell et al (1977) give the weekly number of defrost cycles as a function of mean outdoor temperature for three air-source heat pump installations. Taking the graphical average of all three, for values of the source temperature of 7.0°C and 8.4°C (corresponding to no roof and tiled roof pre-heating respectively), the number of defrost cycles would be about 43 and 33 cycles $week^{-1}$ respectively for these installations.

A plot of the number of hours of defrosting per week against mean outdoor temperature was produced by Heap (1976b) for an air to air heat pump (11.4 kW output at a source temperature of -1°C) in a domestic installation at Alton, Hampshire (about 10 km from the test house, in Long Sutton). This heat pump is of similar manufacture and capacity to the one in the monitored installation and may be taken as a guide to the defrost performance of the monitored unit. From the plot, the number of hours of defrost operation per week at air source temperatures of 7.0°C and 8.4°C is about 1.2 and 0.6 hours respectively for continuous operation of the heat pump. In the monitored installation, however, the heat pump operated, on average, for about 12 hours day^{-1}, so corresponding figures for the weekly defrost duration in this situation could be expected to be about 0.6 and 0.3 hours $week^{-1}$ respectively. Using these figures, estimates may be made of the energy removed from the system during defrost, and also the energy input which would be lost due to the reduced time in the heating mode as a result of the time spent in the defrost mode (assuming the

same fixed 12 hours day^{-1} operation). The total 'loss' to the system then amounts to 192 kWh and 99kWh over the season for no roof and tiled roof pre-heating cases respectively. In the latter case, it is assumed that this seasonal 'loss' of 99 kWh is already included in the figures for the overall analysis of the system (Chapter 6). (It must, therefore, also be assumed that the characteristics obtained for the in situ performance of the heat pump are inclusive of the defrost performance appropriate for the tiled roof pre-heater). The comparative 'loss' as a result of defrost performance in the case of no roof pre-heating is, therefore, 192-99 = 93 kWh over the season; this value changes the figure of 26.5% to 26% for the saving in the requirement of purchased energy over the 1:1 ratio resistance heating system case.

It can be seen that the use of a tiled roof as a pre-heater of the source air for a heat pump can result in fewer defrost cycles and can reduce the time spent in defrosting. These findings are based on the results given for other installations by Blundell et al (1977) and Heap (1976b); in addition, these authors highlight the need for improved defrost control mechanisms to reduce the number of unnecessary defrost cycles which have been observed in some installations. Though reduced defrosting has, in the case of the monitored system, a small effect on the saving of purchased energy, benefit is nevertheless derived in the form of a reduction in wear on the heat pump components. It is therefore concluded that some type of pre-heater, be it only a conventional tiled roof, benefits the performance of a heat pump.

7.3.3 The Effect of a Corrugated Steel Roof

The performance of the heat pump using, as a pre-heater, a corrugated steel roof made up from the panels discussed in Chapter 4 is now assessed. This is of interest for such applications as industrial building retrofitting, or for any new dwelling incorporating a steel roof. Both this assessment and the estimation of the savings in the requirement of purchased energy are undertaken in the context of the monitored installation and heating season (for comparison purposes). Steel panels are regarded as being fitted to both the South East facing and North West facing sides of the test house roof.

To evaluate the performance of the steel roof, use may be made of the 'fin and tube' model discussed in Chapter 4, section 4.2.3. From equations 4.25-4.28, and equation 3.26, values for F', U_L and F_R may be calculated, estimation of the heat transfer coefficients for the test house conditions following the same approach as described in sections 3.2.4 and 4.2.1. For the roof width of 11.925m there would be 95 flow channels each side, giving a mass flow rate of 0.0047 kg s^{-1} through each (the total mass flow rate from both sides is taken as 0.9 kg s^{-1}). The flow in each channel is turbulent, and the Nusselt number is found from equation 3.42, but without the effects of entrance type of entrance length, since for the roof length of 4.52m and for the value for D_e of 0.0329m, $Nu_m/Nu_{fd} \simeq 1$. Roughness was accounted for by equation 3.44. The wind-induced value for h_1 was estimated from equation 3.40 for a wind speed of 4 ms^{-1}, and a sky temperature of -7°C was taken for radiative losses (see section 3.2.5). Application of the appropriate area enhancement factors, adoption of suitable surface temperature values relating to T_1 and T_4

(based on heating season average values and typical laboratory findings), and taking values for the thermal conductivity and thickness of the steel absorber plate of 55 $Wm^{-1} K^{-1}$ and 0.0007m respectively, led to the values and results summarised in Table 7.4.

HEAT TRANSFER COEFFICIENT	ESTIMATED VALUE $Wm^{-2} °C^{-1}$	CALCULATED VALUES FOR F', U_L AND F_R
h_1	10.0	F' : 0.51
h_{r1}	4.8	
U_t	37.2	
h_2	21.6	
h_3	16.9	U_L : 38
h_4	0.2	
h_{r4}	4.8	
U_b	0.6	F_R : 0.20

Table 7.4 Heat transfer coefficients and values for F', U_L and F_R using a 'fin and tube' model for a steel roof. The units of U_L are $Wm^{-2} °C^{-1}$.

Equations 3.4 and 3.49 were used to estimate the temperature rise of air drawn through a steel roof. Values for the average total radiation incident on South East and North West facing sides of the roof were taken as 180 Wm^{-2} and 92 Wm^{-2} respectively, obtained by the method described in Chapter 3, section 3.2.5. For the 'Plastisol' - coated panel surfaces, $(\tau\alpha)_e$ is 0.916 under solar radiation (Chapter 4, section 4.1) and for the 1977/78 heating season, t_i and t_a were both

taken equal to 7°C. Substitution of the calculated values for F_R and U_L, and the above numerical quantities, into equation 3.4 gives a value for η of 0.183. Evaluation of equation 3.49 results in a temperature rise of 3.9°C for the air flowing under the S.E. facing side, and, assuming the same values for F_R and U_L, a similar calculation gives an air temperature rise of 2.0°C for the N.W. facing side. For equal air mass flow rates from each side, the overall average temperature rise after passing through the steel roof is $(3.9 + 2.0)/2 = 3.0$°C, giving a final outlet temperature of $(7.0 + 3.0) = 10.0$°C.

The seasonal average values for t_a and g_a were 7.0°C and 0.005758 kg kg^{-1} of dry air respectively. For the steel roof, the value for t_b is 10.0°C, and that for g_b is assumed the same as g_a. Equations 5.21 and 5.22 then give a value for t_c of 4.92°C, and a value for g_c of 0.005105 kg kg^{-1} of dry air. Taking an average value of 0.9 kg s^{-1} for the mass flow rate of moist air, and assuming the same number of hours of heat pump operation as in the monitored season (2093 hours), Q_2 is calculated to be 12826 kWh for the season. For a corrugated steel roof and ducting, it has been estimated (Chapter 4, section 4.5) that the fan power consumption would be 780 watts. As a result, the COP(H) cannot be determined from equation 6.6 as this equation is based on the fan power for the existing tiled roof system. Instead, use must be made of equation 5.23:

$$P_c = 199\ t_b + 8662 \qquad 5.23$$

The compressor power consumption is a function of t_b and should be unaffected by the fan power consumption. For a value for t_b of

10.0°C and 2093 hours operation, the seasonal value for P_c is 6193 kWh. The new P_f value of 0.780 kW gives a seasonal fan power requirement of 1633 kWh, and from equation 5.20, P_t becomes 7826 kWh. The seasonal COP(H) is found from equation 5.8 to be 2.43. The seasonal requirement of purchased energy becomes 12359 kWh (neglecting any change in Q_{HL} resulting from the overall U-value for the steel roof differing from that for the tiled roof). The saving over the 1:1 ratio resistance heating system case (Table 6.4) is therefore 17005 - 12359 = 4646 kWh, or about 27.3%.

The approximate calculation above shows that use of a corrugated steel roof (in this case on both sides, and for the test house situation during the 1977/78 heating season) can raise the seasonal average temperature of ambient air from 7°C to about 10°C for the conditions and limitations imposed in this procedure. This compares with a value of 8.4°C for the tiled roof. More energy is removed from the source air, Q_2, in the case of the steel roof (Q_2 = 12826 kWh) than in the case of the tiled roof (Q_2 = 12344 kWh) for the same number of heat pump running hours (2093 hours) in each. However, the value for the seasonal COP(H) with the steel roof is only 2.43 because of the increased fan power requirement.

Though there is a higher output temperature of the air from the steel panels compared with that from a tile roof, the values for the COP(H) and the savings are lower because of the increased fan power needed to draw the air through the design of steel panel and ducting considered; if the steel roof design was such that the same output temperature (10°C) could be obtained with the same air mass flow rate but with little or no increase in fan power, such as a

non-corrugated steel roof, then the COP(H) value would be 2.57 (equation 6.6), the seasonal requirement of purchased energy would become 11668 kWh, and the saving over the 1:1 ratio resistance heating system case (Table 6.4) would be 5337 kWh, or 31.4%.

A steel roof would bring other benefits, compared with a tiled roof, with regard to heat pump defrosting. For a source temperature of about 10°C, the number of defrost cycles would be reduced to about 21 per week for the systems discussed by Blundell et al (1977). Using the results for the system discussed by Heap (1976b), the time spent in the defrost mode would be reduced to about 0.3 hours $week^{-1}$ (for continuous heat pump operation) or about 0.15 hours $week^{-1}$ for the 12 hours day^{-1} operation of the monitored system. The estimated 'loss' in energy to the system is then 51 kWh over the season. Comparing this with the seasonal 'loss' of 99 kWh in the tiled roof pre-heating case means that there is an effective 'gain' of 99 - 51 = 48 kWh with the steel roof pre-heater as a result of reduced defrosting. The effect of this on the figure of 27.3% for the saving in the requirement of purchased energy over the 1:1 ratio resistance heating system case would be to change it to a value of 27.6%, which is very small, but there is reduced wear on the heat pump components because of fewer defrost cycles. For the case of a steel roof but with no increase in fan power, the reduced defrosting would change the savings figure from 31.4% to 31.7%.

While metal roofs have potential as pre-heat devices for air source heat pumps, their use can result in an increase in fan power which, in turn, can lower the seasonal COP(H) and hence the savings. This effect is, of course, dependent upon the design and configuration of

the 'ducting' leading to the heat pump, and would be true for any pre-heating system, not only metal roofs. Note that in the case of no roof pre-heating considered earlier, the same fan power as for the existing tiled roof was assumed, which may, in practice, not be the case. For a comparison using the same fan power for no roof, tiled roof and steel roof pre-heating, the steel roof then gives the best COP(H) and savings figures. Careful attention, as regards duct design and fan power requirements, must therefore be paid to the design of pre-heating systems for air source heat pumps. However, in retrofit applications, the prevailing circumstances may predetermine the configuration of roof system used.

7.4 Summary

Three specific modifications to the size and/or the level of insulation of the test house store have been the subject of discussion in the first part of this chapter. The modifications (suggested by the results of the monitoring programme) have been discussed in terms of savings in purchased energy, and it has been shown that, in the case examined of combined size reduction and insulation, a saving of about 40% may be possible over the case of the 1:1 ratio resistance heating system (Table 6.4). Brief comments have been made with regard to cost-effectiveness, but optimisation by computer would be necessary for a full assessment. This discussion has served to show the scope for improvement to the monitored system.

The latter part of this chapter has been concerned with the effect on the seasonal COP(H) of supplying the monitored heat pump with non pre-heated air drawn directly from outdoors, or with air pre-heated by

the existing tiled roof; the effect of a steel roof acting as a pre-heater has also been considered, in the context of the monitored system. The effect on the savings of purchased energy has been estimated for each of the air sources, and comparative figures have been presented.

The likely effect of each air source on the defrost performance of heat pumps in other installations has been discussed (Blundell et al, 1977; Heap 1976b). Since no data on the defrost performance of the monitored heat pump was available, the results of Heap (1976b) for a similar heat pump were used to assess the effect of each air source on the likely defrost performance of the monitored unit and to estimate the corresponding 'losses' to the test house system. The defrost performance was found to have a very small effect on the comparative figures for the seasonal savings of purchased energy. Note that the comparative figures presented for these savings for the cases of no roof and steel roof pre-heating inherently contain the defrost performance for the case of the existing tiled roof, since comparison was based on the heat pump characteristics with the latter as a pre-heater.

The results may be conveniently summarised in the following tables. All savings in purchased energy are compared with the case of the 1:1 ratio resistance heating system (Table 6.4) and the values given are to the nearest whole number. In the case of savings for the different air pre-heating arrangements (ie., the tiled roof, steel roof or no pre-heating at all) the figures given are those which do not take into account the different defrost performances, since the effect of these on savings is negligibly small (i.e. -0.5% and + 0.3% [or + 0.3%

for no change in fan power requirement, i.e. a non-corrugated steel roof] to the values given for percentage savings in seasonal purchased energy for the no roof pre-heating and steel roof pre-heating cases respectively).

STORE MODIFICATION	SAVING IN SEASONAL PURCHASED ENERGY	
	kWh	PER CENT
EXISTING STORE WITHOUT CHANGES	4031	24%
50% SIZE REDUCTION	5017	30%
INSULATE EXISTING STORE ($U = 0.6 Wm^{-2} °C^{-1}$)	6410	38%
INSULATE THE 50% REDUCED STORE ($U = 0.6\ Wm^{-2} °C^{-1}$)	6741	40%

Table 7.5 Progressive improvements to the store and their estimated effect on seasonal savings in purchased energy.

TYPE OF PRE-HEATER	SEASONAL COP(H)	SAVING IN SEASONAL PURCHASED ENERGY*	
		kWh	PER CENT
NONE-USE OUTSIDE AIR DIRECTLY	2.44	4506	27%
THE EXISTING TILED ROOF	2.50	4855	29%
A STEEL ROOF: NON-CORRUGATED CORRUGATED	2.57** 2.43	5337** 4646	31%** 27%

Table 7.6 Effect of different pre-heat systems on the seasonal COP(H), and on the savings in purchased energy for the monitored installation.

* Comparative values only, and no account taken of defrost performance (which has a negligibly small effect on these figures).

** A steel roof, but with no increase in fan power.
These are the true comparative figures for this table.

TYPE OF PRE-HEATER	PROBABLE NUMBER OF DEFROST CYCLES PER WEEK (BLUNDELL ET AL, 1977)*	PROBABLE NUMBER OF HOURS WEEK^{-1} IN DEFROST MODE (HEAP, 1976b)*
NONE-USE OUTSIDE AIR DIRECTLY	43	1.2
THE EXISTING TILED ROOF	33	0.6
A STEEL ROOF	21	0.3

Table 7.7 Likely effect of different pre-heat systems on the defrosting performance of several heat pumps in other installations (see references).

* For continuous operation.

TYPE OF PRE-HEATER	PROBABLE TIME IN DEFROST MODE, HOURS WEEK^{-1} (HEAP, 1976b)	SEASONAL ENERGY 'LOSSES' TO THE MONITORED SYSTEM, kWh		
		REMOVED DURING DEFROSTING	LOST DUE TO REDUCED TIME IN HEATING MODE	TOTAL
NONE-USE OUTSIDE AIR DIRECTLY	0.6	65	127	192
THE EXISTING TILED ROOF	0.3	34	65	99
A STEEL ROOF:				
NON-CORRUGATED	0.15	18*	34*	52*
CORRUGATED	0.15	16	35	51

Table 7.8 Estimated effect of the different defrost performances with each pre-heat system on the monitored installation (based on the results of Heap, 1976b).

* A steel roof, but with no increase in fan power.

These are the true comparative figures for this table.

CHAPTER 8

FINAL DISCUSSION, RECOMMENDATIONS AND CONCLUSIONS

8.1 System Balance Point and Heat Pump Sizing

The balance point of a heat pump system is defined as that value of outdoor temperature at which the rates of energy loss from a building and energy supply by the heat pump to the building are equal, after accounting for incidental gains. For outdoor temperatures lower than the balance point temperature, the heat pump cannot fully meet the load, and supplementary heating is required; for temperatures above the balance point temperature, the heat pump has excess capacity over the load. The value of the balance point for which a particular heating system is designed determines the size (in terms of output capacity) of heat pump required. Careful choice of the balance point is necessary, because designing a system where, for example, the heat pump supply matches the load for the coldest day of the season would render the heat pump oversized for the remainder of the time. For a system incorporating heat storage, a heat pump of sufficient capacity must be installed in order to supply not only the fabric and ventilation heat losses, but also heat losses from the store and the stored energy itself.

For the system monitored, a graph of the rate of energy loss from the living space and store, $(Q_{HL} + Q_L)$, in kW, as a function of outdoor ambient temperature, t_a, in °C, is shown in Figure 8.1; also shown is the rate of energy supply by the heat pump less its contribution to domestic water heating, $(Q_2 + P_c) - Q_W$. Note that, in this case, one is concerned with space heating only - hence the removal of Q_W. The

average weekly energy supplied by incidental gains (including solar gain and the 50% contribution to space heating provided by domestic hot water usage) is 236 kWh $week^{-1}$ (an average rating of 1.40 kW). This is shown as an addition to the heat pump rate of supply.

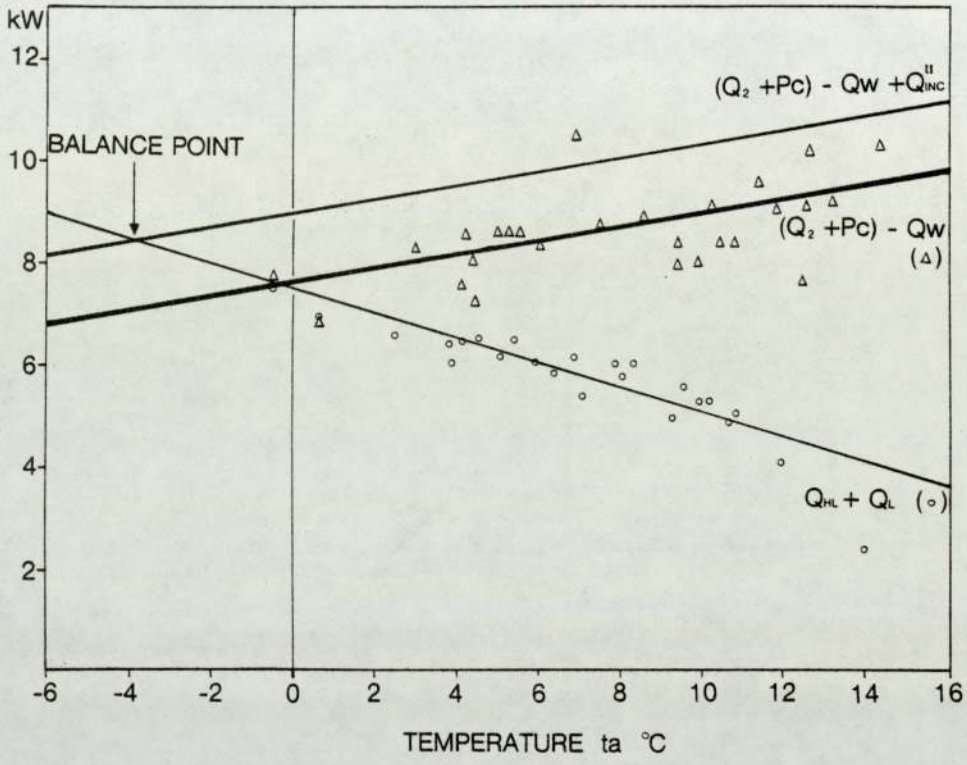

Figure 8.1 Rates of energy loss and supply as a function of outdoor ambient temperature, t_a, and the balance point, for the monitored installation. Note that $Q''_{INC} = Q'_{INC} + Q_{SG}$.

It can be seen that the balance point is -4°C (excluding incidental gains, the balance point would be 0°C). This means that the installed heat pump, if operated continuously, would be of adequate capacity to supply the total rate of loss for the monitored installation down to an outdoor temperature value of -4°C. For $(Q_{HL} + Q_L)$ and $(Q_2 + P_c)$ in kW, and for t_a in °C, linefits give the following relations:

$$(Q_{HL} + Q_L) = - 0.243\ t_a + 7.5 \qquad 8.1$$

Errors: 0.243 ± 0.058 (2 st. dev.); 7.5 ± 0.5 (2 st. dev.).

Measured range of t_a: - 0.5°C to 14.1°C.

$$(Q_2 + P_c) - Q_W = 0.137\ t_a + 7.5 \qquad 8.2$$

Errors: 0.137 ± 0.096 (2 st. dev.); 7.5 ± 0.75 (2 st. dev.).

Measured range of t_a: - 0.5°C to 14.1°C.

Note that a plot of $(Q_2 + P_c)$ against t_a would give:

$$(Q_2 + P_c) = 0.137\ t_a + 7.7 \qquad 8.3$$

Errors: 0.137 ± 0.096 (2 st. dev.); 7.7 ± 0.8 (2 st. dev.).

Measured range of t_a: - 0.5°C to 14.1°C.

The concept of a pseudo-balance point may now be introduced. The pseudo-balance point allows for the hours, or mode, of operation of the heat pump over, for example, the heating season, to be taken into account; it may be defined as that value of outdoor temperature at which the energy supplied to a building over a given time interval is equal to the energy lost from the building over the same time interval, after accounting for incidental gains. The hours, or mode, of operation of a heat pump over the time period concerned are thereby taken into account, provided that the time interval is of sufficient length so as to properly represent the full operational and non-operational periods of the heat pump (a time interval of 24 hours should therefore be the minimum value utilised).

A pseudo-balance point for the monitored system over the heating season 1977/78 was determined for time intervals of one week. Figure 8.2

shows, as a function of temperature t_a, in °C, the ventilation, fabric and store heat loss, due to Q_{HL} and Q_L, over the season in kWh week^{-1}. Shown also is the weekly space heating energy supplied by the heat pump (for the number of hours operated), $(Q_2 + P_c) - Q_W$, and, added to it, the incidental gains of 236 kWh week^{-1}.

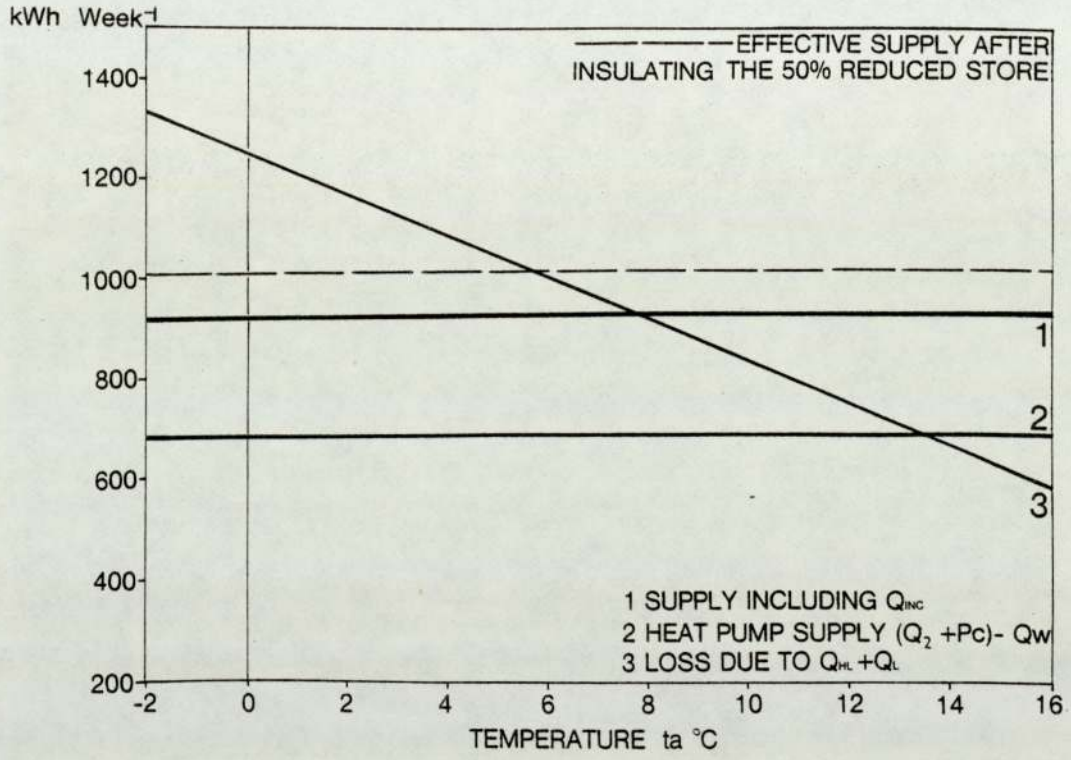

Figure 8.2 Average weekly values of energy loss and supply over the heating season, as a function of outdoor ambient temperature, t_a. The intersection of lines 1 and 3 gives the pseudo-balance point.

This shows the pseudo-balance point for the existing system and mode of operation to be approximately 8°C; the difference between this and the true average value for t_a over the 25-week season gives an indication of the amount of supplementary heating used by the occupants (note that the average value for t_a of 7°C given earlier

is for the hours of heat pump operation only and does not take into account night temperatures, which would make the true seasonal average t_a value lower). The pseudo-balance point gives, therefore, an indication of the supplementary heating requirements over the season for a particular mode of operation of a heating system. Also, it may be used to show the effect of modifications to the installation and/or to the mode of operation of the heating system.

A lower pseudo-balance point would mean a reduction in the requirement of supplementary heating. For the monitored system, this might be achieved by either running the heat pump for a longer time or by insulating and/or reducing the size of the store (or, of course, a combination of both, but this will not be discussed). With regard to changes of the mode of heat pump operation, the on/off times could be set such that the morning operation of the heat pump is reduced and the evening operation increased, but by a greater amount. In this way, the value of the seasonal COP(H) would not fall (but would probably rise) since advantage is taken of the heat storage by the roof tiles and of the evening heat loss from the living space to the loft resulting from occupancy patterns - refer to Figure 6.9. With regard to store modifications, several such changes have already been discussed in Chapter 7. The effect of one of these on the pseudo-balance point, that of insulating the 50% reduced store to a base/ground U-value of 0.6 $Wm^{-2}\,°C^{-1}$, may now be seen in Figure 8.2. The pseudo-balance point is then brought to about 6°C.

The installed heat pump is, therefore, of adequate capacity to supply the total loss rate of the existing installation down to an outdoor temperature of about -4°C (though at this temperature, no energy would

be available for storage). For the hours of heat pump operation and season monitored, however, the system was balanced (the pseudo-balance point) at about 8°C (this would be equivalent to a 4.2 kW heat pump, operating continuously, producing a balance point at 8°C). The pseudo-balance point, and hence the requirement of supplementary heating, may be changed by making adjustments to the system or to its mode of operation. Computer modelling would be needed to determine the optimum pseudo-balance point (and also the optimum balance point) for cost effectiveness.

It therefore becomes possible to relate the pseudo-balance point to real average outdoor temperatures, degree - day figures, and modes of operation of heating systems so as to arrive at an overall approach to the space heating analysis of the built environment.

8.2 Computer Modelling, and Alternative Modes of Operation

Modelling by computer represents a relatively inexpensive means of assessing the change in performance of, for example, a heating system, as components or modes of operation are altered. Numerous computer simulations have been undertaken of various heat pump system configurations - see, for example, Bosio and Suryanarayana, 1975; Freeman et al, 1975; MacArthur, 1976; Carrington, 1978; Sundell and Bubenko, 1979; Freeman et al, 1979. In each of those mentioned, the heat pump performance was based on theoretical analyses or manufacturers' specifications. Berghmans et al (1978) obtained empirical relations for the performance, under controlled laboratory conditions, of a steady state - operated heat pump; in addition, transient operation was simulated. The relations were then used in a computer model

of a heating system incorporating solar collectors, a heat pump and store.

Theoretical analyses and results based on laboratory tests make useful contributions in computer modelling applications. Laboratory testing, in particular, offers the advantages of better control and of improved reproducibility of results, which are important for comparison purposes; in addition, it can provide a valuable guide to the performance that may be expected of a component in operation. It is of equal importance, however, to obtain data from field trials, as computer models incorporating such data would be very effective in the accurate prediction of performance in future installations. The results, presented in this thesis, of the characteristics of an air-source heat pump operating in the U.K. climate fall into the latter category, while the results obtained in the laboratory concerning the behaviour of tiled and corrugated metal roof structures as air heaters fall into the former category. Together, they may be incorporated in computer models which would make possible the estimation of the performance of both retrofitted and newly-designed installations comprised of air-source heat pumps and conventional roof pre-heaters. Furthermore, with the inclusion of appropriate data, a model may be set up which would allow optimisation of the monitored (or another) system to be carried out.

Computer simulation would allow assessment to be made of the effects on performance of changes to the existing system, and of alternative modes of operation to that monitored, some examples of which follow. For a temperature fall from 40°C to 25°C, the existing store has a (usable) energy capacity of about 373 kWh which, from the average

weekly load for the season, gives it a 'range' of about 4-5 days without any input from the heat pump. The effect of a variety of store sizes (and levels of insulation) could be simulated, down to, for example, a 'one-day', or 24 hours, store. A store of this size could be more easily incorporated within a building structure so that the heat losses from the store could help supply the living space heat load. In addition, a small store would be easier to accommodate in retrofitting applications and would reduce the capital cost of installation.

Another mode of operation might be to operate the heat pump at night only, in order to charge a one-day store for daytime use. Though the seasonal COP(H) would fall (due to lower air temperatures at night compared with those in the day), advantage is taken of off-peak electricity tariffs. Initial studies by Neal (1981c) indicate that substantial financial savings over the case of daytime operation are possible, which may prove more attractive to the consumer. (This highlights the fact that there is often a conflict between the saving of primary energy and financial saving). From the viewpoint of electrical demand variation with time, night operation of heat pumps may be preferred by the electricity supply industry. Increased heat pump capacity may, however, be needed to supply the load and remain within the off-peak period.

Several modifications to the existing store have been discussed in this thesis (Chapter 7). The effect of dispensing with heat storage altogether and allowing the heat pump to supply the instantaneous load could not be assessed from the results of the monitored system. This is because such operation would have rendered the existing heat

pump oversized, resulting in transient operation and hence a degradation in performance (Parken et al, 1977; Berghmans et al, 1978). A smaller capacity heat pump, carefully matched to the load, with the inclusion of varying degrees of supplementary heating, would therefore be required, though there are advocates of a balance point being set at -1°C for heat pump sizing (Stokes, 1981). Computer modelling could be used to assess the performance of such systems in both the monitored, and other, installations.

8.3 Summary of Main Results

The objectives set out at the beginning of the thesis have been achieved, except for the design of a heat pump control system. Performance characteristics have, however, been presented upon which a control strategy for such a system could be based.

Though brief comments have been made regarding cost-effectiveness, the time available did not permit a full appraisal to be carried out.

The main results of this work may be summarised as follows:

(1) A conceptual model has been presented which takes into account the finite thickness and thermal conductivity of the absorber plate in the performance analysis of an air-heating solar collector. The model has been shown to satisfactorily describe the behaviour of a tiled roof when used as an air-heating device, for the case of little or no air leakage into the structure. The effect of a wind on an untorched tile surface was found to increase the gain in useful energy and hence the

efficiency compared with a sealed roof. This is caused by air leakage into the airstream from the upper surfaces of the tiles. A theoretical model has been proposed to explain and quantify this effect. A 'fin and tube' model has been shown to be the most suitable for describing the performance, as solar air heaters, of corrugated metal panels that consist of separate flow channels. The models permit estimation of the efficiency of conventional tiled and metal roofs when used as solar collectors. Time constants and fan power requirements for these structures have been determined (Chapters 3 and 4).

(2) A set of empirical relations has been presented, describing the in situ performance of an American air-source heat pump in the U.K. climate. The relations allow calculation of the instantaneous values of the rate of energy extraction from moist air, the latent and sensible heat contributions, and the COP(H) from a knowledge of the psychrometric state and mass flow rate of the air on entry to the evaporator, and the power consumption of the heat pump fan (Chapter 5).

(3) From the overall analysis of the performance of the monitored system over one heating season (based on weekly averages), further equations relating the COP(H) and heating capacity of the heat pump to the dry bulb temperature of the air entering the evaporator have been given, together with a relation between COP(H) and the dry bulb temperature of outdoor air. Results of calculations based on the former relations showed a lack of agreement with the manufacturer's specifications at air source temperatures of +7°C and -7°C (Chapter 6).

(4) An energy balance for the test house and system was carried out, resulting in an expression upon which the analysis of the performance over one heating season (October 1977 - April 1978) could be based. Comparison of the actual variation in stored energy over the season with that estimated from the analysis procedure showed good general agreement and indicated that the ground and house foundations may be acting as a secondary store. With the monitored system, the estimated saving in purchased energy over the case of the same house, but with a 1:1 ratio resistance heating system installed, was found to be 24% (Chapter 6).

(5) The effects of several modifications to the size and level of insulation of the existing store were assessed. Of the changes considered, one gave an estimated saving in the requirement of purchased energy of 40% over the 1:1 ratio resistance heating system case. This indicated the scope for savings in purchased energy (Chapter 7).

(6) The effect was assessed on the seasonal COP(H) of supplying the monitored heat pump with non-pre-heated air or with air pre-heated by the existing tiled roof; the effect of a corrugated steel roof acting as an air pre-heater was also considered, in the context of the monitored system. For each case, comparative figures have been given for the saving in the requirement of purchased energy over the 1:1 ratio resistance heating system case.

In addition, the effect of the three pre-heating arrangements on the likely defrost performance was assessed, based on the

results of Heap (1976b) for a similar heat pump to that monitored. For the cases of no pre-heating, tiled roof and steel roof pre-heating in the monitored system, and for the same fan power requirements in each case, progressive improvements were noted in the values for the seasonal COP(H) (2.44, 2.50 and 2.57 respectively), and in the savings in purchased energy over the 1:1 ratio resistance heating system case (27%, 29% and 31% respectively), these comparative figures being based on relations derived in earlier chapters. Corresponding estimates of the time spent in the defrost mode were also made (0.6, 0.3, 0.15 hours $week^{-1}$ respectively). The different defrost performances were found to have a small effect on the figures for the saving in purchased energy. The relative importance of fan power requirements on seasonal performance was highlighted (Chapter 7).

(7) From a consideration of the balance point of the system, it was found that the heat pump can supply the total system loss rate down to an outdoor temperature of about -4°C. The concept of a pseudo-balance point was introduced, and its value for the monitored system was found to be 8°C. Adjustment may be made to this value by carrying out modifications, either to the installation itself, or to its mode of operation (Chapter 8).

8.4 Recommendations for Future Work

(1) Tests should be conducted, either outdoors or in a solar simulator, to determine the efficiency characteristics and time constants of additional common roofing materials and structures, such as slate and asbestos roofs, and also the

factors affecting efficiency for each roof configuration. Heat transfer coefficients, appropriate to the use of conventional roofs as solar collectors, should be measured.

(2) The analytical models describing the behaviour of tiled and metal roofs as solar collectors, and the in situ performance characteristics of the monitored heat pump, presented in this thesis, should be incorporated into computer models for predicting the likely performance of both retrofitted and newly-designed installations.

(3) Optimisation of the monitored system by computer modelling should be carried out, with regard to store improvements and adjustment to the on/off times of the heat pump (to take advantage of heat storage in the tiles and evening heat loss into the loft). The possibility of night operation should be considered.

(4) Other factors relating to improved system performance could be incorporated into computer models, such as different storage media, different storage temperatures, compressor capacity variation to match the load, and modular heat pump systems.

(5) An overall approach to the space heating analysis of the built environment should be developed which relates the pseudo-balance point to real average ambient temperatures, degree-day figures and modes of operation of heating systems.

8.5 Main Conclusions

(1) Conventional tiled roofs and, in particular, corrugated metal

roofs, when used as air-heating solar collectors, operate at comparable efficiencies for low temperature rises to purpose-designed air panels. There is potential for their use as pre-heaters for air source heat pumps in domestic or industrial installations, and as a means of providing small temperature rises in agricultural applications.

(2) The use of tiled or metal roofs as air pre-heaters improves the performance of a heat pump by increasing the heating mode coefficient of performance and reducing the time spent in the defrost mode. In the monitored installation, the corresponding values for the seasonal COP(H) for the cases of no roof, tiled roof and steel roof pre-heating were 2.44, 2.50 and 2.57 (for equal fan power requirements). Some form of pre-heater is therefore of benefit to the performance of a heat pump.

(3) The analytical models describing the thermal performance of conventional tiled and corrugated metal roofs, and the relations describing the in situ performance of the heat pump, provide data upon which computer simulation studies may be based. Such techniques might be used to optimise the monitored system, to assess the savings resulting from alternative modes of operation, and to predict the performance of both newly-designed and retrofitted installations.

(4) The heating system monitored can, in its present form, save 24% on the requirement of purchased energy compared with the case of the same house, but with a 1:1 ratio resistance heating system installed, and the heat pump can operate with a seasonal value of 2.4 - 2.5 for the heating mode coefficient of performance.

If the coefficient of performance for the system is defined as the ratio of energy required over the season to energy purchased over the season, or $1/(1 - FS)$, where FS is the fractional saving, then the system COP of the monitored installation is $1/(1 - 0.24) \simeq 1.3$. With the improvements to the store discussed in Chapter 7, savings on the requirement of purchased energy of up to 40% may be realised. This would give a system COP of $1/(1 - 0.40) \simeq 1.7$.

The widespread use (through retrofitting) of such heating systems can therefore lead to worthwhile reductions in the United Kingdom's energy consumption for domestic space and water heating.

REFERENCES

Ambrose, E.R., 'Heat Pumps and Electric Heating'. John Wiley and Sons, Inc., New York, 1966.

Andrews, J.W., 'Heat Pump Impact upon Solar Collector Design and Cost'. Proc. I.S.E.S. Congress, Atlanta, Sun II, Vol. 1, pp. 792-796, 1979.

Aranovitch, E., 'The Joint Solar Collector Testing Programme of the European Community'. Proc. U.K. - I.S.E.S. Conf. C11, 'Testing of Solar Collectors and Systems', pp. 49-69, April 1977.

Aranovitch, E., D. Van Hattem et al, 'Performance of Three Years of Operation of a Solar Heating System Combined with a Heat Pump and a Long Term Storage in Northern Italy'. Abstracts, I.S.E.S. Congress, Brighton, Paper I:A2:87, p. 262, August 1981.

ASHRAE, 'Handbook of Fundamentals'. American Society of Heating, Refrigerating and Air-Conditioning Engineers, New York, 1972.

ASHRAE, Standard 93-77, 'Methods of Testing to Determine the Thermal Performance of Solar Collectors'. American Society of Heating, Refrigerating and Air-Conditioning Engineers, New York, 1978.

ASTM, Standard E 424-71 'Standard Test Methods for Solar Energy Transmittance and Reflectance (Terrestrial) of Sheet Materials'. American Society for Testing and Materials, Annual Book of ASTM Standards, Part 46, 1979.

Bansal, P.K. and S.C. Kaushik, 'Analyses of Single and Double Exposure Solar Air Heaters'. Energy Research, Vol. 4, pp. 69-79, 1980.

Berghmans, J., A. Debosscher and E. Debrabander, 'Analysis of Heat Pump Assisted Solar Energy Air Heating Systems'. Report by the Commission of the European Communities - Solar Energy R. and D. Programme, 1978.

Bliss, R.W., 'The Derivations of Several Plate-Efficiency Factors Useful in the Design of Flat-Plate Solar Heat Collectors'. Solar Energy, Vol. 3, No. 4, pp. 55-64, 1959.

Blundell, C.J., 'Optimising Heat Exchangers for Air to Air Space Heating Heat Pumps in the U.K.' Report ECRC/N949, Electricity Council Research Centre, Capenhurst, Chester, June 1976.

Blundell, C.J., R.D. Heap and E.G.A. Goodall, 'Heat Pumps for Space Heating in the U.K. Research and Application'. 4th Electric Space Heating and Air-Conditioning Conference, Bordeaux, October 11-14, 1977.

Boettner, E.A. and L.J. Miedler, 'Simulating the Solar Spectrum with a Filtered High-Pressure Xenon Lamp'. Applied Optics, Vol. 2, No. 1, pp. 105-108, 1963.

Bosio, R.C. and N.V. Suryanarayana, 'Solar Assisted Heat Pump System: A Parametric Study for Space Heating of a Characteristic House in Madison, Wisconsin'. American Society of Mechanical Engineers, Winter Annual Meeting, Paper 75-WA/SOL-8, 1975.

Bourne, R.C., 'A Volume Collector - Heat Pump Demonstration House'. Extended Abstracts, I.S.E.S. Congress, Los Angeles, Paper 14/13, p. 85, 1975.

BSE, 'Guidelines and Directions for Determining the Usability of Solar Collectors, a Solar Collector Efficiency Test'. Bundesverband Solarenergie, Essen, Federal Republic of Germany, May, 1978.

Building Research Establishment, 'Energy Conservation: A Study of Energy Consumption in Buildings and Possible Means of Saving Energy in Housing'. B.R.E. Current Paper CP 56/75, June 1975.

Building Research Establishment, 'Heat Losses from Dwellings'. B.R.E. Digest No. 190, June 1976.

Carrington, C.G., 'Optimising a Heat Pump for Heating Purposes'. Energy Research, Vol. 2, pp. 153-170, 1978.

Charters, W.W.S. and C.W. Dixon, 'Some Performance Characteristics of the Unimelb Air Source Solar Boosted Heat Pump System'. Proc. I.S.E.S. Congress, Atlanta, Sun II, Vol. 1, pp. 807-811, 1979.

Chemical Rubber Company, 'Handbook of Chemistry and Physics, 54th Edition, 1973-74'. C.R.C. Press, Cleveland, Ohio, U.S.A., 1973.

Close, D.J. and M.B. Yusoff, 'The Effects of Air Leaks on Solar Air Collector Behaviour'. Solar Energy, Vol. 20, pp. 459-463, 1978.

Conseil, B., A. Prieur, M. Ronc and G. Rousseau, 'Experimental Study of a Solar Heating System Combining a Solar Roof, a Heat Pump and a Buried Pipes Storage'. Abstracts, I.S.E.S. Congress, Brighton, Paper I:A2:84, p. 259, August 1981.

Cottingham, J.G., 'The Cost-Effective Potential of Optimumly Designed Heat Pumps for the Collection, Storage and Distribution of Solar Energy'. ASHRAE Symposium PH-79-2, 'Solar-Assisted Heat Pumps', Paper No. 1, pp. 345-349, American Society of Heating, Refrigerating and Air-Conditioning Engineers, New York, 1979.

Cur, N. and E.M. Sparrow, 'Measurements of Developing and Fully Developed Heat Transfer Coefficients along a Periodically Interrupted Surface'. Trans. ASME, J. of Heat Transfer, Vol. 101, pp. 211-216, May 1979.

Dean, T.S., 'Low Cost Solar Assist for Air to Air Heat Pumps'. Abstracts, I.S.E.S. Congress, Brighton, Paper I:A2:93, p. 268, August 1981.

Department of Energy, 'Degree Days'. Fuel Efficiency Booklet No. 7, Her Majesty's Stationery Office, 1977.

Department of Energy, 'U.K. Energy Statistics, 1981'. Her Majesty's Stationery Office, 1981.

Diamant, R.M.E., 'Insulation Deskbook'. Heating and Ventilating Publications, 1977.

Dietrich, B.G., 'Energy Roof Systems-Up-to-Date Position and Development Trends in the Federal Republic of Germany'. Abstracts, I.S.E.S. Congress, Brighton, Paper I:A2:89, p. 264, August 1981.

Dittes, W. and D.R. Goettling, 'Testing the Performance of Solar Collectors under Standard Conditions'. Proc. I.S.E.S. Congress, Atlanta, Sun II, Vol. 1, pp. 355-359, 1979.

Drummond, A.J. and J.J. Roche, 'Corrections to be Applied to Measurements Made with Eppley (and other) Spectral Radiometers When Used with Schott Colored Glass Filters'. Journal of Applied Meteorology, Vol. 4, pp. 741-744, 1965.

Duffie, J.A. and W.A. Beckman, 'Solar Energy Thermal Processes'. Wiley - Interscience, 1974.

Duffie, J.A. and W.A. Beckman, 'Solar Engineering of Thermal Processes'. Wiley - Interscience, 1980.

Eckert, E.R.G. and R.M. Drake, 'Analysis of Heat and Mass Transfer'. McGraw Hill, 1972.

Energy Management, Degree Day Table, p. 8, June 1979.

Energy Management, Degree Day Table, p. 7, October 1981.

Eppley Laboratory, Inc., private communication, 1982.

Esbensen, T. and P.E. Kristensen, 'Sun Sec Low Energy House in Sweden'. Abstracts, I.S.E.S. Congress, Brighton, Paper I:A2:88, p. 263, August 1981.

Ferguson, W.E. and P.H. Bailey, 'A Solar Barn for Grain and Hay Drying Experiments in Scotland'. Abstracts, I.S.E.S. Congress, Brighton, Paper D2:5, p. 644, August 1981.

Freeman, T.L., J.W. Mitchell, W.A. Beckman and J.A. Duffie, 'Computer Modelling of Heat Pumps and the Simulation of Solar-Heat Pump Systems'. American Society of Mechanical Engineers, Winter Annual Meeting, Paper 75-WA/SOL-3, 1975.

Freeman, T.L., J.W. Mitchell and T.E. Audit, 'Performance of Combined Solar - Heat Pump Systems'. Solar Energy, Vol. 22, pp. 125-135, 1979.

Fritschen, L.J., 'Miniature Net Radiometer Improvement'. Journal of Applied Meteorology, Vol. 4, pp. 528-532, 1965.

Gillett, W.B., 'Solar Simulators and Indoor Testing'. Proc. U.K. - I.S.E.S. Conf. C11, 'Testing of Solar Collectors and Systems', pp. 31-48, April 1977.

Gillett, W.B., 'The Equivalence of Outdoor and Mixed Indoor/Outdoor Solar Collector Testing'. Solar Energy, Vol. 25, No. 6, pp. 543-548, 1980.

Gillett, W.B., R.W. Rawcliffe and A.A. Green, 'Collector Testing Using Solar Simulators'. Proc. U.K. - I.S.E.S. Conf. C22, 'Solar Energy Codes of Practice and Test Procedures', pp. 57-71, April 1980.

Green, A.A., 'The Influence of Environmental Parameters on Flat Plate Solar Collector Performance'. Proc. U.K. - I.S.E.S. Conf. C18, 'Meteorology for Solar Energy Applications', pp. 95-107, January 1979.

Green, A.A. and W.B. Gillett, 'The Significance of Longwave Radiation in Flat Plate Solar Collector Testing'. Proc. Institution of Electrical Engineers Conf. 'Future Energy Concepts', London, I.E.E. Conf. Publication No. 171, pp. 36-39, 1979.

Green, A.A., J.P. Kenna and R.W. Rawcliffe, 'The Influence of Wind Speed on Flat Plate Solar Collector Performance'. Report No. 601, Solar Energy Unit No. 171, Department of Mechanical Engineering and Energy Studies, University College, Cardiff, July 1980.

Haldane, T.G.N., Journal of the Institution of Electrical Engineers, Vol. 68, p. 666, 1930.

Hatton, A.P. and A. Quarmby, 'The Effect of Axially Varying and Unsymmetrical Boundary Conditions on Heat Transfer with Turbulent Flow Between Parallel Plates'. Int. J. Heat and Mass Transfer, Vol. 6, pp. 903-914, 1963.

Hays, D.K., B.W. Parkinson and C.B. Winn, 'The Development of an Ambient Temperature Observer/Predictor (ATOP) for Use with Solar Heating Systems'. Proc. I.S.E.S. Congress, Atlanta, Sun II, Vol. 2, pp. 1416-1420, 1979.

Heap, R.D., Building Services Engineer, Vol. 44, p. 80, 1976a.

Heap, R.D., 'Domestic Heat Pump Operation in a Large House at Alton'. Report ECRC/M998, Electricity Council Research Centre, Capenhurst, Chester, November 1976b.

Heap, R.D., 'Heat Pumps for Domestic Use'. Proc. 2nd International C1B Symposium on Energy Conservation in the Built Environment, Copenhagen, May 28 - June 1, 1979.

Hill, J.E. and T. Kusada, 'Method of Testing for Rating Solar Collectors Based on Thermal Performance'. NBSIR 74-635, National Bureau of Standards, Washington D.C., December 1974.

Hill, J.E. and E.R. Streed, 'A Method of Testing for Rating Solar Collectors Based on Thermal Performance'. Solar Energy, Vol. 18, pp. 421-429, 1976.

Hill, J.E., J.P. Jenkins and D.E. Jones, 'Testing of Solar Collectors According to ASHRAE Standard 93-77'. ASHRAE Transactions, Vol. 84, Pt. 2, pp. 107-126, 1978.

Hoggarth, M.L., Energy World, No. 85, Supplement, October 1981.

Hollands, K.G.T. and E.C. Shewen, 'Optimisation of Flow Passage Geometry for Air-Heating Solar Collectors'. Proc. I.S.E.S. Congress, Atlanta, Sun II, Vol. 1, pp. 302-306, 1979.

Holman, J.P., 'Heat Transfer'. McGraw Hill Kogakusha Ltd., 4th Edition, 1976.

Hottel, H.C. and B.B. Woertz, 'The Performance of Flat-Plate Solar-Heat Collectors'. ASME Transactions and Journal of Applied Mechanics, Vol. 64, pp. 91-104, 1942.

Hwang, B.C. and W.F. Bessler, 'Economics of Solar Assisted Heat Pump Heating Systems for Residential Use'. Proc. I.S.E.S. Congress, Atlanta, Sun II, Vol. 1, pp. 767-771, 1979.

IHVE, 'IHVE Guide, Book A'. Institute of Heating and Ventilating Engineers, 1970.

IHVE, 'IHVE Guide, Book C'. Institute of Heating and Ventilating Engineers, 1970.

Incropera, F.P. and D.P. De Witt, 'Fundamentals of Heat Transfer'. John Wiley and Sons, Inc., 1981.

Jenkins, J.P., 'A Comparison of Test Results for Flat-Plate Water - Heating Solar Collectors Using the BSE and ASHRAE Procedures'. Proc. I.S.E.S. Congress, Atlanta, Sun II, Vol. 1, pp. 365-369, 1979.

Jones, W.P., 'Air Conditioning Engineering'. 2nd Edition, Edward Arnold, 1973.

Kays, W.M., 'Convective Heat and Mass Transfer'. McGraw Hill, 1966.

Krusi, P. and R. Schmid, 'Design of an Inexpensive Solar Simulator'. Proc. I.S.E.S. Congress, Atlanta, Sun II, Vol. 1, pp. 417-421, 1979.

Laidler, J.R. and G.R. Bainbridge, 'The Development and Construction of a Simulator for the Proof Testing of Solar Power Devices'. Proc. Institution of Electrical Engineers Conf. 'Future Energy Concepts', London, I.E.E. Conf. Publication No. 171, pp. 30-35, 1979.

Lee, S.M. and W.N. Gill, 'Heat Transfer in Laminar and Turbulent Flows Between Parallel Plates with Transverse Flow'. A.I.Ch.E. Journal, Vol. 10, pp. 896-901, Nov. 1964.

Liu, B.Y.H. and R.C. Jordan, 'The Long-Term Average Performance of Flat-Plate Solar Energy Collectors'. Solar Energy, Vol. 7, No. 2, pp. 53-74, 1963.

Lou, D.Y.S., A. Haji-Sheikh, S. Kugle and S. Green, 'Performance of Solar Assisted Heat Pump Systems in Residential Applications'. Abstracts, I.S.E.S. Congress, Brighton, Paper I:A2:83, p. 258, August 1981.

Loveday, D.L., G.L.R. Mair and W.E.J. Neal, 'The Utilisation of Conventional Roofs as Solar Energy Collectors'. Abstracts, I.S.E.S. Congress, Brighton, Paper I:A2:81, p. 256, August 1981.

MacArthur, J.W., 'A Parametric Analysis of a Heat Pump Augmented Solar House and Subsequent Determination of the Optimal Cost Effective System'. M.S. Thesis, University of Rhode Island, Kingston, Rhode Island, U.S.A., 1976.

MacGregor, A.W.K., 'An Experimental Investigation into the Effect of Plate Thermal Capacity on the Performance of Solar Water Heating Systems'. Proc. I.S.E.S. Congress, Atlanta, Sun II, Vol. 1, pp. 278-282, 1979.

Mair, G.L.R. and W.E.J. Neal, 'Study of a Solar Assisted Heating System Incorporating a Heat Pump and Store'. ETSU Contract 174/175/057, 1st Progress Report, 1980.

McAdams, W.H., 'Heat Transmission'. McGraw Hill, New York, 1954.

McMullan, J.T. and R. Morgan, 'Heat Pumps'. Adam Hilger, Bristol, November 1981.

McQuiston, F.C. and J.D. Parker, 'Heating, Ventilating, and Air Conditioning Analysis and Design'. John Wiley and Sons, Inc., New York, 1977.

McVeigh, J.C., 'Sun Power'. Pergamon Press, Oxford, 1977.

Moody, L.F., Trans. ASME, Vol. 66, p. 671, 1944.

Mumma, S.A. and C.F. Sepsy, 'A Comparative Experimental Study of Direct Solar Heating and Solar Assisted Heat Pump Heating'. Extended Abstracts, I.S.E.S. Congress, Los Angeles, Paper 45/2, p. 417, 1975.

Mumma, S.A., J.I. Yellott and B. Wood, 'The Application of ASHRAE Standard 93-77 to the Thermal Performance Testing of Air Solar Collectors'. ASHRAE Transactions, Vol. 84, Pt. 2, pp. 410-418, 1978.

National Engineering Steam Tables, 1964.

Neal, W.E.J., D.L. Loveday and M. Pabon-Diaz, 'A Solar Assisted Heat Pump and Storage System for Domestic Space and Water Heating Using a Conventional Roof as a Radiation Absorber'. Proc. I.S.E.S. Congress, Atlanta, Sun II, Vol. 1, pp. 822-826, 1979.

Neal, W.E.J., 'Collecting Precious Joules'. Inaugural Lecture, University of Aston in Birmingham, 23rd October, 1980.

Neal, W.E.J., 'Thermal Energy Storage'. Physics Technology, Vol. 12, p. 213, 1981a.

Neal, W.E.J., Symposium on Solar Heating and Heat Pumps, 'Klimatherm '81', Nicosia, Cyprus, October 1981b.

Neal, W.E.J., 'Study of a Solar Assisted Heating System Incorporating a Heat Pump and Store'. ETSU Contract 174/175/057, Final Report, 1981c.

Norbäck, K., 'Heat Pumps: Results from Measurements Made on Heat Pump Installations in Small Private Houses'. Electricity Council, Overseas Relations Branch Translation Service, O.A. Trans. 2039, from Elinstallatoren, No. 7, 1975.

Olson, O.H., 'Selected Ordinates for Solar Absorptivity Calculations'. Applied Optics, Vol. 2, No. 1, pp. 109-110, 1963.

Parken, W.H., R.W. Beausoleil and G.E. Kelly, 'Factors Affecting the Performance of a Residential Air-to-Air Heat Pump'. ASHRAE Transactions, Vol. 83, Pt. 1, pp. 839-849, 1977.

Parker, B.F., 'Derivation of Efficiency and Loss Factors for Solar Air Heaters'. Solar Energy, Vol. 26, No. 1, pp. 27-32, 1981.

Philips Lighting Division, private communication, 1982.

Rayment, R., 'Wind Energy in the U.K.' B.R.E. Current Paper CP 59/76, September 1976.

Rogers, G.F.C. and Y.R. Mayhew, 'Engineering Thermodynamics, Work and Heat Transfer'. 2nd Edition, Longman, London, 1978.

Sargent, S.L., 'A Compact Table of Blackbody Radiation Functions'. Bulletin of the American Meteorological Society, Vol. 53, p. 360, April 1972.

Siegel, R. and J.R. Howell, 'Thermal Radiation Heat Transfer'. 2nd Edition, McGraw Hill Book Company, 1981.

Simon, F.F. and P. Harlamert, 'Flat-Plate Collector Performance Evaluation - the Case for a Solar Simulation Approach'. NASA TM X-71427, National Aeronautics and Space Administration, Lewis Research Center, Cleveland, Ohio, U.S.A., 1973.

Siviour, J.B., 'Houses as Passive Solar Collectors'. Report ECRC/M1070, Electricity Council Research Centre, Capenhurst, Chester, July 1977.

Siviour, J.B., 'Energy Flows in Six Experimental Houses'. Proc. 2nd International CIB Symposium on Energy Conservation in the Built Environment, Copenhagen, May 28 - June 1, 1979a.

Siviour, J.B., 'Prospects for Energy Savings in Home Heating'. CIBS Annual Conference, 1979b.

Smithsonian Physical Tables, Table 1, Vol. 815, p. 273, 1954.

Stamper, E. and R.L. Koral (Editors), 'Handbook of Air Conditioning, Heating and Ventilating'. 3rd Edition, Industrial Press Inc., New York, 1979.

Stoecker, W.F., 'Refrigeration and Air Conditioning'. McGraw-Hill, New York, 1958.

Stokes, J.W., Heating and Ventilating News, 19th September, 1981.

Sumner, J.A., 'Domestic Heat Pumps'. Prism Press, Dorchester, 1976.

Sundell, J. and J.A. Bubenko, 'Heat Pump Application to Single Family Dwellings - an Analysis by Computer Model'. Proc. Institution of Electrical Engineers Conf. 'Future Energy Concepts', London, I.E.E. Conf. Publication No. 171, pp. 73-76, 1979.

Taussig, R., J. Lockett, J. Isakson, M. Storie and B. Levy, 'Solar Assisted Heat Pump Performance and Computer Simulation'. Proc. I.S.E.S. Congress, Atlanta, Sun II, Vol. 1, pp. 835-839, 1979.

Temps, R.A. and K.L. Coulson, 'Solar Radiation Incident Upon Slopes of Different Orientations'. Solar Energy, Vol. 19, pp. 179-184, 1977.

Terrell, R.E., 'Performance of a Heat Pump - Assisted Solar Heated Residence in Madison, Wisconsin'. Proc. Annual Meeting American Section of I.S.E.S., Denver, Colorado, Vol. 2.1, pp. 299-302, August 28-31, 1978.

Thomson, W., Proc. of the Glasgow Philosophical Society, Vol. 3, 1852.

Touloukian, Y.S., D.P. De Witt and R.S. Hernicz, 'Thermophysical Properties of Matter'. Vol. 9, Plenum Pub. Corp., New York, 1972.

U.S. Naval Observatory, 'The American Ephemeris and Nautical Almanac for the Year 1950'. U.S. Naval Observatory, Washington D.C., 1948.

Welty, J.R., 'Engineering Heat Transfer'. John Wiley, New York, 1978.

Whillier, A., 'Performance of Black-Painted Solar Air Heaters of Conventional Design'. Solar Energy, Vol. 8, No. 1, pp. 31-37, 1964.

Whittle, G.E. and P.R. Warren, 'The Efficiency of Domestic Hot Water Production out of the Heating Season'. B.R.E. Current Paper CP 44/78, July 1978.

Yass, K. and H.B. Curtis, 'Low-Cost, Air Mass 2 Solar Simulator'. NASA TM X-3059, National Aeronautics and Space Administration, Washington D.C., June 1974.

Young, J.F., 'Humidity Control in the Laboratory Using Salt Solutions - A Review'. Journal of Applied Chemistry, Vol. 17, pp. 241-245, September 1967.

Zemansky, M.W., 'Heat and Thermodynamics'. 5th Edition, McGraw-Hill, 1968.

APPENDIX

PUBLICATIONS

(1) Neal, W.E.J., D.L. Loveday and M. Pabon-Diaz, 'A Solar Assisted Heat Pump and Storage System for Domestic Space and Water Heating Using a Conventional Roof as a Radiation Absorber'. Proc. I.S.E.S. Congress, Atlanta, Sun II, Vol. 1, pp. 822-826, 1979.

A SOLAR ASSISTED HEAT PUMP AND STORAGE SYSTEM FOR DOMESTIC SPACE AND WATER HEATING USING A CONVENTIONAL ROOF AS A RADIATION ABSORBER

W.E.J.Neal
D.L.Loveday
M.Pabon-Diaz
Physics Department,
The University of Aston,
Birmingham, B4 7ET, U.K.

ABSTRACT

A domestic space and water heating system will be described. It comprises three main components:- a radiation absorber - the normal roof of a house, a split heat pump situated in the roof space and a thermal store comprising $22m^3$ of water located below the ground floor. A prototype unit has been installed in an owner occupied house with three bedrooms and a summary of some of the results of monitoring for one heating season is given. An indication of the contribution of energy from N.W. and S.E. facing roofs is given together with the average seasonal coefficient of performance for the heat pump and the relative contributions from the three low grade sources: ambient air, solar boost and heat loss from the house to the roof space during operation.

1. INTRODUCTION

Before describing the system it is relevant to comment on the United Kingdom situation and to consider the system in an appropriate context. The U.K. lies between latitudes 50^oN and 58^oN with a high proportion of the population in the South. It has a relatively mild climate and the occasions when temperatures are less then 0^oC for 10 consecutive days are rare. The extremes between summer and winter radiation levels are $\sim 800Wm^{-2}$ and $\sim 150Wm^{-2}$ respectively. There are few completely cloudless days even in summer so that there is a high proportion of diffuse radiation. Degree days - defined in terms of a base temperature of 15.5^oC (60^oF) range from 1900 in the South to 2900 in the extreme North. Under average climatic conditions there is little or no cooling requirement for dwellings so the use of heat pumps presents quite a different picture from that in the United States of America for example where there is a considerable domestic cooling requirement. The operation of air to air heat pumps in the U.K. almost exclusively in the heating mode and for 50% to 60% of the year raises the serious question of cost effectiveness in view of the capital outlay for such equipment.

The average household in the U.K. uses $0.15m^3$ of water every day at 55^oC to 60^oC which represents 25% of the household's annual demand - the remaining 75% being for space heating. Annual savings in energy which may be expected from the use of solar panels to provide pre-heated water amount to $\sim$ 12.5%. For solar energy to make any appreciable contribution to the annual heating load some provision for both space and water heating is necessary.

One of the objectives of the present work was to consider a solar-assisted heating system which fulfilled the above requirement and which could be installed in existing houses at minimal cost and with few structural alterations. (The provision of a system, based on the same principles, for new dwellings would present fewer difficulties). Another objective was to determine and optimise the performance over a heating season - October to April. The system described takes advantage of the diffuse radiation on a North facing roof as well as diffuse and direct radiation on a South facing roof and, as has already been mentioned, diffuse radiation in the U.K. constitutes the larger proportion. A prototype unit incorporating a split heat pump and thermal store was installed in two occupied privately owned dwellings (one with a tile roof and one with a slate roof) by Helix Multi-professional Services. The discussion in this paper arises from results which were obtained from the house with the tiled roof.

2. DESCRIPTION OF HOUSE AND HEATING SYSTEM

The house is a detached three bedroom dwelling situated at 51^oN with a floor area of $147m^2$ and living accommodation on two levels. The calculated roof, wall and window fabric loss is 4.6kw under wind still

conditions for a 20 deg C difference between the inside and outside. The two sides of the delta-tiled roof each of 55m^2 face South East and North West with a pitch of 25^o. Figure 1 represents a section through the roof space, the floor of which is covered with the equivalent of 150mm of fibre glass wool.

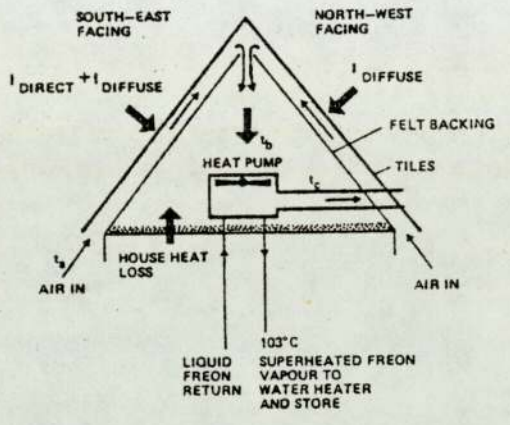

Fig.1. Roof Space System

Air from outside the building at an external ambient temperature t_a is drawn through channels, on both sides of the roof, formed by the underside of the roof tiles and a roof felt backing attached to the tile support structure. The air enters the channels at the eaves and its temperature is raised during its passage to the apex by heat exchange with the roof which absorbs direct and indirect radiation. The air enters the evaporator of the split heat pump at a temperature t_b and is expelled to the outside at a temperature t_c. In general $t_b > t_a > t_c$. The heat extracted at the evaporator is obtained from ambient air with the addition of heat derived from radiation and any heat losses from the living space to the roof space. Figure 2 is a diagrammatic representation of the system. Superheated freon vapour is cooled and heat is supplied to a domestic hot water feed tank which reaches a temperature of 55^{o}C. Condensation of freon takes place in a freon -water heat exchanger. The water circulates through the store either directly or through the water-air heat exchanger of the warm air heating system. The store comprises 22m^3 of water in three polypropylene bags recessed into the lower floor and contained within the building structure. Although as shown the evaporator and compressor are situated in the roof space, in practice the heat pump could be located elsewhere if an

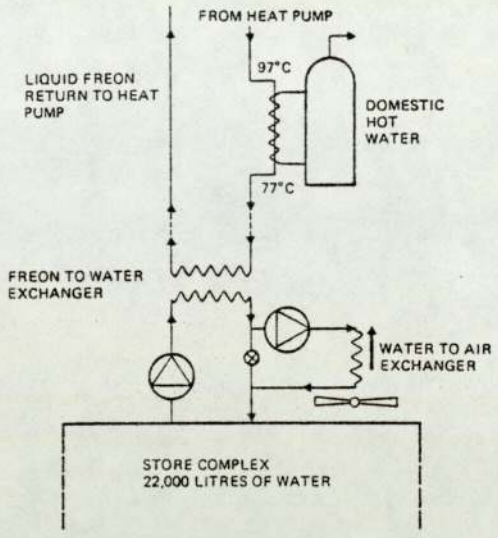

Fig.2. General System.

insulated air duct connects the roof space to the evaporator. The system is switched on during October to initiate the charging of the store and the normal procedure has been to operate the heat pump during daylight hours in an attempt to maximise the seasonal coefficient of performance of the heat pump. Temperatures were monitored at 30 strategic points using thin film platinum sensors and sampled hourly throughout the day and night. Electrical energy consumption was also monitored. Data on solar radiation, wind velocity, relative humidity and weather conditions was initially obtained from a local weather station.

3. RESULTS

Figures 3(a,b,c) are typical plots of temperature rises in air which has passed through the channels in the North West and South East facing roofs for the same air flow rate 740 litre s^{-1} under different weather conditions. Table I gives radiation, wind and relative humidity data for the same days. Normally the heat pump was run during daylight hours. [On a few occasions the pump was run for 24 hours to obtain contributions only from ambient and heat losses from the house].
Under the conditions relating to Figure 3c the contributions from both sides of the roof are almost identical and due to diffuse radiation and any radiation from the surroundings.

Although it has not yet been possible to correlate values of the roof efficiency with

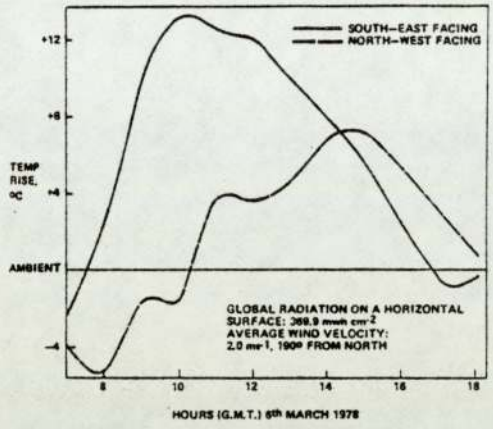

Fig.3(a)

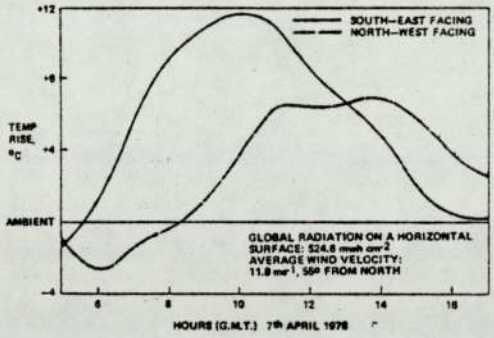

Fig.3(b)

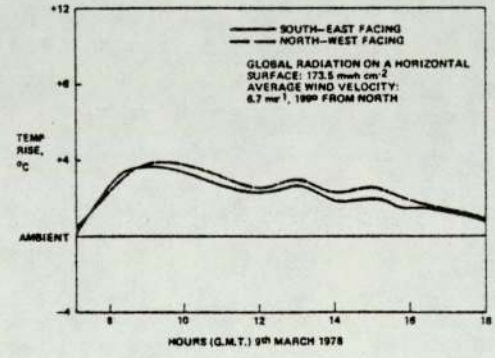

Fig.3(c)

Fig.3(a,b,c). Air temperature rises, S.E. and N.W. facing sides.

weather conditions we have found values ranging from 6% to 12%. In the laboratory in still conditions and high ambients efficiencies of over 40% have been obtained for low radiation levels when re-radiation is also low. The evaluation of the factor 'f' in equation (1) is still being pursued.

TABLE I

Meteorological Data for Figures 3(a,b,c)

Data	6.3.78	9.3.78	7.4.78
A	369.9	173.5	524.6
B	71.7	125.7	198.6
C	38.5	51.5	82.6
D	521.4	145.6	427.8
E	10.4	0.7	10.7
F	73.0	94.0	59.0
G	190.0	199.0	55.0
H	2.0	6.7	11.8
J	06-36	06-29	05-24
K	17-49	17-54	18-44

A=Global Radiation on a Horizontal Surface, mWh cm^{-2}
B=Diffuse Radiation on a Horizontal Surface, mWh cm^{-2}
C=Global Radiation on a Vertical Surface facing North, mWh cm^{-2}
D=Global Radiation on a Vertical Surface facing South, mWh cm^{-2}
E=Number of Hours of Sunshine
F=Relative Humidity at 0900 hrs, %.
G=Average Wind Direction, degrees from North.
H=Average Wind Speed, m s^{-1}
J=Time of Sunrise, Hours G.M.T.
K=Time of Sunset, Hours G.M.T.

4. DISCUSSION

In comparing the performance of a system of the type described and one where an air to air heat pump extracts heat directly from ambient and transfers it to the living area as and when required there are two important factors which need to be known:
(i) The function of a normal roof as a radiation absorber and the proportion of incident radiation which can be transferred to the air flowing in the roof channels.
(ii) The percentage of total energy extracted which can be attributed to the solar boost.

4.1 The roof efficiency

An efficiency f can be defined as:

$$f_{SE} = Q_{SE} / E_{SE} \qquad (1)$$

where the suffix SE refers to the South East facing roof.
Q_{SE} is the rate of energy gain by the air.

$$E_{SE} = A\, I_{SE} \qquad (2)$$

I_{SE} is the radiation energy intensity on the roof in W m^{-2} and A is the area of each roof surface ($55m^2$).

$$Q_{SE} = \dot{m}\, C_p \left(t_{Apex} - t_a \right)_{SE} \Big/ 2 \qquad (3)$$

C_p is the specific heat of the air, $\dot{m}$ is the total mass flow rate of air assumed to be equal on both roof sides.

$\left(t_{Apex} - t_a \right)_{SE}$ is the temperature rise in the channel for the South East facing roof. Similar expressions can be given for the roof surface facing NW.

The ratio f is dependent on climatic conditions and we have not yet been able to quantify all effects of external influences on the heat transfer characteristics. Separate tests are being undertaken on a laboratory simulation rig under more controlled conditions.

4.2. Sources of energy

The maximum theoretical performance of a heat pump is given by the ratio $T_1/(T_1-T_2)$ where T_1 and T_2 are the absolute temperatures of sink and source respectively. In practice one can define a real coefficient of perform -ance for an electrically driven compressor as:-

$$C.O.P.(H) = Q_1/(Q_1-Q_2) = Q_1/W \qquad (4)$$

where Q_1 is the heat rejected per cycle
Q_2 is the heat absorbed per cycle at a temperature T_2
W is the electrical energy consumed per cycle.

The performance can also be expressed in terms of Q_2

$$C.O.P.(H) = (Q_2 + W)/W \qquad (5)$$

For the purposes of this paper we shall use the latter definition in order to arrive at an estimate of the relative contributions from the various sources of low grade heat.

$$Q_2 = Q_A + Q_S + Q_{HL} \qquad (6)$$

Q_A, Q_S and Q_{HL} are the contributions from ambient air, the solar boost and the heat losses from the living space to the roof space respectively. For moist ambient air Q_A will be made up from sensible and latent heat contributions. The various contributions are depicted in Figure 4 which gives the specific enthalpies of air at the different stages. Ambient air is represented

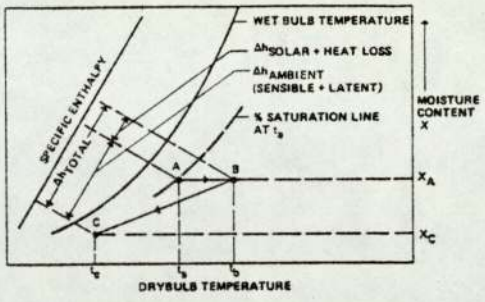

Fig.4. Psychrometric Changes as Air Passes Through the Roof System.

by the point A and in passing through the roof channel we assume no change in moisture content. The air arriving at the evaporator is represented by B and the move BC takes place at the evaporator.

$Q_A = \dot{m}\, \Delta h_{AMBIENT}$, $Q_S = \dot{m}\Delta h_{SOLAR}$, $Q_{HL} = \dot{m}\Delta h_{HEAT\ LOSS}$

The data for each day of the heating season 1977-1978 has been analysed in order to obtain performances over the season. Figure 5 is a plot of average weekly coefficients of performance and it can be seen that they vary between 3.30 and 1.96 with an average seasonal value of 2.4. Attention is drawn to the fact that the heat pump energy consumption used in the calculation includes that used by the compressor and the fan to draw air over the evaporator. The effective seasonal C.O.P.(H)s were: with compressor only 2.76; compressor and fan 2.43; compressor, fan and ancillary system equipment 1.96. Taking into account the additional electrical energy for boosting the temperature of domestic hot water the value is reduced to 1.8.

The curves in figure 6 show the variations of contributions from ambient, solar and heat loss over the season assuming 100% heat recovery of the losses from the house to the loft during the operation of the heat pump. The effect of less than 100% recovery would be to increase the solar contribution as can be seen from figure 4, since the sum of solar and heat loss contributions is fixed for a given situation and is represented by the movement from A-B. In calculating the heat loss contribution still wind conditions have been assumed. [A wind speed of 6 m s^{-1} for example leads to relative changes between solar and heat loss of the order of 0.1%]. The average contributions over the season from either ambient, solar or heat loss is defined as:

$$\frac{\text{Total heat extracted from a given source}}{\text{Total heat extracted from all sources}} \times 100\%$$

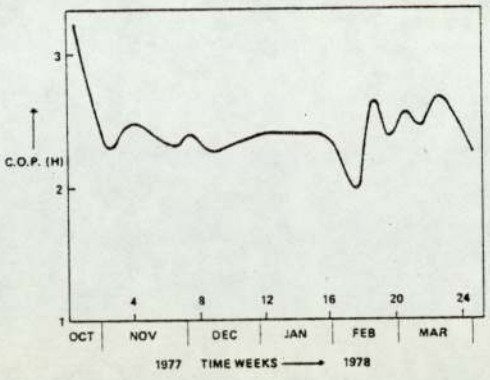

Fig.5. Coefficients of Performance Over a Heating Season.

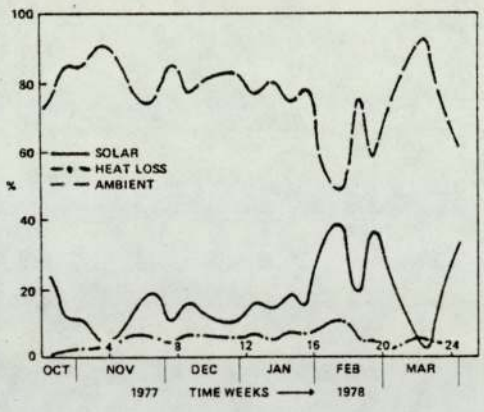

Fig.6. % Contribution of Ambient, Solar and Heat Loss Over a Heating Season.

During the experimental period October to April for the 1977-1978 heating season the values were found to be 77%, 17.5% and 5.5% for ambient, solar and heat loss respectively. There is no doubt that the utilisation of the normal roof as a radiation absorber and air panel can provide a useful addition to a heat pump system in mild climates. The provision of a store enables the pump to be operated at times when higher C.O.P.(H)s can be achieved and the slightly higher air temperature over external ambient provided at the evaporator reduces the frosting problem in addition to improving the performance. In fact a fully charged store in the system described provides for 10 consecutive days with a temperature difference of 20 deg C between the outside and inside without the operation of the heat pump. As mentioned in the introduction this would be a rare condition for most regions in the U.K.

Several authors have reported on computer modelling of solar assisted heat pump systems, see for example Freeman et al(1), Bosio and Suryanarayana (2), Freeman et al(3). The operational experience gained with this relatively simple prototype system together with the laboratory simulated tests on roof structures has provided the basis for an engineering design of an integrated heating and cooling system which includes heat pumping from store and a new store configuration. The objective has been to match the heat pump to the supply and the load in order to achieve an improved seasonal C.O.P.(H) and to provide a unit suitable for any house in any locality without the need for auxiliary space heating. It is expected to commence a computer modelling exercise on the new system in the Autumn of 1979.

5. ACKNOWLEDGMENTS

A Grant from the Science Research Council (U.K.) to enable part of the monitoring programme to be undertaken is gratefully acknowledged, and Mr.D.L.Loveday acknowledges a studentship from the same body. We are grateful to Mr.B.Wilson for the use of his house for experimental purposes.

6. REFERENCES

(1) Freeman, T.L., Beckman, W.A., Mitchell, J.W. and Duffie, J.A. Computer Modelling of Heat Pumps and the Simulation of Solar-Heat Pump Systems. ASME paper 75-WA/SOL-3, ASME Winter Annual Meeting (1975).

(2) Bosio, R.C. and Suryanarayana, N.V. Solar Assisted Heat Pump System: A Parametric Study for Space Heating of a Characteristic House in Madison, Wisconsin. ASME paper 75-WA/SOL-8 ASME Winter Annual Meeting (1975).

(3) Freeman, T.L., Mitchell, J.W., Audit, T.E. Performance of Combined Solar-Heat Pump Systems. Solar Energy 22 125 (1979).

(2) Loveday, D.L., G.L.R. Mair and W.E.J. Neal, 'The Utilisation of Conventional Roofs as Solar Energy Collectors'. Abstracts, I.S.E.S. Congress, Brighton, Paper I:A2:81, p. 256, August 1981.

THE UTILISATION OF CONVENTIONAL ROOFS AS SOLAR ENERGY COLLECTORS

D.L. Loveday, G.L.R. Mair and W.E.J. Neal

Department of Physics, University of Aston in Birmingham,
Birmingham B4 7ET, U.K.

ABSTRACT

Indoor tests using a heating simulator were carried out on a $1m^2$ section of tiled roof and a $1m^2$ corrugated steel panel with backing insulation to determine their instantaneous steady-state efficiencies and time constants with a view to solar applications. The tests and presentation of results followed, as closely as possible, the ASHRAE 93-77 (1978) standard procedure. In addition, it was considered appropriate to conduct some tests of particular relevance to U.K. conditions. Plots of efficiency η against $(t_i - t_a)/I$ are presented for the tiled structure and the steel panel and are compared with that of a double glazed flat plate air heater. It is shown that the effect of wind on an untorched tiled surface raises the η intercept

KEYWORDS

Solar simulation; energy collection by roofs; tile roof; metal roof; ASHRAE 93-77 procedure; solar panel efficiency; solar-assisted heat pump.

INTRODUCTION

The laboratory investigation reported here forms part of an experimental programme of work in which the objective was to look into the potential of utilising existing roofs of houses as absorbers of solar energy. This would not only be of particular relevance for the retro-fitting of some form of solar-assisted heating system to the existing housing stock, but could also be of benefit in the construction of new buildings from the points of view of cheapness of materials, reliability and safety. In a field trial, a conventional tiled roof, where air has been heated as it passes between tiles and a backing of felt, has been used as the pre-heat component for a heat pump in a domestic space and water heating installation near Basingstoke, U.K. (Neal, Loveday and Pabon-Diaz, 1979). Laboratory tests allow a comparison to be made between conventional roofing materials (when used as air-heating energy collectors) and purpose-designed collectors.

COLLECTOR TESTING

The performance of a solar collector is commonly described by the equations

$$\eta = F'(\tau\alpha)_e - F'U_L(\bar{t}_f - t_a)/I \quad (1)$$

or $$\eta = F_R(\tau\alpha)_e - F_R U_L (t_i - t_a)/I \quad (2)$$

The efficiency, η, is given by

$$\eta = q_u/IA \quad (3)$$

and $$q_u = \dot{m}Cp(t_o - t_i) \quad (4)$$

where q_u is the useful energy collected and IA the incident energy, both per unit time for the collector area, A, considered; $\dot{m}$ and Cp are the mass flow rate and specific heat of the transfer fluid respectively, $(\tau\alpha)_e$ is the effective cover transmittance plate absorptance product (Duffie and Beckman, 1974), U_L the overall heat loss coefficient, $\bar{t}_f$, t_o and t_i the average heat transfer fluid temperature, and fluid outlet and inlet temperatures respectively and t_a the surrounding ambient temperature. F' is the plate efficiency factor and F_R the heat removal efficiency factor introduced by Bliss (1959). These forms, of what has now come to be known as the Hottel-Whillier-Bliss equation, are those most frequently used in collector testing; $(\tau\alpha)_e$, U_L and the factors F' and F_R are generally taken as constants (within limited operating conditions) characterising a given collector's performance.

The use of standard test procedures (NBS, 1974; ASHRAE, 1978 ; BSE, 1978) allows universal comparison of the thermal performance of collectors, since tests are conducted under similar specified conditions, and results presented in the same format. The format given in the ASHRAE standard is widely used and was chosen for the results in this paper.

HEATING SIMULATOR

Indoor testing offers the advantage of closely controlled conditions which in turn reduce scatter in efficiency plots and aid comparison of results. "Solar simulators" are usually employed and several have been described (Yass and Curtis, 1974 ; Gillett, 1977; Krusi and Schmid, 1979). A facility giving full spectral simulation is expensive. In view of this, a simulator was constructed which reproduced the heating effect of solar radiation rather than its actual spectrum. (Fig. 1).

A square array of sixteen Philips 300 watt tungsten filament infra red reflecting (IRR) heat lamps was used to heat a $1m^2$ section of "roof". The glass envelopes of the lamps were 0.5m from the test surface. A crossflow fan drew air under the tiles (Fig.1) or through the flutes formed in the corrugated steel panel with backing insulation, while another crossflow fan simulated the effect of a $2m.s^{-1}$ wind parallel to the collector surface. A pre-heat module served to vary t_i and hence generate the efficiency graphs.

Comparative indoor testing of collectors is unaffected by the use of IRR lamp radiation provided that the appropriate values for absorptivity are used. Relating the indoor IRR to the equivalent outdoor solar radiation intensity can be achieved in terms of the level of solar radiation needed to maintain the same collector temperatures but under outdoor heat loss conditions; a knowledge of the collector surface absorptivity to each radiation distribution is also required .

This approach gave equivalent solar radiation values of 934 Wm^{-2} and 457 Wm^{-2} for the indoor IRR radiation values of 813 Wm^{-2} and 327 Wm^{-2} respectively, for the tiled roof.

All radiation intensities, I, presented in the results which follow, are the indoor IRR values, corrected for the indoor field of view temperature (Gillett, Rawcliffe and Green, 1980). Airstream temperature differences were measured with differential thermopiles.

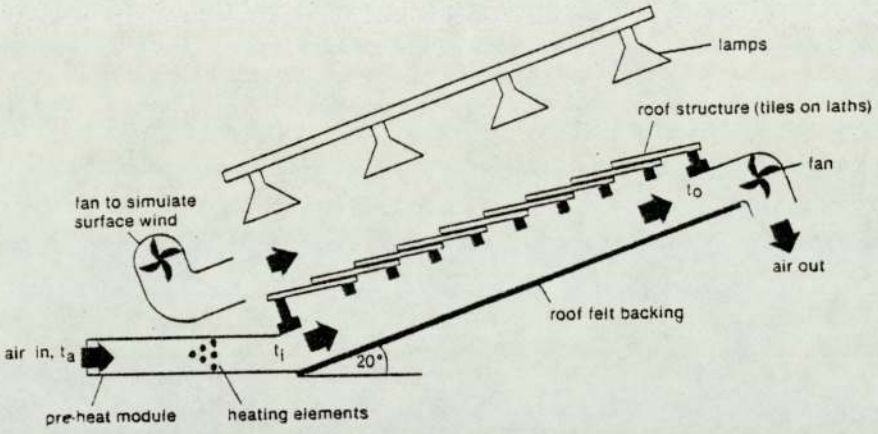

Fig. 1. Schematic diagram of the heating simulator with the tiled surface under test.

RESULTS AND DISCUSSION

When a wind blows over the untorched experimental tile surface, air ingress to the tile/felt duct takes place. This effect augments the air mass flow rate. However, the mass flow rates for efficiency plots in this report relate to non-augmented values throughout.

Fig. 2 refers to the tiled surface. Fig. 3 relates to a double glazed flat plate solar air heater, adapted from the ASHRAE Standard (1978) and originally reported by Hill, Jenkins and Jones (1978). It can be seen that the efficiency intercepts are 0.30 and 0.50 for the tile surface and the air panel respectively at an air mass flow rate of $\simeq$0.13 kg s^{-1}. The results also highlight the fact that the specially designed panel has a lower heat loss coefficient and can run with higher inlet fluid temperatures. The roof structure therefore has a role to play as a pre-heating device for an air source heat pump, the applications of which are to be discussed elsewhere.

The results presented in Figs. 4 and 5 were obtained for a lower radiation level and a mass flow rate closer to that utilised in the air source heat pump system reported by Neal, Loveday and Pabon-Diaz (1979).

The efficiencies were lower but for a larger range of $(t_i - t_a)/I$ values. The results also show an enhanced efficiency with wind. This is mainly due to the ingress air removing heat from the tile upper surfaces and transporting the energy to the air stream in the duct. This effect was confirmed by sealing the tile

overlaps and repeating the tests.

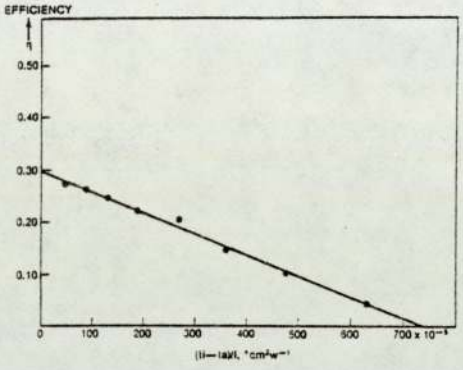

Fig. 2. Tiled roof: I = 813 Wm^{-2}; $\dot{m}$ = 0.12 kg s^{-1}; wind = 2 m s^{-1}

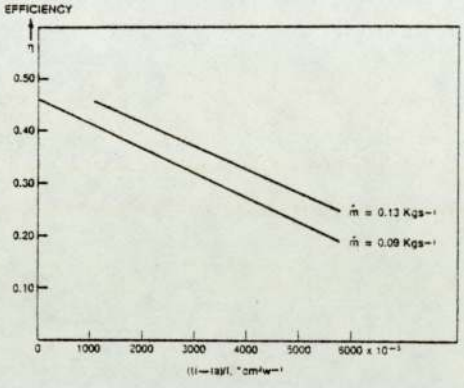

Fig. 3. Air Panel (from Hill, Jenkins and Jones, 1978).

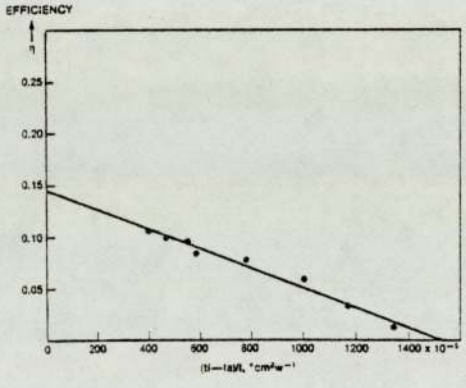

Fig. 4. Tiled roof: I = 327 Wm^{-2}; $\dot{m}$ = 0.03 kg s^{-1}; no wind.

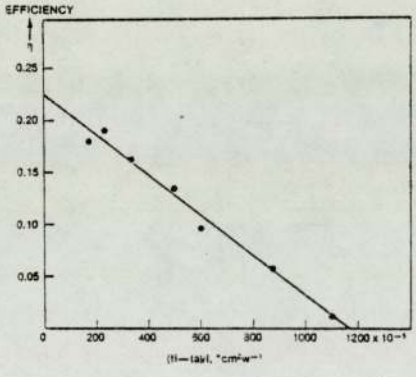

Fig. 5. Tiled roof: I = 327 Wm^{-2}; $\dot{m}$ = 0.03 kg s^{-1}; wind 2 m s^{-1}.

The plot for the sealed roof was almost identical to Fig. 4, but the application of wind now reduced rather than enhanced efficiency.

Several authors have discussed the effects of leaks on the efficiency of air heating solar collectors (see for example, Close and Yusoff, 1978, Mumma, Yellott and Wood, 1978). In the present work benefit is derived since the ingress introduces a supplementary source of heat, which raises the outlet air temperature.

Tests were also conducted on corrugated steel and aluminium panels with backing insulation and the results for a steel panel are shown in Figs. 6 and 7.

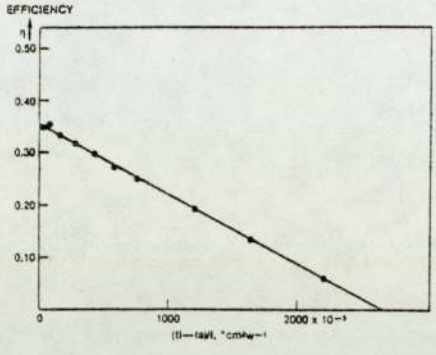

Fig. 6. Steel Panel: I = 817 Wm^{-2}; $\dot{m}$ = 0.03 Kg s^{-1}; wind 2 m s^{-1}.

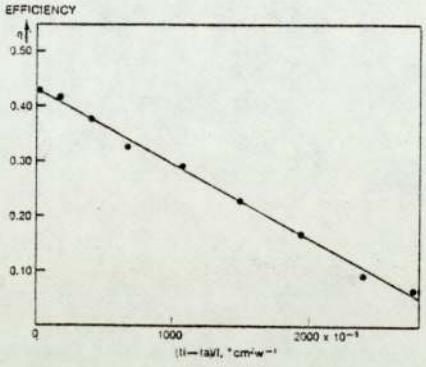

Fig. 7. Steel Panel: I = 327 Wm^{-2}; $\dot{m}$ = 0.03 kg s^{-1}; wind 2 m s^{-1}.

The increase in the η intercept in the lower radiation case for the steel panel could be due to selectivity. This phenomenon is under further investigation.

Values for the time constants (defined in ASHRAE 93-77) with wind for the unsealed tiled roof section, corrugated steel panel and the air panel (Hill, Jenkins and Jones, 1978) were 40.0, 7.0 and 12.7 minutes respectively.

REFERENCES

A.S.H.R.A.E.(1978). ASHRAE Standard 93-77, American Society of Heating, Refrigerating and Air-Conditioning Engineers, Inc., New York.

Bliss, R.W. (1959). Solar Energy, Vol. III, No.4, 55-64.

B.S.E. (1978). Efficiency Test. Bundesverband Solarenergie, Essen, Federal Republic of Germany.

Close, D.J. and M.B. Yusoff (1978). Solar Energy, Vol. 20, 459-463.

Duffie, J.A. and W.A. Beckman (1974). Solar Energy Thermal Processes, Wiley Interscience, New York.

Gillett, W.B. (1977). Proc. Conf. (U.K)-I.S.E.. . C11, 31-48.

Gillett, W.B., R.W. Rawcliffe and A.A. Green (1980). Proc. Conf. (U.K)-I.S.E.S. C22, 57-71.

Hill, J.E., J.P. Jenkins and D.E. Jones (1978). A.S.H.R.A.E. Trans., Vol. 84, Pt.2, 107-126.

Krusi, P. and R. Schmid (1979). Proc. I.S.E.S. Silver Jubilee Congress, Atlanta, Georgia, Sun II, Vol. 1, 417-421.

Mumma, S.A., J.I. Yellott and B. Wood (1978). A.S.H.R.A.E. Trans. Vol. 84, Pt.2, 410-418.

N.B.S. (1974). NBSIR 74-635, National Bureau of Standards, Washington, D.C.

Neal, W.E.J., D.L. Loveday and M. Pabon-Diaz (1979). Proc. I.S.E.S. Silver Jubilee Congress, Atlanta, Georgia, Sun II, Vol. I, 822-826.

Yass, K. and H.B. Curtiss (1974). NASA TM X-3059, National Aeronautics and Space Administration, Washington, D.C.

ACKNOWLEDGEMENT

The authors are grateful to Dr. M.G. Hutchins of University College, Cardiff, for reflectivity measurements.